

STRUCTURE AND PROPERTIES OF π - π INTERACTING COMPLEXES OF CARBON NANOTUBES

Ph.D. Thesis

by

ANKITA JOSHI



DEPARTMENT OF CHEMISTRY
INDIAN INSTITUTE OF TECHNOLOGY ROORKEE
ROORKEE – 247667 (INDIA)
AUGUST, 2019



STRUCTURE AND PROPERTIES OF π - π INTERACTING COMPLEXES OF CARBON NANOTUBES

A THESIS

*Submitted in partial fulfilment of the
requirements for the award of the degree*

of

DOCTOR OF PHILOSOPHY

in

CHEMISTRY

by

ANKITA JOSHI



DEPARTMENT OF CHEMISTRY
INDIAN INSTITUTE OF TECHNOLOGY ROORKEE
ROORKEE – 247667, INDIA
AUGUST, 2019



©INDIAN INSTITUTE OF TECHNOLOGY ROORKEE, ROORKEE- 2019
ALL RIGHTS RESERVED



INDIAN INSTITUTE OF TECHNOLOGY ROORKEE

STUDENT'S DECLARATION

I hereby certify that the work presented in the thesis entitled **STRUCTURE AND PROPERTIES OF π - π INTERACTING COMPLEXES OF CARBON NANOTUBES** is my own work carried out during a period from July, 2014 to August, 2019 under the supervision of Dr. Ramachandran C. N., Assistant Professor, Department of Chemistry, Indian Institute of Technology Roorkee, Roorkee.

The matter presented in the thesis has not been submitted for the award of any other degree of this or any other Institute.

Dated: December 3, 2019

(ANKITA JOSHI)

SUPERVISOR'S DECLARATION

This is to certify that the above mentioned work is carried out under my supervision.

Dated: December 3, 2019

(Ramachandran C. N.)

Supervisor

The Ph.D. Viva-Voice Examination of Ankita Joshi, Research Scholar, has been held on **December 3, 2019**.

Chairperson, SRC

External Examiner

This is to certify that the student has made all the corrections in the thesis.

Supervisor

Head of the Department

Dated: December 3, 2019



Abstract

Functionalization of carbon nanotubes (CNTs) has gained wide attention during the last two decades due to their applications in various optoelectronic devices. Such functionalization has been achieved by either covalently or non-covalently. The non-covalent functionalization is further classified into endohedral and exohedral. The endohedral functionalization involves the encapsulation of guest molecules inside the cavity of host CNT while in the exohedral one the molecules are adsorbed non-covalently on the surface of CNT. The non-covalently interacting endo- and exohedral complexes of CNTs are often stabilized by weak interactions such as π - π , C-H... π and N-H... π , depending on the functional groups present in the attached molecule. Among these, the π - π interactions are more common and exist between aromatic rings and CNT. Such interactions also exist between π -donor and π -acceptor molecules. In general, the various interactions such as dispersion, electrostatic and polarization stabilize the complex while the exchange interaction destabilizes it. Such complexes exhibit distinctive optoelectronic and charge transport properties which makes them suitable for their applications in organic electronic, organic light-emitting diode (OLED) and organic transistor devices. The donor-acceptor complexes of CNTs are particularly useful in OLEDs. The organic semiconducting complexes of CNTs with good carrier mobilities are potential candidates for organic transistors. They can be of p-type, n-type or ambipolar in nature depending on the magnitude of electron and hole mobility. Most of the studies on optoelectronic properties of the non-covalent complexes of CNTs have been done without an in-depth understanding of charge transfer at the molecular level. Besides, a molecular level understanding of the charge transport properties of such complexes are also lacking. In this regard, the computational investigation of the optoelectronic as well as the charge transport properties of non-bonded complexes of CNTs with donor or acceptor molecules is of utmost important.

A new type of non-covalent functionalization of CNT is the mechanically interlocked nanotubes (MINTs). In MINTs, the movement of macrocycles on the surface of CNT is possible in presence of external stimuli such as light and can be used for various applications including molecular motors. In the present thesis, dispersion-corrected density functional theoretical methods are employed to study the interaction of carbon nanotubes (CNTs) with selected macrocyclic host molecules to explore their optoelectronic properties.

The thesis is divided into seven chapters. In chapter 1, different types of functionalization of CNTs, mechanically interlocked nanotubes, their properties and applications are discussed. The earlier reported studies on the complexes of CNTs are also briefly reviewed.

The important computational methodologies used in the present thesis are described in the second chapter. Beginning with Schrödinger equation, the quantum chemical methods such as Hartree-Fock and Post-Hartree-Fock methods are briefly discussed. Apart from these wavefunction-based methods, density functional methods used in the present work are also discussed. A brief outline of different types of functionals and basis sets is presented. This chapter also provides basic concepts of ground- and excited-state electron transfer processes for donor-acceptor compounds. Various charge transport parameters such as reorganization energy, transfer integral and carrier mobility are explained.

In chapter 3 of the thesis, stability, optoelectronic and charge transport properties of endo- and exohedral complexes of CNT with indigo are investigated using dispersion-corrected density functional B97-D in conjunction with 6-31G(d,p) basis set. The stabilization energy, ionization energy, electron affinity, the energy gap between the highest occupied and lowest unoccupied molecular orbitals ($\Delta E_{\text{HOMO-LUMO}}$), and absorption spectra of the complexes as well as their free components are determined. The $\Delta E_{\text{HOMO-LUMO}}$ of about 1 eV is obtained for the complexes indicating them as organic semiconductors. The effect of number of indigo molecules on the above mentioned properties of their exohedral complexes with CNT is examined. The dependence of diameter of CNT on the stability and properties of its endohedral complexes with indigo is investigated. The effect of hybrid functional B3LYP-GD3 and long-range corrected hybrid functional ω B97X-D on the properties of most stable endohedral complex is examined. The photoinduced charge transfer for the exohedral complexes in which CNT behaves as a donor and indigo acts as an acceptor is observed. The optical absorption spectra of the complexes are simulated using the time-dependent density functional theoretical (TD-DFT) method. The complexes show charge transfer peaks in the visible and near-infrared regions of the electromagnetic spectrum. Based on the Marcus theory, the carrier mobility is calculated from the charge hopping rate. The carrier mobility calculations reveal that the exohedral complexes exhibit p-type character due to significantly higher hole mobility than electron mobility while the endohedral complexes possess nearly the same value of hole and electron mobilities. The results for the exohedral complexes of long and closed CNTs are similar to those obtained for the complexes of CNT of relatively small length as well as with open ends. Apart from this, the

exohedral complex in which indigo is aligned parallel to the tube-axis exhibits almost similar value of hole and electron mobilities.

The structure, optoelectronic and charge transport properties of the exohedral complex of (6,6)CNT with perylene bisimide (PBI) are investigated using different dispersion-corrected density functionals (B97-D, B3LYP-GD3 and ω B97X-D) in conjunction with 6-31G(d,p) basis set and the results are discussed in chapter 4. The electron density distribution in the frontier molecular orbitals of the complex indicates the possibility of photoinduced charge transfer from donor CNT to acceptor PBI constituting a donor-acceptor complex between them. Due to inappropriate size of the cavity of (6,6)CNT to host PBI, a relatively larger diameter (8,8)CNT is used for the encapsulation. The calculations of stabilization energy reveal that the endohedral complex PBI@(8,8)CNT is more stable than the exohedral complex PBI-(8,8)CNT. The energy decomposition analysis of the complexes suggests that the dispersion and the electrostatic interactions are predominant for endo- and exohedral complexes, respectively.

In chapter 5 of the thesis, the structure and properties of endo- and exohedral complexes of (6,6)CNT with electron donor molecule quaterthiophene (4T) are investigated using various dispersion-corrected density functionals. A comparative study on the charge transport properties of both types of complexes is presented. The results indicate a n-type charge transfer characteristics owing to remarkably higher electron mobility than hole mobility, irrespective of the type of functionalization. The excited state calculations of the complexes carried out in the framework of TD-DFT indicate several charge transfer transitions from donor 4T to acceptor CNT in the visible region of the electromagnetic spectrum. The complexes also show very high light-harvesting efficiency implying their possible application in solar cells.

The optoelectronic properties of the complexes of guest (6,6)CNT with macrocyclic hosts [10]cycloparaphenylene ([10]CPP) and its derivatives are studied using dispersion-corrected density functional method and are discussed in chapter 6. The various derivatives of [10]CPP are modelled by doping nitrogens as well as by substituting hydrogens with electron-donating amino/electron-accepting fluorine groups. The values of stabilization energy indicate that the complexes CNT@[10]CPP and CNT@*n*F-[10]CPP (*n* = 10, 20 and 40) are energetically stable. The frontier molecular orbital analysis predicted the occurrence of photoinduced charge transfer in the complex CNT@40F-[10]CPP. The optical absorption spectrum of the complex CPP-CNT indicates absorption in the near-ultraviolet and visible regions, whereas that of the complexes CNT@*n*F-[10]CPP show absorption in a wide range starting from near-ultraviolet to near-infrared region of the electromagnetic spectrum. Among the complexes, high values of light-

harvesting efficiency are obtained for CNT@*n*F-[10]CPP. The change in potential energy for the translational movement of CPP over CNT for both ground and excited states is examined. The results indicate an energy barrier for the piston type movement of CNT in the complexes for the ground state, but not for its excited states. The barrier for rotation of bare and fluorinated CPP over CNT suggests the application of these complexes as components in molecular wheels and shuttles.

The summary and conclusions of the thesis are provided in chapter 7.



Acknowledgement

First of all, I would like to express my sincere gratitude and thanks to my supervisor **Dr. C.N. Ramachandran**. This work would not have been possible without his guidance, support and motivation. Under his supervision, I successfully overcame with many difficulties and extended my problem solving and creative abilities. His calm demeanour and positive approach to research made working under his supervision a very enjoyable experience.

I would also like to thank my research committee members, **Dr. P. Jeevanandam** (Chairman), **Dr. Pallavi Debnath** (Internal Expert) and **Dr. Moumita Maiti** (External Expert) for their availability and insightful comments, which were determinant for the completion of the work present in this thesis.

I gratefully acknowledge **Prof. K. R. Justin Thomas**, Head of the Department of Chemistry, Indian Institute of Technology Roorkee and former head, **Prof. M. R. Maurya** for providing necessary infrastructure and resources to accomplish my research work.

I take this opportunity to thank all the chemistry faculty members for their contributions to my academic activities.

I would also like to thank other teachers who taught me at various stages of my academic career. I have reached to this level because of their teaching, advice, guidance and support.

Thanks to all my lab-mates **Dr. K.S. Sujith, Dr. Surinder Pal Kaur, Vinit, Mohan Tiwari, Peeyush Gangwar, Angat Dhiman, Paras, V. Shilpi, Bhawna Singh Tomar, Km Suman Lata, Rajdeep, Rajat, Sakshi Ganotra, Manisha Singh, Mohit Rohilla, Laukesh Sharma, Vishal Chhikara, Shivam Rawat and Kapil**. I expand my thanks to **Dr. P. Smitha** for her constant moral and emotional support.

I would also like to thank staff members at IIT Roorkee, Department of Chemistry for their help and support. I am also thankful to Dr. Navneet Gupta, Computer Centre, IIT Roorkee, for providing the computation facility.

I am thankful to Indian Institute of Technology Roorkee (**IITR**) for providing infrastructure and fellowship for my research work.

Last but not least, I would like pay high regards to my parents and special gratitude to my brother and sister for their sincere encouragement and inspiration throughout my research work. I owe everything to God. Besides this, several people have knowingly and unknowingly helped me in the accomplishment of this research work.

Ankita Joshi
IIT Roorkee
August, 2019



Table of Contents

Candidate's Declaration

Abstract	i
Acknowledgement	v
Table of Contents	vii
List of Tables	xi
List of Figures	xv
List of Publications	xix
List of Conferences Attended/Presented	xxi
CHAPTER 1 Introduction	
1.1 Structure and Properties of Carbon Nanotubes	1
1.1.1 Experimental Studies	1
1.1.2 Theoretical Studies	2
1.2 Functionalization of Carbon Nanotubes	3
1.2.1 Covalent Functionalization	4
1.2.2 Non-Covalent Functionalization	4
1.2.2.1 Weakly Interacting Complexes of Carbon Nanotubes	6
1.3 Donor-Acceptor Complexes of Carbon Nanotubes	8
1.4 Charge Transport Properties of Functionalized Carbon Nanotubes	10
1.5 Optoelectronic Properties of Functionalized Carbon Nanotubes	11
1.6 Mechanically Interlocked Nanotubes (MINTs)	12
1.7 Objectives of the Thesis	13
1.8 Outline of the Thesis	14

CHAPTER 2 Theoretical Background

2.1 Electronic Structure Methods	17
2.2 <i>Ab-initio</i> Methods	18
2.2.1 Hartree-Fock Method	18
2.2.2 Post-Hartree-Fock Methods	20
2.3 Density Functional Theory (DFT)	20
2.3.1 Thomas-Fermi Model	21
2.3.2 Hohenberg-Kohn (H-K) Theorems	21
2.3.2.1 First H-K Theorem	21
2.3.2.2 Second H-K Theorem	22
2.3.3 Kohn-Sham Theory	22
2.3.4 Local Density Approximation (LDA)	23
2.3.5 Generalized Gradient Approximation (GGA)	24
2.3.5.1 Meta-GGA Functionals	25
2.3.6 Hybrid Functionals	25
2.3.7 Improvement in Density Functionals	26
2.3.7.1 Long-Range Corrected Functionals	26
2.3.7.2 Dispersion-Corrected Functionals	26
2.3.8 Time-Dependent Density Functional Theory (TD-DFT)	27
2.3.9 Applications of DFT and TD-DFT	27
2.4 Basis Set	27
2.4.1 Split-Valence Basis Set	28
2.4.1.1 Polarization Basis Function	29
2.4.1.2 Diffuse Basis Function	29

2.5 Basis Set Superposition Error (BSSE)	29
2.6 Photoinduced Charge Transfer	30
CHAPTER 3 Structure, Stability and Properties of the Complexes of Carbon Nanotubes with Indigo	
3.1 Introduction	33
3.2 Computational Methods	36
3.3 Results and Discussion	37
3.3.1 Exohedral complexes of CNT with indigo	37
3.3.2 Endohedral complexes of CNTs with indigo	51
3.4 Conclusion	73
CHAPTER 4 Structure, Stability and Properties of the Complexes of Carbon Nanotube with Perylene Bisimide	
4.1 Introduction	75
4.2 Computational Methods	76
4.3 Results and Discussion	77
4.3.1 Optimized structures and stability	77
4.3.2 Electronic Properties	78
4.3.3 Charge Transport properties	80
4.3.4 Optical absorption properties	80
4.3.5 Effect of nanotube length on stability and properties of PBI-CNT complexes	82
4.3.6 Effect of nanotube diameter on the stability of PBI-CNT complexes	97
4.4 Conclusion	98
CHAPTER 5 Structure, Stability and Properties of the Complexes of Carbon Nanotube with Quaterthiophene	
5.1 Introduction	99
5.2 Computational Methods	100

5.3 Results and Discussion	101
5.3.1 Geometries and stabilization energies of the complexes of CNT with 4T	101
5.3.2 Electronic properties	102
5.3.3 Charge transport properties	108
5.3.4 Optical absorption properties	110
5.4 Conclusion	119
CHAPTER 6 Structure, Stability and Properties of the Complexes of Carbon Nanotube with Cycloparaphenylene and its Derivatives	
6.1 Introduction	121
6.2 Computational Methods	122
6.3 Results and discussion	124
6.3.1 Mechanically Interlocked Complex of CPP with CNT	124
6.3.2 Amino- and fluorine-substituted derivatives of CPP	126
6.3.3 Complexes of amino- and fluorine-substituted CPP derivatives with CNT	134
6.3.4 N-doped derivatives of CPP	138
6.3.5 Potential energy profiles for translational and rotational motions of CPP over CNT	140
6.4 Conclusion	149
CHAPTER 7 Summary and Conclusions	151
A Appendix	155
Bibliography	159

List of Tables

Table No.	Title	Page No.
3.1	The stabilization energy of dyad and triad obtained for different functional at 6-31G(d,p)level	40
3.2	The vertical ionization energy (VIE), adiabatic ionization energy (AIE), vertical electron affinity (VEA), adiabatic electron affinity (AEA) and the HOMO-LUMO energy gap for indigo, CNT and their complexes obtained at the B97-D/6-31G(d,p) level. All the energy values are in eV	41
3.3	The calculated parameters of transfer integral (t), internal reorganization energy (λ), rate constant (k), diffusion coefficient (D), and carrier mobility (μ) for the complexes at different distances	43
3.4	The calculated values of absorption wavelengths, corresponding oscillator strengths, prominent molecular orbitals involved in transition and the respective percentage contribution for indigo, CNT and their complexes. The isodensity plot of molecular orbitals is also shown	46
3.5	Calculated stabilization energy of the complexes with and without basis set superposition error (BSSE) and zero-point energy (ZPE) corrections at B97-D/6-31G(d, p) level. All the energy values are in kcal/mol	54
3.6	Percentage contribution of various interaction energy components (dispersion, electrostatic and induction) for the exo- and endohedral complexes of indigo with CNTs	56
3.7	Calculated values of ionization energy (IE), electron affinity (EA), energy of HOMO and LUMO orbitals (E_{HOMO} , E_{LUMO}) and their energy gap ($\Delta E_{\text{HOMO-LUMO}}$) for various systems obtained at B97-D/6-31G(d, p). All the energy values are in eV	56
3.8	Calculated values of hole and electron reorganization energy (λ_+ and λ_-) for free indigo, CNTs and their complexes at B97-D/6-31G(d,p) level	58
3.9	Calculated values of the transfer integral (t), internal reorganization energy (λ), rate constant (k) and carrier mobility (μ) for the complexes at different distances (d) obtained at B97-D/6-31G(d,p)	59
3.10	The absorption wavelength (λ), oscillator strength (f), corresponding electronic transitions, percentage contribution and molecular orbitals involved for the complex indigo@(7,7)CNT obtained at B97-D/6-31G(d,p)	62

3.11	Computed values of ionization energy (IE), electron affinity (EA), energy of HOMO and LUMO orbitals (E_{HOMO} , E_{LUMO}) and their energy gap ($\Delta E_{\text{HOMO-LUMO}}$) for indigo, (7,7)CNT and their complex obtained at B3LYP-GD3/6-31G(d,p) level. All the energy values are in eV	64
3.12	Calculated values of the transfer integral (t), internal reorganization energy (λ), rate constant (k) and carrier mobility (μ) for the most stable complex indigo@(7,7)CNT at different distances (d) obtained at B3LYP-GD3/6-31G(d,p) level	64
3.13	The absorption wavelength (λ), oscillator strength (f), corresponding electronic transitions, percentage contribution and molecular orbitals involved for the complex indigo@(7,7)CNT obtained at B3LYP-GD3/6-31G(d,p) level	65
3.14	Computed values of ionization energy (IE), electron affinity (EA), energy of HOMO and LUMO orbitals (E_{HOMO} , E_{LUMO}) and their energy gap ($\Delta E_{\text{HOMO-LUMO}}$) for indigo, (7,7)CNT and their complex obtained at ω B97X-D/6-31G(d,p) level. All the energy values are in eV	68
3.15	Calculated values of the transfer integral (t), internal reorganization energy (λ), rate constant (k) and carrier mobility (μ) for the most stable complex indigo@(7,7)CNT at different distances (d) obtained at ω B97X-D/6-31G(d,p) level	68
3.16	The absorption wavelength (λ), oscillator strength (f), percentage orbital contribution and molecular orbitals involved in the transition for the complex indigo@(7,7)CNT obtained at ω B97X-D/6-31G(d,p) level	70
4.1	The stabilization energies (ΔE_{stab}) of the complex PBI-CNT with and without BSSE corrections using various dispersion-corrected density functionals and 6-31G(d,p) basis set. All the energy values are in kcal/mol	81
4.2	Percentage contribution from various components of interaction energy for the complex PBI-CNT using zeroth-order symmetry adapted perturbation theory (SAPT0) and 6-31G basis set	81
4.3	The vertical ionization energy (VIE), adiabatic ionization energy (AIE), vertical electron affinity (VEA), adiabatic electron affinity (AEA) and the energy gap between HOMO and LUMO ($\Delta E_{\text{HOMO-LUMO}}$) of PBI, (6,6)CNT and their complex obtained for different functionals using 6-31G(d,p) basis set. All the energy values are in eV	83
4.4	Calculated values of transfer integral (t), internal reorganization energy (λ), rate constant (k) and carrier mobility (μ) of the complex	86

	PBI-(6,6)CNT obtained for different functionals using 6-31G(d,p) basis set	
4.5	The maximum absorption wavelength (λ_{\max}), oscillator strength (f), light-harvesting efficiency (LHE), molecular orbitals involved in the transitions and the orbital contribution of the complex PBI-(6,6)CNT for different functionals using 6-31G(d,p) basis set. Only those transitions of minimum orbital contribution 15% are considered	88
4.6	The absorption wavelength (λ), oscillator strength (f), light-harvesting efficiency (LHE), molecular orbitals involved in the transition and the orbital contribution of the complex PBI-(6,6)CNT at B3LYP-GD3/6-31G(d,p) level. Only those transitions of oscillator strength more than 0.05 and of minimum orbital contribution 15% are considered	89
4.7	The electronic properties such as vertical ionization energy (VIE), adiabatic ionization energy (AIE), vertical electron affinity (VEA), adiabatic electron affinity (AEA) and the energy gap between HOMO and LUMO ($\Delta E_{\text{HOMO-LUMO}}$) of long CNT and its complex with PBI obtained at B97-D/6-31G(d,p) level. All the energy values are in eV	94
4.8	The calculated values of transfer integral (t), internal reorganization energy (λ), rate constant (k) and carrier mobility (μ) of the complex PBI with long (6,6)CNT at B97-D/6-31G(d,p) level	94
4.9	The stabilization energies (ΔE_{stab}) of the complexes formed between PBI and (8,8)CNT calculated with and without BSSE corrections using various dispersion-corrected density functionals and 6-31G(d,p) basis set. All the energy values are in kcal/mol	96
4.10	Percentage contribution from various components of interaction energy for the complexes of PBI with (8,8)CNT obtained using zeroth-order symmetry adapted perturbation theory (SAPT0) and 6-31G basis set	96
5.1	Stabilization energies (ΔE_{stab}) of endo-and exohedral complexes formed between CNT and 4T obtained for different functionals using 6-31G(d,p) basis set. All the energy values are in kcal/mol	104
5.2	Percentage contribution of various components of interaction energy for the complexes of CNT with 4T calculated using zeroth-order symmetry adapted perturbation theory (SAPT0) and 6-31G basis set	105
5.3	Calculated values of ionization energy (IE), electron affinity (EA), energy gap between HOMO and LUMO ($\Delta E_{\text{HOMO-LUMO}}$) for 4T, CNT and their complexes obtained for different functionals using 6-31G(d,p) basis set. All the energy values are in eV	107

5.4	Calculated values of transfer integral (t), internal reorganization energy (λ), rate constant (k) and carrier mobility (μ) for the complexes at different distances between centre of 4T and that of nearby surface of CNT (d_{c-c}) obtained for different functionals using 6-31G(d,p) basis set	109
5.5	Calculated values of maximum absorption wavelength (λ_{max}), oscillator strength (f) and light-harvesting efficiency (LHE) of 4T obtained for different functionals using 6-31G(d,p) basis set	112
5.6	The maximum absorption wavelength (λ_{max}), light-harvesting efficiency (LHE) and the molecular orbitals involved in the electronic transitions of the complexes 4T@CNT and 4T-CNT obtained for different functionals using 6-31G(d,p) basis set	113
5.7	The absorption wavelength, oscillator strength, orbital contribution and molecular orbitals involved in the transition of the complex 4T@CNT obtained for different functionals using 6-31G(d,p) basis set	115
5.8	The absorption wavelength, oscillator strength, orbital contribution and molecular orbitals involved in the transition of the complex 4T-CNT obtained for different functionals using 6-31G(d,p) basis set	117
6.1	The values of stabilization energy (ΔE_{stab}) for the complexes of CPP, its substituted and doped derivatives with CNT. All the energy values are in kcal/mol	127
6.2	Percentage contribution of various components of energy for the interactions of CPP, its fluorine-substituted derivatives with CNT	128
6.3	Computed values of ionization energy (IE), electron affinity (EA), energy of HOMO (E_{HOMO}), energy of LUMO (E_{LUMO}) and energy gap between HOMO-LUMO ($\Delta E_{HOMO-LUMO}$) of [10]CPP, its substituted and doped derivatives, CNT and the corresponding complexes of CPP with CNT. All the energy values are in eV	130
6.4	The values of maximum absorption wavelength (λ_{max}), light-harvesting efficiency (LHE) for [10]CPP, its substituted-/doped-derivatives, CNT and their corresponding complexes	132
6.5	Frontier molecular orbitals of the fluorine-substituted derivatives with CNT	137
6.6	The molecular orbital involved in the electronic transition corresponding to the maximum absorption wavelength (λ_{max}) of the complexes of the fluorine-substituted derivatives with CNT	141

List of Figures

Figure No.	Title	Page No.
2.1	The ground state charge transfer in electron donor-acceptor (EDA) complexes	31
2.2	The excited state charge transfer in electron donor-acceptor (EDA) complexes	31
3.1	The optimized geometries of (a) indigo, (b) (6,6)CNT, (c) indigo-(6,6)CNT dyad and (d) indigo-(6,6)CNT triad	39
3.2	Electrostatic potential maps for the indigo-CNT complexes	39
3.3	The frontier molecular orbitals and the corresponding energy level diagram of indigo, CNT and their complexes	41
3.4	Optimized geometry of the complex in which indigo is aligned parallel to the tube-axis	45
3.5	The absorption spectra of indigo, CNT and their complexes	45
3.6	Optimized geometries of (a) (7,7)CNT, (b) (8,8)CNT and (c-e) the respective complexes indigo@(n,n)CNT, where $n = 6-8$ obtained at B97-D/6-31G(d,p) level	53
3.7	Optimized geometry of the exohedral complex of indigo with (7,7)CNT obtained at B97-D/6-31G(d,p) level of theory	54
3.8	The frontier molecular orbitals of the complexes (a) indigo@(6,6)CNT (b) indigo@(7,7)CNT and (c) indigo@(8,8)CNT obtained at B97-D/6-31G(d,p) level	55
3.9	The optical absorption spectra of indigo, (7,7)CNT and their complex indigo@(7,7)CNT obtained at B97-D/6-31G(d,p) level	61
3.10	Optimized geometry of the complex indigo@(7,7)CNT obtained at B3LYP-GD3/6-31G(d,p) level of theory	64
3.11	The optical absorption spectra of indigo, (7,7)CNT and the complex indigo@(7,7)CNT obtained at B3LYP-GD3/6-31G(d,p) level	67
3.12	Optimized geometry of the complex indigo@(7,7)CNT obtained at ω B97X-D/6-31G(d,p) level	68
3.13	The optical absorption spectra of indigo, (7,7)CNT and the complex indigo@(7,7)CNT obtained at ω B97X-D/6-31G(d,p) level	69

4.1	Optimized geometries of the complex PBI-(6,6)CNT (left: side view, middle: front view and right: top view) obtained at (a) B3LYP-GD3, (b) B97-D and (c) ω B97X-D levels	79
4.2	Frontier molecular orbitals of the complex PBI-(6,6)CNT obtained at (a) B3LYP-GD3/6-31G(d,p), (b) B97-D/6-31G(d,p) and (c) ω B97X-D/6-31G(d,p) levels	84
4.3	Schematic representation of the mechanism of photoinduced electron transfer (PET) for the complex PBI-CNT at B3LYP-GD3/6-31G(d,p) level.	85
4.4	Optical absorption spectra of the PBI, (6,6)CNT and their complex obtained using the functionals (a) B3LYP-GD3 (b) B97-D and (c) ω B97X-D along with 6-31G(d,p) basis set	87
4.5	Optimized geometries (a) side view and (b) front view of the complex PBI with relatively long (6,6)CNT obtained at B97-D/6-31G(d,p) level	91
4.6	Frontier molecular orbitals of the complex PBI with long (6,6)CNT obtained at B97-D/6-31G(d,p) level	92
4.7	Optical absorption spectra of long (6,6)CNT and its complex with PBI obtained at B97-D/6-31G(d,p) level	93
4.8	Optimized geometries of the complexes (a-c) PBI-(8,8)CNT and (d-f) PBI@(8,8)CNT each set obtained using B3LYP-GD3, B97-D and ω B97X-D functionals, respectively	95
5.1	Optimized geometries of (a) 4T (b) 4T@CNT and (c) 4T-CNT obtained for different functionals using 6-31G(d,p) basis set	103
5.2	Schematic representation of the stepwise photoinduced electron transfer (PET) between 4T and CNT	106
5.3	Simulated absorption spectra of (a) 4T (b) 4T@CNT and (c) 4T-CNT obtained for different functionals using 6-31G(d,p) basis set	111
6.1	Schematic diagram of [10]CPP, its derivatives and their complexes with CNT	123
6.2	Optimized geometries of (a) [10]CPP, (b) CNT, and (c) the complex CNT@[10]CPP	125
6.3	Frontier molecular orbital of the complex CNT@[10]CPP	129
6.4	The molecular orbital involved in the transition corresponding to the maximum absorption wavelength (λ_{\max}) of the complex CNT@[10]CPP	129

6.5	Absorption spectra of [10]CPP, CNT and the complex CNT@[10]CPP	131
6.6	Optimized geometries of fluorine-substituted CPPs (side view and front view) and their complexes with CNT	133
6.7	Optimized geometries of the amino-substituted derivatives of CPP (side view and front view) and their corresponding complexes with CNT	135
6.8	The absorption spectra of various fluorine-substituted derivatives of CPP and their complexes with CNT obtained at B3LYP-GD3/6-31G(d,p) level	139
6.9	The absorption spectra of (a) [10]CPP, (b) 40F-[10]CPP and (c) CNT@40F-[10]CPP obtained at ω B97XD/6-31G(d,p) level	143
6.10	Optimized geometries of the nitrogen-doped derivatives of CPP (side view and front view) and their corresponding complexes	144
6.11	Potential energy profile for the translational movement of CPP over the surface of CNT. For clarity, only the front portion of CPP is shown	145
6.12	Potential energy profile for the rotation of CPP over the surface of CNT keeping their geometric centres coincide. For clarity, only the front portion of CPP is shown	146
6.13	Potential energy profile for the translational movement of 40F-[10]CPP over the surface of CNT. For clarity, only the front portion of 40F-[10]CPP is shown	147
6.14	Potential energy profile for the rotation of 40F-[10]CPP over the surface of CNT keeping their geometric centres coincide. For clarity, only the front portion of 40F-[10]CPP is shown	148



List of Publications from the Thesis

1. **Ankita Joshi**, C. N. Ramachandran. Charge transport and optical properties of the complexes of indigo wrapped over carbon nanotubes. *Phys. Chem. Chem. Phys.*, **2016**, 18, 14040-14045.
2. **Ankita Joshi**, C. N. Ramachandran. Structural, optoelectronic and charge transport properties of the complexes of indigo encapsulated in carbon nanotubes. *Phys. Chem. Chem. Phys.*, **2018**, 20, 15158-15167.
3. **Ankita Joshi**, C. N. Ramachandran. Optoelectronic Properties of Cycloparaphenylene–Carbon Nanotube Based Molecular Architectures. *J. Phys. Chem. C*, **2018**, 122, 19904-19912.
4. **Ankita Joshi**, C. N. Ramachandran. Optoelectronic and Charge Transport Properties of the Complex of Carbon Nanotube with Perylene Bisimide. *Int. J. Quantum Chem.*, **2019**, 119, e26026.
5. **Ankita Joshi**, C. N. Ramachandran. Switching the charge transfer characteristics of quaterthiophene from p-type to n-type via interactions with carbon nanotubes. *Phys. Chem. Chem. Phys.*, **2019**, 21, 24820-24827.

Other Publications

6. Manisha Prakashni, **Ankita Joshi**, C.N. Ramachandran. Electronic and optical absorption properties of the derivatives of 1,3,4-Oxadiazole. *Chem. Data Collect.*, **2016**, 5-6, 99-95.
7. **Ankita Joshi**, C.N. Ramachandran. A comprehensive study of the optoelectronic properties of donor-acceptor based derivatives of 1,3,4-oxadiazole. *Chem. Phys. Lett.*, **2017**, 679, 102-111.

8. Rakesh Kumar, Harshita Jain, Parveen Gahlyan, **Ankita Joshi**, C. N. Ramachandran. A highly sensitive pyridine-dicarbohydrazide based chemosensor for colorimetric recognition of Cu^{2+} , AMP^{2-} , F^- and AcO^- ions. *New J. Chem.*, **2018**, 42, 8567-8576.
9. **Ankita Joshi**, C. N. Ramachandran, High-bias Negative Differential Resistance Effect in Pure, Doped and Co-Doped Carbon Nanotubes Connected to Boron Nitride Nanotubes. *Physica E Low Dimens. Syst. Nanostruct.*, **2019**, 113, 1-7.
10. Harshita Jain, **Ankita Joshi**, C. N. Ramachandran and Rakesh Kumar, Synthesis of highly efficient multifunctional Cu (II)-pyridyl complex for adsorption and photocatalytic degradation of organic dyes. *ChemistrySelect*, **2019**, 4, 4952-4961.
11. Parveen Gahlyan, Rashim Bawa, Harshita Jain, Manu Dalela, **Ankita Joshi**, C. N. Ramachandran, Ashok K. Prasad, Arunjit Kaur and Rakesh Kumar, Isatin-triazole tethered rhodamine based dual sensor for recognition of Cu^{2+} and Fe^{3+} ions and its application in live cell imaging. *ChemistrySelect*, **2019**, 4, 7532-7540.
12. Harshita Jain, Nidhi Deswal, **Ankita Joshi**, C. N. Ramachandran and Rakesh Kumar, Triazole-appended pyrano[2,3-c]pyrazolone based colorimetric chemosensors for recognition of Fe^{3+} ions and their molecular logic gate behavior. *Anal. Methods*, **2019**, 11, 3230-3243.

List of Conferences Attended/Presented

1. **Ankita Joshi** and C. N. Ramachandran, Asian Academic Seminar and School organized by IISER Kolkata, IACS Kolkata and NINS, Okazaki, Japan and IMS, Okazaki, Japan at IISER and IACS, Kolkata, March 6-10, **2015**.
2. **Ankita Joshi** and C. N. Ramachandran, International Conference on Advanced Materials for Energy, Environment and Health (ICAM-2016) organized by Indian Institute of Technology Roorkee (IITR), March 4-7, **2016**.
3. **Ankita Joshi** and C. N. Ramachandran, 18th CRSI National Symposium in Chemistry organized by Panjab University and Institute of Nano Science and Technology at Panjab University, Chandigarh, February 5-7, **2016**.
4. **Ankita Joshi** and C. N. Ramachandran, 15th Theoretical Chemistry Symposium organized by University of Hyderabad and Indian Institute of Chemical Technology, Hyderabad at University of Hyderabad, December 14-17, **2016**.
5. **Ankita Joshi** and C. N. Ramachandran, ACS on Campus organized by Indian Institute of Technology Roorkee on February 7, **2018**.
6. **Ankita Joshi** and C. N. Ramachandran, 16th Theoretical Chemistry Symposium organized by BITS Pilani at Pilani Campus, February 13-16, **2019**. (*Best Poster Presentation Award*)
7. **Ankita Joshi** and C. N. Ramachandran, 3rd North-West Meeting on Spectroscopy, Structure and Dynamics (SSD-2019) by Department of Chemistry, IIT Roorkee, April 5-7, **2019**.



CHAPTER 1

Introduction

1.1 Structure and Properties of Carbon Nanotubes

Carbon nanotubes, especially single-walled nanotubes (SWNTs), have engrossed great attention owing to their distinctive structural, electronic, optical and transport properties.[1, 2] Like fullerenes and graphenes, carbon nanotube (CNT) is the allotrope of carbon discovered by Iijima in 1991.[3] The hybridization of each carbon atoms of CNT lies between sp^2 and sp^3 leading to non-planarity to the structure. CNTs have hollow cylindrical structure in which electrons move on the surface along the tube-axis and hence they are considered as one-dimensional conductors.[4] Due to the long tubular structure, CNT exhibits high aspect ratio (length/diameter). Similarly, the surface-to-volume ratio is also notably high.

Broadly, CNTs are divided into two categories *viz.*, single-walled nanotubes (SWNTs) and multi-walled nanotubes (MWNTs). SWNT is formed by rolling one of the graphene sheets by specific chiral angle. Based on the magnitude of chiral angle and chiral indices (n and m , where n is any natural number and m is any whole number), nanotubes are classified as armchair, zigzag and chiral. For armchair nanotubes, both chiral indices are same and are denoted as (n,n) CNTs. The zigzag and the chiral ones are designated as $(n,0)$ and (n,m) CNTs, respectively. The diameter (d) of any (n,m) CNT can be determined using the formula: $d = 0.783 \sqrt{n^2 + m^2 + nm} \text{ \AA}$. [5]

1.1.1 Experimental Studies

The synthesis of CNT of a particular chirality is a challenge for experimentalists although some progresses have been made in this direction over the past few years.[6, 7] Liu *et al.* reviewed different approaches employed for the chirality-selective synthesis of CNTs.[8] One such approach is the seeded growth method, wherein the short CNTs used as a seed to grow long CNTs of specific chirality.[9-12] Another approach is based on the utilization of metal-nanoparticles as catalysts for the disproportion reaction of carbon monoxide resulting in the formation of chirality-selective synthesis of CNT.[13-16] In other studies, carbonaceous compounds like one end capped CNT, carbon nanoring, diamond and C_{60} have been used as precursors for initiating the growth of CNT.[17-21]

In 2004, the thinnest CNT with a diameter of 3 Å referred to as (2,2)CNT was synthesized by Zhao and group.[22] CNTs of diameter as large as 30 Å have also been studied.[23] Similarly, CNTs of length in centimetres have been grown.[24] It is well known that CNTs of finite length

is difficult to synthesize. Two approaches *viz.*, bottom-up and top-down are normally used to obtain finite-length CNTs. Jasti and group synthesized the shortest possible segments of armchair CNT known as [9]-, [10]- and [18]cycloparaphenylene (CPP) with different diameters.[25] An attempt towards the synthesis of CNT from [9]- and [10]CPP was put forth by Itami and group.[21] Similarly, the synthesis of armchair (5,5)CNT, utilizing [5]CPP was reported by Jasti and Bertozzi.[26] The bottom-up synthesis of three different zigzag CNTs ($C_{120}H_{136}$) has been achieved from the racemic mixture of (16,0)-[4]cyclo-3,9-chrysenylene in methanol or methylene chloride.[27] The bottom-up synthesis of CNT through macrocyclization of [4]phenacene is also reported.[28] Wang and colleagues reviewed the recent advancements in the synthesis of CNTs of finite-length using bottom-up approach.[29] The top-down approach for the synthesis of CNT by employing various physical and chemical methods to shorten the length below 1 μm has been studied extensively during the last decade.[30-36] Warner *et. al.* performed a comparative study of the stability of CNTs with varying diameter under electron beam irradiation.[37] Their study indicated defects in CNTs of diameter less than 10 \AA . In 2013, Naumov and co-workers investigated the optical properties of long SWNTs as a function of their length and could not find any relationship between the two.[38] A study conducted by Kataura *et. al.* on the optical properties of CNT showed that the absorption peaks shift to shorter wavelength with a decrease in the diameter of tube.[39] They also demonstrated that the optical absorption of CNT occurs in the near-ultraviolet (350 nm) to near-infrared (2500 nm) region of electromagnetic spectrum. Due to the absorption of CNTs in the near-infrared region, they were found to be useful in photothermal therapy for the treatment of cancer.[40] The unique properties of CNTs enable their application in optoelectronic devices such as organic solar cells [41], field-effect transistors [42] and light-emitting diodes.[43]

1.1.2 Theoretical Studies

Theoretical studies of finite-length CNT have been performed even before their first time synthesis.[44] Matsuo *et. al.* also investigated the structural properties of finite-length armchair CNTs.[45] They divided (n,n) CNTs ($n = 5$ and 6) into three types of structures *viz.*, Kekulé, incomplete and complete Clar, based on the alteration in the length of carbon-carbon bond. Several theoretical studies on the passivation of terminals of CNTs by hydrogens have been reported.[46-48]

The studies of CNTs are interesting as their energetics and properties can be modulated by varying length as well as diameter. The properties of infinite length CNTs differ significantly from their finite length counterparts. The armchair nanotubes of infinite-length are metallic in

nature, whereas the finite-length nanotubes are semiconducting.[44] This is due to the Peierls instability leading to alteration in the carbon-carbon bond lengths.[49] Odom *et al.* examined the quantum size effects on the electronic properties of three short CNTs of length 3, 5 and 6 nm.[50] Recently, Hedman and Larsson carried out a study on the dependence of length on the stability of armchair and zigzag CNTs.[51] Petrushenko and Ivanov examined the correlation between structure and electronic properties of finite CNTs.[52] Their results inferred that vertical and adiabatic ionization energies are different for finite CNTs while they are same for infinite CNTs. They also reported a significant change in carbon-carbon bond length upon ionization of CNT. Okada studied the energy gap between highest occupied molecular orbital (HOMO) and lowest unoccupied molecular orbital (LUMO) of armchair CNTs of length upto 100 Å.[53] The finite-length CNTs showed non-zero energy gap that decreases on increasing the length of the tube. Gao *et al.* examined the dependence of energy gap on the length of semiconducting chiral CNTs (less than 100 Å) employing density functional theoretical method.[54] A similar study on the variation in energy gap between HOMO-LUMO of semiconducting zigzag CNT as a function of its length (ranging from 4 to 44 Å) was also conducted by Ahmadpour and co-workers.[48] Ghosh *et al.* reported that CNTs of larger diameter are less reactive due to less curvature compared to those of smaller diameter.[55] Galano investigated the structural and electronic properties of (n,n) CNTs ($n = 3-6$) of diameter about 4-8 Å and length about 6-30 Å.[56] They found that the variation in length or diameter of CNT leads to changes in various properties such as binding energy, electronegativity, chemical potential, chemical hardness, ionization energy, electron affinity, energy gap between frontier orbitals and optical transitions. The same study also found that CNT of minimum length and diameter as the most reactive. Recently, the optical properties of long CNT (10-20 Å) have been explored using time-dependent density functional theory.[57] The study reported a red shift in absorption maximum for CNT of length 20 Å compared to that of length 10 Å.

1.2 Functionalization of Carbon Nanotubes

Despite outstanding properties of CNTs, they suffer from a major drawback in the fabrication of devices. This is mainly due to the van der Waals (vdW) interactions between carbon nanotubes leading to the formation of bundles thereby hindering their use for practical purposes. The above problem can be circumvented by the functionalization of CNTs which can be achieved in two ways *viz.*, covalent and non-covalent functionalization.

1.2.1 Covalent Functionalization

In the covalent functionalization of CNT, the hybridization of carbon atoms linked to guest species changes, resulting in the modifications of its electronic properties.[58] The properties of CNT are strongly influenced by other molecules either by adsorbing over the nanotube or by encapsulating inside CNT. The unique structure of CNT allows the species to interact both from inside and outside the cavity. In this regard, CNTs can be functionalized in two ways *viz.*, endo- and exohedral. Endohedral functionalization is done by encapsulating molecule within the hollow space of CNT. Exohedral functionalization is also known as surface functionalization. However, the covalent functionalization is usually preferred on the surface of CNT. In 2004, Kar and co-workers carried out an investigation on the covalent functionalization of CNT with O₃ and 2-phenyl-1 H-imidazole.[59] Later, in 2004, Zhao *et al.* found a drastic change in the electronic states of CNT near the fermi level by covalently attaching -NH₂, -CH₃, -OH or -COOH groups.[60] However, a new method of covalent functionalization via [2+1] cycloaddition was presented in which the π -conjugation of CNT remains unchanged.[61] Prato and group reviewed various covalent complexes of CNT with organic species *viz.*, carboxylic acid, fluorine, carbene, nitrene, alkyl and aryl groups.[62] The covalent functionalization of CNT with amine-terminated organic monolayer on gold and silicon surfaces has been explored using experimental as well as theoretical methods.[63] The density functional theoretical investigation on the covalent interaction of non-functionalized, OH- and COOH-functionalized CNTs with ethylene glycol (EG) by Subramanian *et al.* demonstrated that EG exhibits stronger interaction with functionalized CNTs.[64] Ghosh and co-workers demonstrated that covalently functionalized CNTs with Na atoms can be used as hydrogen storage materials.[65]

1.2.2 Non-Covalent Functionalization

The bundling of CNTs leads to solubility issues and hinders their use for various applications. The non-covalent functionalization of CNTs helps in circumventing the above problem by dispersing them in solvents while preserving the properties of pristine CNT.[66] Several research groups have reviewed the non-covalent functionalization of CNTs.[67-73] The non-covalent functionalization of CNT can be done either endohedrally or exohedrally. The exohedral functionalization is generally performed by non-covalently attaching molecule over the surface of CNT. The adsorption affinity of 30 aromatic compounds on the surface of CNT has been examined theoretically.[74] The non-covalent complex CNT-porphyrin was synthesized by Murakami and co-workers.[75] In a study by Anderson and group, the relationship between the binding energy of the complexes of CNTs with porphyrin oligomers has been investigated.[76]

Their results indicated that larger the porphyrin units, greater the binding affinity for CNTs. Using various functionals with and without dispersion correction, Chermahini *et al.* studied the adsorption of lactic acid on the surface of CNTs of different chirality.[77] Ghosh *et al.* investigated the structural properties of the endohedral complexes of (n,n) CNT, $n = 4-8$ with Zundel cation.[78] They found that among the complexes studied, the complex of $(6,6)$ CNT as the most stable due to its least deformation energy.

Endohedral functionalization is a special case of non-covalent functionalization. In 2003, Takenobu *et al.* reported the inclusion complexes of CNT with various organic molecules such as anthracene, tetrathiafulvalene (TTF), tetracyanoquinodimethane (TCNQ), C_{60} , to name a few.[79] The literature is abundant with a number of studies performed on the encapsulation of fullerenes, heterofullerenes and metallofullerenes into the hollow space of CNT and such type of systems are commonly known as peapods.[80-87] Munusamy and Wheeler explored the exohedral as well as endohedral complexes of CNT with substituted benzenes and found that the endohedral complexes are more stable than their exohedral counterparts.[88] In a combined theoretical and experimental study performed by Stobinski and co-workers on the complexes of CNT with carotenoids such as β -carotene and lycopene, it has been found that the endohedral complex in which carotenoids act as acceptors are more stable than the corresponding exohedral complex.[89] Very recently, the structural and electronic properties of endo- as well as exohedral complexes of CNTs with different nucleic acids have been reported using DFT method by Kumar and his group.[90] Their results also revealed that the endohedral complexes are energetically more stable than their exohedral counterparts.

The non-covalent complexes of CNT with inorganic molecules have also been studied although not extensively as those of organic molecules. For instance, Chang and Lee conducted density functional theoretical investigation on the adsorption of NH_3 and NO_2 over CNT surface.[91] A similar study has been performed by Dai *et al.* on the adsorption of NO_x (where, $x = 1, 2$ and 3) molecules on CNT.[92] The encapsulation of uranyl complexes inside CNT was studied for the storage of nuclear waste.[93] Mejri and co-workers conducted molecular dynamics studies on the encapsulation and subsequent release of cisplatin from the cavity of CNT.[94] The encapsulation of atoms such as Li and Na within CNTs of varying diameter has been investigated and the results revealed that the density of state generally increases as a function of the number of encapsulated species.[95] Another theoretical investigation has been performed by Roztoczyńska and group on the exo-and endohedral complexes of HF dimer with CNT.[96] Their results indicated a stronger interaction of HF dimer when it was confined inside the cavity of CNT. Kumar *et al.* studied the interaction of encapsulated noble gas dimers *viz.*,

He₂, Ne₂, Ar₂ and Kr₂ with the inner wall of CNT and found that dimers aligned parallel to the tube-axis rather than perpendicular forming stable complexes.[97] An investigation of the rare gas dimers (He₂, Ne₂, and Kr₂) encapsulated inside BN-substituted CNT has been conducted by Chakraborty and Chattaraj.[98] In the complexes, a parallel alignment of dimers with respect to the tube-axis was preferred. Subramanian and co-workers have examined the possibility of encapsulation of ice nanotubes inside CNTs and observed that the cavity size of host plays an important role in the stabilization of the complexes.[99]

1.2.2.1 Weakly Interacting Complexes of Carbon Nanotubes

Non-covalent interactions, particularly the π - π interactions is the major reason for the attraction between the stacked π -systems. These interactions provide stability to the complexes which are formed from π -conjugated molecules. In the last decade, several efforts have been made both experimentally and theoretically to explore the complexes of CNT which are stabilized by π - π and X-H... π (X = C, N, O etc.) interactions. Using density functional theoretical methods, the adsorption of benzene derivatives which are formed by attaching electron-donating groups (methyl and amino) and -accepting group (nitro) on CNT has been studied by Woods and co-workers.[100] They showed that the physisorption of above derivatives occurs through π - π interactions. In a study by Chin and Tsai, it was found that the π - π interactions between CNT and benzene can be strengthened by substituting the latter by either -CH₃ or -Cl.[101] Kar *et. al.* carried out an MP2 study on the complexes of CNT with benzene and naphthalene which are stabilized by π - π and C-H... π interactions.[102] The π -stacking interactions of CNT with polycyclic aromatic compounds such as benzene, pyrene and azulene were investigated by Tournus and co-workers.[103] The π -stacking interaction between CNT and benzylmercaptan has been revealed by Sacher and group using X-ray photoelectron spectroscopic studies.[104] In a study by Cohen *et al.*, pyridine was substituted on a polymeric moiety named poly(methyl methacrylate) so as to have favourable π - π interactions with CNT.[105] The π - π interactions in various complexes formed between CNT and planar molecules like π -extended tetrathiafulvalene (exTTF), TCNQ, guanine, thymine and cytosine were reviewed by Pérez and Martin.[106] Another study reported that the complex with parallel orientation of cytosine over CNT is stabilized mainly by π - π interaction, whereas NH... π and CH... π interactions are predominant in its perpendicular counterpart.[107] A dispersion-corrected density functional theoretical study (DFT-D) on the complexes of functionalized CNT with histidine was reported by Wang and group and found that the complexes are stabilized by π - π interactions.[108] Recently, the interactions between CNT as host and various pyrene derivatives as guests have been studied

using both experimental and theoretical means.[109] Based on the molecular dynamic studies, Gorantla and co-workers demonstrated the π - π interactions between C_{60} and bent double-walled carbon nanotube (DWCNT).[110] Using the combined molecular mechanical and quantum mechanical study, the π - π interactions between CNT and amino acid derivatives were explored by Yang and co-workers.[111] Recently, Yumura and Yamamoto performed a dispersion-corrected density functional study (DFT-D) on the endohedral complexes of p'(dimethylamino)-p'-nitrostilbene (DANS) with CNT.[112] They found that the atoms of DANS in the vicinity of tube interact via π - π and C-H... π interactions. Nogueira *et al.* synthesized the π -conjugated compounds containing thiophene, dialkoxyphenylene and imidazole units for the dispersion of CNTs in water.[113] Very recently, the role of π - π interactions in the purification of phenol-contaminated water has been highlighted in a density functional theoretical investigation by Moradi and co-workers.[114] In their study, CNT and its functionalized derivatives were selected due to their favourable π - π interactions with phenol. The π - π interaction between CNT and phthalocyanine has been demonstrated in a study conducted by Zhang and Shao.[115] The π - π interactions between aromatic units of CNT with those of amino acid molecules have been investigated by several research groups.[111, 116, 117]

The interactions of CNT with large π -conjugated structures have also been studied extensively. In 2002, Chen and group reported that the solubility of CNTs can be achieved via π - π interactions with poly(arylenethylene) and its derivatives rather than by wrapping with polymers.[118] The π - π interactions in the encapsulated complexes of carbon nanotube with small as well as large molecules such as acetylene, terthiophene, anthracene, perylene, coronene, C_{60} , graphene nanoribbons and biomaterials such as DNA and lamivudine were reviewed by Dappe.[119] Other examples are polymer as well as DNA wrapped around CNT.[120, 121] Numata and co-workers reported that the complex in which CNT is wrapped by water-soluble polymer β -1,3-glucan is stabilized by π - π and O-H... π interactions.[122] In 2015, different polymer-wrapped CNTs were reviewed and it was demonstrated that polymer and CNT are held together primarily by π - π and C-H... π interactions.[121] Wang and Ai claimed that the complexes in which tripeptides moieties adsorbed on the surface of CNT are stable due to π - π , C-H... π , N-H... π and O-H... π interactions.[123] Poenitzsch *et al.* showed that CNT-peptide complexes are stabilized by π - π stacking interactions between CNT and phenylalanine unit of the peptide.[124]

1.3 Donor-Acceptor Complexes of Carbon Nanotubes

The charge transfer phenomenon involves the transfer of a fraction of charge from one species to another when two such species interact. The resulting complexes are stabilized mainly via electrostatic interactions. The charge transfer interactions also exist between CNT and several organic molecules as elucidated from both theory and experiments. Raman spectroscopy is one such experimental technique that can be used to study the charge transfer interactions between the constituents of the complex. Raman studies have shown that G-band of CNT at 1600 cm^{-1} becomes slightly narrow on forming charge transfer complex with Poly(3,4-ethylenedioxythiophene) (PEDOT).[125] The charge transfer in the encapsulated complexes of CNT with oligothiophene and its derivatives have been reported using infrared and Raman spectroscopic methods.[126, 127]

Earlier studies have also shown that CNTs can act as donor or acceptor depending on the electronic properties of the molecule attached. In a review by Fukuzumi, it is reported that CNT acts as an electron donor with coenzyme Q_{10} , whereas it behaves as an electron acceptor with polypeptide $P(H_2P)_{16}$. [128] The charge transfer from donor polypyrrole (PPy) to acceptor CNT was studied by Tang and group.[129] Very recently, an investigation was carried out by a group of researchers on the exohedral complex formed between donor decamethylcobaltocene and acceptor CNT.[130] Their study revealed that the complex exhibits n-type charge transfer characteristics. The photoinduced electron-transfer in the complex of CNT wrapped with coenzyme Q_{10} was explained on the basis of frontier orbital energy levels of individual units by Ontami and Fukuzumi.[131] They showed that the photoexcitation of electron takes place from the valence band to the conduction band of CNT followed by transfer of the photoexcited electron to the lowest unoccupied molecular orbital of coenzyme Q_{10} . In a study by Weaver *et al.*, the charge transfer phenomena was reported in the composites of perylene derivatives and CNT. They found that CNT acts as an acceptor while the other species behave as donors.[132] In 2016, Strauss *et al.* examined the complexes formed between CNT and n-type semiconductors such as pyridyloxy group substituted Zn-pthalocyanine, perylene bisimide and TCNQ.[133] All the above complexes were found to be stabilized via π - π , hydrophobic and charge-transfer interactions. Rao and co-workers performed an experimental investigation of charge-transfer complexes formed between CNT and several donor-acceptor species such as aniline, TTF, nitrobenzene, TCNQ and TCNE using Raman spectroscopy.[134] Their results revealed that compared to the G-band maximum of CNT (1585 cm^{-1}), a band maximum of its complexes with aniline and TTF is decreased while that of its complexes with nitrobenzene, TCNQ and TCNE is increased. Another experimental study by Wu and co-workers indicated the

possibility of charge transfer from donor tetrathiafulvalene (TTF) to acceptor CNT.[135] The charge transfer effects have also been observed in the complexes of CNT with organometallic compounds.[136]

In 2000, Jhi and co-workers investigated the electronic properties of the complexes of CNT with O₂ by means of density functional theory.[137] Their results from density of states calculations revealed the charge transfer from CNT to O₂. Zhao and Lu performed theoretical studies on the complexes of CNT with benzene, cyclohexane, DDQ and O₂. [138] Based on the Mulliken population analysis, they reported charge transfer within the complexes. CNT behaved as an acceptor in the presence of benzene or cyclohexane while CNT acted as a donor in the presence of DDQ or O₂. Later, Tournus *et. al.* studied the physisorption of aromatic molecules such as benzene, azulene and DDQ on the surface of CNT and noticed the charge transfer interactions between CNT and DDQ.[139] The possibility of charge transfer interactions in the complexes of CNTs with small molecules like naphthalene, anthracene, TCNQ and DDQ were also examined theoretically by Lu and co-workers.[140] Among these complexes, TCNQ-CNT and DDQ-CNT were found to be stabilized by charge transfer interactions. A similar study was performed by Manna and Pati on the charge transfer complexes of metallic and semiconducting CNTs with TTF, TCNQ and TCNE.[141] Their study revealed that the electronic properties of CNT can be changed from metallic to semiconducting and vice-versa on doping different donor or acceptor moieties. The charge transfer interactions of CNT with carbene and its halogen substituted derivatives were explored by Kakkar and group using density functional theoretical methods.[142] Umadevi and Sastry studied the adsorption of gas molecules (H₂, CO₂, H₂O, NH₃, CH₄) on the surface of CNTs.[143] From the Mulliken population analysis, they inferred that the above gas molecules behave as electron donors in their complexes with CNTs. The charge transfer interactions between electron-accepting CNTs and electron-donating mono-, di-, tri-, tetra-, penta- and hexa-chloro substituted benzenes have been investigated by Balamurugan and Subramanian.[144] They observed that the maximum charge transfer occurs between CNT and highly substituted benzene. A recent study by Pati *et. al.* has shown the charge transfer interactions occur in the complexes of hazardous molecules such as dichlorodiphenyldichloroethane (DDD), dichlorodiphenyltrichloroethane (DDT), and dichlorodipenyldichloroethylene (DDE) with nitrogen and transition-metal-doped CNTs rather than their complexes with pure CNT.[145] In 2016, Ivanov and group examined the charge transfer interactions between the components of the endohedral complexes formed between CNTs and lithium monophosphide chains.[146] In another study

on the endohedral complexes of CNT with polyiodide, it has been reported that the charge transfer takes place from donor CNT to acceptor iodide ions.[147]

The donor-acceptor complexes of CNT find applications in various devices. For example, the donor-acceptor complexes of CNT with polymer of porphyrin have been found suitable for applications in photovoltaic (PV) devices.[148] The composite CNT-poly(p-phenylene vinylene) (PPV) wherein hole transfer takes place from PPV to CNT has been shown to exhibit photovoltaic properties.[149] The donor-acceptor nanohybrid composed of CNT, pyrene and porphyrin has been found to exhibit a significant absorption in the visible region (600-800 nm) of the spectrum and therefore considered as an ideal candidate for PV cells.[150] Other donor-acceptor systems which have been found suitable for PVs are quantum dot-CNT-thiol functionalized perylene derivatives and carboxylated CNT-C₆₀. [132, 151] The complexes in which CNT acted as a donor and C₆₀ as well as silicon as acceptors have also been reported to be suitable for PV applications.[152, 153] The nanocomposite formed by wrapping CNT by helical isoalloxazine ring containing aliphatic spacer unit having 12 carbon atoms attached to C₆₀-functionalized flavin has been reported as a useful component in PV devices.[154] Guldi reported that the device consisting of nanohybrid SWNT/Pyrene⁺/ZnP⁸⁻ and indium tin oxide (ITO) electrode can be used to convert solar energy to electrical energy.[155] This is due to the flow of electrons from nanohybrid to electrode in presence of light. The organic-inorganic nanohybrid system made up of CNT, pyrene⁺ and CdTe wherein CNT acts as an acceptor moiety has been found useful in photoelectrochemical cell by Guldi and co-workers.[156]

1.4 Charge Transport Properties of Functionalized Carbon Nanotubes

The carrier mobility (μ) is a crucial parameter to decide the nature of charge transport in organic semiconductors. The compounds with significantly higher hole mobility than electron mobility show p-type semiconducting characteristics. On the other hand, n-type semiconducting characteristics are observed for those compounds which exhibit electron mobility much higher than hole mobility. However, an ambipolar behaviour is observed for those having equal or nearly same values of electron and hole mobilities.

In 2014, Peng *et. al.* reviewed the recent advances in p-type as well as n-type field-transistor devices based on CNT.[157] Cao and co-workers fabricated p-type thin-film transistor that based on CNT with mobility of $12.04 \text{ cm}^2\text{V}^{-1}\text{s}^{-1}$. [158] The mobility as high as $77 \text{ cm}^2\text{V}^{-1}\text{s}^{-1}$ has been reported for CNT based thin-film transistor.[159] In another study, p-type carbon nanotube field-effect transistor (CNTFET) exhibited mobility of $35 \text{ cm}^2\text{V}^{-1}\text{s}^{-1}$. [160] McGuire *et. al.* fabricated p-type CNT transistor via doping of boron atoms.[161] Park and co-workers showed that p-type

CNT can be prepared by electrochemical doping of CNT by perchlorate anions .[162] The p-type doping of CNT with the adsorption of O₂ was achieved by Kang and colleagues.[163]

It is well known that pristine CNTs are p-type semiconductors. Thus, there is a great interest in the designing of n-type semiconductors based on CNT. One such study conducted by Xu *et al.* on the charge transfer complexes of CNT with decamethylcobaltocene (DMC) in which the former acted as an acceptor while the latter as a donor.[130] Based on the results obtained from the electrical characterization, they inferred that a conversion from p-type to n-type characteristics occurs when CNT is doped by DMC. Another study showed that the doping of CNT by Al changes the charge transfer characteristics from p-type to n-type.[164] A similar investigation was carried out by Czerw *et al.*, showing p-type to n-type conversion of CNT on doping nitrogen.[165] Nouchi and co-workers fabricated p-type as well as n-type carbon nanotube based field effect transistors using TCNQ and polyethyleneimine (PEI) as dopants, respectively.[166] The n-type transistors made up of CNT and SiN_x thin films exhibit a maximum electron mobility of 10 cm²V⁻¹s⁻¹. [167] The complex formed by functionalizing CNT with amine-rich polymer showed high electron mobility (8×10^3 cm²V⁻¹s⁻¹) thereby serving as an n-type field-effect transistor.[168]

Huang and Jiang fabricated the carbon nanotube based field-effect transistors which exhibit ambipolar behaviour due to nearly the same values of electron and hole mobilities.[169] Baeg and co-workers also reported the ambipolar charge transfer characteristics for the polymer-wrapped CNTs.[170] The conversion of p-type conductivity of CNT to ambipolar-type for CNT/carbide heterostructures was observed by Martel and co-workers.[171] Another approach of modifying the electrical characteristics of CNT from unipolar to ambipolar has been achieved in polystyrene coated CNT.[172]

1.5 Optoelectronic Properties of Functionalized Carbon Nanotubes

The complexes of CNT with appreciable band gap (< 2 eV) act as semiconductors and they can be used in various optoelectronic devices. Very recently, a combined theoretical and experimental study reported that the band gap of metallic CNT becomes non-zero on forming complexes with dendrimers.[173] Xu and co-workers pointed out that the metal-to-semiconductor transition can be done by co-doping CNT with boron and nitrogen atoms.[174] Besides, a number of studies are available on the conversion of metallic CNTs to semiconducting ones by different methods including irradiation with low-energy electrons [175], treatment with hydrogen plasma [176] and by applying high axial strain.[177]. In contrast to the above metal-semiconductor transition, Rao and co-workers showed that semiconducting CNTs when attached

to metal nanoparticles become metallic due to charge transfer between them.[178] Later, Rao and Voggu suggested that the metal to semiconductor transition of CNT takes place on forming charge transfer complex with electron acceptor molecules while its semiconductor to metal transition occurs in the presence of electron donor molecules.[179]

In an experimental study performed by Tsuchikawa *et. al.*, it has been shown that the optical properties of CNT can be altered to a large extent by functionalizing with squaraine dyes.[180] Their results indicated that pure CNT does not absorb visible light, whereas a prominent absorption is observed for the dye functionalized CNT. Bunes and co-workers studied the optoelectronic properties of the complexes formed by interacting carbazolyethynylene oligomer with CNT.[181] Their study also showed that although the absorption of CNT is negligible, its complexes show significant absorption in the visible region of the electromagnetic spectrum. Cheng and co-workers reported that the absorption wavelengths of CNT have been red-shifted on complexation with fluorene-based polymers.[182] Interaction between CNT and oligonucleotides of DNA was examined by Tan and group.[183] Their results demonstrated that the wavelengths as well as the absorption intensities of free CNT differ significantly from those of its complexes with DNA. Another group of researchers showed that the nanohybrids formed from zinc porphyrin (ZnP) and CNTs can be used for light-harvesting applications.[184] The above nanohybrids showed photoinduced electron transfer from ZnP to CNT.

1.6 Mechanically Interlocked Nanotubes (MINTs)

The mechanically interlocked molecules (MIMs) have gained increased attention in the past decades. They are basically of two types *viz.*, rotaxanes and catenanes. The rotaxanes are those in which a linear macrocycle is surrounded by macrocyclic ring, whereas the catenanes are those in which macrocyclic rings are intertwined with each other. The work on mechanically interlocked molecular architectures was acknowledged with Nobel Prize in Chemistry awarded to Feringa, Sauvage and Stoddart in 2016 for the designing and synthesising molecular machines at the nanoscale.[185-188].

The mechanically interlocked nanotubes (MINTs) fall into the categories of MIMs. The two main advantages of MINTs are (i) their stability is comparable to that of the covalent complexes of CNT and (ii) they do not modify the electronic properties of CNT similar to the non-bonded complexes of CNT. Among MINTs, the rotaxane-like structures have been widely investigated both theoretically and experimentally.[189-194] There are many examples of such structures which include the complexes formed by encapsulation of CNT within macrocycle composed of two π -extended TTF units [191, 193], wrapping of CNT by pyrene-based macrocycle [192, 193]

and by confining CNT into macrocyclic systems made up of two porphyrin units.[194] Akola and co-workers studied the electronic properties of rotaxane-like MINTs formed by the complexation of CNT with crown ethers or β -cyclodextrin.[189] Their results indicated that the structures without any cross-linking preserves the electronic properties of CNT similar to the supramolecular non-covalent complexes. Juan and Pérez reviewed the endohedral complexes of CNT on comparing their properties with that of rotaxane-like MINTs.[190] They showed that the topology of both types of complexes of CNT is the same.

Since CNTs have large surface area, the molecules can easily move on their surface in presence of external stimuli like temperature, voltage, pH and light. Recently, the light and electricity responsive materials of aligned CNT with polymers were reviewed by Luo and Hu.[195] Jintoku *et. al.* studied the optically responsive complexes of CNTs with azobenzene-based dispersant.[196] They observed the photo-isomerisation of azobenzene molecule upon irradiation of ultraviolet light on its complexes. The photomechanical effect in bilayer systems composed of CNT and polycarbonate polymer was elucidated by Zhang and co-workers.[197] They suggested the future applications of above systems as light-driven motors, oscillators and sensors. Temperature and voltage driven molecular motors in which short CNT translates over long CNT have also been reported.[198, 199]

1.7 Objectives of the Thesis

Although there are reports on the π - π and the charge transfer complexes of CNT, a systematic study on the stability, optoelectronic and charge transport properties of these complexes is still deficit at the molecular level which motivated us to carry out further investigations. The main objective of the present thesis is to study the interactions between CNT and various π -electron species such as indigo, perylene bisimide (PBI), quaterthiophene (4T), [10]cycloparaphenylene ([10]CPP) and substituted as well as doped derivatives of [10]CPP. For this purpose, we used different dispersion-corrected density functional methods *viz.*, B97-D [200], B3LYP-GD3 [201] and ω B97X-D [202] which account for the weak van der Waal interactions between the constituent units.

In the present study, the armchair nanotubes were selected as they are semiconducting in nature. Zigzag nanotubes were not used because of their half-metallic nature for the finite-length. We could not use chiral nanotubes because of the high computational cost required due to their unsymmetrical nature. As CNTs have the ability to adsorb as well as to encapsulate the organic molecules, both endo- and exohedral complexes are considered for the investigation. Further, it is imperative to understand the structural stability of these complexes. It is also important to

examine how different components of interaction energy contributes towards the stability of each of the complexes.

One of the objectives of the present study is to unravel the mechanism of photoinduced electron transfer in the complexes based on the analysis of frontier molecular orbitals of the components of the complex. Earlier studies on the non-covalent complexes of CNT did not consider the nature of excited state transitions. The thesis aims to find out whether the excited state transitions occur due to intermolecular charge transfer. The thesis also attempts to find out the role of CNT as an electron donor or as an electron acceptor in its complexes with several π -conjugated molecules (indigo, PBI, 4T and CPPs). A molecular level analysis of charge transport properties of non-covalent complexes of CNT is lacking in earlier studies. Therefore, the thesis aims on whether the complexes of CNT with indigo, PBI and 4T exhibit p-type, n-type or ambipolar behaviour for organic transistors. Since CPP and its derivatives act as macrocyclic host for CNT and together they constitute the mechanically interlocked systems, the molecular level understanding of energy barriers for the translational and rotational motions of CPP over CNT is needed for their application in molecular machines.

1.8 Outline of the Thesis

The chapters of the present thesis are organised as follows:

The first chapter gives an introduction to CNTs and a literature review focussed on non-functionalized and functionalized CNTs. The structure and properties of non-covalently bound charge transfer complexes of CNTs are reviewed. A brief review on the mechanically interlocked nanotubes and their applications is also given. Following this, the objectives of this thesis are presented.

In the second chapter, the theoretical methods commonly used in computational studies are discussed. An introduction to the Schrödinger equation followed by various theoretical methods such as Hartree-Fock, post-Hartree-Fock and density functional theory are briefly explained. Different types of Pople basis sets along with the basis set superposition error are discussed. This chapter also presents the details of photoinduced electron transfer within donor-acceptor systems. The research works done are covered in next four chapters of the thesis. In Chapter 3-6, the structure-property relationships for the various complexes of CNT is established.

Chapter 3 presents the study of stability, optoelectronic and charge transport properties of endo- and exohedral complexes of CNT with indigo at B97-D/6-31G(d,p) level. The effect of length and the capping of CNT on the charge transport properties of the above complexes with

indigo is examined. Three types of CNTs of same chirality but different diameters are used for the confinement of indigo to investigate the optoelectronic and charge transport properties of their complexes. The effect of different dispersion-corrected density functionals is studied for the endohedral complex of maximum stability.

In Chapter 4, the stability and above mentioned properties of exohedral complex of CNT with perylene bisimide are examined using different dispersion-corrected density functionals. A similar investigation on the stability of its endohedral complex is also performed.

Chapter 5 discusses the structure, optoelectronic and charge transport properties of endo- as well as exohedral complexes of CNT with quaterthiophene. The charge transport properties of these complexes are compared to those of the complexes reported in other chapters.

Chapter 6 describes the optoelectronic properties of the complexes of CNT with cycloparaphenylene (CPP) and its derivatives. The effect of substituents and dopants on the stability of CPP-CNT complexes is investigated. The occurrence of charge transfer to or from CNT is established for its complexes with CPP and its fluorine-substituted derivatives. The role of these systems in the molecular machines such as wheels and shuttles is also highlighted.

Chapter 7 culminates the results of the work done in the thesis followed by the future scope of the present work.



CHAPTER 2

Theoretical Background

Quantum chemistry describes atoms and molecules at microscopic level, in terms of structures, energetics and properties which can be assessed through different electronic structure methods. Some of the above methods with necessary theoretical background are discussed below.

2.1 Electronic Structure Methods

With the advent of quantum mechanics in the early 20th century, Heisenberg in 1925 gave the formulation of quantum mechanics by using matrix mechanics.[203] In 1926, Erwin Schrödinger proposed the wave equation which describes how the wave evolves in space and time.[204] The entire endeavour is solving Schrödinger equation. The time-independent Schrödinger equation is given by:

$$\hat{H}|\psi\rangle = E|\psi\rangle \quad (2.1)$$

where ψ is the wave function of the particle, \hat{H} is the Hamiltonian and E is the total energy of the system. The time-dependent Schrödinger equation is the first-order differential equation of the evolution of wave function in time,

$$\hat{H}|\psi(t)\rangle = i\hbar \frac{d}{dt} |\psi(t)\rangle \quad (2.2)$$

Paul Dirac, in 1926, demonstrated that both Heisenberg and Schrodinger methods are equivalent.[205] Since Schrodinger's version was relatively easy to understand, it was used for further development of quantum mechanics. Thereafter, Born and Oppenheimer in 1927 assumed that the total wave function (ψ_{total}) is the product of electron wave function ($\psi_{electron}$) and nuclear wave function ($\psi_{nuclear}$).[206]

$$\psi_{total} = \psi_{electron}\psi_{nuclear} \quad (2.3)$$

According to Born-Oppenheimer approximation, the Hamiltonian for an electron in an interacting many electron system is defined as the sum of the kinetic energy operator (\hat{T}_e), potential due to electron-electron interactions (V_{ee}) and external potential (V_{ext}) due to electron-nucleus interactions for fixed position of nuclei,

$$\hat{H} = \hat{T}_e + V_{ee} + V_{ext} \quad (2.4)$$

where $\hat{T}_e = -\frac{\hbar^2}{2m} \sum_i \nabla_i^2$

Considering the Born-Oppenheimer approximation, the Schrodinger's equation can be written as:

$$-\frac{\hbar^2}{2m} \left(\frac{\partial^2 \psi}{\partial x^2} + \frac{\partial^2 \psi}{\partial y^2} + \frac{\partial^2 \psi}{\partial z^2} \right) + V\psi = E\psi \quad (2.5)$$

Based on this approximation, one can separate the electronic and nuclear motions so as to partition the respective wavefunction and Hamiltonian. On solving the above equation, the wave function can be determined. The wave function is a function of the coordinates that contains all the information necessary to define a system. The Schrödinger's wave was interpreted correctly by Max Born as the probability amplitude which means the wave function must be squared in order to obtain the probability.[207]

2.2 *Ab-initio* Methods

According to the fundamental postulate of quantum mechanics, a system can be described completely using its wave function. The Schrödinger equation for one-electron system can be solved analytically, whereas solving many-electron Schrödinger equation is a tedious task and needs approximation methods like variational and perturbation methods.

2.2.1 Hartree-Fock Method

Hartree and Fock proposed an iterative self-consistent field method for many electron systems. The procedure for achieving self-consistency has been discussed in many books.[208-210] The Hartree-Fock self-consistent field (HF-SCF) method is an *ab-initio* approach based on the variational method which assumes the total wave function as a product of one electron wave functions. The idea behind the assumption taken by Hartree is that each electron moves independent of each other and hence experiences only the average electrostatic field from all other electrons. [211] In order to construct one electron operator, an initial wave function is taken. Then, the equations are solved to get new wavefunction. Fock extended the Hartree method to incorporate the electron exchange effect applying Slater determinant.[212] HF method employs a Hartree potential and an exchange interaction that forces the antisymmetry of the wavefunction. For N-particle system, the trial wavefunction (ψ) satisfying the antisymmetry condition for electron can be written in the form of Slater determinant.

$$\psi(x_1, x_2, x_3, \dots, x_N) = \frac{1}{\sqrt{N!}} \begin{vmatrix} \chi_1(x_1) & \chi_2(x_1) & \chi_3(x_1) & \dots & \chi_N(x_1) \\ \chi_1(x_2) & \chi_2(x_2) & \chi_3(x_2) & \dots & \chi_N(x_2) \\ \chi_1(x_3) & \chi_2(x_3) & \chi_3(x_3) & \dots & \chi_N(x_3) \\ \vdots & \vdots & \vdots & \ddots & \vdots \\ \chi_1(x_N) & \chi_2(x_N) & \chi_3(x_N) & \dots & \chi_N(x_N) \end{vmatrix} \quad (2.6)$$

where x_1, x_2, \dots, x_N denotes the coordinates and $\chi_1 \chi_2 \chi_3 \dots \chi_N$ represent the one-electron spin orbitals for a set of N-particles.

For i^{th} -orbital (φ_i), one-electron Fock operator (\hat{F}) is given by,

$$\hat{F}[(\varphi_i)] = \hat{H} + \sum_{i=1}^{N/2} [2\hat{J}_i - \hat{K}_i] \quad (2.7)$$

where \hat{H} is the Hamiltonian operator which is the sum of kinetic energy operator for electron and potential energy operator due to electron-nucleus interaction. \hat{J}_i is the Coulomb operator that defines the repulsion between two electrons occupying the same i^{th} orbital and \hat{K}_i is the exchange operator arises due to the antisymmetric nature of the wavefunction for N-electrons. In terms of occupied spin-orbitals (a and b), the Coulomb operator (\hat{J}_{ab}) and the exchange operator (\hat{K}_{ab}) are given by

$$\hat{J}_{ab} = \int d^3r_1 d^3r_2 |\psi_a(r_1)|^2 \frac{1}{r_{12}} |\psi_b(r_2)|^2 \quad (2.8)$$

$$\hat{K}_{ab} = \int d^3r_1 d^3r_2 \psi_a^*(r_1) \psi_b^*(r_1) \frac{1}{r_{12}} \psi_a(r_2) \psi_b(r_2) \quad (2.9)$$

Equation (2.7) is non-linear and has to be solved iteratively by self-consistent procedure. As this equation is difficult to solve, Roothaan and Hall (1951) proposed a detailed way of solving this by expanding molecular orbitals as a linear combination of atomic orbitals. Roothaan and Hall matrix [213, 214] equation has the form

$$\hat{F}C = \varepsilon SC \quad (2.10)$$

where \hat{F} is the effective one electron Fock operator, C is the coefficient matrix, S is the overlap matrix and ε is the matrix for orbital energies.

Once the approximated wave function and Hamiltonian are formulated, one can invoke the variational principle to solve the electronic Schrödinger equation. According to variational principle, the expectation energy obtained by solving the Schrödinger equation using variational principle is always the upper bound of the true ground state energy. By solving the HF equations,

lowest energy for the ground state is obtained. This energy tends to HF limit with the improvement of wave functions. Nevertheless, this method suffers from a major drawback that it considers only the average interaction among electrons. The main drawback of Hartree-Fock method is that it does not take into account of the electron correlation due to the assumption of independent particle model. Other drawbacks include bond lengths are underestimated and non-covalent interactions, particularly dispersion forces are not described correctly.

2.2.2 Post-Hartree-Fock Methods

The exchange interaction that occurs between electrons is the result of Pauli exclusion principle. The correlated motion between electrons of anti-parallel spins arises because of their mutual coulombic repulsion. The electron correlation energy is calculated as the difference between exact energy and HF energy. Since the Hartree-Fock method does not take into account the complete correlation between electrons, post Hartree-Fock methods were introduced which refine HF method either variationally or perturbatively. These include Møller-Plesset (MP) perturbation, configuration interaction (CI) and coupled-cluster (CC) methods.

In Møller-Plesset perturbation (MP) methods, the sum of the Fock operators forms the unperturbed Hamiltonian. Here, the electron correlation effects are included using perturbation method. In case of MP2, the perturbation is limited to second order. The full configuration interaction method treats the electron correlation effectively, even better than the higher order Møller-Plesset perturbation methods. The coupled cluster single, double and perturbative triple excitation, CCSD(T) is regarded as “the gold standard of quantum chemistry” as it fulfils the requirements of accuracy and cost. However, these methods are computationally expensive for large systems and are not considered for the present study.

2.3 Density Functional Theory (DFT)

It is an alternate approach to Hartree-Fock (HF) theory for determining the electronic structure of a chemical system. The main advantage of DFT is that it takes into account the electron correlation effect which is neglected in HF theory. Instead of computing the multi-electron and multi-dimensional wave function, the density functional theory is concerned only with the computation of electron density that depends on three variables compared to $3N$ variables in wave-function based approaches. In DFT, function used in wave-function-based approaches is replaced by functional. It implies that the wave function ($\psi[n(r)]$) depends on the electron density $n(r)$, which in turn depends on the three-dimensional spatial coordinates (r) of the system. This theory has great success in the past few decades.

It is the most widely used computational method which describes the ground state properties of any system under consideration. By employing this method, the approximate solutions of Schrödinger equation can be determined. Although DFT is less accurate than other ab-initio methods, it is rather more versatile. DFT methods take approximately the same computational time as HF methods and have almost the same accuracy compared to MP2 method.

2.3.1 Thomas-Fermi Model

Prior to the introduction of density functional theory, Thomas and Fermi in 1927 proposed a Jellium model or uniform gas model.[215] In this model, an imaginary system named Jellium is composed of large number of electrons in an infinite space with evenly distributed positive charges. For the above system, Thomas and Fermi calculated the kinetic energy using the fermion statistical mechanics as,

$$T[\rho(r)] = \frac{3}{10} (3\pi^2)^{2/3} \int \rho^{5/3}(r) dr \quad (2.11)$$

Here, kinetic energy is the function of electron density, which in turn is the function of three-dimensional spatial coordinates.

In 1951, Slater determined the exchange energy (E_x) as a function of electron density [216] and is given by

$$E_x[\rho(r)] = -\frac{9\alpha}{8} \left(\frac{3}{\pi}\right)^{1/3} \int \rho^{4/3}(r) dr, \text{ where } \alpha = 1 \quad (2.12)$$

Thereafter, Bloch and Dirac derived a similar equation but changed the value of α to $2/3$. Together, the equations (2.11) and (2.12) with $\alpha = \frac{2}{3}$ are known as Thomas-Fermi-Dirac equation.[217] Thomas-Fermi Statistical model which is based on this equation does not explain the bonding between the atoms, which in turn, cannot be considered appropriate for molecules and solids.

2.3.2 Hohenberg-Kohn (H-K) Theorems

An approach that treats electron density as basic variable was laid in 1964 by Hohenberg and Kohn.[218] They explained the density functional theory via first and second H-K theorems.

2.3.2.1 First H-K Theorem

The first theorem states that the “external potential is the functional of electron density”. The

Hamiltonian operator and hence the total energy ($E[\rho(r)]$) is described by the ground state electron density ($\rho(r)$) as,

$$E[\rho(r)] = \int \rho(r) v_{ext}(r) dr + F[\rho(r)] \quad (2.13)$$

where $v_{ext}(r)$ is the external potential and $F[\rho(r)]$ is the universal functional of electron density.

The universal functional is the sum of kinetic energy and of electron-electron interaction energy which is same for all the electrons present in a system. Hence, total energy of any two systems is different due to their varying values of $v_{ext}(r)$. This theorem is also known as the existence theorem.

2.3.2.2 Second H-K Theorem

The second theorem states that the ground state energy of a system can be determined by minimizing the total energy of the system, which in turn, depends on the external potential. Hohenberg and Kohn determined the energy of the ground state using density. It is based on the variational principle, according to which, the ground state energy (E_{GS}) is given by,

$$E_{GS} \leq \langle \psi | \hat{H} | \psi \rangle \quad (2.14)$$

$$E[\rho(r)] = \int \rho(r) v_{ext}(r) dr + F[\rho(r)] \geq E_{GS} \quad (2.15)$$

In order to obtain the ground state density and hence the energy, the universal functional has to be minimized. Although H-K theorems formed the basis of DFT, the exact functional form of the total energy was still unknown and thus many approximate methods have been given in last few decades.

2.3.3 Kohn-Sham Theory

It is based on the assumption that the density of an unreal system with non-interacting electrons is same as that of a real system with interacting electron. The replacement of many-electron problem with a single-particle problem by Kohn and Sham leads to much lower computational cost. The K-S equations [219] is written in terms of the one-electron Schrödinger equation as given by,

$$\left(\frac{-\hbar^2}{2m} \nabla^2 + v_{eff}(r) \right) \varphi_i(r) = \varepsilon_i \varphi_i(r) \quad (2.16)$$

where $\varphi_i(r)$ is the Kohn-Sham orbital and ε_i is the orbital energy. For n-electron system, the density in terms of Kohn-Sham orbital is given by

$$\rho(r) = \sum_i^n |\varphi_i(r)|^2 \quad (2.17)$$

The total energy is thus written as

$$E[\rho] = T_s[\rho] + V_{ext}[\rho] + E_H[\rho] + E_{xc}[\rho] \quad (2.18)$$

where kinetic energy $T_s[\rho]$ is for the non-interacting electrons and is written as

$$T_s[\rho] = \sum_i^n \int dr \varphi_i^*(r) \left(-\frac{1}{2} \nabla^2 \right) \varphi_i(r) \quad (2.19)$$

and $E_H[\rho]$ is the Coulomb energy.

Here, the equations are solved to get Kohn-Sham orbitals using self-consistent procedure starting with an initial guess of charge density (ρ). The process of iteration is repeated till the value of density and exchange-correlation energy lie within their respective tolerance values. The theories by Hohenberg-Kohn and Kohn-Sham are termed as density functional theory (DFT).

In equation (2.18), the exact form of exchange-correlation energy was not known. Thus, two main approximations were used *viz.*, local density approximation (LDA) and gradient density approximation (GGA) so as to determine the functional form of exchange and correlation energies and are discussed in detail below.

2.3.4 Local Density Approximation (LDA)

It is the simplest approximation for determining the exchange-correlation (E_{xc}) that depends on the electron density,

$$E_{xc}[\rho] = \int \varepsilon_{xc}[\rho] \rho(r) d^3r \quad (2.20)$$

where $\varepsilon_{xc}[\rho]$ is the exchange-correlation energy per electron.

The exchange-correlation potential is related to the total exchange-correlation energy by,

$$V_{xc}(r) = \frac{\delta E_{xc}^{LDA}}{\delta \rho(r)} \quad (2.21)$$

For spin-polarized system, the exchange-correlation energy is calculated using local-spin density approximation (LSDA) and is

$$E_{xc}^{LSDA}[\rho_{\uparrow}, \rho_{\downarrow}] = \int dr \rho(r) \epsilon_{xc}(\rho_{\uparrow}, \rho_{\downarrow}) \quad (2.22)$$

The above approximations describe the uniform electron gas using Thomas-Fermi theory underestimating the interactions between electrons. Here, the exchange energy [217] is given by,

$$E_x^{LDA}[\rho(r)] = -\frac{3}{4} \left(\frac{3}{\pi}\right)^{1/3} \int \rho^{4/3}(r) dr \quad (2.23)$$

and the correlation energy can be determined by Monte-Carlo simulation and fit to analytical form by Vosko, Wilk, and Nusair (VWN).[220] However, this method overestimates the correlation energy and thus, better approximations are required. With this approximation, the chemical bonds like covalent, metallic and ionic are well described, however, hydrogen bond as well as the van der Waals bond are not described adequately. It also gives a fairly accurate value of bond length whereas a large error is obtained in the calculation of molecular energies. The exchange-correlation functional based on this approximation is SVWN which is the combination of exchange functional (Slater functional) with local VWN correlation functional.[220, 221] The magnitude of exchange-correlation energy on the basis of Hartree-approach is zero due to complete negligence of the exchange-correlation effects.

2.3.5 Generalized Gradient Approximation (GGA)

The exchange-correction functionals based on LDA involve slow changes in the electron density over the small region of space. Therefore, they are used to accurately predict the properties of only those systems in which the electron density distribution remains uniform. GGA circumvent this problem by incorporating the gradient of density in the calculation of exchange-correlation energies. Therefore, it gives a better description of the systems taking into account the derivative of density based on the Kohn-Sham theory. By applying GGA, the exchange-correlation energy is written as:

$$E_{xc} = \epsilon_{xc}[\rho(r), \nabla\rho(r)] \quad (2.24)$$

$$\text{where, } \epsilon_{xc}^{GGA}[\rho(r), \nabla\rho(r)] = \epsilon_x^{GGA}[\rho(r), \nabla\rho(r)] + \epsilon_c^{GGA}[\rho(r), \nabla\rho(r)] \quad (2.25)$$

The functionals such as Becke (B97) [222] and Becke-Lee-Yang-Parr (*BLYP*) [223, 224] belong to this class of functionals. GGA functionals are also known as non-local functionals and describe correctly those systems with inhomogeneous electron distribution. It provides an improvement in the bond energies but not in the band gaps of the molecules.

Both LDA and GGA functionals fairly describe the structural as well as electronic properties of many solids but are relatively less accurate to predict the properties of a molecular system.

2.3.5.1 Meta-GGA Functionals

In 2005, the first work on meta-GGA functional was published by Truhlar and his co-workers and it was denoted as M05.[225] The meta-GGA exchange-correlation energy as a function of electron density is given by,

$$E_{xc}^{meta-GGA}[\rho(r)] = \int \varepsilon_{xc}^{meta-GGA}[\rho(r), \nabla\rho(r), \tau(r)] \rho(r) d^3r \quad (2.26)$$

where, τ is the kinetic energy density and is equal to $\frac{1}{2} \sum_i (\nabla\varphi_i)^2$.

Other type of meta-GGA functional is Toa-Perdew-Staroverov-Scuseria (TPSS) [226]. In general, these functionals are accurate than GGA functionals but the disadvantage is that meta-GGA functionals are relatively more expensive in terms of computational cost.

2.3.6 Hybrid Functionals

The main problem with the above exchange-correlation functionals based on LDA, GGA and meta-GGA is that they all lead to self-interaction error, whereas exact DFT does not include any self-interactions. This problem is circumvented largely by using hybrid functional that helps to reduce the self-interaction error. The exchange-correlation energy in hybrid functionals involves a contribution from Fock exchange along with the exchange and correlation energy from various approximations.

$$E_{hybrid}[\rho] = \alpha E_X^{exact}[\rho] + (1 - \alpha)E_X[\rho] + E_c[\rho] \quad (2.27)$$

where, the parameter α can be obtained by fitting it to experimental data of the molecules.

The exact exchange energy functional is defined by Kohn-Sham orbitals and not by electron density. The hybrid functionals are most popular among different class of functionals and some of the examples are Becke-3-LYP [223, 224, 227], ω B97X [228] and CAM-B3LYP [229]. The functional Becke-3-LYP (B3LYP) includes 20% of HF exchange, 80% of Dirac or Slater exchange, 72% of Becke exchange, 81% of Lee-Yang-Parr correlation and 19% of Vosko, Wilk, and Nusair correlation. B3LYP adequately considers the effect of both exchange and correlation energy and thus, gives better result than pure functionals based on LDA and GGA. Due to the additional HF exchange energy term in hybrid functional, it becomes slower than GGA functional. With hybrid functionals, bond energies are significantly improved in comparison to

GGA functionals. Further, the hybrid functionals also improve the band gaps and the electron affinities of molecules. A new class of functionals called double-hybrid density functionals have also been introduced in which exchange-correlation functionals are mainly composed of (i) HF exchange and (ii) perturbative correlation term of second-order (PT2).[230] The double hybrid functionals are more accurate, however, far more expensive in terms of their computational cost than hybrid functionals.

2.3.7 Improvement in Density Functionals

The density functionals without any long range or dispersion corrections do not define accurately the properties of such systems which are stabilized predominantly by van der Waals (vdW) forces. Since these forces play an important role in stabilizing the complexes, it becomes imperative to include long-range and dispersion corrections in the total exchange-correlation energy.

2.3.7.1 Long-Range Corrected Functionals

In this type of functionals, the exchange part of Hartree-Fock is simply replaced by the long-range exchange functional. Examples of such functionals include CAM-B3LYP and ω B97X which are the long-range corrected version of B3LYP and B97 functionals, respectively. They are used mainly for improving the charge transfer excitation energies and oscillator strength which are underestimated by the conventional DFT methods.

2.3.7.2 Dispersion-Corrected Functionals

In KS-DFT, the long-range electron correlation effects are not incorporated and hence the total energy with dispersion interactions is given by

$$E_{DFT-D} = E_{KS-DFT} + E_{disp} \quad (2.28)$$

and

$$E_{disp} = -s_6 \sum_{i=1}^{N-1} \sum_{j=i+1}^N \frac{c_6^{ij}}{R_{ij}^6} f_{dmp}(R_{ij}) \quad (2.29)$$

where s_6 is the scaling factor, N is the number of atoms, c_6^{ij} is the dispersion-coefficient for the atom pair ij and f_{dmp} is the damping function.

Commonly used DFT methods supplemented with dispersion corrections are DFT-D, DFT-D2 and DFT-D3. The first two involves pair of atoms while the other include upto three-body effects. Some examples of such functionals given by Grimme and co-workers are B2PLYPD [231], B97-D [200], ω B97X-D [202], B3LYP-GD2 [200, 224, 227] and B3LYP-GD3 [201, 232].

2.3.8 Time-Dependent Density Functional Theory (TD-DFT)

In this method, the excitations are defined in terms of the electronic density which is time-dependent and can be used for excited state calculations. Here, the exchange-correlation functional is non-local with respect to time and space. The time-dependent generalization of Hohenberg-Kohn theorem was given by Runge and Gross[233], thus constituting mathematical form of TD-DFT.

$$\hat{H}(t) |\psi(t)\rangle = i\hbar \frac{\partial}{\partial t} |\psi(t)\rangle \quad (2.29)$$

where,
$$\hat{H}(t) = \hat{T} + \hat{V}_{ext}(t) + \hat{V}_{ee} \quad (2.30)$$

From equation (2.30), it is clear that external potential (\hat{V}_{ext}) depends only on time and thus $\hat{V}_{ext}(t)$ is defined by electron density which can be determined using equation (2.29).

TD-DFT method is useful for understanding the optical response in molecules. Although TDDFT method depends on functionals selected, it is considered more accurate than Configuration Interaction Singles (CIS) method. TD-DFT is suitable for studying the excited-state properties of large systems due to relatively lower computational cost than coupled cluster and configuration interaction methods. With TD-DFT, absorption spectra of any system can be calculated. It is not always true that one type of functional can give accurate values of both absorption wavelength and oscillator strength. Therefore, different functionals are employed usually to obtain their correct values.

2.3.9 Applications of DFT and TD-DFT

To date, numerous applications of DFT have been reported. Using this method, the structure of solids without a priori knowledge of crystal structure can be predicted. One can also determine the most stable conformer. The thermodynamic properties such as Gibbs free energy, a quantity useful for determining the feasibility of a reaction can be computed. With DFT, it is also possible to calculate the electronic properties like ionization energy, electron affinity, band structure and density of states. Using TD-DFT method, the optical properties such as band gap and absorption spectrum of any system can be determined.

2.4 Basis Set

A basis set is a set of functions used to construct wave function. The use of larger basis set provides a better estimation of atomic orbitals. Generally, it is used to build molecular orbitals (ψ), which can be written as a linear combination of atomic orbitals (φ) with coefficients (c) and is given as

$$\psi_i(r) = \sum_{\mu=1}^k c_{\mu i} \varphi_{\mu}(r) \quad (2.31)$$

where, k is the total number of basis set.

Such basis sets are usually employed which resembles closely to the actual wave function and give accurate results at lower cost. The most common basis function used in computational study is Slater-type orbitals (STOs) and their radial part has the form $N r^{n-1} e^{-\zeta r}$. Here, N is the normalization constant, n is the principal quantum number, r is the distance of electron from the nucleus and ζ is a constant that gives the idea about the effective charge of the nucleus. The larger value of ζ gives tight function while its smaller value gives diffuse function. Initially, STOs were used as basis functions to perform the quantum chemical calculations since they resemble the eigenfunctions of hydrogen atom (e^{-zr/a_0}). The advantage of STOs is that they have direct physical interpretation and the disadvantage is that the computation of large number of integrals during self-consistent field (SCF) convergence is tedious, which in turn, reduces the computational speed. To overcome this problem, STOs were approximated as a linear combination of Gaussian orbitals. In case of Gaussian Type Orbitals (GTOs), the product of two Gaussians centered on two different locations gives another Gaussian and the calculations of orbital integrals are very fast. The other type of basis set is Gaussian type orbitals (GTOs) for which the radial part has the form $N r^{n-1} e^{-\alpha r^2}$. Although they differ from hydrogen atom type orbital, their calculations are easy which makes GTOs used universally in quantum chemistry. Generally, contracted basis sets, for example, STO-nG, 6-31G, 6-31++G, 6-31G(d, p) etc. are used in the calculations. The STO-3G basis set is a minimal basis set where each atomic orbital is made up of three primitive Gaussians. Other types of basis set are double zeta basis set that uses two basis functions for each atomic orbital. Similarly, there are triple-zeta and quadruple-zeta basis sets which employ three and four basis functions, respectively. Generally, extended basis sets are used for the system with large number of electrons. The different types of extended basis sets are discussed below.

2.4.1 Split-Valence Basis Set

These basis sets are used separately for core and valence orbitals. They are formed by two or more basis functions having different exponents. Unlike minimal basis set, they allow for size variations that occur in the bonding process. For instance, in case of 3-21G basis set, three Gaussians are used for the core orbitals and for the valence orbitals a split basis set is employed where two Gaussians are used for a contracted part of the wavefunction and one for the diffuse part. This is important for atoms like oxygen and fluorine where the minimal basis sets don't

allow for the valence orbitals to expand or contract during bond formation. It is also possible to add polarization and diffuse functions to the split valence basis set which are discussed below in detail.

2.4.1.1 Polarization Basis Function

They include flexibility within the basis set owing to which the molecular orbitals become more asymmetric about the nucleus. These basis sets are important to explain accurate bonding between the atoms as the spherical symmetry of atoms sometimes get distorted in presence of neighbouring atoms. For example, 6-31G* basis set include the d functions on the heavy atoms while 6-31G** basis set include the d functions on heavy atoms and the p functions on hydrogen and helium atoms.

2.4.1.2 Diffuse Basis Function

These basis functions have additional functions with small exponents and are thus, large in size. They are generally used for anions and also, for the weaker bonds. The use of this basis set mainly affects the properties like dipole moments and polarizabilities. For example, 6-31+G adds diffuse functions on the heavy atoms while 6-31++G adds diffuse functions on heavy atoms as well as hydrogen atoms.

2.5 Basis Set Superposition Error (BSSE)

The overestimation of the stabilization energy in a quantum chemical calculation arises generally due to the basis set superposition error (BSSE). This mainly results from the artificial stabilization of the dimer owing to the inclusion of additional basis function for each of the monomers. To determine the BSSE-corrected stabilization energy, a counterpoise correction scheme was proposed by Boys and Bernardi.[234]

When two monomers A and B combine to form dimer AB, the stabilization energy for the dimer AB without any BSSE correction, $\Delta E_{stab}^{AB}(AB)$ can be written as:

$$\Delta E_{stab}^{AB}(AB) = E^{AB}(AB) - E^A(A) - E^B(B) \quad (2.32)$$

where, $E^{AB}(AB)$, $E^A(A)$ and $E^B(B)$ denote the energies of the complex, monomer A and monomer B in their respective basis.

The BSSE for the monomer A; $E_{BSSE}(A)$ and the monomer B; $E_{BSSE}(B)$ in the combined basis function AB is computed as:

$$E_{BSSE}(A) = E^{AB}(A) - E^A(A) \quad (2.33)$$

$$E_{BSSSE} (B) = E^{AB} (B) - E^B (B) \quad (2.34)$$

where, $E^{AB} (A)$ and $E^{AB} (B)$ represent the energies of A and B in the basis of the complex AB. Subtracting the equations 2.33 and 2.34 from equation 2.32, we get the BSSE corrected stabilization energy $\Delta E_{stab}^{CP} (AB)$,

$$\Delta E_{stab}^{CP} (AB) = E_{stab}^{AB} (AB) - [E_{BSSSE} (A) + E_{BSSSE} (B)] \quad (2.35)$$

2.6 Photoinduced Charge Transfer

Interactions between the electron-donor and the electron-acceptor systems lead to the formation of an electron donor-acceptor (EDA) complex. The donor molecule is the one with low ionization energy, whereas the acceptor molecule is the one with high electron affinity. In contrast to ionic or covalent compounds, the complex is formed due to weak electrostatic attraction between the donor and the acceptor molecules. Such complexes are also known as charge-transfer complexes. In π -electron donor-acceptor complexes, the charge is transferred from the π -bonding orbital of the donor to the π^* -antibonding orbital of the acceptor. These complexes absorb in the visible region of the electromagnetic spectrum.

The charge transfer in EDA complexes can take place either in the ground state or in the excited state as illustrated in figures 2.1 and 2.2. According to the frontier molecular orbital (FMO) theory, the interaction occurs between the highest occupied molecular orbital (HOMO) of the donor and the lowest unoccupied molecular orbital (LUMO) of the acceptor molecule in the ground state. On the other hand, in the case of excited state charge-transfer, the electron is first excited from HOMO of the donor to its LUMO upon irradiation, followed by the transfer of electron to LUMO of the acceptor. The charge transfer phenomenon plays an important role in various physical, chemical and biological systems. Compared to the charge transfer in inorganic species, that in organic species are more useful as latter are inexpensive, fabricated easily and mechanically flexible.

One can predict the rate at which electron transfers from donor to acceptor moiety by applying Marcus theory. In the presence of a neighbouring molecule A^* , the intermolecular hole/electron transfer from the molecule in cationic/anion state ($A^{+/-}$) is denoted by



Since the electron transfer takes place at the transition state, activation energy is needed to distort the reactant from its equilibrium state. The rate constant for the intermolecular charge transfer (k_{CT}) is given by,

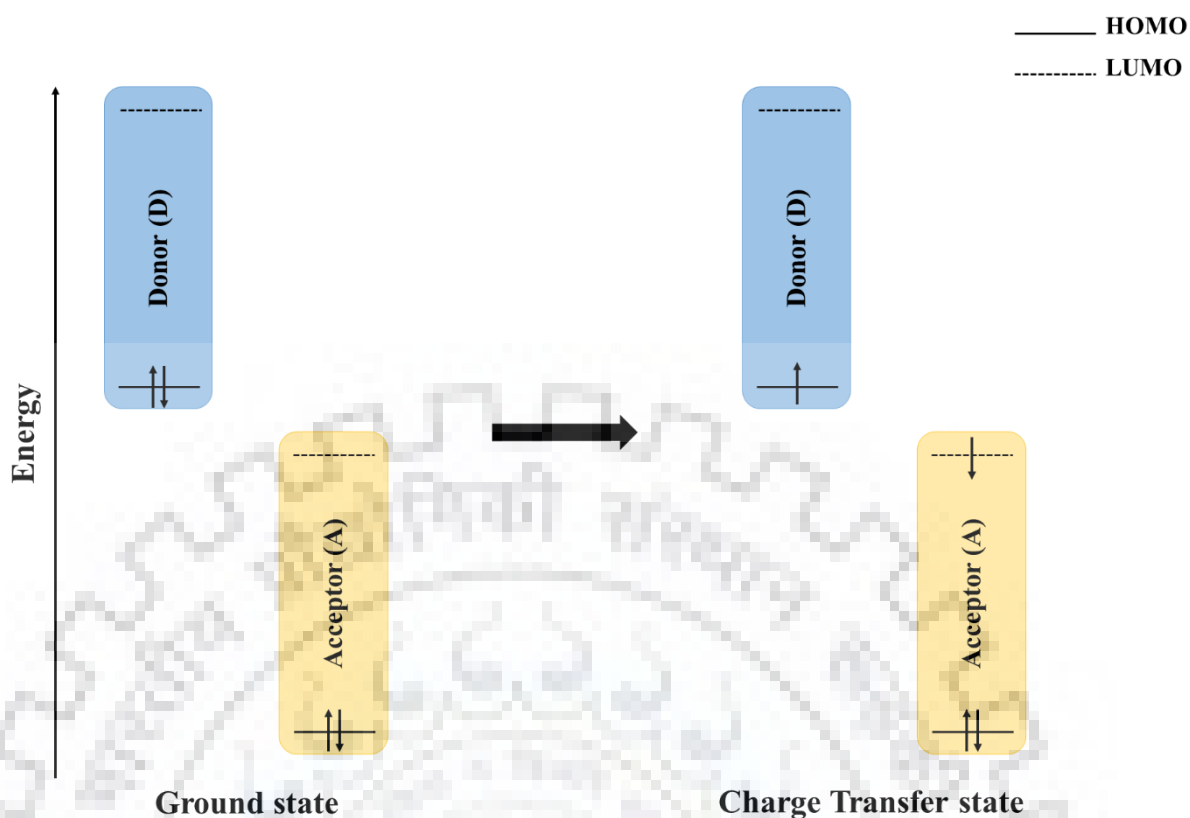


Figure 2.1 The ground state charge transfer in electron donor-acceptor (EDA) complexes

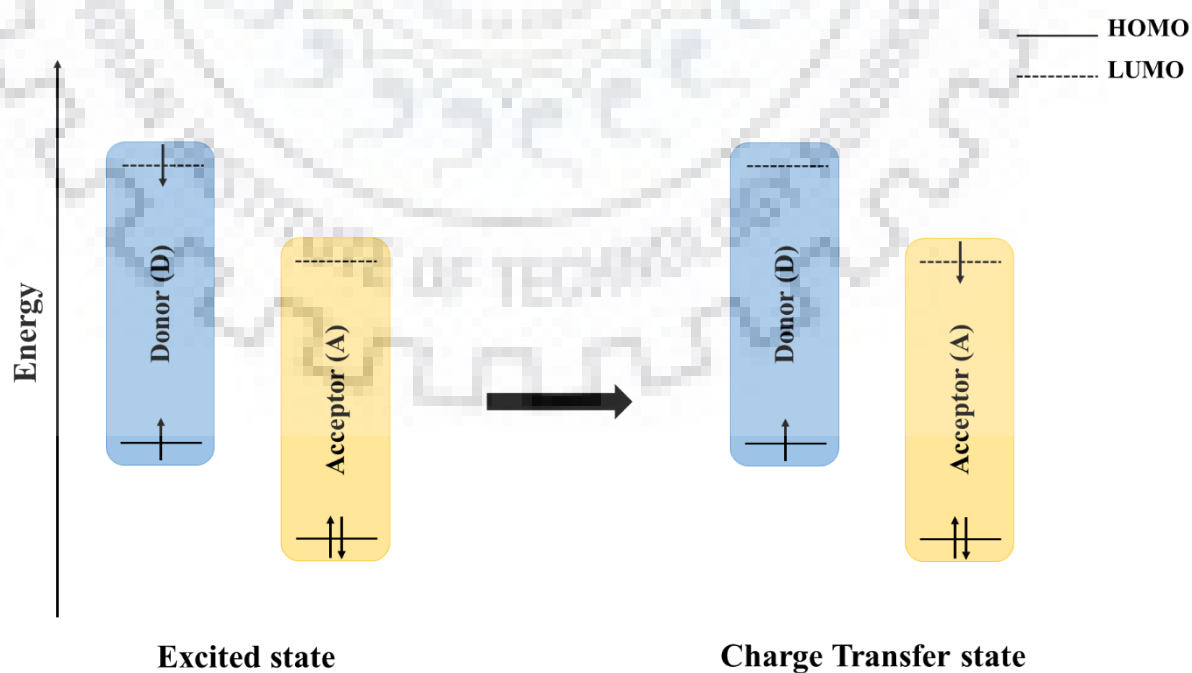


Figure 2.2 The excited state charge transfer in electron donor-acceptor (EDA) complexes

$$k_{CT} = \frac{4\pi^2}{h} \frac{1}{\sqrt{4\pi\lambda k_B T}} t^2 e^{-\lambda/4k_B T} \quad (2.37)$$

where λ is the reorganization energy, t is the transfer integral, h is the Planck's constant, T is the temperature (298 K) and k_B is the Boltzmann's constant. From the above equation, it is clear that the activation energy of carrier transport depends largely on λ at a given temperature.

For determining the rate constant for the hole transport, the values of hole transfer integral (t_+) and reorganization energy (λ_+) are used. Similarly, the rate constant for the electron transport can be determined from electron transfer integral (t_-) and reorganization energy (λ_-).

The reorganization energy for electron/hole transport ($\lambda_{-/+}$) can be calculated as (E (charged species) - E^o (charged species)) + (E (neutral geometry obtained from the charged species) - E^o (neutral geometry)), where E is the single-point energy and E^o is the optimized energy.

The transfer integral for an electron, t_- can be written in terms of energies of LUMO+1 (E_{L+1}) and LUMO (E_L),

$$t_- = \frac{E_{L+1} - E_L}{2} \quad (2.38)$$

The transfer integral for hole, t_+ can be approximated from the energies of HOMO (E_H) and HOMO-1 (E_{H-1}),

$$t_+ = \frac{E_H - E_{H-1}}{2} \quad (2.39)$$

The electron/hole diffusion coefficient (D) is calculated using the Smolchowski equation as follows

$$D_{-/+} = \frac{L^2 k_{-/+}}{2} \quad (2.40)$$

where, L denotes the centre-to-centre equilibrium distance.

From the values of diffusion coefficient (D), the electron/hole mobility ($\mu_{-/+}$) can be calculated using the Einstein relation given by

$$\mu_{-/+} = \frac{eD_{-/+}}{k_B T} \quad (2.41)$$

CHAPTER 3

Structure, Stability and Properties of the Complexes of Carbon Nanotubes with Indigo

3.1 Introduction

As mentioned in chapter 1, the derivatization of nanotube has the advantage that it prevents their association into bundles and thus provides dispersion in a selected solvent.[235-237] The non-covalently functionalized complexes of CNT are among the various derivatives which find myriad of applications in organic electronics,[238, 239] light-harvesting [240, 241] and organic field-effect transistors (OFETs).[242] In the non-covalent complexes, the nature of interactions between host and guest plays a crucial role in determining their stability. The non-covalent complexes of CNTs are stabilized by van der Waals, electrostatic, π - π stacking, X-H... π (where X= C, N, and O) and charge transfer interactions.[70, 150, 243-246] The importance of π - π interactions in the complexes such as oligothiophene@CNT, [247, 248] pioglitazone@CNT, [249] acetone@CNT [250] and diamond nanowire@CNT [251] was elucidated by several groups through theoretical and experimental methods. The above studies reported that the attractive interactions between π -conjugated CNT and encapsulated moiety impart stability to these complexes. Using density functional theory, Chang *et al.* showed that the inclusion complexes of amino acids with CNTs are stabilized either by π - π or by charge transfer interactions depending on the amino acid encapsulated.[252] In 2016, Wang and Xu theoretically studied the endohedral complexes of CNTs with doxorubicin and found that π - π and X-H... π (X = C, N, and O) interactions are responsible for the stabilization of resulting complexes.[253]

Recent studies have shown that the structure and properties of carbon nanotubes can be altered significantly by functionalization.[60, 254-261] The developments made in the field of functionalized CNTs have been summarized in a review by Meng and co-workers.[73] Both experimental and theoretical studies have revealed that the complexes of single-walled carbon nanotubes (SWCNTs) possess enhanced electronic properties compared to free carbon nanotubes and can be used in electronic devices.[68, 238, 262, 263] Sumanasekera *et al.* investigated the complexes of single-walled carbon nanotube (SWCNT) with various six-membered cyclic hydrocarbons having different number of π -electrons and showed an enhancement in the transport parameters of CNT with an increase in the number of π -electrons of the hydrocarbon.[264] Manzetti reported the tuning of energy levels of highest occupied molecular orbital and lowest unoccupied molecular orbital of CNT with a variety of molecules such as linear carbon chains, carbon sheets, oligomers and polymers.[265] Using the first principle

density functional theoretical (DFT) method, Khorshand and co-workers carried out investigation on the structural, energetic and electrical properties of the complexes of pencillamine with armchair and zigzag CNTs.[266] Mulliken population and molecular orbital analyses revealed that charge-transfer occurs from the electron donor pencillamine to the electron acceptor CNT. Debbichi *et al.* examined the effect of van der Waals interactions on the transport properties of the complex formed by encapsulating anthracene in CNT.[267] They observed that the rotation of anthracene within the cavity of CNT leads to varying amount of charge transfer between two units, which in turn alters the conductance of CNT. Shiraishi and co-workers reported that inclusion complexes formed between 7,7,8,8-tetracyano-p-quinodimethane (TCNQ) and CNTs can be used as p-type semiconductors in organic field-effect transistors.[268] Recently, the endohedral complexes of metallic CNT with viologen derivatives have been employed for the fabrication of organic field-effect transistor (OFET) devices due to their semiconducting nature.[261] Experimentally, it has been shown that CNT doped with electron acceptor TCNQ results in enhanced field emission characteristics compared to bare CNT.[269] This suggests the importance of the endohedral complexes of CNTs with organic molecules for optoelectronic applications.

The functionalization of CNTs alters the optical properties to a large extent as was reported in the CNT-squarylium complex in which the squarylium dye acts as a photosensitizer.[270] The study also revealed that the confinement results in the appearance of an additional peak in the absorption spectrum of pristine CNT. Chernov's group examined the optical properties of the endohedral complexes of CNTs with graphene nanoribbon (GNR).[271] They found that the complexes exhibit photoluminescence in the visible and infrared regions of the spectrum. The complexes formed by confining the asymmetric dye *p,p'*-dimethylaminonitrostilbene (DMANS) in CNT exhibit a large non-linear optical response.[272] In a study conducted by Campo and co-workers on the encapsulated complexes of CNTs with 20 different organic molecules, including various alkanes and their derivatives, an alteration in the optical properties of CNTs was observed.[273] Very recently, Wang *et al.* examined the electronic and optical properties of the inclusion complexes of CNTs with diamond nanowires.[251] Their study showed that the absorption spectrum of the complexes covers a wide spectral range from the ultraviolet to near-infrared, suggesting that they are useful in the areas of nano-optoelectronics. The encapsulation of flat molecules such as perylene based nanoribbon in carbon nanotube (CNT) leads to low charge recombination which is an important property required for solar cell applications.[119]

In a donor-acceptor (D-A) system of CNT with hydrocarbons, the direction of charge transfer between molecules can be ascribed to the electron donating or withdrawing group attached to

hydrocarbon. Upon functionalizing a nanotube with tetrathiafulvalene (TTF), the former acts as an acceptor,[135] whereas on functionalizing with tetracyanoquinodimethane (TCNQ), CNT acts as a donor.[140, 274] Recently, Caruso et. al highlighted the significance of the HOMO-LUMO energy level diagram to understand the electron transfer processes in weakly interacting donor-acceptor compounds.[275] Their studies illustrated that the electron transfer in the excited state occurs when the HOMO of the donor is lower in energy than the LUMO of the acceptor (*i.e.* $E_{CT} > 0$), whereas the charge transfer occurs in the ground state for the systems when LUMO of the acceptor is lower in energy than HOMO of the donor.

The charge transport properties of the nanotube are crucial in determining the conductivity of donor-acceptor complexes. Depending on the donor-acceptor nature of the molecule attached non-covalently to CNTs, the complex can be either an n-type semiconductor or a p-type semiconductor.[276] In this context, indigo can be envisaged as an interesting and promising molecule that exhibits several properties such as semiconductivity and high carrier mobility, making it useful as a component in thin films and organic field-effect transistors.[277] Indigo is an ampielectronic system with its amino group acting as an electron donor and the carbonyl group as an electron acceptor. The complexes of indigo and (6,6)CNTs can be used in the semiconductor devices only if the chosen CNT is of finite length. The C-C bond length alternation of about 0.03 Å for (6,6) CNT considered in this study is in analogy with the Peierls instability reported in the case of semiconducting armchair carbon nanotubes of finite length.[49, 278] Several methods for synthesizing such finite length CNT have been discussed in the literature, which include cutting of long CNTs into small fragments, Diels-Alder reaction of aromatic rings with an acetylene molecule or its derivatives and the addition of carbon units to cyclic aromatic compounds using Friedel-Crafts reaction.[26] Apart from these, methods such as dispersion followed by ultrasonic treatment,[279] and reversible debundling of carbon nanotubes upon illumination of light [280] are promising in the direction of synthesis and separation of specific tubes.

The present study aims to obtain a molecular level understanding of yet uninvestigated system, indigo-CNT. Here, we study the stability of the complexes of indigo wrapped over CNTs for their valuable transport and optical properties. It is very clear from the above studies that the endohedral complexes of CNTs with organic molecules are promising for optoelectronic and transport applications. In this chapter, we modelled the complexes of armchair CNTs of varying diameter with encapsulated indigo. Assuming the encapsulation of indigo can alter the properties of CNTs, we carried out a detailed investigation into the structural, optoelectronic and charge transport properties of various complexes of indigo@(n,n)CNT, where $n = 6, 7$ and 8 . The

electronic transitions of indigo, nanotube and their complexes are simulated using the time-dependent density functional theoretical method [233] and the results are analysed using the frontier molecular orbitals involved.

3.2 Computational Methods

The geometry optimization and vibrational frequency calculations of the exohedral complexes of indigo with (6,6)CNT in the ratio of 1:1 (dyad) and 2:1 (triad) were done using the dispersion-corrected density functional theoretical method. Similarly, the geometry optimization and frequency calculations of the endohedral complexes of indigo with (*n,n*)CNTs (*n* = 6-8) were also performed. The above computations were also carried out for their individual components. The lack of any imaginary frequency assures that a minimum is achieved in their respective potential energy surface. The B97-D functional in conjunction with 6-31G(d,p) basis set was employed for the calculations.[200] The above functional is capable of describing the dispersion interaction among components of each complex.[281-283] The stabilization energies (ΔE_{stab}) of the complexes were computed using supermolecular approach by taking the difference in energies of the complexes and their components in their respective optimized geometries as follows;

$$\Delta E_{\text{stab}} = E_{\text{complex}} - (E_{\text{CNT}} - n \times E_{\text{indigo}}) \quad (3.1)$$

where, *n* is the number of indigo molecules present in the complex.

These values were further corrected for basis set superposition error (BSSE) using the counterpoise correction scheme.[234, 284] They were also corrected for zero-point energy (ZPE). The electronic properties, such as vertical ionization energy (VIE) and vertical electron affinities (VEA), were calculated using the expressions:

$$\text{VIE} = E_{+} - E^{\text{opt}} \quad (3.2)$$

$$\text{VEA} = E_{-} - E^{\text{opt}} \quad (3.3)$$

where E^{opt} denotes the energy of optimized neutral species and E_{+}/E_{-} denotes the energy of charged species using the optimized neutral geometries. Similarly, the adiabatic ionization energy (AIE) and the adiabatic electron affinity (AEA) were determined using the energies of optimized neutral and charged species as:

$$\text{AIE} = E_{+}^{\text{opt}} - E^{\text{opt}} \quad (3.4)$$

$$\text{AEA} = E_{-}^{\text{opt}} - E^{\text{opt}} \quad (3.5)$$

where, E^{opt} denotes the energy of optimized neutral system and E_+^{opt} (E_-^{opt}) denotes the energies of optimized cationic (and anionic) system. Here, both the cationic and anionic systems are in their doublet state. It is assured that these states has no spin contamination.

As mentioned in chapter 2, the charge transport properties of the holes and electrons at room temperature were studied using the hopping model [285, 286]. The transfer integral (t) and internal reorganization energy (λ) of the carriers were computed to assess the rate constant of charge transfer (k_{CT}). The foregoing parameters along with diffusion coefficient (D) and charge carrier mobility (μ) were determined using the equations discussed in chapter 2. The excited state calculations were done using the TD-DFT formalism at B97-D/6-31G(d,p) level. All the calculations mentioned above were performed using Gaussian 09 suite of programs.[287] The optimized geometries and molecular orbital (MO) diagrams were generated using the visualization program Gauss View 5.0.[288]

To study the effect of functionals on the properties of the studied complexes, calculations were also performed using the dispersion-corrected hybrid functional B3LYP-GD3 [201, 232] and the range-separated functional ω B97X-D [202] for the most stable complex indigo@(7,7)CNT. By employing time-dependent density functional theoretical (TD-DFT) method, the optical absorption properties were determined for indigo@(7,7)CNT at three different levels B97-D/6-31G(d,p), B3LYP-GD3/6-31G(d,p) and ω B97X-D/6-31G(d,p).

3.3 Results and Discussion

3.3.1 Exohedral complexes of CNT with indigo

The optimized geometries of indigo, CNT and their complexes are shown in figure 3.1. The diameter and length of (6,6) carbon nanotube used are 8.14 Å and 16.69 Å, respectively. In the complexes, indigo loses its planarity and bents along the curved surface of CNTs. However, the structure of CNTs is not much affected. Figure 3.1 depicts two different distances from the surface of CNTs at which indigo is adsorbed. These include the distance to (i) apex of the bent indigo molecule and, (ii) centre of the imaginary plane connecting four terminal hydrogen atoms at the concave surface of indigo. In the dyad, the distance from the nearest surface of CNTs to the apex of indigo molecule is 3.16 Å, whereas that for the triad is 3.05 Å. The above distances lie in the range of π - π stacking distances usually found in the non-covalent complexes formed between benzene and carbon nanotubes.[103] The distance between indigo and CNT is an important parameter in the charge transport calculations of the complexes and is discussed later.

To get insight on the interaction between indigo and CNTs, we evaluated the stabilization energy (ΔE_{stab}) of the complexes using equation 3.1. The values of ΔE_{stab} without BSSE and ZPE corrections for the dyad and the triad are -28.28 and -56.76 kcal/mol, respectively. The BSSE corrections for the dyad and the triad are 7.81 and 15.62 kcal/mol. After incorporating BSSE and ZPE corrections, the stabilization energies of dyad and triad are found to be -19.25 and -38.92 kcal/mol, respectively. The stabilization energies of the complexes for different functional are also calculated using the optimized geometries obtained at the B97-D/6-31G(d,p) level and are listed in table 3.1. The values indicated that there is no cooperative effect in the triad due to the large distance between indigo molecules. The natural bond orbital (NBO) analysis of the complexes based on the values of second-order perturbation energy indicated that the interaction between the carbonyl group of indigo and the nearest carbon-carbon double bond of CNT mainly contributes to the stabilization energy. The electrostatic potential (ESP) maps for the complexes as shown in figure 3.2 also support the above findings. From the figure, it is evident that the carbonyl groups of indigo with maximum electron density interacts with CNT.

To study the electronic properties of the complexes, ionization energy and electron affinity of individual molecules and their complexes are determined from the energies of the corresponding charged and neutral species. Table 3.2 lists the computed values of ionization energy (IE) and electron affinity (EA) of indigo, CNT and their complexes. It is found that the vertical ionization energy (VIE) of free indigo is 6.58 eV which is in reasonable agreement with the experimental value of 7.0 eV.[289] Similarly, the CNT molecule chosen in the present study has a VIE of 4.93 eV which is in good agreement with the value of 5.02 eV obtained for (5,5) CNT of same length.[290] A comparison of ionization energies of indigo and CNT suggests that the nanotube can act as an electron donor owing to its low IE. The ionization energy of the complexes differs slightly from that of CNT and varies in the order: CNT > dyad > triad. The electron affinity also follows a similar trend as reflected from the values listed in table 3.2. The ionization energy and the electron affinity are also calculated adiabatically. It can be seen that the ionization energy obtained by adiabatic and non-adiabatic methods are nearly the same. This holds true for the corresponding electron affinities as well. A careful examination of the results indicates that there is a modest change in the above electronic properties by about 0.05 and 0.10 eV for the dyad and the triad, respectively, with respect to free CNT. The relatively low value of ionization energy and high value of electron affinity for the complexes with respect to those of CNT imply that they are ideal for OLED applications.

The frontier molecular orbitals play an important role in the charge transport properties. The highest occupied molecular orbital (HOMO) and lowest unoccupied molecular orbital (LUMO)

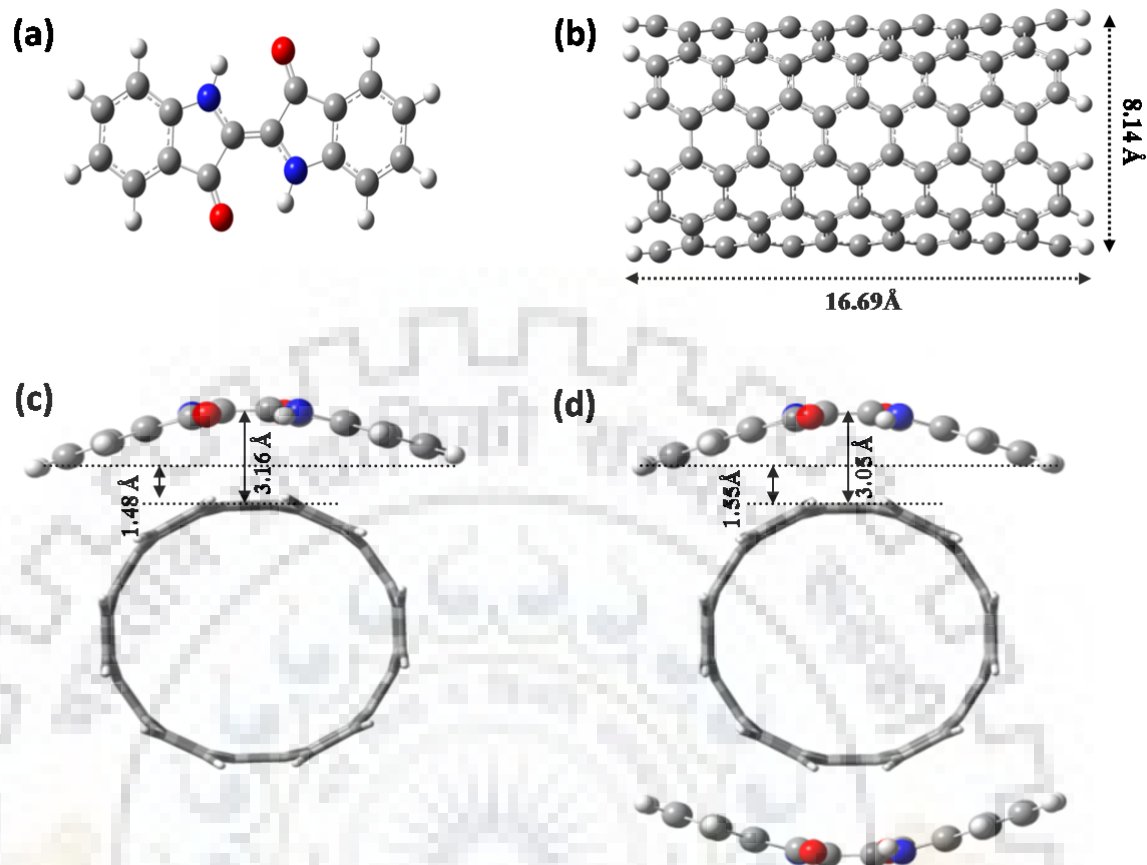


Figure 3.1 The optimized geometries of (a) indigo, (b) (6,6)CNT, (c) indigo-(6,6)CNT dyad and (d) indigo-(6,6)CNT triad.

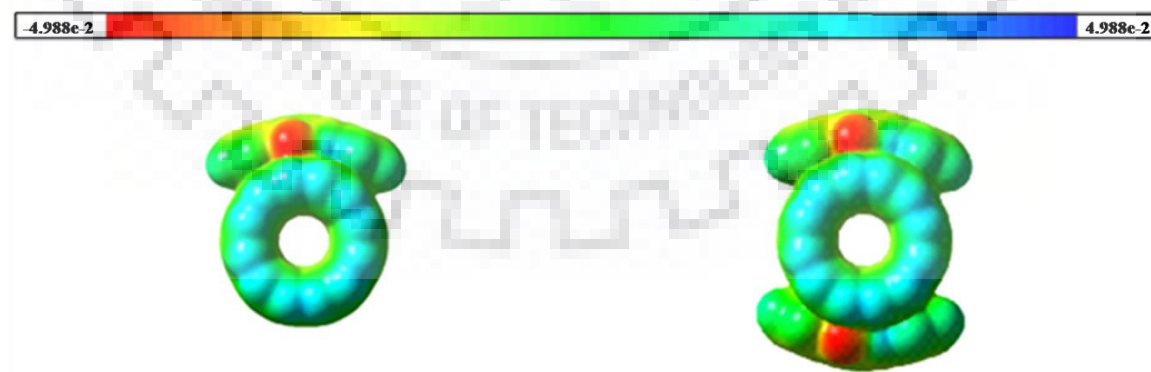


Figure 3.2 Electrostatic potential maps for the indigo-CNT complexes.

of the complexes are depicted in figure 3.3. It can be inferred from the figure that HOMO of the dyad is mainly formed from the molecular orbitals of nanotube, whereas its LUMO is formed from those of both indigo and CNT. A similar observation can be deduced from the frontier orbitals of the triad. The energy gap between HOMO and LUMO ($\Delta E_{\text{HOMO-LUMO}}$) can be correlated to the conductivity of the complex. It is reported that the armchair nanotubes of finite-length ($<100 \text{ \AA}$) have a HOMO-LUMO energy gap of $\sim 1\text{eV}$. [44, 291] Table 3.2 also lists the $\Delta E_{\text{HOMO-LUMO}}$ for indigo, CNT and their complexes. The HOMO-LUMO energy gap of free indigo is 1.31 eV, which is close to the experimental value of 1.70 eV. [277] The $\Delta E_{\text{HOMO-LUMO}}$ of free CNT is 0.80 eV, which is decreased to 0.76 eV for the dyad. Introducing a molecule of indigo into the dyad does not change the energy gap significantly suggesting that the electronic properties of the nanotube remain the same upon further addition of indigo.

The frontier molecular orbital energy level diagram for free indigo, CNT and their corresponding complexes is depicted in figure 3.3. It suggests that there can be photoexcitation

Table 3.1 The stabilization energy of dyad and triad obtained for different functional at 6-31G(d,p) level. All the energy values are in kcal/mol.

Functional	ΔE_{stab} of dyad		ΔE_{stab} of triad	
	Without BSSE correction	With BSSE correction	Without BSSE correction	With BSSE correction
B97-D	-28.28	-20.47	-56.76 (-28.38)	-41.14 (-20.57)
B3LYP-GD2	-27.85	-19.28	-55.94 (-27.97)	-38.78 (-19.39)
M06-2X	-18.36	-11.01	-37.03 (-18.51)	-22.32 (-11.16)

The values given in the parentheses correspond to respective stabilization energy per indigo.

Table 3.2 The vertical ionization energy (VIE), adiabatic ionization energy (AIE), vertical electron affinity (VEA), adiabatic electron affinity (AEA) and the HOMO-LUMO energy gap for indigo, CNT and their complexes obtained at the B97-D/6-31G(d,p) level. All the energy values are in eV.

System	VIE	AIE	VEA	AEA	$\Delta E_{\text{HOMO-LUMO}}$
Indigo	6.58	6.52 (7.0) ^a	-1.25	-1.38	1.31
CNT	4.93	4.90	-2.15	-2.17	0.80
Dyad	4.88	4.85	-2.20	-2.22	0.76
Triad	4.84	4.82	-2.24	-2.27	0.74

^aExp. value [289]

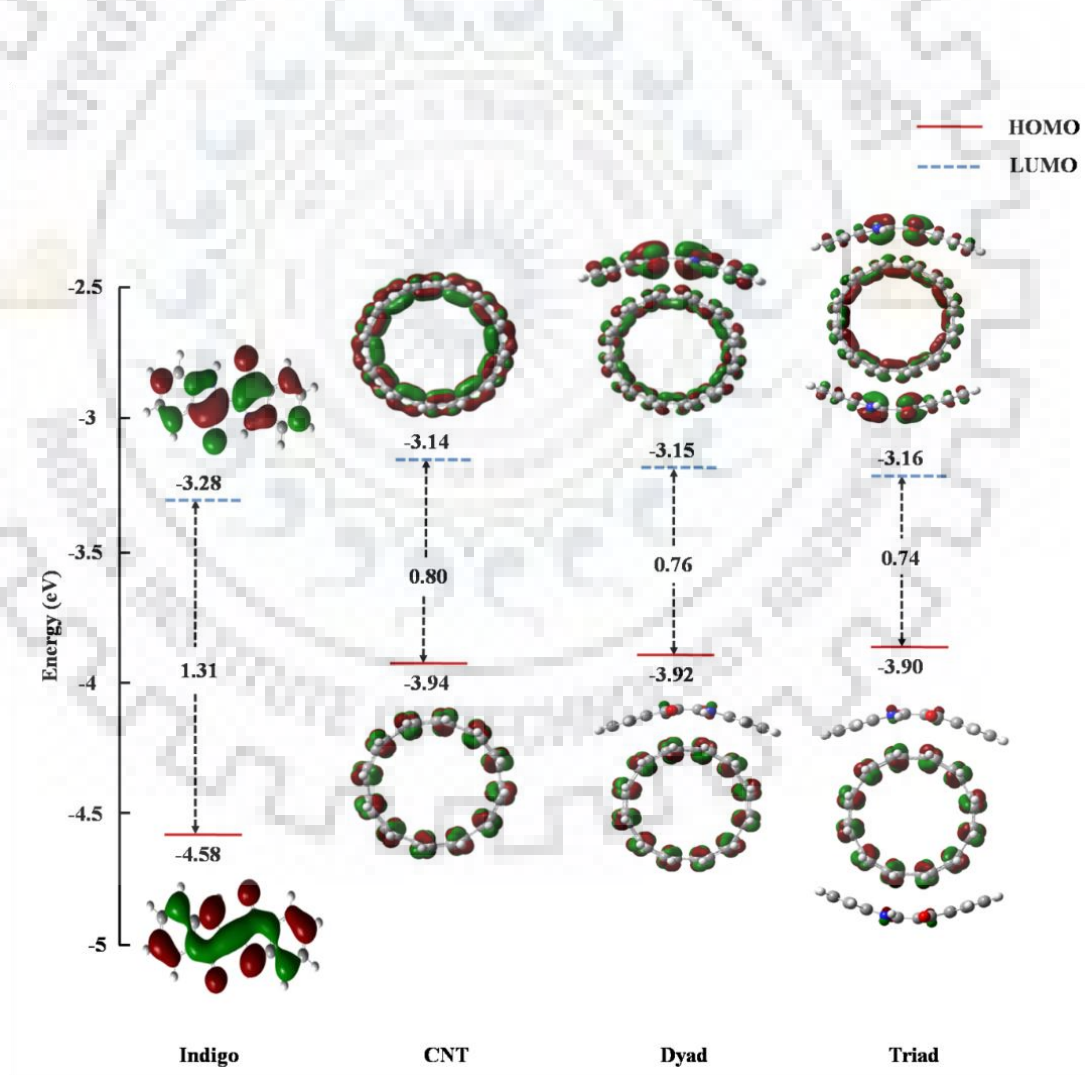


Figure 3.3 The frontier molecular orbitals and the corresponding energy level diagram of indigo, CNT and their complexes.

of an electron from the HOMO of CNT to its LUMO followed by the transfer of that electron to the LUMO of indigo, thereby suggesting the photoinduced charge transfer phenomenon. The charge transfer effects coupled with $\Delta E_{\text{HOMO-LUMO}}$ (about 0.7-0.8 eV) and the absorption in the near-infrared region make the complexes suitable for light absorbing devices such as solar cells,[292] especially in the miniaturized electronic devices.

High charge carrier mobility is one of the prerequisites for a molecule to be exploited in organic transistor devices. The carrier mobility depends on various parameters including transfer integral, reorganization energy, rate constant of charge carrier transport and the centre-to-centre distance between molecules. The calculated values of these parameters are listed in table 3.3, where + and – signs represent hole and electron, respectively. From the table, it can be seen that the values of transfer integral (t) for hole and electron transport in the dyad are 0.11 and 0.03, respectively. In the case of triad, the transfer integral for hole transport is the same as that of dyad. However, for electron transport it is decreased by one-third of the value obtained for dyad. Furthermore, the high values of rate constant and diffusion coefficient for hole transport can be correlated to high value of transfer integral which in turn increases the hole mobility. The distance between molecules affects the diffusion coefficient and hence the mobility. Therefore, carrier mobilities are calculated for two distinct distances between indigo and CNT and are listed in table 3.3. For indigo-CNT dyad in which the components are separated by a distance of 3.16 Å, hole mobility is exceptionally high with a value of 8.94 $\text{cm}^2\text{V}^{-1}\text{s}^{-1}$. Both hole and electron mobilities of the dyad are nearly one order higher than that of the triad. The above results indicate that surface modification of carbon nanotube can alter its transport properties. The higher hole mobility makes these complexes useful for their applications in p-type semiconductor devices.

To understand the effect of length of CNT on the charge transport properties, a relatively long carbon nanotube having a length of 31.55 Å was used. As is evident from table 3.3, the complex so formed shows an enhancement in electron mobility; a trend similar to the conducting behaviour of long armchair carbon nanotubes. Further, to know about edge effects of the tube, we calculated charge transport properties of the complex by capping the carbon nanotube. As can be seen from table 3.3, the electron mobility of the complex of capped carbon nanotube is enhanced seven times relative to that of the complex of uncapped CNT. Unlike electron mobility, hole mobility does not change significantly with respect to the change in length or capping of the tube. However, it should be mentioned that all of the above complexes show a higher hole mobility than electron mobility.

To investigate the effect of orientation of indigo on carbon nanotube, the complex in which indigo is planar and aligned parallel to the tube axis was modelled. Such a planar geometry for

Table 3.3 The calculated parameters of transfer integral (t), internal reorganization energy (λ), rate constant (k), diffusion coefficient (D), and carrier mobility (μ) for the complexes at different distances.

System	Distance (Å)	λ_+ (eV)	t_+ (eV)	k_+ (s ⁻¹)	D_+ (cm ² s ⁻¹)	μ_+ (cm ² V ⁻¹ s ⁻¹)	λ_- (eV)	t_- (eV)	k_- (s ⁻¹)	D_- (cm ² s ⁻¹)	μ_- (cm ² V ⁻¹ s ⁻¹)
Dyad	3.16				0.23	8.94	0.04	0.03	0.40×10^{14}	0.03	1.16
	1.48	0.06	0.11	0.45×10^{15}		1.94				0.01	0.39
Triad	3.05				0.02	0.77				0.03×10^{-1}	0.12
	1.55	0.07	0.11	0.59×10^{14}	0.05×10^{-1}	0.19	0.05	0.01	0.18×10^{13}	0.08×10^{-2}	0.03
Dyad of long CNT	3.15				0.20	7.62				0.18	7.08
	1.43	0.03	0.11	0.42×10^{15}	0.42×10^{-1}	1.65	0.02	0.09	0.39×10^{15}	0.39×10^{-1}	1.54
Dyad of capped CNT	3.12				0.22	8.45				0.21	8.18
	1.49	0.53×10^{-1}	0.22	0.45×10^{15}	0.49×10^{-1}	1.93	0.46×10^{-1}	0.18	0.43×10^{15}	0.48×10^{-1}	1.87
Dyad of planar indigo	3.15	0.06	0.10	0.66×10^{14}	0.33×10^{-1}	1.27	0.05	0.09	0.10×10^{15}	0.50×10^{-1}	1.93

indigo is also expected when it is sandwiched between two carbon nanotubes. This also justifies to some extent the limitation of the present study that does not consider the effect of nearby tubes due to the high computational cost required. The optimized geometry of the above complex in which indigo is aligned parallel to the tube axis is shown in figure 3.4. The charge transport properties of the complex are also listed in table 3.3. Interestingly, electron mobility of this complex is higher than hole mobility. This can be correlated to the direction of electron flow in the carbon nanotube. The above results suggest that the charge transport properties of a complex can be tuned by changing the orientation of adsorbed molecule.

The absorption spectra of constituent molecules and their complexes are determined using the time-dependent density functional theoretical method and are depicted in figure 3.5. The absorption wavelength, oscillator strength and the details of orbitals involved in the electronic transitions having an oscillator strength of more than 10% are listed in table 3.4 of the supplementary information. The molecular orbitals those mainly involved in the electronic transitions are also given in the supplementary information. The absorption maximum (λ_{\max}) of free indigo obtained at 614 nm is in close agreement with the experimental value of 610 nm.[293] The corresponding electronic excitation can be featured as a π - π^* transition (HOMO \rightarrow LUMO). The calculation also predicts a signal of low intensity at 384 nm which is dominated by HOMO-4 to LUMO transition. The absorption spectrum of carbon nanotube exhibits multiple peaks in the visible and near- infrared regions in accordance with the observations reported by Naumov *et al.* on semiconducting CNTs.[294] The prominent peaks for CNT appear at 399 nm, 538 nm, 548 nm and 874 nm. In the absorption spectra of the complexes, the peaks due to indigo are disappeared, probably due to the loss of planarity of indigo upon complex formation. It should be mentioned that in the leuco form (water-soluble form) of indigo, the absorption maximum shifted from 610 nm to 442 nm due to the lack of conjugation owing to non-planarity of the structure.[295] The oscillator strength of the absorption wavelength near 400 nm for CNT is reduced by \sim 30% for each addition of indigo molecule. Similarly, oscillator strength for the absorption of CNT in the near-infrared region is also decreased consistently upon complex formation by \sim 15%. Ultimately, the most intense peak for triad appears in the near-infrared region compared to the ultraviolet region for CNT. Apart from this, a red shift of 10-13 nm is also observed for the peak in the near-infrared region. Although intensity and absorption wavelength of the remaining peaks of CNT are unaltered in the complexes, several new peaks of lower intensity appear in visible region. Unlike bare CNT and indigo, the complexes absorb in a broad range of visible region, making them suitable for solar cell applications.

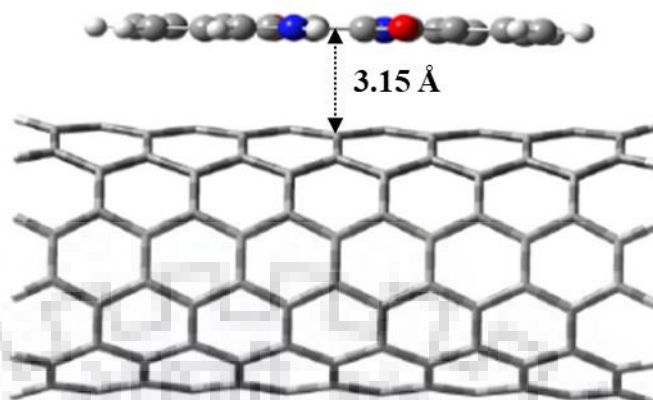


Figure 3.4 Optimized geometry of the complex in which indigo is aligned parallel to the tube-axis.

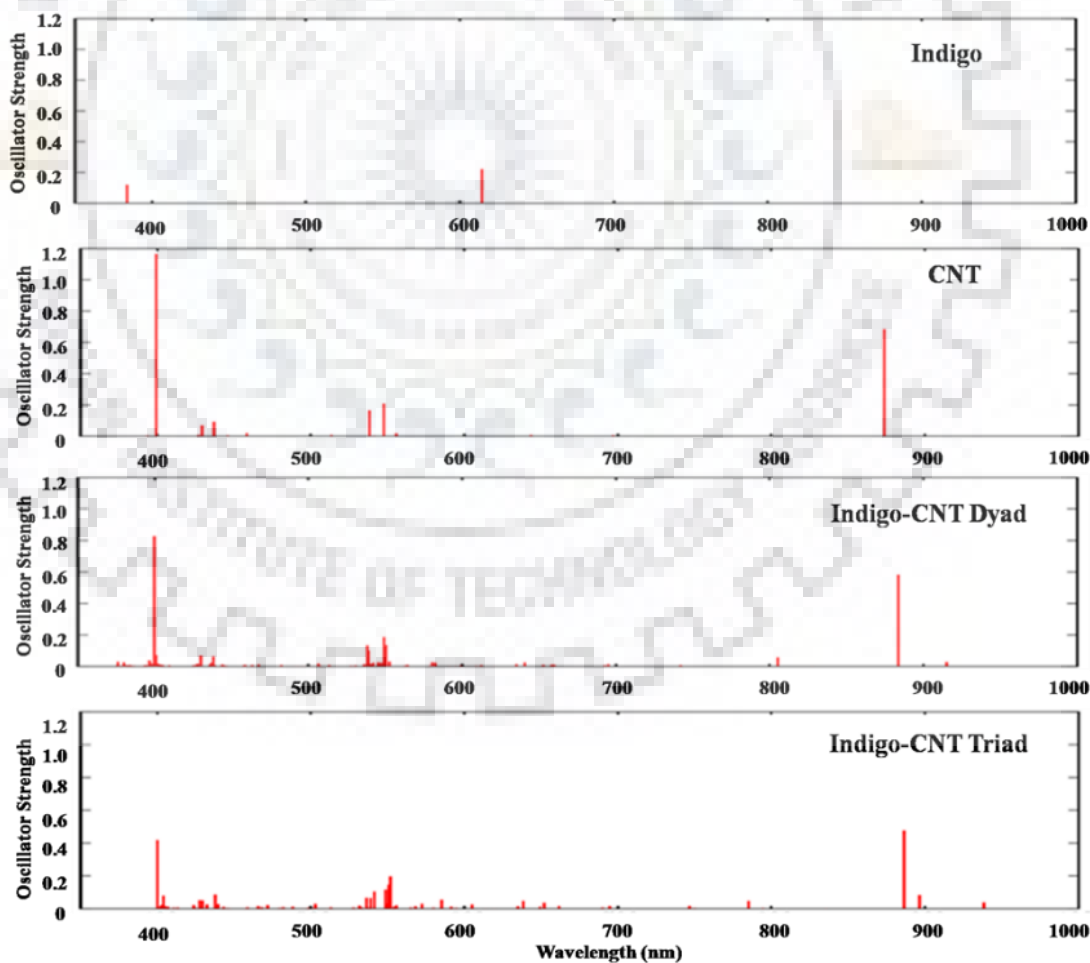
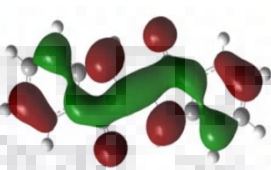
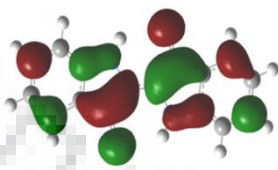
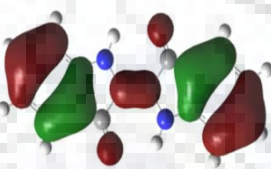
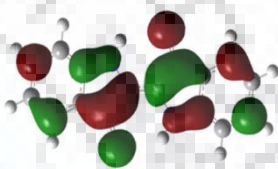


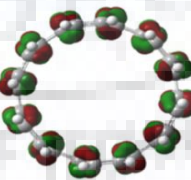
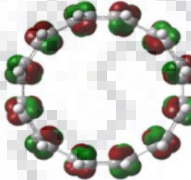

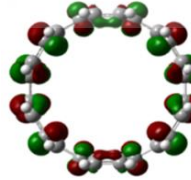
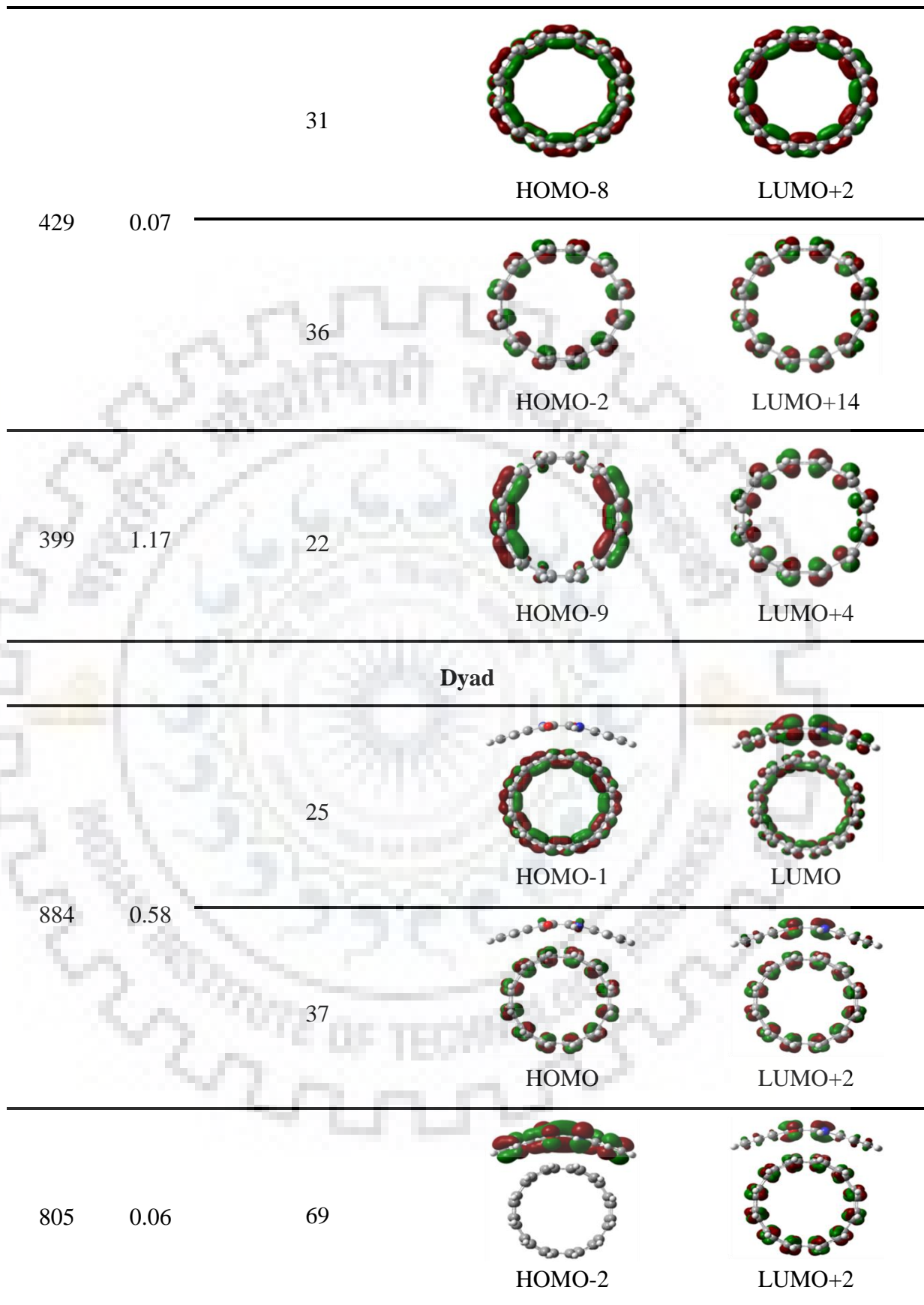
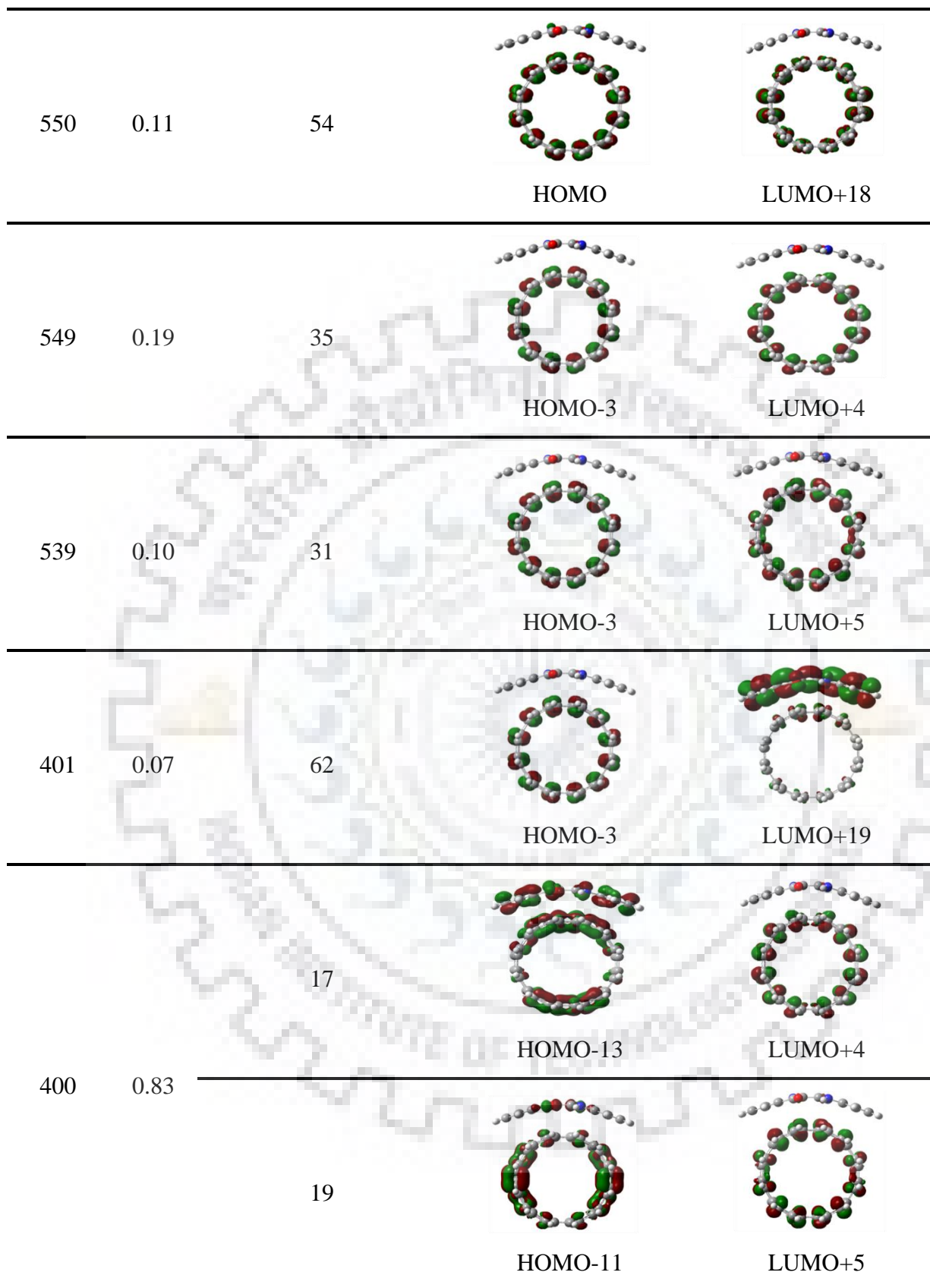


Figure 3.5 The absorption spectra of indigo, CNT and their complexes.

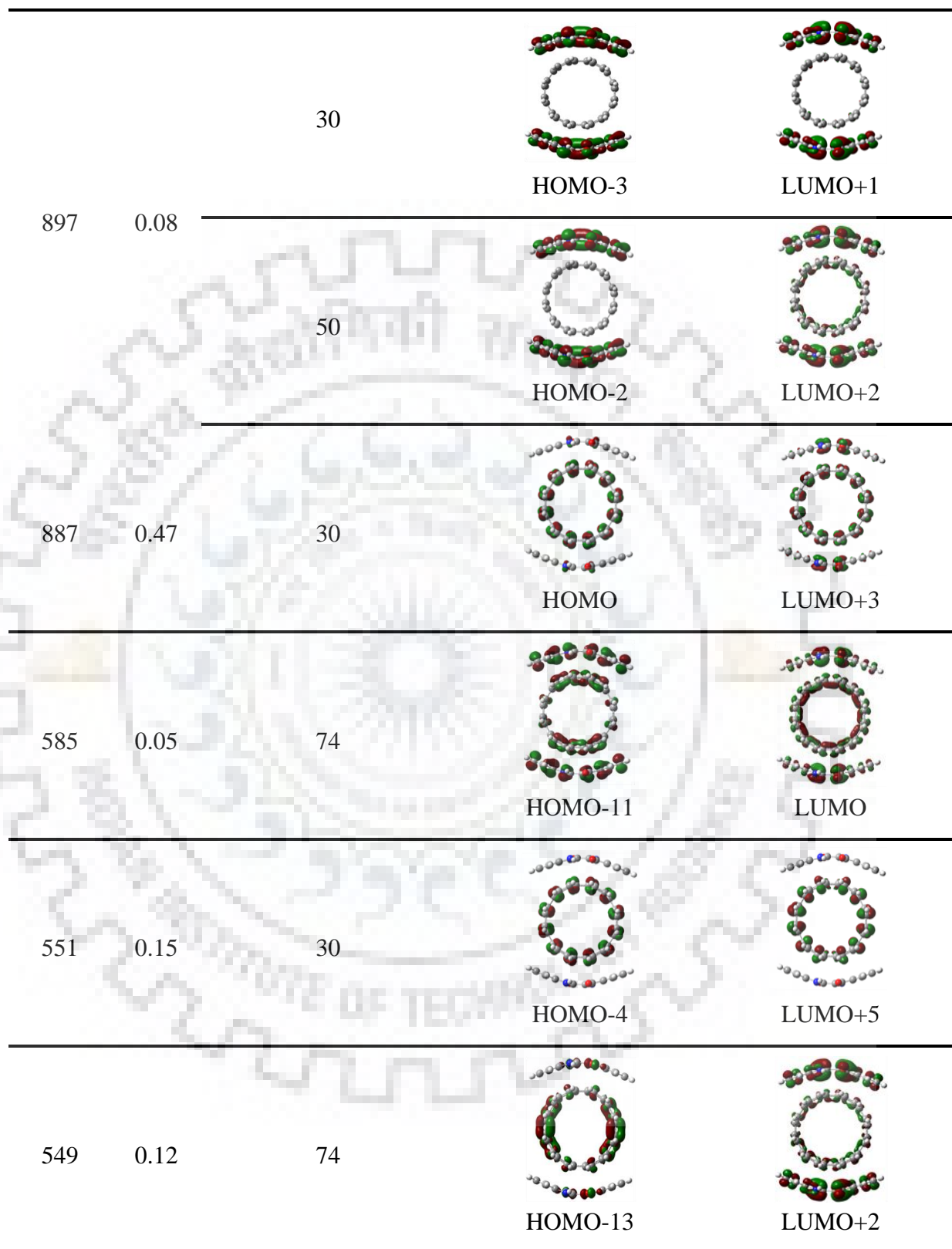
Table 3.4 The calculated values of absorption wavelengths, corresponding oscillator strengths, prominent molecular orbitals involved in transition and the respective percentage contribution for indigo, CNT and their complexes. The isodensity plot of molecular orbitals is also shown.

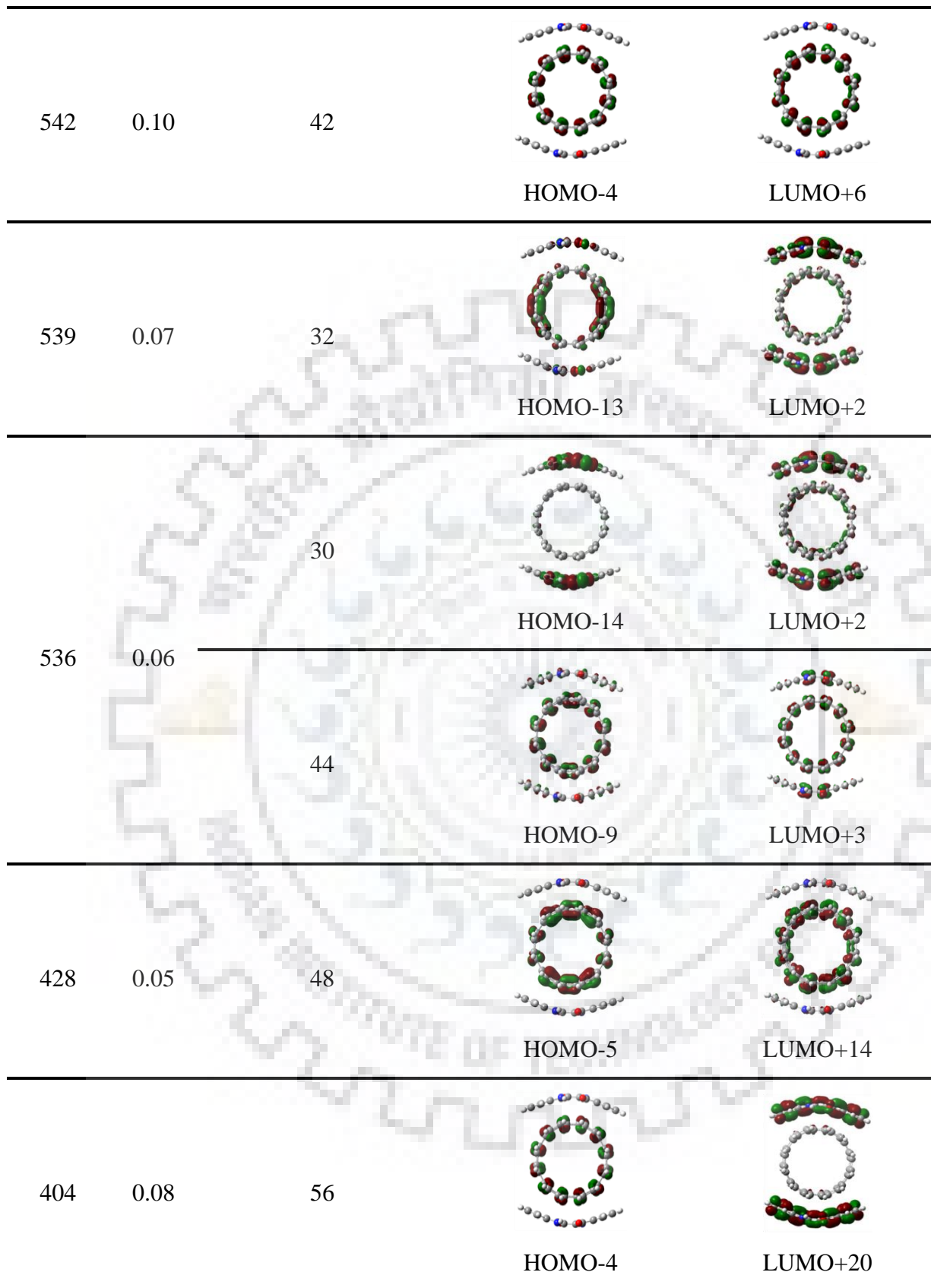
λ (nm)	f	Orbital Contribution (%)	Molecular orbitals involved in the transition	
Indigo				
614	0.22	99		
			HOMO	LUMO
384	0.12	89		
			HOMO-4	LUMO
CNT				
874	0.68	51		
			HOMO-1	LUMO
		46		
			HOMO	LUMO+1
548	0.21	37		
			HOMO-2	LUMO+3

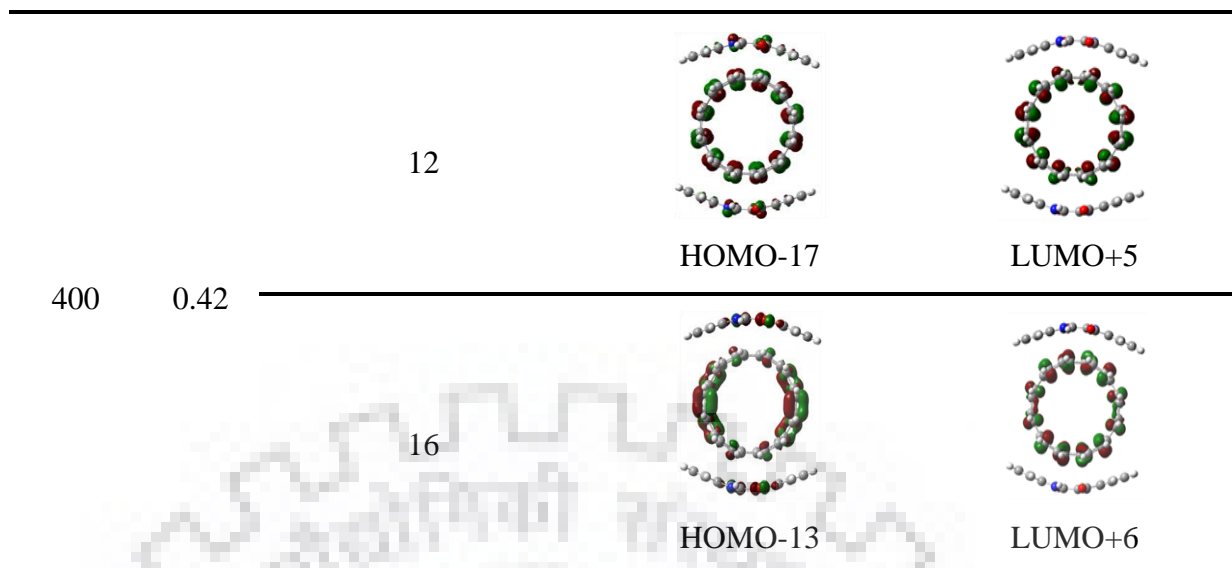




Triad







3.3.2 Endohedral complexes of CNTs with indigo

Figures 3.1 and 3.6 show three different carbon nanotubes *viz.* (6,6), (7,7) and (8,8) of diameter 8.14 Å, 9.49 Å, and 10.84 Å, respectively. The reason for selecting CNTs of varying diameter was to find a suitable host for indigo based on the host-guest interactions. The length of ~17 Å for CNT used is large enough to host indigo inside the cavity along the tube-axis. Figure 3.6 shows the optimized geometries of the complexes indigo@(n,n)CNT (where $n = 6, 7$ and 8). As can be seen from figure 3.6, the geometry of CNTs is squeezed in a direction perpendicular to the tube-axis in the complexes indigo@(6,6)- and (7,7)CNT to facilitate π - π interactions. It is worth mentioning that in a recent molecular dynamic study on the encapsulation of liquid droplets inside CNT, the latter was reported to change its cylindrical shape to a distorted geometry with an increase in the number of droplets.[296] In another study, Wang *et al.* reported a distortion in the structure of CNTs with encapsulation of carbon nanowires.[251] Unlike in indigo@(6,6)CNT, in all other complexes indigo was found to be slightly tilted with respect to the tube-axis, keeping the geometric centres of indigo and CNT coincident with each other. Compared to indigo@(7,7)CNT, for indigo, a larger inclination with respect to the tube-axis was observed inside (8,8)CNT so as to bring the distance between phenyl groups of indigo and (8,8)CNT into the range of π - π stacking. As shown in figure 3.6, the center-to-center distances between indigo and the nearby surface of (6,6), (7,7) and (8,8)CNT are 3.41, 4.67 and 5.40 Å, respectively. The shortest distance between indigo and the nearby surface of (7,7) and (8,8)CNT is 2.97 and 3.04 Å, respectively. It can be seen from the figure that various types of interactions such as π - π , C-H... π and N-H... π exist between the components of all the complexes. The various bond lengths in free indigo as well as those in its respective endo- and exohedral complexes with

CNT were calculated for the B97-D optimized structures and are given in figure A1 of the Appendix-A. Comparison of the bond lengths indicate that there is a significant change in the bond lengths of indigo in its endohedral complex rather than in its exohedral counterpart. Compared to the C-H bond lengths of indigo in free state, those in its endohedral complex has significantly shortened although that remained nearly the same in its exohedral complex. From the optimized geometries of endo- and exohedral complexes of indigo with CNT shown in figures 3.1 and 3.6, it was found that indigo lost its planarity upon exohedral complexation. This indicates a significant change in the bond angles and dihedral angles of indigo in its exohedral complex.

Table 3.5 lists the stabilization energy (ΔE_{stab}) with and without BSSE and ZPE corrections for the abovementioned complexes. As can be deduced from the table, the complexes are energetically stable. From the table, it is evident that the stability of complexes follows the order: indigo@(7,7)CNT > indigo@(8,8)CNT > indigo@(6,6)CNT. From the table, it can be seen that ΔE_{stab} of indigo@(7,7)CNT is only ~2 kcal/mol more than that of indigo@(8,8)CNT, whereas it is ~49 kcal/mol more than that of indigo@(6,6)CNT. Thus, it is found that among CNTs of different diameter, (7,7)CNT of diameter ~9.5 Å is an ideal host for indigo. The lower stabilization for indigo@(6,6)CNT can be accounted due to the repulsive interactions at very short distances between indigo and nearby surface of CNT. From the values listed in table 3.5, a comparison of ΔE_{stab} of indigo@(6,6)CNT with that of indigo wrapped over (6,6)CNT [297] revealed the latter complex to be more stable than the former by ~17 kcal/mol. On the other hand, indigo@(7,7)CNT is stabilized more by ~30 kcal/mol than its exohedral complex in which indigo is wrapped over (7,7)CNT (shown in figure 3.7). A significantly high value of BSSE for indigo@(6,6)CNT arises because of the close proximity between indigo and CNT. As mentioned earlier, the complexes indigo@(n,n)CNT ($n = 6, 7$ and 8) considered in this study are stabilized by cumulative weak interactions such as π - π , C-H... π and N-H... π . To know more about the stabilization of these endohedral complexes, energy decomposition analysis was performed and the contribution of different components of energy (dispersion, electrostatic and induction) was determined using the symmetry adapted perturbation theoretical (SAPT) method [298] and 6-31G basis set as reported in the earlier studies of different non-covalent complexes.[299-301] Various components of interaction energy such as dispersion, electrostatic and induction were determined and their values are listed in table 3.6. All these components were found to stabilize the complexes. It is found that for indigo@(6,6)CNT, the contribution of dispersion energy (56%) is maximum followed by electrostatic energy (37%). A similar trend is observed for indigo@(7,7)CNT with contributions of 69% and 24% for the above components. For indigo@

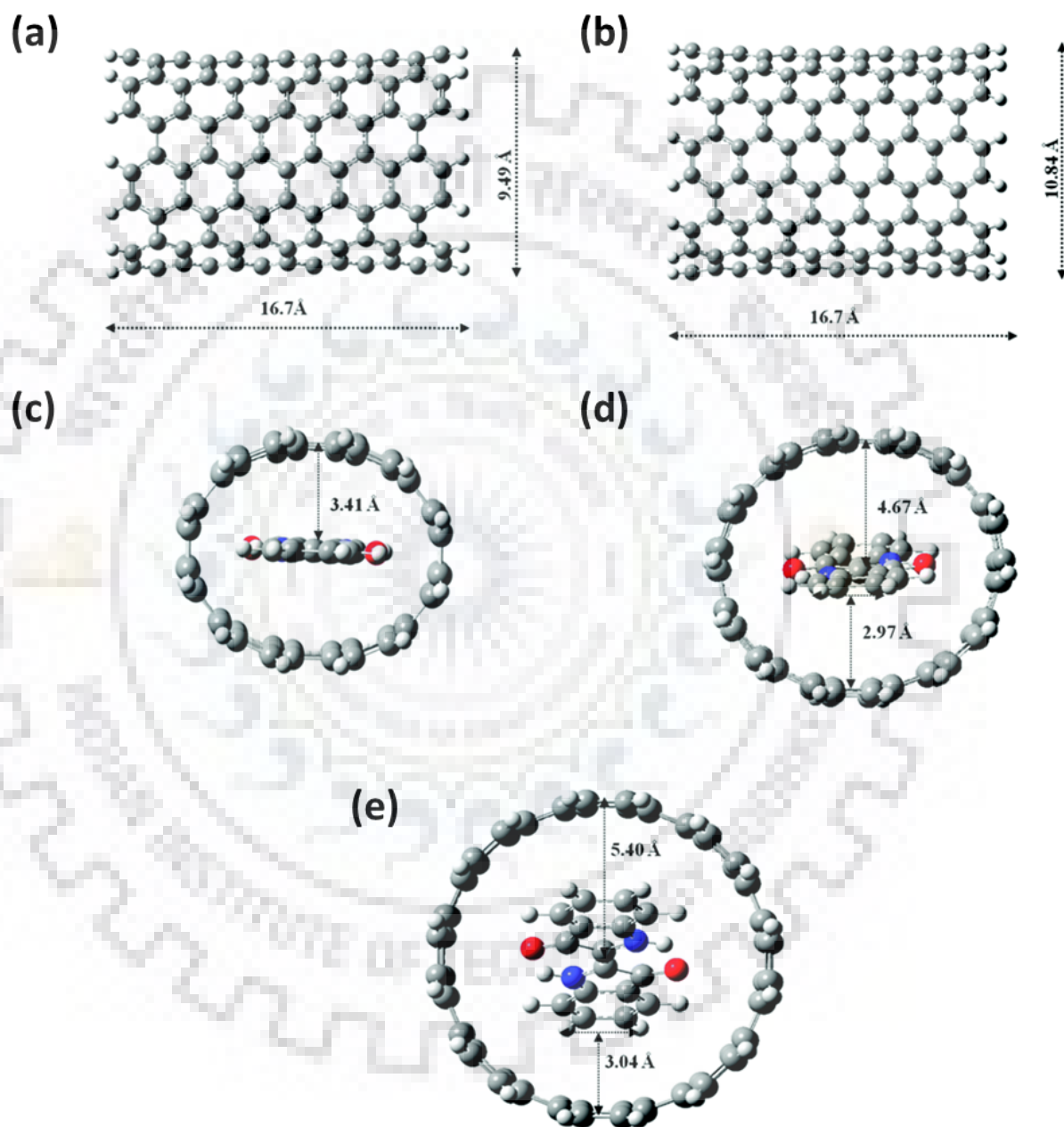


Figure 3.6 Optimized geometries of (a) (7,7)CNT, (b) (8,8)CNT and (c-e) the respective complexes indigo@(n,n)CNT, where $n = 6-8$ obtained at B97-D/6-31G(d,p) level.

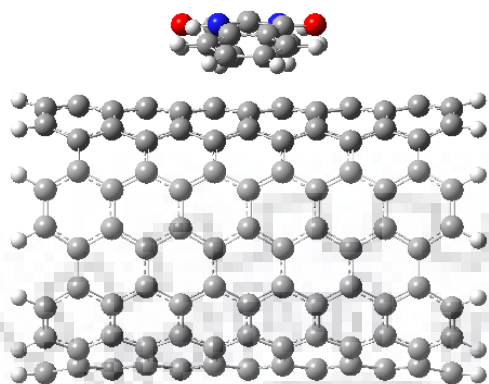


Figure 3.7 Optimized geometry of the exohedral complex of indigo with (7,7)CNT obtained at B97-D/6-31G(d,p) level of theory.

Table 3.5 Calculated stabilization energy of the complexes with and without basis set superposition error (BSSE) and zero-point energy (ZPE) corrections at B97-D/6-31G(d, p) level. All the energy values are in kcal/mol.

Complex	Without BSSE Correction	With BSSE Correction	With ZPE and BSSE corrections
Indigo-(6,6)CNT dyad	-28.28	-20.47	-19.25
Indigo-(7,7)CNT dyad	-29.78	-21.97	-20.93
Indigo@(6,6)CNT	-28.47	-4.84	-2.08
Indigo@(7,7)CNT	-66.80	-52.48	-50.76
Indigo@(8,8)CNT	-61.16	-50.60	-48.33

(8,8)-CNT, dispersion energy contributes 68% while electrostatic energy contributes 24%. Based on the above discussion, it can be concluded that the dispersion interaction is maximum for indigo@(7,7)CNT, the most stable among the complexes studied. The electronic properties such as ionization energy (IE) and electron affinity (EA) were computed for free indigo, CNTs and their complexes as discussed earlier and are listed in table 3.7. From the table, it can be seen that both IE and EA decrease with an increase in the diameter of CNT in agreement with the trend reported earlier.[302] On encapsulating indigo inside a CNT, only a negligible change in IE and EA is observed with respect to those of free CNTs. The values of IE and EA for indigo@(6,6)CNT are also found to be close to those of its exohedral complex. The frontier molecular orbital (FMO) diagrams of the complexes considered are depicted in figure 3.8. From the figure, it is clear that the electron density for highest occupied molecular orbital (HOMO) and lowest unoccupied molecular orbital (LUMO) of the complexes is localized over CNT without any contribution from indigo, suggesting that the complexes do not exhibit photoinduced charge transfer. Table 3.7 also lists the values of the energy gap between HOMO and LUMO ($\Delta E_{\text{HOMO-LUMO}}$) for all the systems studied. As can be seen from the table, CNTs show a $\Delta E_{\text{HOMO-LUMO}}$ in the range of 0.80-0.94 eV. Compared to this, a slight decrease in $\Delta E_{\text{HOMO-LUMO}}$ is observed for the complexes. The $\Delta E_{\text{HOMO-LUMO}}$ of ~ 1 eV for the complexes indicates that they can be used as narrow energy gap semiconductors.

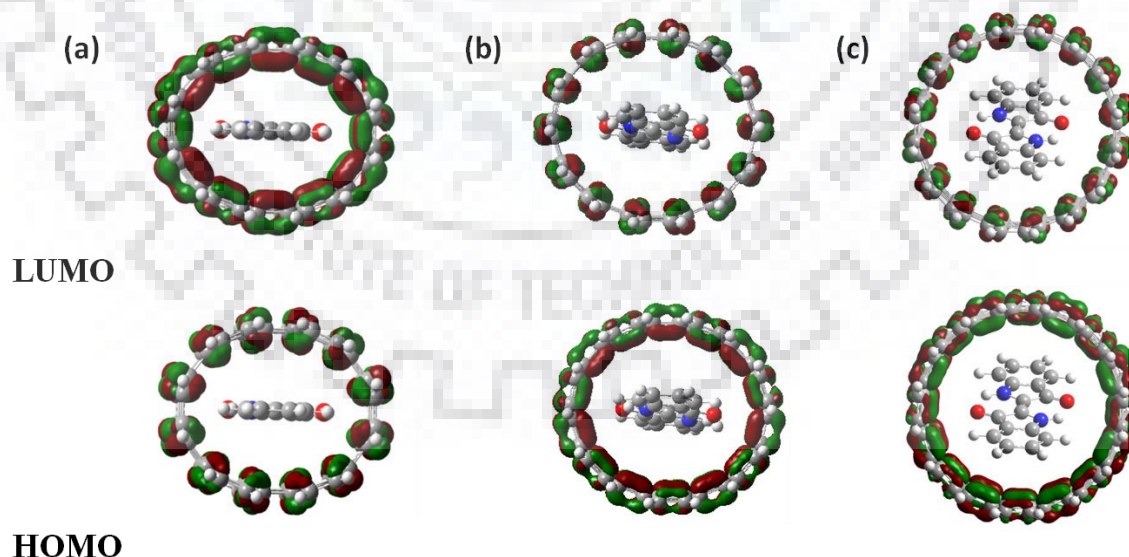


Figure 3.8 The frontier molecular orbitals of the complexes (a) indigo@(6,6)CNT (b) indigo@(7,7) CNT and (c) indigo@(8,8)CNT obtained at B97-D/6-31G(d,p) level.

Table 3.6 Percentage contribution of various interaction energy components (dispersion, electrostatic and induction) for the exo- and endohedral complexes of indigo with CNTs.

Complex	Dispersion	Electrostatic	Induction
Indigo-(6,6)CNT dyad	62	32	6
Indigo@(6,6)CNT	56	37	7
Indigo@(7,7)CNT	69	24	7
Indigo@(8,8)CNT	68	24	8

Table 3.7 Calculated values of ionization energy (IE), electron affinity (EA), energy of HOMO and LUMO orbitals (E_{HOMO} , E_{LUMO}) and their energy gap ($\Delta E_{\text{HOMO-LUMO}}$) for various systems obtained at B97-D/6-31G(d, p). All the energy values are in eV.

System	VIE	AIE	VEA	AEA	E_{HOMO}	E_{LUMO}	$\Delta E_{\text{HOMO-LUMO}}$
Indigo	6.58	6.52	-1.25	-1.38	-4.58	-3.28	1.30
(6,6)CNT	4.93	4.90	-2.15	-2.17	-3.94	-3.14	0.80
(7,7)CNT	4.90	4.88	-2.20	-2.21	-4.00	-3.11	0.89
(8,8)CNT	4.89	4.88	-2.24	-2.26	-4.04	-3.10	0.94
Indigo@(6,6)CNT	4.90	4.87	-2.14	-2.19	-3.92	-3.15	0.77
Indigo@(7,7)CNT	4.89	4.86	-2.18	-2.20	-3.97	-3.10	0.87
Indigo@(8,8)CNT	4.88	4.86	-2.23	-2.25	-4.02	-3.09	0.93

Charge transport parameters such as reorganization energy, transfer integral, rate of charge transfer and carrier mobility are of utmost importance in assessing the performance of organic field-effect transistors and organic light-emitting diodes.[303, 304] The hole reorganization energy (λ_+) and the electron reorganization energy (λ_-) for indigo, CNTs and their complexes were calculated and are listed in table 3.8. From the table, it is clear that the reorganization energy of the complexes is slightly higher than free components, in general. For all the complexes, the value of reorganization energy clearly indicates a relatively higher λ_+ than λ_- . As evident from the table, both λ_+ and λ_- decrease with an increase in the diameter of CNT. However, all the complexes show a lower value of λ_+ than λ_- , irrespective of the diameter of CNT. The small values of reorganization energy of complexes are advantageous in that they decrease the possibility of charge recombination during the charge transport process.[305-308] In addition to the reorganization energy, the intermolecular transfer integral for holes and electrons is also a crucial parameter which affects the rate of hole and electron transfer. It can be seen from table 3.9 that the values of transfer integral (t) and rate constant (k) for the complexes decrease with an increase in the diameter of CNT. One can also see from the table that the carrier mobilities are calculated for center-to-center distance of 3.41 Å between indigo and the nearest surface of (6,6)CNT. For other complexes, owing to the tilted orientation of indigo, carrier mobilities are calculated for two different distances (shown in figure 3.6). The carrier mobilities (μ_+ and μ_-) presented in table 3.9 follow the same trend as those of transfer integral (t_+ and t_-) with increase in the diameter of CNT. Among the complexes studied, indigo@(6,6)CNT has maximum μ_+ and μ_- (8.025 and 9.768 $\text{cm}^2\text{V}^{-1}\text{s}^{-1}$, respectively). Irrespective of the diameter of CNT, all the complexes exhibit a value of μ_- slightly higher than the respective value of μ_+ . The ratio of hole and electron mobility for the complexes is close to that of indigo [309] and differs largely from that of pristine CNT.[310] Thus, it can be inferred that unlike electronic properties, transport properties of CNT are significantly altered on encapsulating indigo. It is also observed that the transport properties of endohedral complexes considered in this study are significantly different from those of exohedral complex, wherein the hole mobility was higher than the electron mobility.[297] It is worth mentioning that a much lower number of compounds have been reported that exhibit higher electron mobility than hole mobility,[311, 312] showing the importance of endohedral complexes of indigo with CNTs.

The optical absorption spectra of indigo, (7,7)CNT and indigo@(7,7)CNT were obtained using the time-dependent density functional theoretical method and are depicted in figure 3.9. It can be seen from the figure that indigo absorbs strongly in the visible region of electromagnetic spectrum. The absorption spectrum of CNT spreads in the near ultraviolet- visible-near infrared

Table 3.8 Calculated values of hole and electron reorganization energy (λ_+ and λ_-) for free indigo, CNTs and their complexes at B97-D/6-31G(d,p) level.

System	λ_+ (eV)	λ_- (eV)
Indigo	0.197	0.272
(6,6)CNT	0.051	0.038
(7,7)CNT	0.028	0.033
(8,8)CNT	0.029	0.027
Indigo@(6,6)CNT	0.047	0.040
Indigo@(7,7)CNT	0.038	0.033
Indigo@(8,8)CNT	0.032	0.029

Table 3.9 Calculated values of the transfer integral (t), internal reorganization energy (λ), rate constant (k) and carrier mobility (μ) for the complexes at different distances (d) obtained at B97-D/6-31G(d,p).

Complex	Distance (Å)	λ_+ (eV)	t_+ (eV)	k_+ (s ⁻¹)	μ_+ [cm ² V ⁻¹ s ⁻¹]	λ_- (eV)	t_- (eV)	k_- (s ⁻¹)	μ_- [cm ² V ⁻¹ s ⁻¹]
Indigo@(6,6)CNT	3.41	0.047	0.085	35.449×10^{13}	8.025	0.040	0.087	43.145×10^{13}	9.768
	4.67				7.644				8.918
Indigo@(7,7)CNT	2.97	0.038	0.055	18.002×10^{13}	3.092	0.033	0.056	21.022×10^{13}	3.067
	5.40				2.556				3.323
Indigo@(8,8)CNT	3.04	0.032	0.024	3.973×10^{13}	0.812	0.029	0.029	5.852×10^{13}	1.053

regions of the spectrum with a maximum absorption at ~425 nm. Compared to the absorption spectrum of free CNT, that of the complex has several peaks in visible region and the most intense peak of the complex lies in near-infrared region. The absorption in near-infrared region makes the complex suitable as a heat absorber.[313] For the above complex, absorption wavelength (λ), oscillator strength (f), molecular orbitals involved in the electronic transitions and their percentage contributions are listed in table 3.10 and are further analysed. Only those transitions for which the oscillator strength and the orbital contribution are greater than 0.05 and 25%, respectively, are considered in this analysis. From the table, one can see that the maximum absorption for the complex occurs at 934 nm with an oscillator strength of 0.56, the transition associated with the molecular orbitals HOMO-1 \rightarrow LUMO (orbital contribution of 46%) and HOMO \rightarrow LUMO+2 (orbital contribution of 33%). It is evident that the former one with more orbital contribution is not associated with photoinduced charge transfer phenomena as the electron density of the corresponding molecular orbitals is localized only on CNT. However, the latter is a charge transfer transition as the electron density of HOMO is located on CNT and that of LUMO+2 is located on indigo. The next intense absorption occurs at a wavelength of 427 nm with an oscillator strength of 0.33 and does not belong to any charge transfer transition. The examination of the molecular orbitals associated with other electronic transitions indicated the presence of several charge transfer transitions in visible (423, 587 and 591 nm) region emphasizing the importance of these complexes in organic solar cell devices.[314]

In order to study the effect of density functionals on the structural, energetic, electronic, charge transport and optical properties of the complexes, these properties were also calculated using the hybrid functional B3LYP-GD3 for the most stable complex indigo@(7,7)CNT. The optimized geometry of the complex is depicted in figure 3.10, in which the shape of indigo is slightly distorted. The computed value of ΔE_{stab} after incorporating BSSE and ZPE corrections for indigo@(7,7)CNT was found to be -50.27 kcal/mol, which is very close to that obtained for B97-D functional. From the values listed in table 3.11 for B3LYP-GD3 and table 3.7 for B97-D, it can be observed that a change in functional does not significantly affect the values of IE and EA. However, $\Delta E_{\text{HOMO-LUMO}}$ calculated using the B3LYP-GD3 functional is relatively higher than that obtained for B97-D functional by ~0.7 eV. Although the carrier mobilities obtained using the B3LYP-GD3 functional are lower than those obtained for B97-D functional, in both cases, electron mobility is higher than hole mobility as reflected from the values listed in table 3.9 for B97-D and in table 3.12 for B3LYP-GD3. The computed hole mobility for the complex is found to be close to hole mobility of carbon nanotube-C₆₀ bi-layer system.[315] The absorption spectra of indigo@(7,7)CNT and its components obtained at the B3LYP-GD3/6-31G(d,p) level are

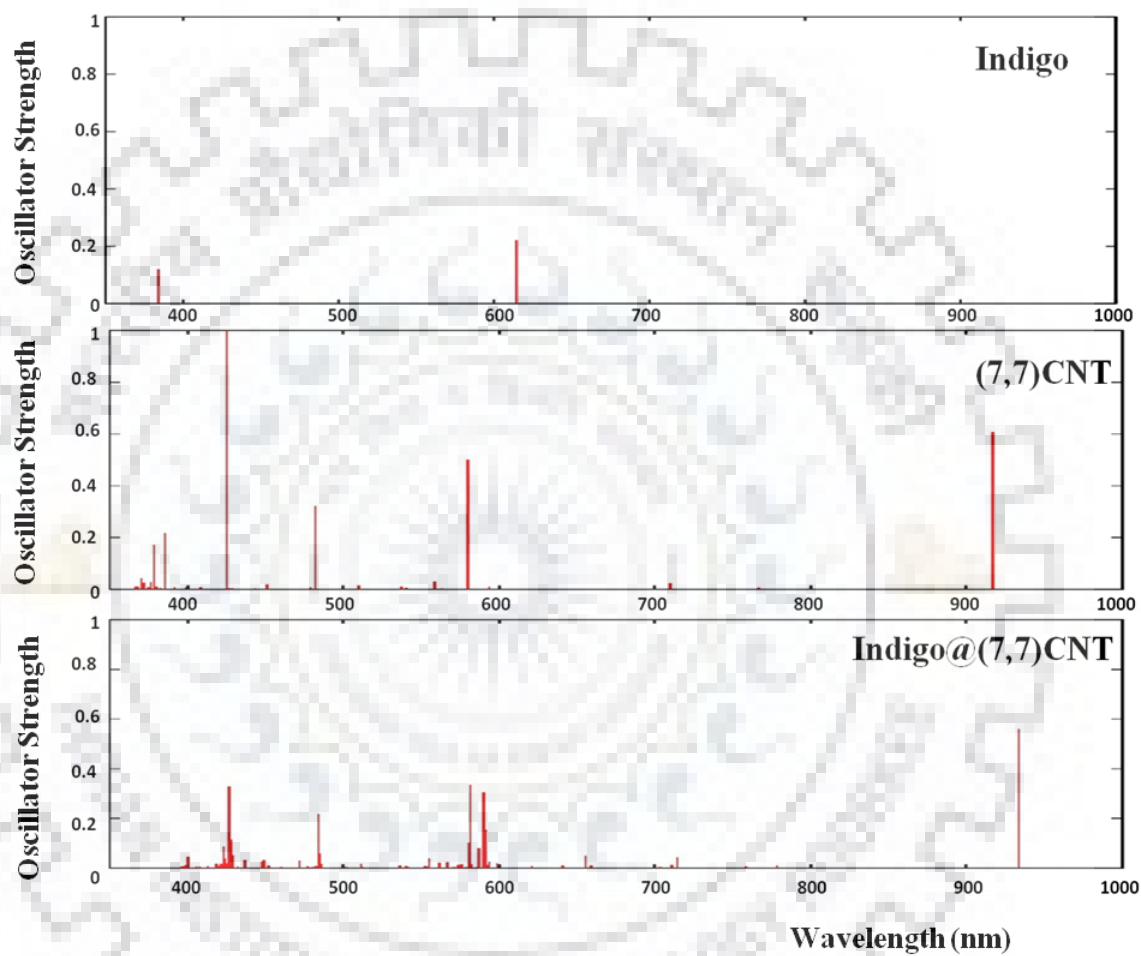
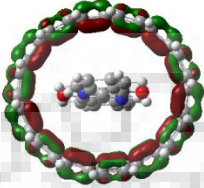
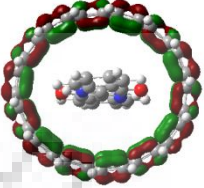
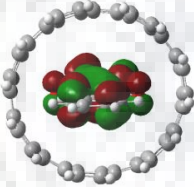
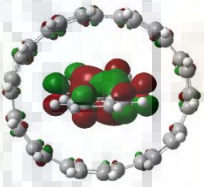
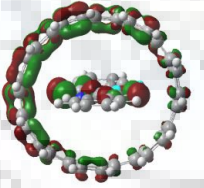
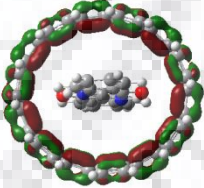
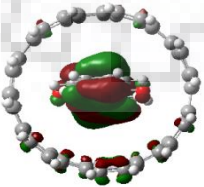
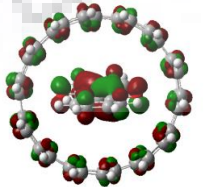
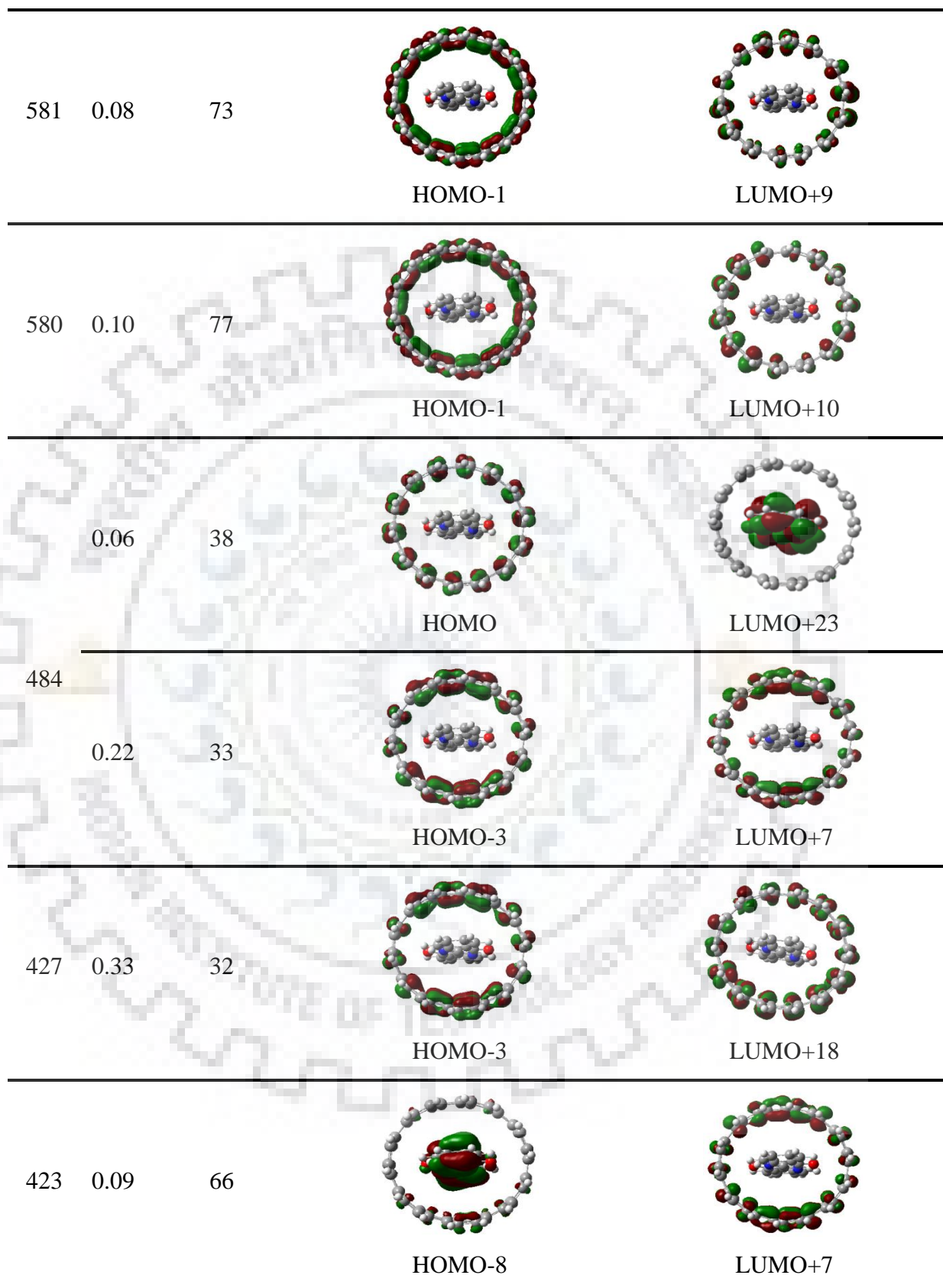


Figure 3.9 The optical absorption spectra of indigo, (7,7)CNT and their complex indigo@(7,7)CNT obtained at B97-D/6-31G(d,p) level.

Table 3.10 The absorption wavelength (λ), oscillator strength (f), corresponding electronic transitions, percentage contribution and molecular orbitals involved for the complex indigo@(7,7)CNT obtained at B97-D/6-31G(d,p).

λ (nm)	f	% Orbital contribution	Molecular orbitals involved in the transition	
934	0.56	46	 HOMO-1	 LUMO
656	0.05	45	 HOMO-2	 LUMO+1
591	0.15	27	 HOMO-9	 LUMO
587	0.08	49	 HOMO-8	 LUMO+2



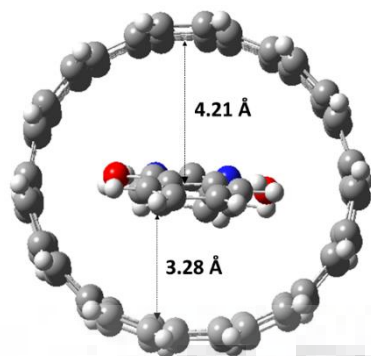


Figure 3.10 Optimized geometry of the complex indigo@(7,7)CNT obtained at B3LYP-GD3/6-31G(d,p) level of theory.






Table 3.11 Computed values of ionization energy (IE), electron affinity (EA), energy of HOMO and LUMO orbitals (E_{HOMO} , E_{LUMO}) and their energy gap ($\Delta E_{\text{HOMO-LUMO}}$) for indigo, (7,7)CNT and their complex obtained at B3LYP-GD3/6-31G(d,p) level. All the energy values are in eV.

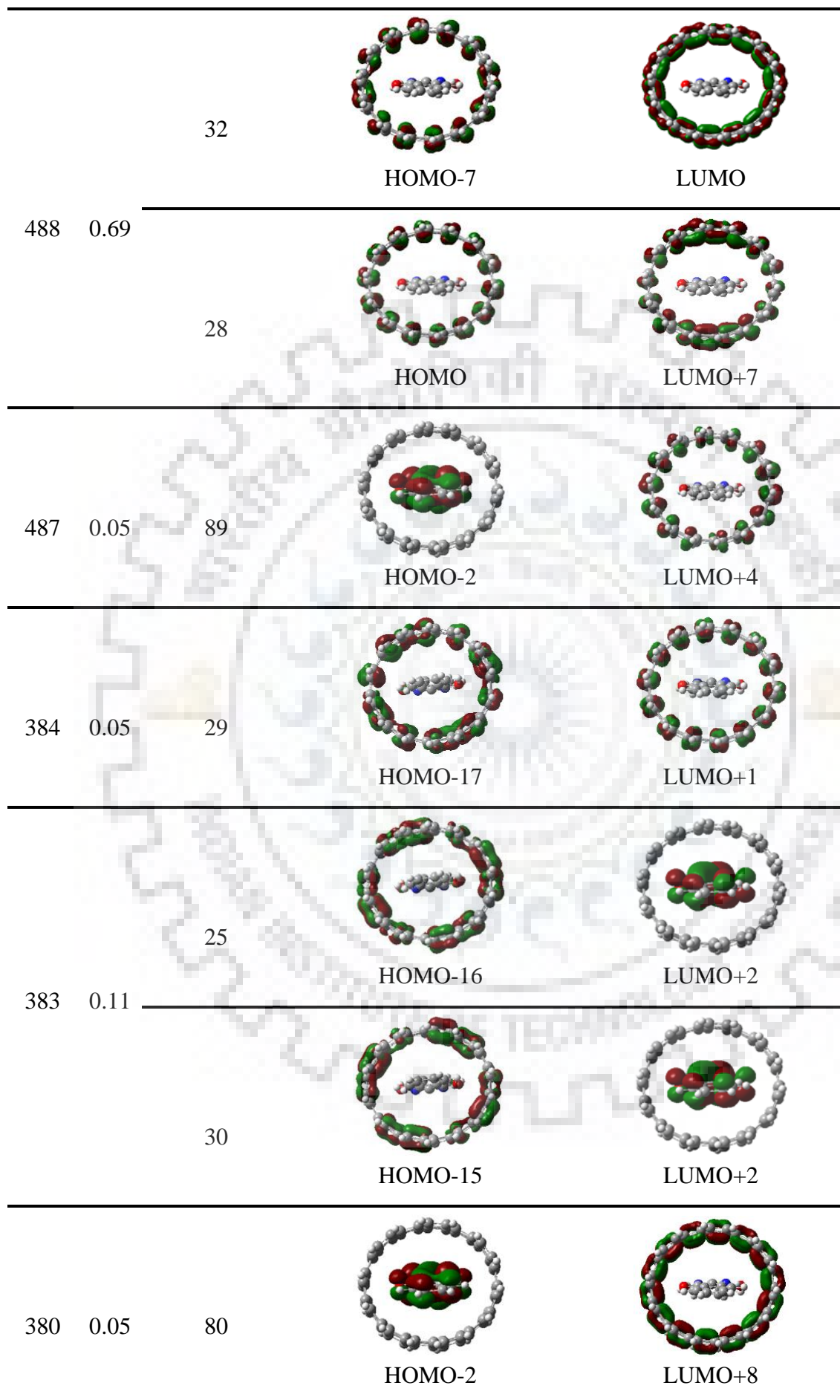
System	VIE	AIE	VEA	AEA	E_{HOMO}	E_{LUMO}	$\Delta E_{\text{HOMO-LUMO}}$
Indigo	6.77	6.68	-1.25	-1.42	-5.27	-2.77	2.51
(7,7)CNT	5.07	5.04	-2.09	-2.12	-4.35	-2.80	1.55
Indigo@(7,7)CNT	5.04	5.01	-2.08	-2.10	-4.33	-2.79	1.54

Table 3.12 Calculated values of the transfer integral (t), internal reorganization energy (λ), rate constant (k) and carrier mobility (μ) for the most stable complex indigo@(7,7)CNT at different distances (d) obtained at B3LYP-GD3/6-31G(d,p) level.

Method	d (Å)	λ_+ (eV)	t_+ (eV)	k_+ (s^{-1})	μ_+ [cm^2 $\text{V}^{-1}\text{s}^{-1}$]	λ_- (eV)	t_- (eV)	k_- (s^{-1})	μ_- [cm^2 $\text{V}^{-1}\text{s}^{-1}$]
B3LYP-GD3	4.21				0.895				1.401
		0.059	0.061	2.299×10^{13}		0.053	0.061	4.070×10^{13}	
	3.28				0.544				0.851

Table 3.13 The absorption wavelength (λ), oscillator strength (f), corresponding electronic transitions, percentage contribution and molecular orbitals involved for the complex indigo@(7,7)CNT obtained at B3LYP-GD3/6-31G(d,p) level.

λ (nm)	f	% Orbital contribution	Molecular orbitals involved in the transition	
751	0.78	48		
			HOMO-1	LUMO
		49		
			HOMO	LUMO+1
562	0.08	77		
			HOMO-2	LUMO+2
495	0.66	32		
			HOMO-6	LUMO
		26		
			HOMO	LUMO+6



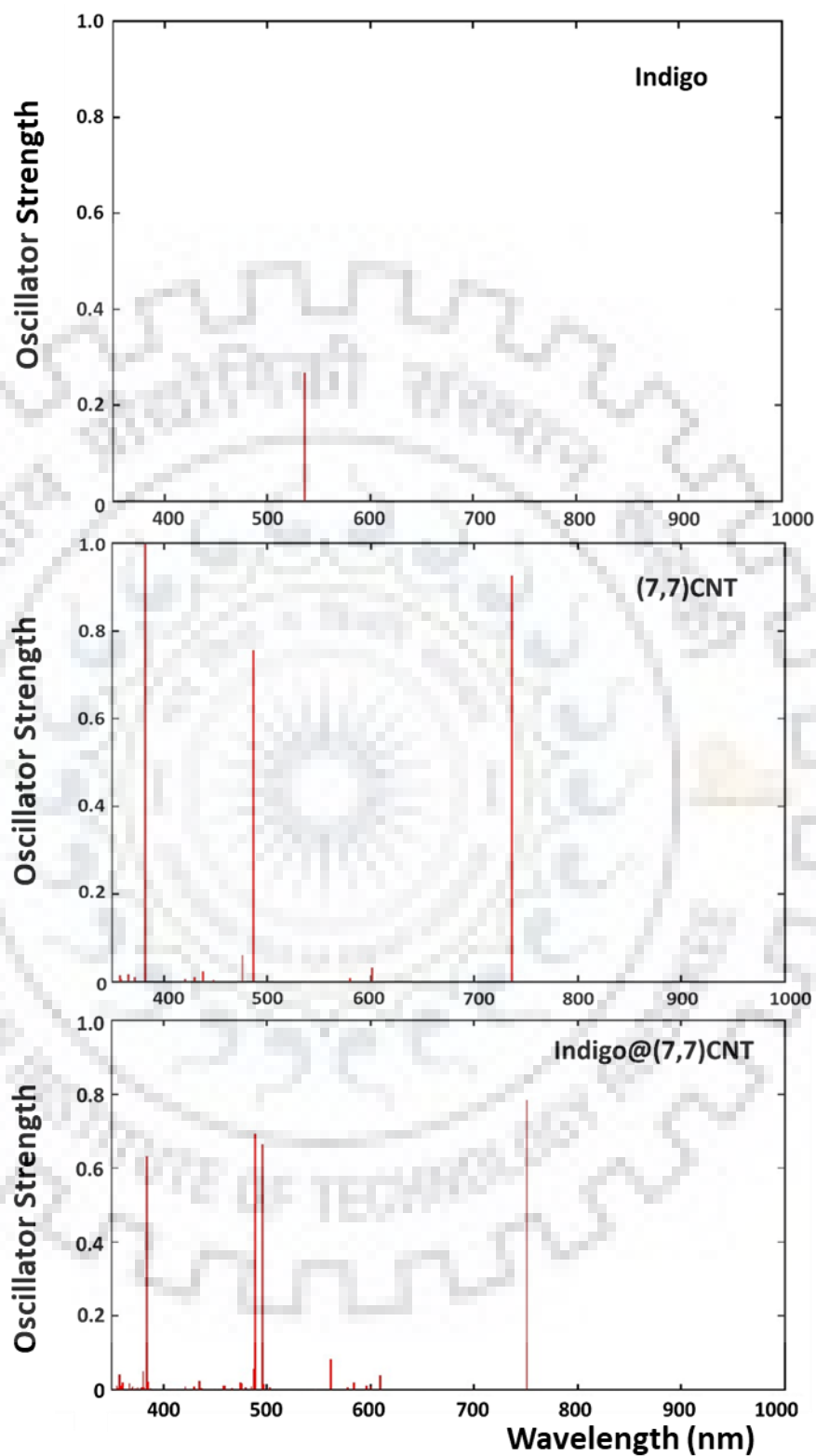


Figure 3.11 The optical absorption spectra of indigo, (7,7)CNT and the complex indigo@(7,7)CNT obtained at B3LYP-GD3/6-31G(d,p) level.

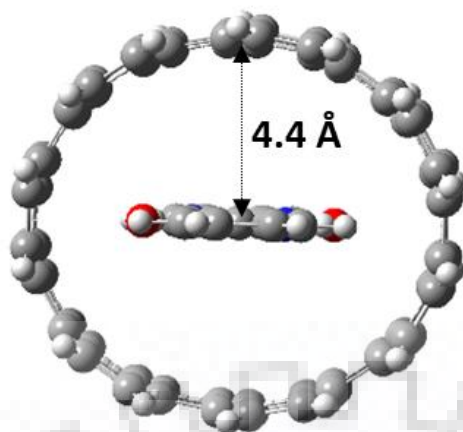


Figure 3.12 Optimized geometry of the complex indigo@(7,7)CNT obtained at ω B97X-D/6-31G(d,p) level.

Table 3.14 Computed values of ionization energy (IE), electron affinity (EA), energy of HOMO and LUMO orbitals (E_{HOMO} , E_{LUMO}) and their energy gap ($\Delta E_{\text{HOMO-LUMO}}$) for indigo, (7,7)CNT and their complex obtained at ω B97X-D/6-31G(d,p) level. All the energy values are in eV.

System	VIE	AIE	VEA	AEA	E_{HOMO}	E_{LUMO}	$\Delta E_{\text{HOMO-LUMO}}$
Indigo	6.98	6.81	-1.24	-1.43	7.10	1.09	6.01
(7,7)CNT	5.02	4.38	-2.34	-2.99	-5.16	-2.19	2.97
Indigo@(7,7)CNT	5.51	5.49	-1.80	-1.86	-5.65	-1.67	3.98

Table 3.15 Calculated values of the transfer integral (t), internal reorganization energy (λ), rate constant (k) and carrier mobility (μ) for the most stable complex indigo@(7,7)CNT at different distances (d) obtained at ω B97X-D/6-31G(d,p) level.

Method	d (Å)	λ_+ (eV)	t_+ (eV)	k_+ (s^{-1})	μ_+ [cm^2 $\text{V}^{-1}\text{s}^{-1}$]	λ_- (eV)	t_- (eV)	k_- (s^{-1})	μ_- [cm^2 $\text{V}^{-1}\text{s}^{-1}$]
ω B97X-D	4.40	0.131	0.060	1.080×10^{12}	0.041	0.122	0.076	2.619×10^{12}	0.098

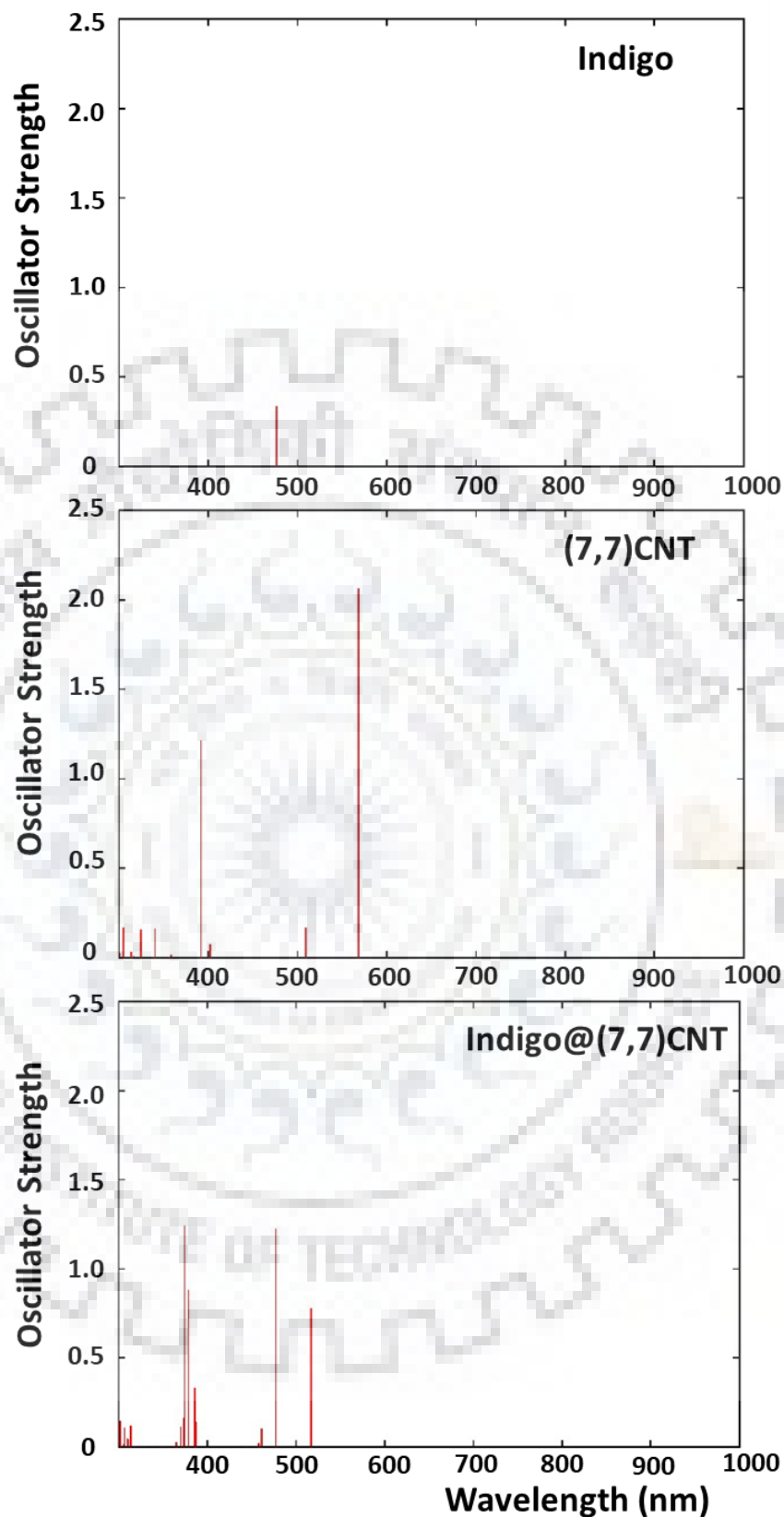
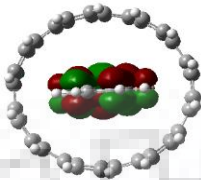
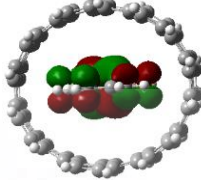

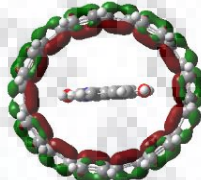
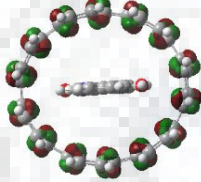
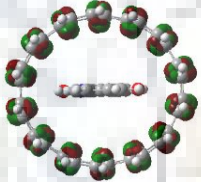
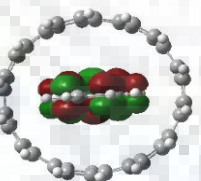
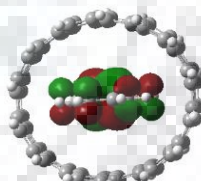
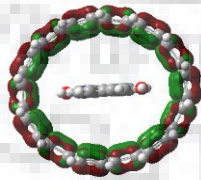


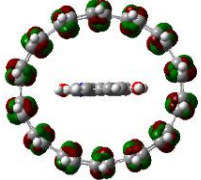
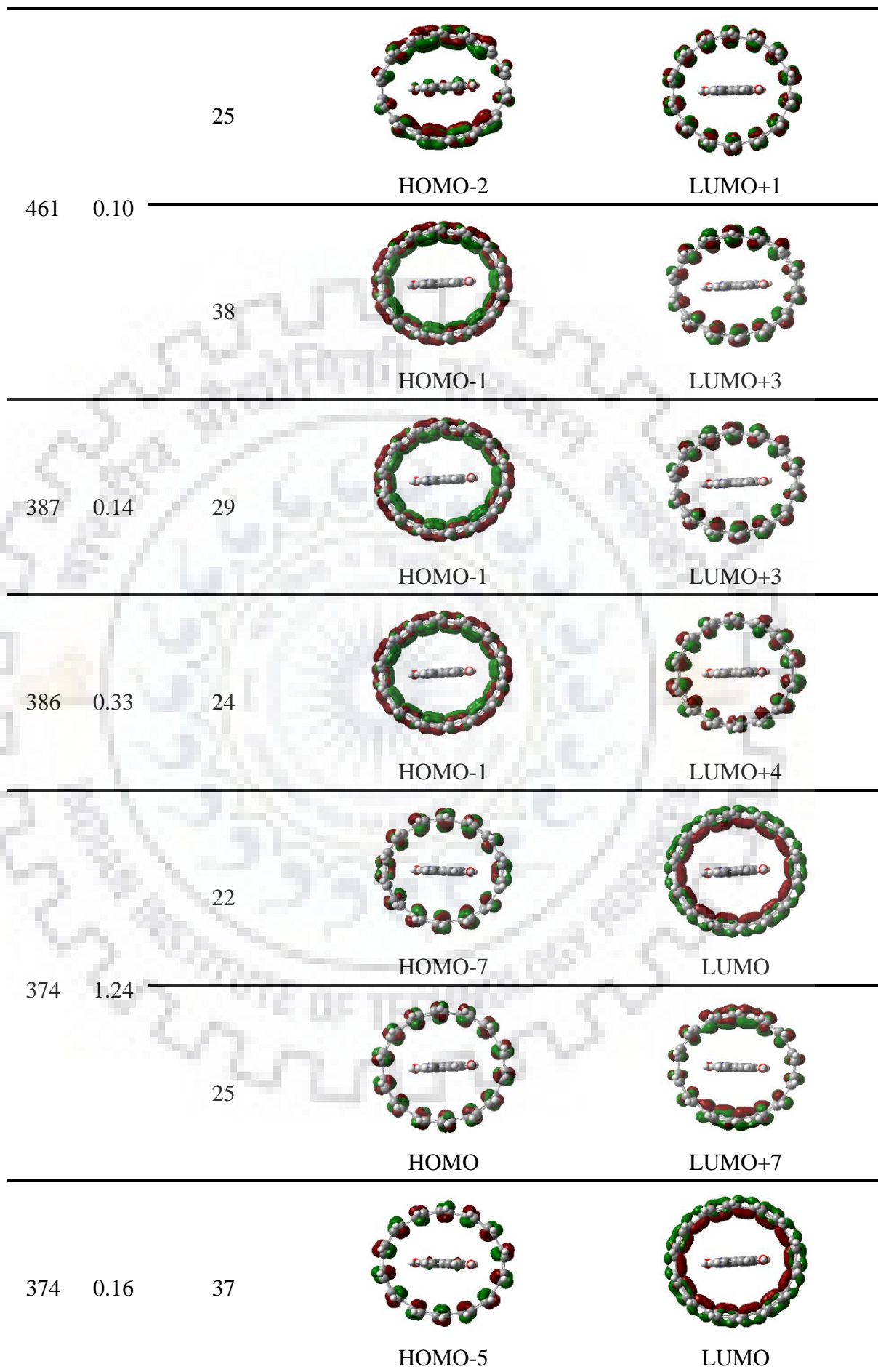
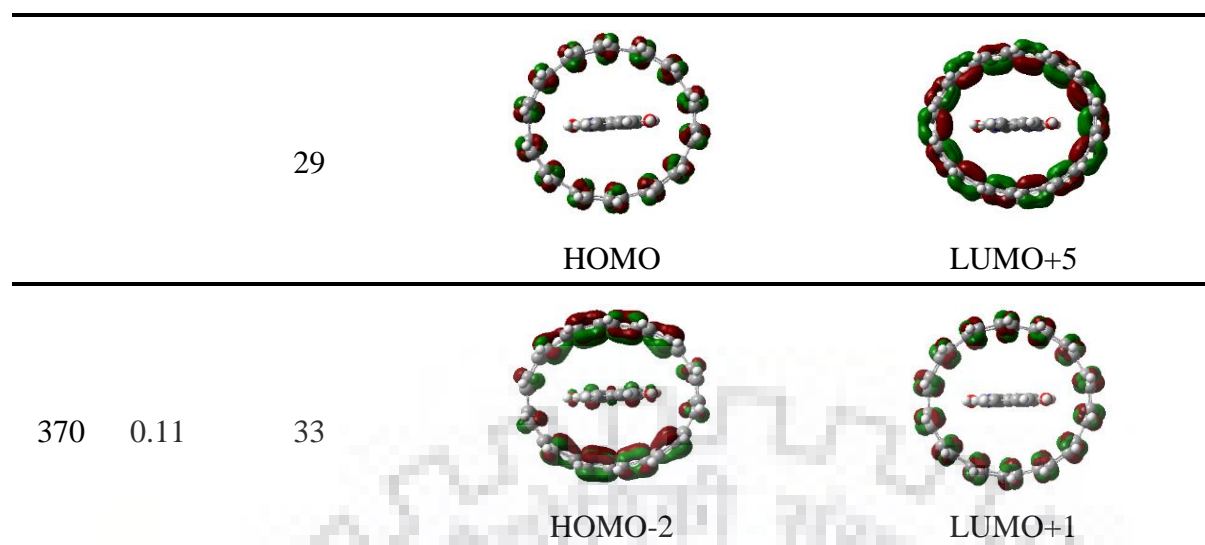


Figure 3.13 The optical absorption spectra of indigo, (7,7)CNT and the complex indigo@(7,7)CNT obtained at ω B97X-D/6-31G(d,p) level.

Table 3.16 The absorption wavelength (λ), oscillator strength (f), percentage orbital contribution and molecular orbitals involved in the transition for the complex indigo@(7,7)CNT obtained at ω B97X-D/6-31G(d,p) level.

λ (nm)	f	% Orbital contribution	Molecular orbitals involved in the transition	
		37		
			HOMO-4	LUMO+2
517	0.77	27		
			HOMO-1	LUMO
		29		
			HOMO	LUMO+1
		50		
			HOMO-4	LUMO+2
477	1.22	20		
			HOMO-1	LUMO
		21		
			HOMO	LUMO+1





shown in figure 3.11. It can be seen that the absorption maximum decreased to a lower wavelength for all the above systems compared to the respective values obtained using the B97-D functional. The absorption parameters of indigo@(7,7) CNT for the functional B3LYP-GD3 are tabulated in table 3.13. As in the case of B97-D functional, three charge transfer transitions are also observed for the B3LYP-GD3 functional. From the above discussion, it can be seen that the conclusions drawn using the B97-D functional qualitatively remain the same for the functional B3LYP-GD3.

In order to know the effect of functional, the long-range corrected hybrid functional (ω B97X-D) which has 100% HF-exchange was further used for the most stable complex indigo@(7,7)CNT. In this case, indigo aligned parallel to the tube-axis as depicted in figure 3.12. The BSSE and ZPE corrected value of ΔE_{stab} for indigo@(7,7)CNT is -106.47 kcal/mol. It is clear from table 3.14 that the values of IE and EA show negligible change compared to those obtained using the functionals B97-D and B3LYP-GD3 as presented in tables 3.7 and 3.11. However, a significant increase in $\Delta E_{\text{HOMO-LUMO}}$ is observed for ω B97X-D. The results obtained using ω B97X-D as tabulated in table 3.15 indicate remarkably lower carrier mobilities with respect to those using other functionals as listed in tables 3.9 and 3.12. As evident from figure 3.13, for this functional the absorption spectrum of the complex shifts towards smaller wavelength compared to that obtained by other functionals. Accordingly, the charge-transfer transitions also shifted to lower wavelengths (370 and 461 nm) as illustrated in table 3.14. Thus, it can be concluded that the charge-transfer excitations depend on the functional to a large extent.

3.4 Conclusion

The non-bonded interactions in the complexes of indigo wrapped over CNTs were studied by means of the dispersion-corrected density functional theoretical method. It was found that indigo forms stable non-covalent complexes with carbon nanotubes. These complexes showed distinct electronic properties compared to the component species. The frontier molecular orbital analysis of the complexes revealed that HOMO is mainly localized on CNT, whereas their LUMO is delocalized over both indigo and CNT. The energy gap between HOMO and LUMO of the complexes is less than that of the individual molecules and is in the range of 0.7-0.8 eV. The HOMO-LUMO energy level diagram of the complexes suggests the possibility of photoinduced charge transfer from CNT to indigo. The complexes also showed exceptionally high hole mobility compared to their electron mobility making them useful for their applications in p-type semiconductor devices. The TD-DFT calculations showed that indigo-CNT complexes absorb in visible and near-infrared region of the electromagnetic spectrum. The peculiar charge transport and optical properties of the complexes suggest that they can be used for the miniaturization of optoelectronic devices. The studies on the charge transport properties of the complexes of indigo with long carbon nanotube and also with capped carbon nanotube indicated an enhancement in their electron mobility compared to that formed from carbon nanotube of finite length. Unlike the electron mobility of the above complexes, a significant change in hole mobility was not observed. In contrast to high hole mobility than electron mobility for indigo wrapped over CNT complexes, the complex with planar indigo showed higher electron mobility than hole mobility. In summary, we have shown that the exohedral complexes of CNTs can be exploited for their electronic, optical and charge transport properties.

The structure and properties of various endohedral complexes formed by encapsulating indigo in CNTs of different diameter were also studied using different dispersion-corrected density functional theoretical methods. The stabilization energy of various endohedral complexes follow the order: indigo@(6,6)CNT < indigo@(8,8)CNT < indigo@(7,7)CNT. The analysis of host-guest interactions in the complexes was carried out using the energy decomposition approach based on symmetry-adapted perturbation theory. It was revealed that all the complexes are stabilized mainly by dispersion interactions. However, a major contribution from dispersion interactions was observed for the most stable complex indigo@(7,7)CNT. Properties such as ionization energy, electron affinity and energy gap between HOMO and LUMO ($\Delta E_{\text{HOMO-LUMO}}$) of the complexes indigo@(n,n)CNTs were changed slightly with respect to the corresponding free CNTs. It was also found that these properties are nearly independent of the diameter of CNT. The complexes showed a low $\Delta E_{\text{HOMO-LUMO}}$ (~1 eV) indicating their semiconducting nature. One

of the most important findings of the present study is that the carrier mobility can be tuned by selecting suitable CNTs. Unlike free CNTs, the complexes showed higher electron mobility than hole mobility suggesting that one can alter the transport properties of a CNT by encapsulating indigo. Using the time-dependent density functional theoretical method, absorption spectrum of indigo@(7,7)CNT was obtained over a wide range covering the near-ultraviolet to the near-infrared region of the electromagnetic spectrum. The absorption maxima in the near-infrared region of this complex corresponds to a charge transfer transition. In addition, several other charge transfer transitions were observed in the visible region. Although the properties obtained using various functionals differ in their respective values, the conclusion drawn based on the results of each functional remained the same. Based on the above discussion, it can be concluded that the complexes obtained by the encapsulation of indigo in CNTs can be used for various optoelectronic applications in organic semiconducting devices.



CHAPTER 4

Structure, Stability and Properties of the Complexes of Carbon Nanotube with Perylene Bisimide

4.1 Introduction

The application of CNT in optoelectronic devices is possible through the functionalization of tube as was discussed in detail in chapter 1.[86, 274, 297, 316-322] In this regard, different derivatives of perylene-3,4,9,10-tetracarboxylic acid bisimide have been used as functionalized molecules to form exohedral complexes with CNT.[323-329] For endohedral functionalization of CNT, size of its cavity should be large enough to encapsulate guest molecules. Few examples of organic molecules reported as guests for CNTs of different diameter are 7,7,8,8-tetracyanoquinodimethane,[274] oligomers of thiophene [316, 319] and fullerene.[86, 87, 317]

Recently, there is a growing interest for the charge-transfer complexes of carbon nanotube to be used in photovoltaic,[330] light-harvesting [331] and electronic devices.[332] In 2006, Lu *et al.* examined the non-bonded interactions of CNT with molecules such as naphthalene, anthracene, 7,7,8,8-tetracyanoquinodimethane (TCNQ) and 2,3-dichloro-5,-dicyano-1,4-benzoquinone (DDQ).[140] They found that among various molecules considered, only TCNQ and DDQ form charge transfer complexes with CNT. It was also revealed that the amount of charge transferred from donor CNT to acceptors TCNQ or DDQ depends on the orientation of the molecules adsorbed. In 2010, Manna *et al.* carried out an investigation on the adsorption of electron donor tetrathiafulvalene (TTF) as well as electron acceptors tetracyanoethylene (TCNE) and tetracyanoquinodimethane (TCNQ) on the surface of metallic and semiconducting CNTs.[141] They showed that the above electron donor-acceptor molecules can tune the band gap of pristine CNT and change its metallic character. The complexes of indigo wrapped over CNT exhibit p-type charge transfer characteristics as was mentioned in previous chapter.[297] Very recently, Ketolainen *et al.* examined the adsorption of nitrates on the surface of CNT and reported a p-type characteristics owing to the charge transfer from donor CNT to acceptor nitrates.[333] On the other hand, Koizhaiganova and co-workers reported n-type charge-transfer characteristics for the complexes of CNT with aromatic amines in which CNT acts as an acceptor for donor amines.[334] Recently, Brownlie and Shapter reviewed the synthesis, properties and applications of the complexes of CNT with n-type characteristics.[335]

The charge-transfer complexes of CNT with perylene bisimide (PBI) have stimulated significant interest in the field of supramolecular chemistry, especially host-guest chemistry.[132, 336, 337] It is known that PBI exhibits attractive structural and optoelectronic

properties and belongs to one of the most investigated dyes. PBI has the peculiar property that its perylene core behaves as an electron donor whereas the bisimide group acts as the electron acceptor. In addition, the high electron affinity of PBI makes it useful as a non-fullerene acceptor for applications in organic photovoltaic devices.[338-340] The energy gap of 2.5 eV of PBI implies its semiconducting nature and its absorption in the visible region of electromagnetic spectrum. Due to high electron mobility of PBI, it acts as an n-type semiconductor suitable for applications in organic transistor.[341] Tsarfati and co-workers elucidated that the complexes of PBI with CNT are stabilized by π - π and charge transfer interactions.[329] The possibility of charge transfer between electron donor CNTs and electron acceptor PBI has also been reported.[323] Weaver and co-workers studied a photoinduced charge transfer system composed of cadmium selenide quantum dot, thiol based perylene derivative and CNT in which the perylene derivative acts as a linker between quantum dot and CNT.[132] Although some experimental works have been done to understand the charge transfer properties of the complexes of PBI with CNT, not much is known about the nature of interactions and stability of such complexes.

In this chapter, we carried out an in-depth molecular level investigation on the optoelectronic and charge transport properties of PBI-(6,6)CNT by employing dispersion-corrected density functional theory (DFT). The electronic and charge transport properties of the above complex as well as its free components are examined. Further, the time-dependent density functional theory (TD-DFT) is used to infer about the absorption properties of the complex.

4.2 Computational Methods

For the quantum chemical calculations of PBI, CNT and their complex, various types of functionals such as GGA-type Becke-97D,[200] hybrid B3LYP-GD3 [201, 232] and range-separated hybrid ω B97X-D [202] were employed as implemented in Gaussian 09 program.[287] The above functionals were used in conjunction with the basis set 6-31G(d,p). It is noteworthy that these functionals are capable of handling the dispersion interactions between PBI and CNT. Geometry optimization and vibrational frequency calculations were carried out for all the systems considered. The stabilization energy of the complex was calculated and also, corrected for the basis set superposition error (BSSE) using the counterpoise method proposed by Boys and Bernardi.[234] Based on the zeroth-order symmetry-adapted perturbation theory (SAPT0), the energy decomposition analysis was performed for the complex using PSI4 software package.[342] All the electronic properties which have been calculated in the previous chapter for various indigo-CNT complexes were also computed for the complex PBI-(6,6)CNT in the present chapter. Similar to indigo-CNT complexes discussed in previous chapter, the optimized

geometries and the molecular orbitals of the complex were analysed using Gauss View 5.0 suite of program.[288] The charge transport parameters such as reorganization energy (λ), transfer integral (t) and rate of charge transfer (k) of the complex were also explored using Marcus theory as was done in indigo-CNT complexes.[307, 343] These parameters were further used for calculating the carrier mobility (μ).[286] By means of time-dependent density functional theoretical method,[233] the absorption wavelengths and corresponding oscillator strengths were computed for the complex. The light-harvesting efficiency (LHE) was determined from the oscillator strength (f) using the formula:

$$LHE = 1 - 10^{-f} \quad (4.1)$$

4.3 Results and Discussion

4.3.1 Optimized structures and stability

The optimized geometries of the complex formed between PBI and CNT obtained at B3LYP-GD3/6-31G(d,p), B97-D/6-31G(d,p) and ω B97XD/6-31G(d,p) levels are shown in figure 4.1. It can be seen from the figure that PBI aligns parallel to the tube-axis. The distance between the centre of PBI and the surface of CNT is approximately 3.1-3.4 Å for the above functionals that lies in the range of π - π interacting distances. In order to study the effect of functionals on the stability of the complex, both BSSE uncorrected and corrected stabilization energies (ΔE_{stab}) at three different levels were calculated and are listed in table 4.1. From the negative values of BSSE corrected stabilization energy, it can be inferred that the complex is energetically stable for all the functionals used. The stabilization of the complex can be attributed to the attractive π - π , C-H... π and N-H... π interactions between PBI and CNT. A significant π - π interaction is expected due to large number of π -electrons present in both species. Among these interactions, N-H... π interaction is widely known in biological systems.[344, 345] An energy decomposition analysis was performed by employing SAPT0 method along with 6-31G basis set as reported in earlier studies for π - π interacting systems.[297, 320, 346] The percentage contributions of various components of interaction energy such as dispersion, electrostatic and induction were determined and are presented in table 4.2. From the table, it can be seen that the dispersion interaction is mainly responsible for the stabilization of the complex followed by electrostatic interaction. This is in agreement with the conclusions of a previous study that reported the dispersion interaction is the major force contributing to π - π stacked complexes.[347] The reason behind the significant contribution from electrostatic interaction is probably the charge transfer

interactions between CNT and PBI which is discussed in later part of the present chapter. However, the contribution of induction energy to the stabilization is found to be almost negligible.

4.3.2 Electronic properties

The electronic properties such as vertical ionization energy (VIE), adiabatic ionization energy (AIE), vertical electron affinity (VEA) and adiabatic electron affinity (AEA) of the complex and its free components were calculated and are listed in table 4.3. Both the cationic and anionic systems are in their doublet state. It is assured that these states has no spin contamination. The calculated values of VIE (7.43 eV) and VEA (-2.28 eV) for PBI at B3LYP-GD3/6-31G(d,p) level match exactly with those reported earlier using the self-consistent-field methods.[341] For CNT, the corresponding values of VIE and VEA are 5.06 and -2.06 eV. Compared to IE of CNT, that of PBI is more, suggesting that the former acts as an electron donor on forming the complex. On the other hand, the VEA of CNT is less than that of PBI, and hence the latter acts as an electron acceptor. The above conclusions also hold true with the results obtained at other levels of calculations. Based on the above discussion, it can be inferred that PBI and CNT can form donor-acceptor complexes in the ground state. It is worth to mention here that other PBI-based donor-acceptor compounds are known and were found useful for organic photovoltaics.[348]

To get more insight on the donor-acceptor nature of the complex, the frontier molecular orbitals (FMOs) obtained at different levels were plotted based on the electron density distribution obtained from the population analysis and are shown in figure 4.2. The frontier molecular orbital analysis revealed that in the complex PBI-CNT, the electron density of HOMO and LUMO is localized on donor CNT and acceptor PBI molecules, respectively. This clearly indicates the transfer of electron density from CNT to PBI and thereby suggesting the possibility of photoinduced charge transfer within the complex. For indigo-CNT, the electron density of HOMO is localized on donor CNT while that of LUMO is delocalized over both donor and acceptor molecules. Herein, the electron density is transferred completely from CNT to PBI while in the case of indigo-CNT complexes, the electron density is transferred only partially from CNT to indigo as discussed in the previous chapter. [297-320] Further, the mechanism of photoinduced electron transfer (PET) between CNT and PBI is depicted in figure 4.3. Initially, the electron present in HOMO of CNT gets excited to its LUMO and then, the photoinduced electron is transferred to LUMO of PBI. Thus, photoinduced electron transfer occurs from CNT to PBI although the reverse is not possible. This also supports the complete charge transfer within the complex as seen from the electron density distribution in its frontier molecular orbitals. The

energy gap between HOMO and LUMO ($\Delta E_{\text{HOMO-LUMO}}$) of the complex and that of its components were calculated for various functionals and are listed in table 4.3. The calculated value of $\Delta E_{\text{HOMO-LUMO}}$ (2.54 eV) for PBI obtained at B3LYP-GD3/6-31G(d,p) level is the same as that reported earlier.[349] The $\Delta E_{\text{HOMO-LUMO}}$ of free CNT is found to be 1.47 eV and that of the complex is 1.02 eV. Such a considerable decrease in $\Delta E_{\text{HOMO-LUMO}}$ for the complex occurs

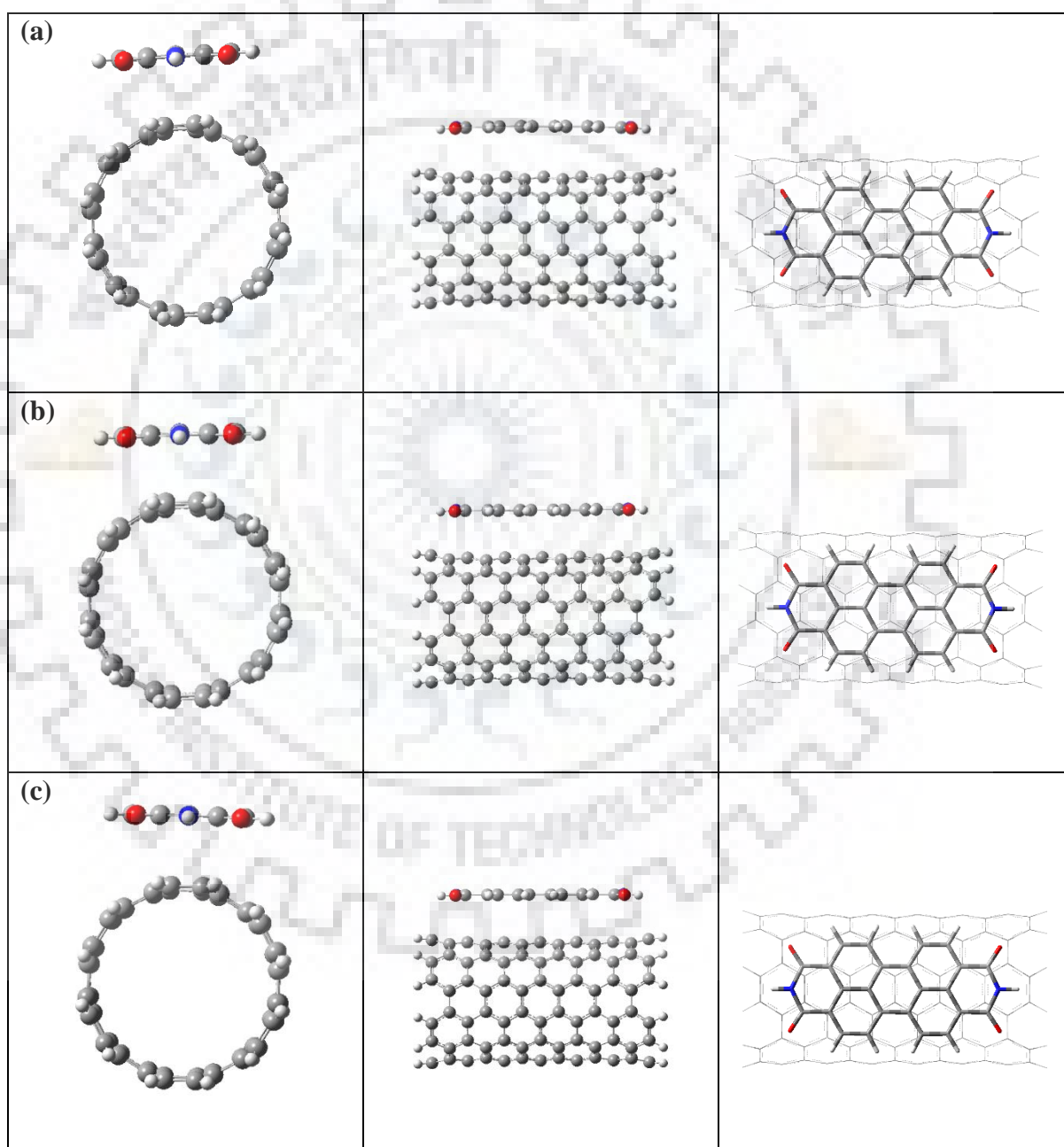


Figure 4.1 Optimized geometries of the complex PBI-(6,6)CNT (left: side view, middle: front view and right: top view) obtained at (a) B3LYP-GD3, (b) B97-D and (c) ω B97X-D levels.

due to the charge transfer between PBI and CNT. Unlike in the studies on indigo-CNT complexes,[297, 320] the present study demonstrates that energy gap between frontier molecular orbital of CNT alters remarkably on forming the complex with PBI. This suggests that PBI has the ability to tune the orbital energy gap. From the tabulated values, it can be seen that the values of $\Delta E_{\text{HOMO-LUMO}}$ obtained using the functional $\omega\text{B97X-D}$ deviate significantly from those using B97-D and B3LYP-GD3 functionals.

4.3.3 Charge transport properties

In order to test the suitability of the complex PBI-CNT for its use in organic transistors, it is of utmost importance to examine the charge transport properties. Based on the difference in the magnitude of the mobilities of holes and electrons, one can predict the p-type/ n-type charge-transport characteristics of a system. It is worth to mention here that the carrier mobility of a donor-acceptor complex is directly proportional to the square of the centre-to-centre distance between donor and acceptor species. Table 4.4 lists the values of reorganization energy (λ), charge transfer integral (t), rate of charge transfer (k) and carrier mobilities (μ) computed using three different functionals. It can be inferred from the tabulated values that the complex exhibits higher hole mobility than the corresponding electron mobility and therefore, acts as a p-type semiconductor. It can also be seen from the table that hole mobility is significantly more than electron mobility obtained at both B3LYP-GD3 and $\omega\text{B97X-D}$ levels.

4.3.4 Optical absorption properties

To comprehend more about the nature of charge-transfer in the excited states of the complex, its optical properties were simulated using the time-dependent density functional theoretical method. The absorption spectra of PBI, CNT and their complex were plotted using different functionals and are shown in figure 4.4. As evident from figure, the maximum absorption wavelength (λ_{max}) of PBI lies at 571, 505 and 431 nm using B97-D, B3LYP-GD3 and $\omega\text{B97X-D}$, respectively. It should be noted that λ_{max} of PBI at B3LYP/6-31G(d) level is 507 nm as reported by Calbo and co-workers.[349] The experimentally obtained λ_{max} of PBI is ~525 nm in chloroform.[350, 351] Unlike PBI, CNT has several peaks in its absorption spectrum covering a wide range of the electromagnetic spectrum starting from near-ultraviolet to near-infrared region at B97-D/6-31g(d,p) level and from near-ultraviolet to visible region for other two levels. It can be seen from the figure that λ_{max} of the complex remains almost unchanged compared to that of free CNT using B97-D. On the other hand, λ_{max} of complex is slightly more than that of CNT for B3LYP-GD3 and $\omega\text{B97X-D}$ functionals.

Table 4.1 The stabilization energies (ΔE_{stab}) of the complex PBI-CNT with and without BSSE corrections using various dispersion-corrected density functionals and 6-31G(d,p) basis set. All the energy values are in kcal/mol.

Complex	Functional	ΔE_{stab} without BSSE corrections	ΔE_{stab} with BSSE corrections
PBI-(6,6)CNT	B3LYP-GD3	-36.55	-27.06
	B97-D	-41.07	-31.38
	ω B97X-D	-39.48	-31.83

Table 4.2 Percentage contribution from various components of interaction energy for the complex PBI-CNT using zeroth-order symmetry adapted perturbation theory (SAPT0) and 6-31G basis set.

Complex	Functional	Dispersion (%)	Electrostatic (%)	Induction (%)
PBI-(6,6)CNT	B3LYP-GD3	66	29	5
	B97-D	62	32	6
	ω B97X-D	65	30	5

Table 4.5 lists the values of λ_{\max} , oscillator strength (f), light-harvesting efficiency (LHE), molecular orbitals involved in the transitions and the corresponding orbital contribution for the complex. Only those transitions are considered for which the orbital contribution is minimum 15%. From oscillator strength, light-harvesting efficiency (LHE) was determined. Studies have been reported on the suitability of density functionals on the study of optical properties showing the usefulness of long-range corrected functional ω B97X-D for calculating the oscillator strengths of perylene, perylene bisimide and their dimeric structures.[352, 353] For the complex PBI-CNT considered in the present study, a very high LHE (94%) is obtained using ω B97X-D, the functional which is reported suitable for the calculation of oscillator strengths.[354] The molecular orbital analysis revealed that the absorption corresponding to λ_{\max} does not arise due to any charge transfer transition, irrespective of the functional used. Further, a close examination of molecular orbitals corresponding to the transitions other than that of λ_{\max} was performed for B3LYP-GD3 (see table 4.6), the functional widely used for studying the optical properties of charge-transfer complexes.[355, 356] Only those transitions with minimum oscillator strength of 0.05 are considered. The charge transfer analysis was performed only for wavelength ranging from 300-600 nm owing to the very low orbital contribution for the transitions in near-infrared region. It can be seen from table 4.6 that the photoinduced charge transfer transitions from CNT to PBI occur at different wavelengths *viz.*, 455, 463 and 505 nm. Among these, the wavelength at 463 nm corresponds to maximum LHE (61%) and the molecular orbitals involved in the transition are HOMO-1 and LUMO+10. Thus, the complex shows reasonable light harvesting properties in the visible region making it suitable to be used in solar cells.

4.3.5 Effect of nanotube length on stability and properties of PBI-CNT complexes

To determine the edge effects of CNT on the optoelectronic and charge transport properties of its complex with PBI, a comparatively long CNT (21.66 Å) was used. The optimized geometry obtained at B97-D/6-31G(d,p) level is depicted in figure 4.5. The distance between the centre of PBI to the nearby surface of CNT is about 3 Å. The stabilization energy with and without BSSE is found to be -40.93 and -31.63 kcal/mol, which is very close to the complex of PBI formed with CNT of small length (16.69 Å) discussed before. The electronic properties of long CNT as well as its complex are presented in table 4.7. Compared to the ionization energy of CNT of small length and its complex, that of relatively long CNT and its complex is decreased. In contrast to ionization energy, their electron affinity is increased. As observed in the case of small CNT, the energy gap between the HOMO and LUMO of long CNT is decreased significantly on forming the complex. The complex of long CNT also showed photoinduced charge transfer as evident

Table 4.3 The vertical ionization energy (VIE), adiabatic ionization energy (AIE), vertical electron affinity (VEA), adiabatic electron affinity (AEA) and the energy gap between HOMO and LUMO ($\Delta E_{\text{HOMO-LUMO}}$) of PBI, (6,6)CNT and their complex obtained for different functionals using 6-31G(d,p) basis set. All the energy values are in eV.

Functional	System	VIE	AIE	VEA	AEA	$\Delta E_{\text{HOMO-LUMO}}$
B3LYP-GD3	PBI	7.43	7.35	-2.28	-2.40	2.54
	(6,6)CNT	5.06	5.03	-2.06	-2.09	1.47
	PBI-(6,6)CNT	5.09	5.05	-2.36	-2.44	1.02
B97-D	PBI	7.21	7.16	-2.30	-2.39	1.50
	(6,6)CNT	4.93	4.90	-2.15	-2.17	0.80
	PBI-(6,6)CNT	4.94	4.92	-2.14	a	0.24
ω B97X-D	PBI	7.69	7.58	-2.15	-2.34	5.09
	(6,6)CNT	5.50	5.43	-1.83	-1.90	3.97
	PBI-(6,6)CNT	5.53	5.45	-2.17	-2.36	3.89

^a Convergence criteria not met.

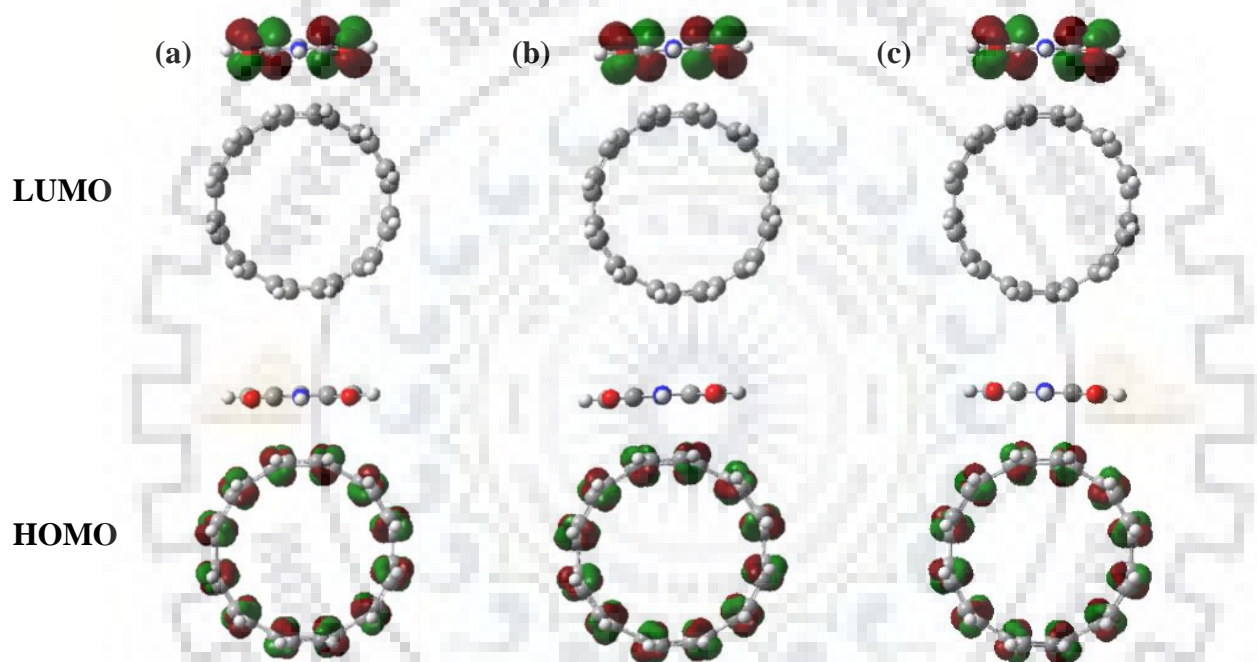


Figure 4.2 Frontier molecular orbitals of the complex PBI-(6,6)CNT obtained at (a) B3LYP-GD3/6-31G(d,p), (b) B97-D/6-31G(d,p) and (c) ω B97X-D/6-31G(d,p) levels.

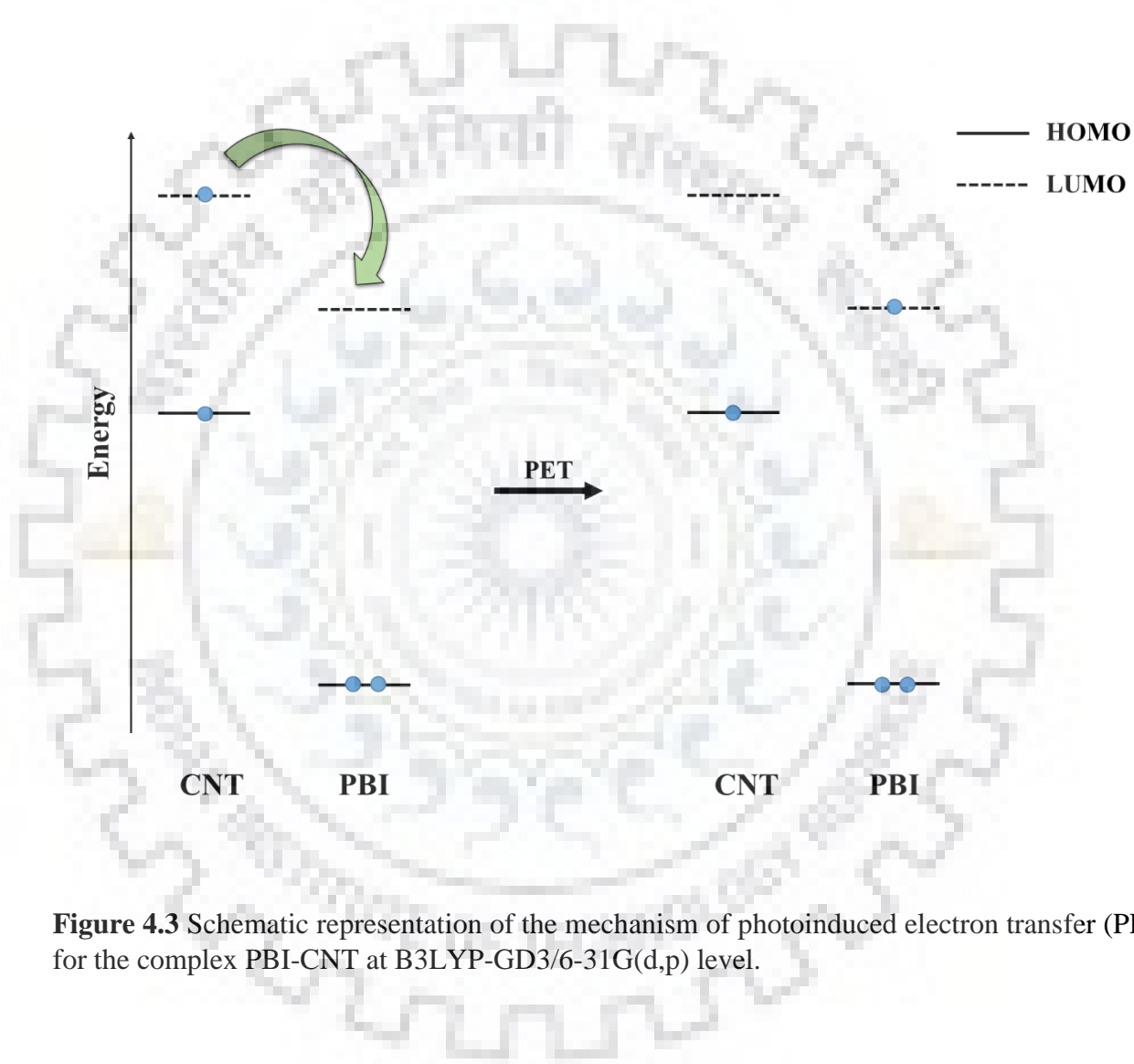


Figure 4.3 Schematic representation of the mechanism of photoinduced electron transfer (PET) for the complex PBI-CNT at B3LYP-GD3/6-31G(d,p) level.

Table 4.4 Calculated values of transfer integral (t), internal reorganization energy (λ), rate constant (k) and carrier mobility (μ) of the complex PBI-(6,6)CNT obtained for different functionals using 6-31G(d,p) basis set.

Method	Distance (Å)	λ_+ (eV)	t_+ (eV)	k_+ (eV)	μ_+ (cm ² V ⁻¹ s ⁻¹)	λ_- (eV)	t_- (eV)	k_- (eV)	μ_- (cm ² V ⁻¹ s ⁻¹)
B3LYP-GD3	3.29	0.08	0.11	3.17×10^{13}	0.66	0.18	0.23	0.19×10^{13}	0.04
B97-D	3.13	0.06	0.10	6.63×10^{13}	1.26	--- ^a	0.28	--- ^a	--- ^a
ω B97X-D	3.25	0.16	0.12	0.12×10^{13}	0.02	0.38	0.03	0.09×10^8	1.88×10^{-7}

^aConvergence criteria not met.

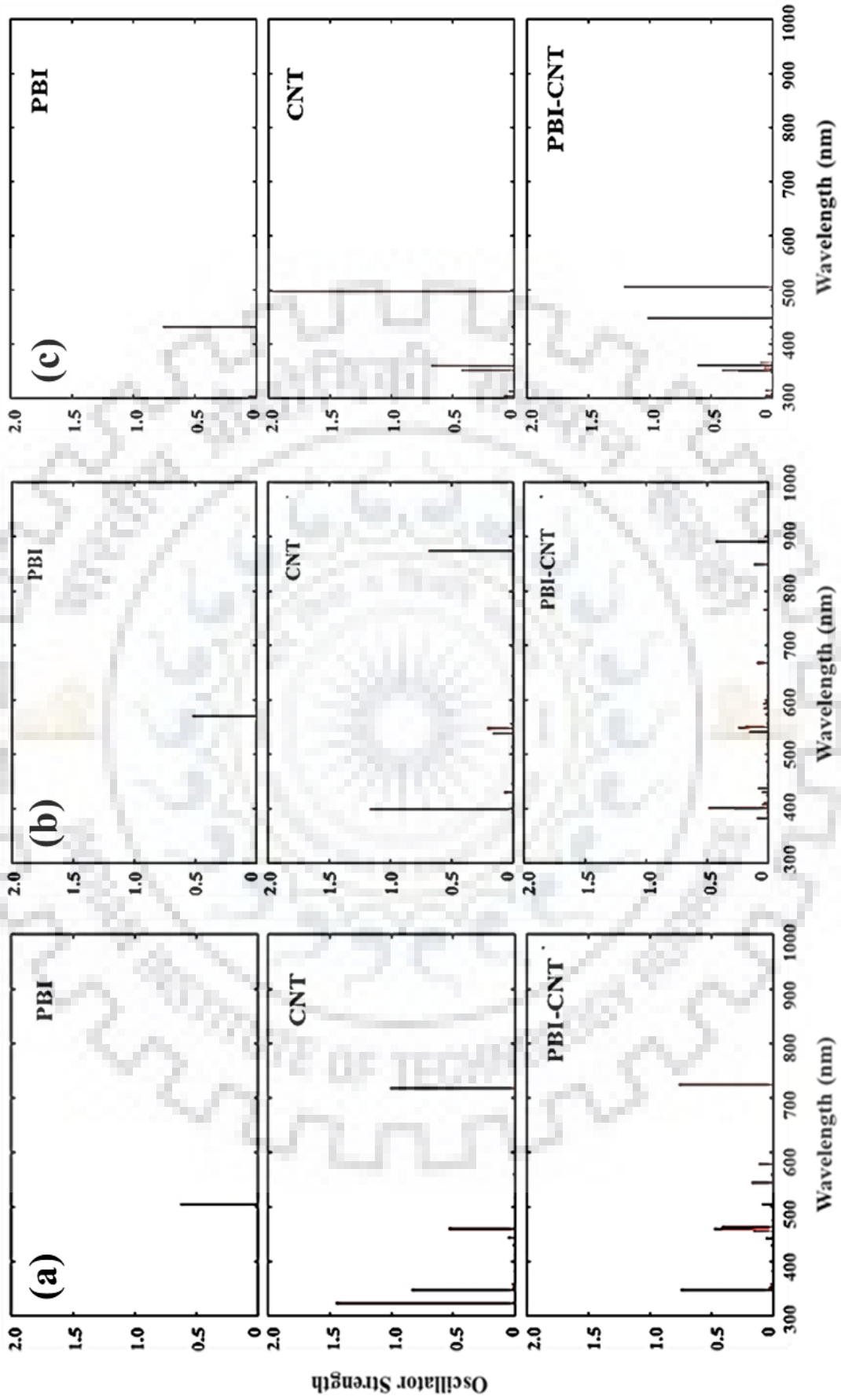


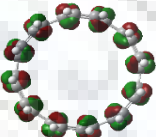
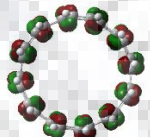
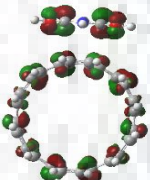
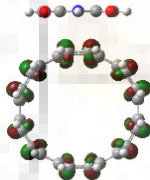
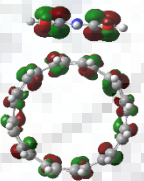
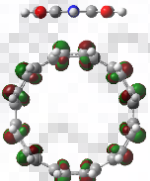
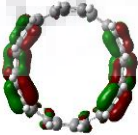



Figure 4.4 Optical absorption spectra of the PBI, (6,6)CNT and their complex obtained using the functionals (a) B3LYP-GD3 (b) B97-D and (c) ω B97X-D along with 6-31G(d,p) basis set.

Table 4.5 The maximum absorption wavelength (λ_{\max}), oscillator strength (f), light-harvesting efficiency (LHE), molecular orbitals involved in the transitions and the orbital contribution of the complex PBI-(6,6)CNT for different functionals using 6-31G(d,p) basis set. Only those transitions of minimum orbital contribution 15% are considered.

Functional	λ_{\max} (nm)	f	LHE (%)	Orbital Contribution (%)	Molecular orbitals involved in the transitions	
B3LYP- GD3	724	0.77	83	50		
					HOMO-1	LUMO+1
				46		
				HOMO	LUMO+2	
B97-D	401	0.49	68	23		
					HOMO-7	LUMO+11
				19		
				HOMO-5	LUMO+11	
				18		
					HOMO-11	LUMO+5

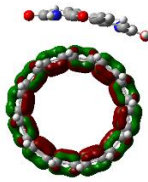
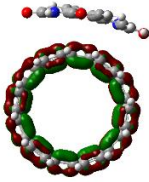
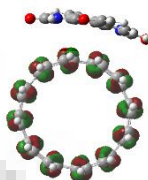
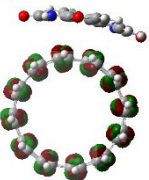
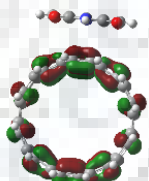
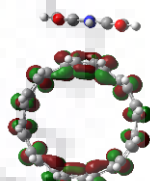
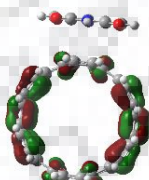
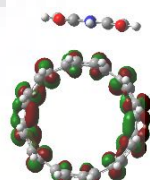
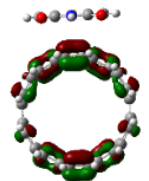
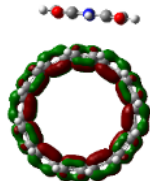
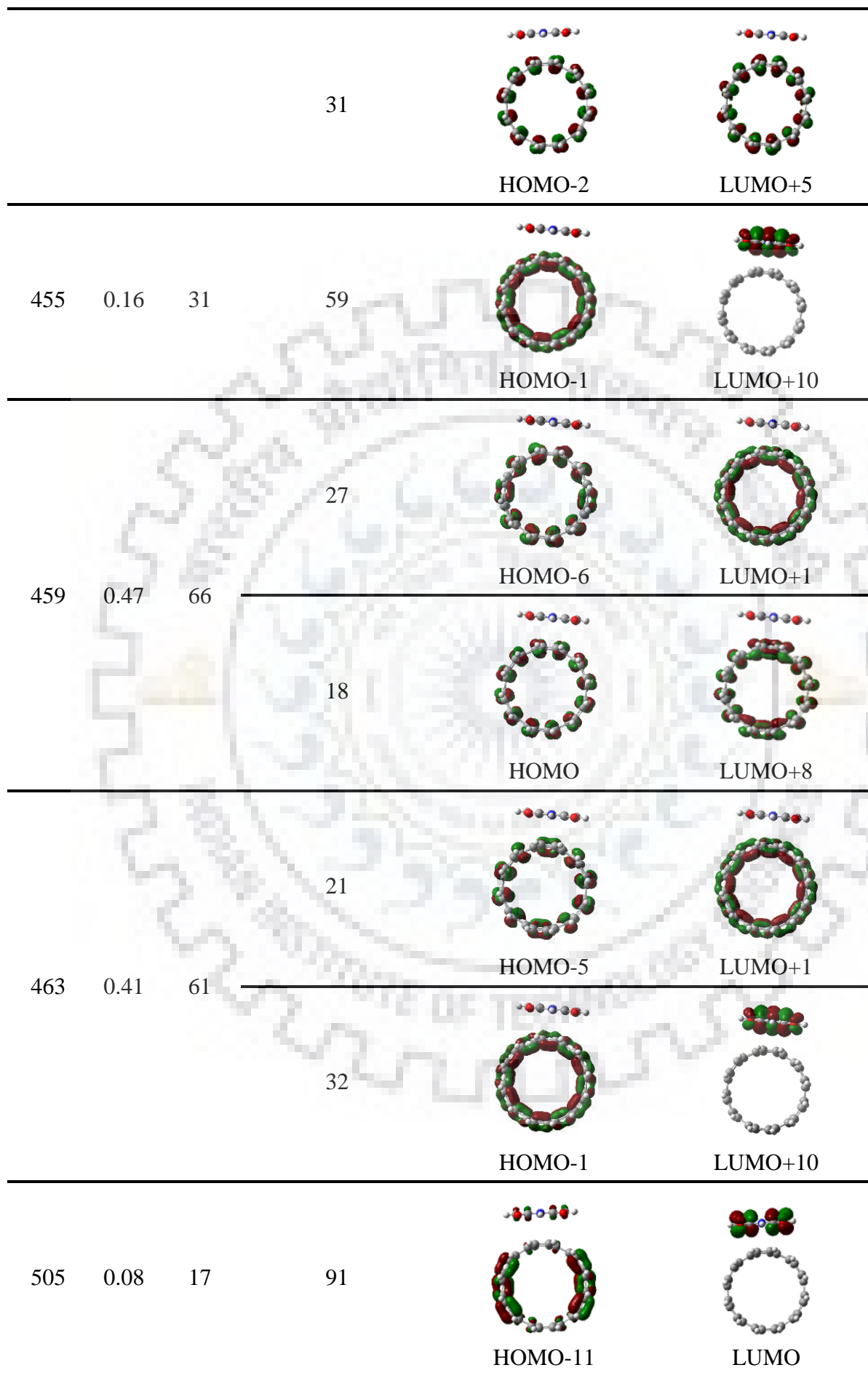
ω B97X-D	507	1.35	95	45		
					HOMO-1	LUMO+1
				45		
					HOMO	LUMO+2

Table 4.6 The absorption wavelength (λ), oscillator strength (f), light-harvesting efficiency (LHE), molecular orbitals involved in the transition and the orbital contribution of the complex PBI-(6,6)CNT at B3LYP-GD3/6-31G(d,p) level. Only those transitions of oscillator strength more than 0.05 and of minimum orbital contribution 15% are considered.

λ (nm)	f	LHE (%)	Orbital Contribution(%)	Molecular orbitals involved in the transition	
348	0.75	82	23		
				HOMO-4	LUMO+8
			20		
				HOMO-3	LUMO+7
443	0.06	13	59		
				HOMO-10	LUMO+1



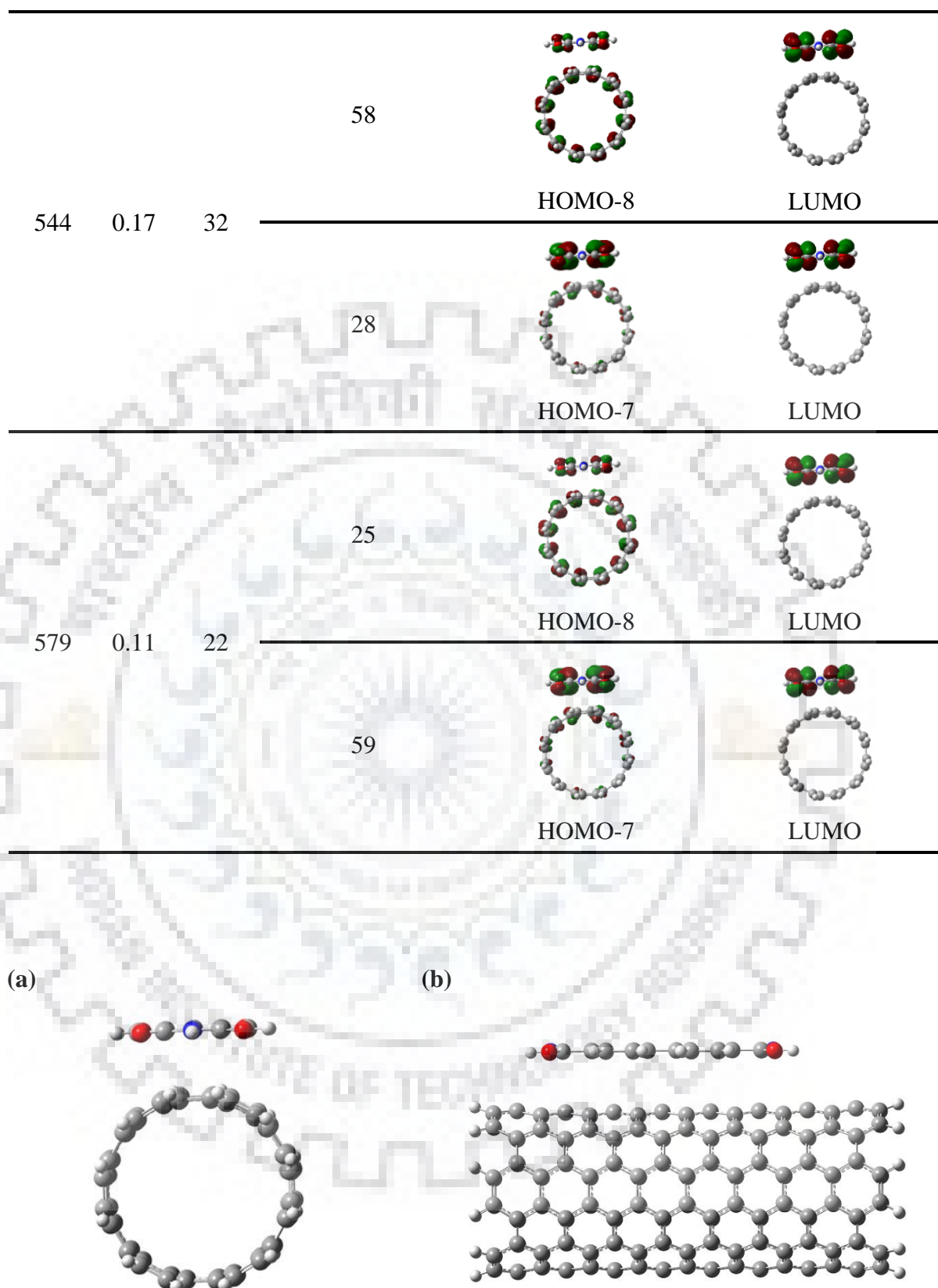


Figure 4.5 Optimized geometries (a) side view and (b) front view of the complex PBI with relatively long (6,6)CNT obtained at B97-D/6-31G(d,p) level.

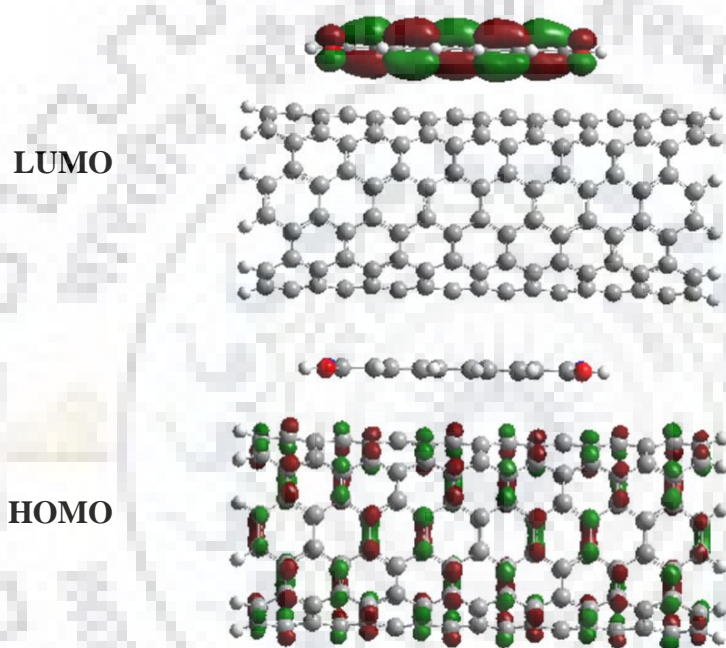


Figure 4.6 Frontier molecular orbitals of the complex PBI with long (6,6)CNT obtained at B97-D/6-31G(d,p) level.

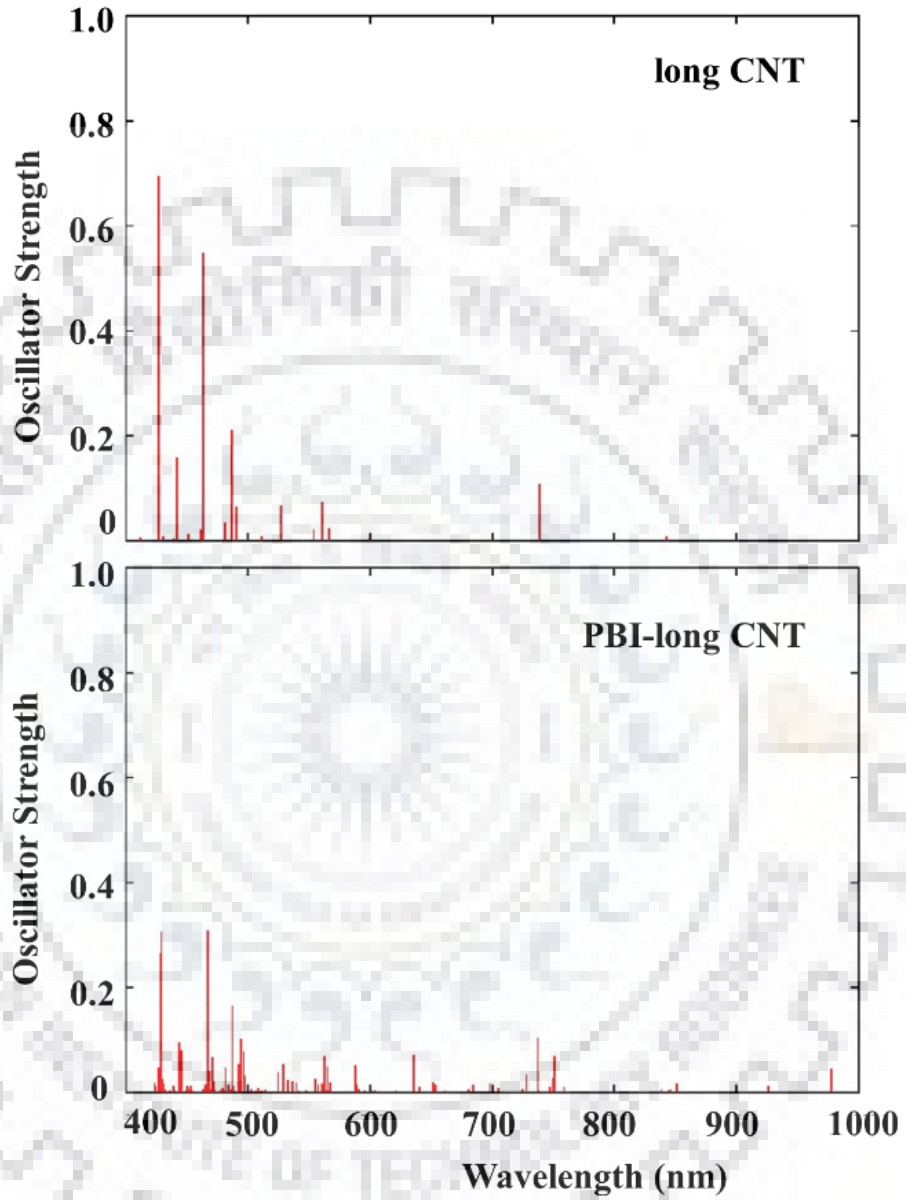


Figure 4.7 Optical absorption spectra of long (6,6)CNT and its complex with PBI obtained at B97-D/6-31G(d,p) level.

Table 4.7 The electronic properties such as vertical ionization energy (VIE), adiabatic ionization energy (AIE), vertical electron affinity (VEA), adiabatic electron affinity (AEA) and the energy gap between HOMO and LUMO ($\Delta E_{\text{HOMO-LUMO}}$) of long CNT and its complex with PBI obtained at B97-D/6-31G(d,p) level. All the energy values are in eV.

System	VIE	AIE	VEA	AEA	$\Delta E_{\text{HOMO-LUMO}}$
long (6,6)CNT	4.72	4.71	-2.46	-2.48	0.50
PBI with long (6,6)CNT	4.74	4.72	-2.67	-2.69	0.14

Table 4.8 The calculated values of transfer integral (t), internal reorganization energy (λ), rate constant (k) and carrier mobility (μ) of the complex PBI with long (6,6)CNT at B97-D/6-31G(d,p) level.

Distance (Å)	λ_+ (eV)	t_+ (eV)	k_+ (s ⁻¹)	μ_+ (cm ² V ⁻¹ s ⁻¹)	λ_- (eV)	t_- (eV)	k_- (s ⁻¹)	μ_- (cm ² V ⁻¹ s ⁻¹)
3.02	0.03	0.11	33.18×10^{13}	5.84	0.06	0.19	23.69×10^{13}	4.24

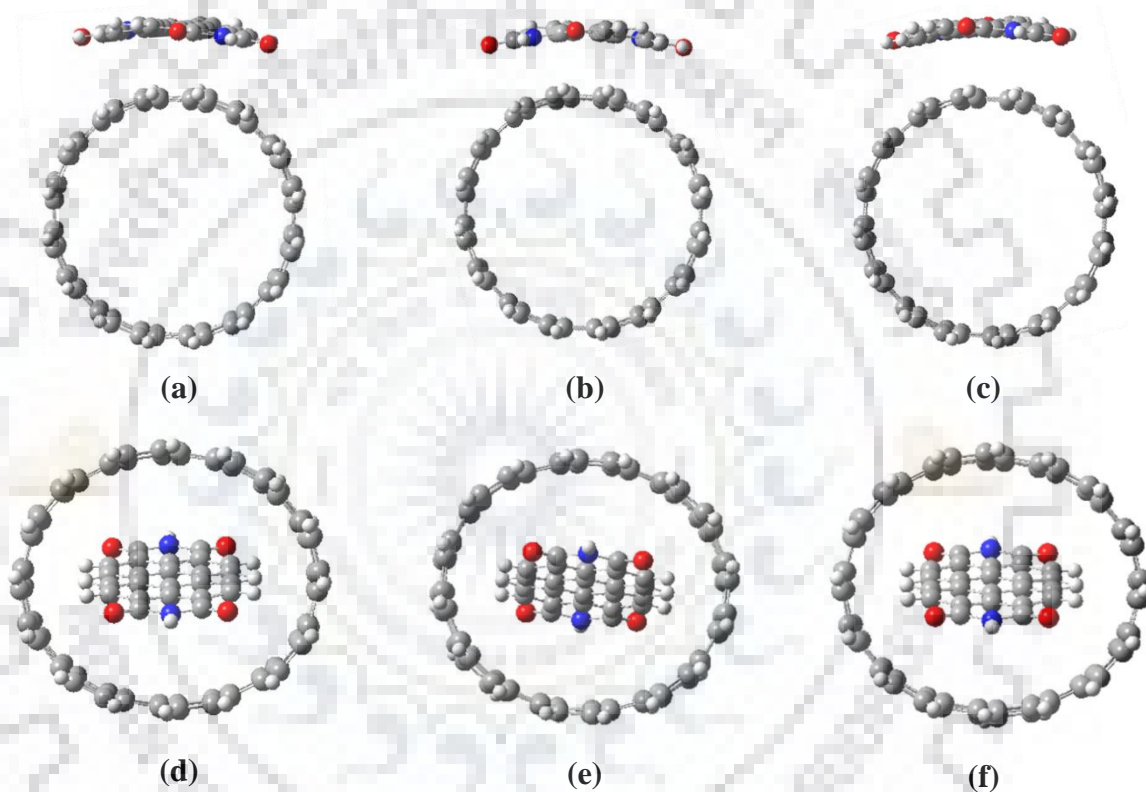


Figure 4.8 Optimized geometries of the complexes (a-c) PBI-(8,8)CNT and (d-f) PBI@(8,8)CNT each set obtained using B3LYP-GD3, B97-D and ω B97X-D functionals, respectively.

Table 4.9 The stabilization energies (ΔE_{stab}) of the complexes formed between PBI and (8,8)CNT calculated with and without BSSE corrections using various dispersion-corrected density functionals and 6-31G(d,p) basis set. All the energy values are in kcal/mol.

Complex	Functional	ΔE_{stab} without BSSE corrections	ΔE_{stab} with BSSE corrections
PBI-(8,8)CNT	B3LYP-GD3	-39.32	-29.42
	B97-D	-44.90	-34.73
	ω B97X-D	-41.97	-34.17
PBI@(8,8)CNT	B3LYP-GD3	-74.95	-59.82
	B97-D	-79.50	-65.06
	ω B97X-D	-71.81	-59.15

Table 4.10 Percentage contribution from various components of interaction energy for the complexes of PBI with (8,8)CNT obtained using zeroth-order symmetry adapted perturbation theory (SAPT0) and 6-31G basis set.

Complex	Functional	Dispersion (%)	Electrostatic (%)	Induction (%)
PBI-(8,8)CNT	B3LYP-GD3	66	29	5
	B97-D	62	32	6
	ω B97X-D	67	28	5
PBI@(8,8)CNT	B3LYP-GD3	72	19	9
	B97-D	71	20	9
	ω B97X-D	71	20	9

from figure 4.6. As can be discerned in tables 4.4 and 4.8, hole mobility is more than electron mobility for the complexes of CNTs of different lengths. The higher hole mobility for the complex of long CNT than that of small CNT is due to lower reorganization energy for hole transport. Similarly, the maximum absorption wavelength of both CNTs and their complexes also remained nearly the same independent of the length of CNT as reflected from figures 4.4 and 4.7. In addition, several new peaks arise in visible region of the electromagnetic spectrum for both long CNT and its complex compared to those of small CNT and its complex, respectively.

4.3.6 Effect of nanotube diameter on the stability of PBI-CNT complexes

To understand the dependence of diameter on the stability of the complexes, a carbon nanotube of relatively large diameter (8,8)CNT is selected. The stability of the endohedral complex PBI@(8,8)CNT was determined. The optimized geometries of the complexes obtained at different levels are shown in figure 4.8. It can be seen from the figure that the encapsulated PBI is slightly tilted with respect to the tube-axis in order to have maximum interactions with the inner wall of CNT. Unlike PBI-(6,6)CNT; PBI-(8,8)CNT indicates slight distortion in the structure of PBI. Comparison of the optimized structures of the exohedral complex PBI-(8,8)CNT with that of the endohedral counterpart indicated a distortion in the structure of PBI in the former. The various bond lengths of free PBI as well as those of its respective endo- and exohedral complexes with (8,8)CNT were calculated for the B97-D optimized structures and are given in figure A2 of the Appendix-A. From the figure, it is found that there is a significant change in the bond lengths of PBI in its respective endohedral complexes rather than in their exohedral counterparts. Similar to indigo, PBI also showed a significant decrease in its C-H bond lengths for the endohedral complex. For the complexes of PBI with (8,8)CNT, the stabilization energies with and without incorporating BSSE correction were calculated and are summarized in table 4.9. From the values of stabilization energies, it can be inferred that PBI can form both exo- and endohedral complexes with (8,8)CNT, although the latter is stabilized more by about 25-30 kcal/mol depending on the functional used. The percentage contribution of various components of interaction energy for these complexes was also determined and the values are presented in table 4.10. The analysis revealed that the higher stability of the endohedral complex arises mainly due to the dispersion interaction. In contrast, the electrostatic interaction is found to be more for the exohedral complex.

4.4 Conclusion

In this chapter, the stability and properties of the complex formed between PBI and (6,6)CNT were studied using different dispersion-corrected density functionals. It was found that the complex formed is energetically stable, irrespective of the functionals used. The energy decomposition analysis of the complexes revealed that the stability arises mainly from the dispersion interactions between the components. The lower ionization energy of CNT compared to that of PBI along with more negative electron affinity of PBI than that of CNT suggested that CNT acts as an electron donor while PBI behaves as an electron acceptor on forming the complex. Compared to IE and EA of CNT, those of the complex did not change significantly for all the functionals. The donor-acceptor nature of the complex was also confirmed by analysing the frontier molecular orbitals of the complex wherein photoinduced charge transfer takes place from CNT to PBI. The photoinduced electron transfer was also observed for the complex wherein the transfer of photoinduced electron takes place from LUMO of CNT to that of PBI. Compared to the energy gap between HOMO and LUMO of free CNT, that of complex is reduced significantly suggesting the use of PBI in tuning the energy gap of CNT. The complex showed an energy gap of about 1 eV at B3LYP-GD3/6-31G(d,p) level thereby suggesting it to be used as organic semiconductors for optoelectronic applications. The complex exhibited p-type charge transfer characteristics due to greater hole mobility than electron mobility. The time-dependent density functional theoretical calculations showed that the complex absorbs in the wide spectral range starting from near ultraviolet to near infrared region. The studies also suggested a very high light-harvesting efficiency (94%) for the complex formed between PBI and CNT. The molecular orbital analysis was also performed for the complex that indicated several charge transfer transitions in the visible region of the electromagnetic spectrum. The above calculations were also performed for the complex with relatively long CNT. The conclusions drawn from the studies on short CNT and its complex remained the same for long CNT and its complex as well.

Further, the investigation on the stability of endo- and exohedral complexes formed between PBI and (8,8)CNT indicated a higher stability for the endohedral complex. The results of energy decomposition analysis showed that the contribution of dispersion interaction is higher for the endohedral complex while that of electrostatic interaction is more for the exohedral complex.

CHAPTER 5

Structure, Stability and Properties of the Complexes of Carbon Nanotube with Quaterthiophene

5.1 Introduction

The charge transfer interactions between electron donor CNT and electron acceptors (indigo and PBI) were discussed in chapters 3 and 4. The present chapter seeks to explore the donor or acceptor nature of CNT when attached to oligothiophene molecule. There are ample evidences for the strong electron donor behaviour of oligothiophenes.[357-359] Among these, quaterthiophene (4T) is a p-type organic semiconductor which has been used in a variety of optoelectronic devices.[360-364] The largest band gap reported for the single-crystals of 4T is 2.37 eV.[365] The energy gap between highest occupied and lowest unoccupied molecular orbital ($\Delta E_{\text{HOMO-LUMO}}$) of 4T was reported as 3 eV.[366, 367] Its optical properties have also been investigated by several research groups.[368-371] Aschi *et. al.* measured the absorption spectrum of 4T in chloroform and dichloromethane wherein the most intense absorption occurs at 393 nm.[371] It has also been reported by Becker and group that 4T absorbs strongly at wavelengths of 391 and 386 nm in dioxane and methylcyclohexane, respectively.[368] The $S_0 \rightarrow S_1$ transition energy of 3.01 eV has been obtained for 4T.[369] In another study, it has been found that 4T exhibits $\pi-\pi^*$ transition around 400 nm.[370]

It is well-known that carbon nanotubes (CNTs) in their charge transfer complexes behave as electron donor or acceptor depending on the electronic nature of the molecule used for their functionalization. Since oligothiophenes are electron-donating in nature, it implies that CNT can act as an acceptor in their donor-acceptor complexes. There are several reports on the structure, stability and properties of the complexes of CNT with oligothiophenes. For instance, Orellana and Vázquez examined the encapsulation of terthiophene (3T) in CNTs of varying diameter using density functional theoretical study.[316] Their results revealed that the above complexes formed are stable. In another study, the endo- and exohedral complexes of CNT with 3T have been studied both theoretically and experimentally.[372] The analysis revealed the endohedral complexes as relatively more stable than their exohedral counterparts. Almadori and co-workers carried out experimental studies on the structural properties of the complexes formed by encapsulating 4T inside CNTs of varying diameter.[247] Their study revealed that the number of 4T molecules trapped inside CNT depends on the diameter of tube. The infrared spectra of endo- and exohedral complexes of CNT with 4T have been studied both by theoretical and experimental means.[373] Using Raman and infrared spectroscopy techniques, Alvarez and

group investigated the possibility of charge transfer in the endohedral complexes of CNT with methyl-terminated 4T.[127]

The optical properties of the complexes $nT@SWNT$ ($n = 4-6$) have been studied experimentally by Gao and co-workers.[374] Their results showed that the complexes emit visible light. Picard *et al.* demonstrated that the complexes of CNTs with an oligomer of bis-4T-fluorenone can be used in solar cells.[375] Yamashita and Yumura conducted several theoretical studies on the structure and properties of the complexes of CNT with methyl-terminated oligothiophenes.[248, 281, 376] The interaction of the encapsulated derivatives of oligothiophenes with CNT was studied using dispersion-corrected density functional methods.[281] Later, the electronic and absorption properties of endohedral complexes of multiple 3T units with CNT were investigated.[376] Recently, a comparative study was carried out on the properties of the complexes methyl-terminated terthiophenes@CNT and methyl-terminated terfurans@CNT.[248] It was reported that the major forces responsible for the stabilization of these complexes are π - π and C-H... π interactions. Very recently, Miyaura *et al.* showed that the empty cavity of CNT can be utilized for the polymerization of thiophenes.[319]

From the above studies, it can be seen that there is an emerging interest in the complexes of oligothiophenes and CNT. Although some studies have been done on the complexes of 4T with CNT, their charge transport properties have not been investigated yet. In this chapter, a comparative study on the structural, optoelectronic and charge transport properties of endo- and exohedral complexes of CNT with 4T which are hereafter referred to as 4T@CNT and 4T-CNT, respectively, is performed. The possibility of switching of charge transfer characteristics of the above complexes with regard to those of indigo-CNT and PBI-CNT discussed in previous chapters is explored. The analysis of frontier molecular orbitals of free 4T and CNT are performed to know the effect of light irradiation on intermolecular charge transfer. The intermolecular charge transfer phenomena is also examined in the excited states of the complexes using the time-dependent density functional theoretical method.

5.2 Computational Methods

The computations of various systems *viz.*, 4T, CNT, 4T@CNT and 4T-CNT were carried out using dispersion-corrected density functionals (non-hybrid B97-D [200], hybrid B3LYP-GD3 [201] and range-separated hybrid ω B97X-D [202]) along with 6-31G(d,p) basis set as implemented in the Gaussian 09 software package.[287] A detailed investigation is performed on the effect of different functionals on the structure and properties of the above systems. As a first step, the geometry optimization was done for the complexes and their component species.

The vibrational frequencies of the optimized systems were computed to ensure that they are the minimum energy structures. The stabilization energies (ΔE_{stab}) of the complexes were calculated as:

$$\Delta E_{stab} = E_{complex} - E_{4T} - E_{CNT} \quad (5.1)$$

where, $E_{complex}$ represents the energy of the exo-/endohedral complex. The stabilization energy was corrected for the basis set superposition error (BSSE) based on the counterpoise method proffered by Boys and Bernardi.[234] The above values were also corrected due to zero-point energy (ZPE) error. The interaction energy of each of the complexes was decomposed into various components such as dispersion, electrostatic, induction and exchange using symmetry-adapted perturbation theory (SAPT) [377] available in the PSI4 software.[378] The electronic properties such as ionization energy (IE), electron affinity (EA) and energy gap between highest occupied and lowest unoccupied molecular orbitals ($\Delta E_{HOMO-LUMO}$) were determined for all the systems as was discussed in chapters 3 and 4. Both the cationic and anionic systems are in their doublet state. It is assured that the spin contamination is negligible for these states. The charge transport parameters such as reorganization energy, transfer integral, rate of charge transfer and carrier mobility of the complexes were determined from the equations discussed in chapter 2. The optical absorption spectra were obtained using the time-dependent density functional theory (TD-DFT) proposed by Runge and Gross.[233] The light-harvesting efficiency (LHE) was evaluated from the oscillator strength as mentioned in the previous chapter. The optimized structures and molecular orbitals were generated by Gauss View 5.0 software.[288]

5.3 Results and Discussion

5.3.1 Geometries and stabilization energies of the complexes of CNT with 4T

The (6,6)CNT of length ~ 17 Å and diameter ~ 8 Å used in the previous chapters was employed to model its endo- and exohedral complexes with 4T.[297, 320] Herein, the functionals *viz.*, B97-D, B3LYP-GD3 and ω B97X-D were employed to study various properties of 4T, 4T@CNT and 4T-CNT. The above functionals have been widely used in the non-covalent interactions reported earlier.[379-381] Their optimized geometries obtained at different levels are depicted in figure 5.1. It is known that 4T exists either in cis or trans form although the latter is reported to be the most stable one.[382] Therefore, only the trans isomer is considered which is slightly non-planar. The major-axis of 4T is ~ 16 Å in length which is comparable to the length of CNT justifying the length of the latter used for the present work. As shown in figure 5.1, endo- as well as exohedral complexes were formed by aligning 4T along the tube-axis so as to have maximum π - π interactions

between the species involved. The other possible interactions include C-H... π and S... π . Although π - π and C-H... π interactions are prevalent in the complexes of carbon-based nanostructures [106, 383], S... π interaction is usually found in protein structures and occurs between its constituent amino acids.[384]. Further, it can be noticed from the figure that the structure of 4T is non-planar on the surface of CNT, on the other hand, the encapsulation of 4T inside CNT leads to planarity in its structure. The various bond lengths in free 4T as well as those in its respective endo- and exohedral complexes with (6,6)CNT were calculated for the B97-D optimized structures and are given in figure A3 of the Appendix-A. Comparison of various bond lengths of 4T with those of its endo- and exohedral complexes indicates that there is a significant change in the bond lengths of 4T in its endohedral complex rather than in its exohedral counterpart. A similar change in C-H bond length was also observed for 4T as in the case of indigo and PBI. Similar to PBI, the optimized geometry of 4T in its exohedral complex is slightly different from its free state as shown in figure 5.1.

To assess the relative stability of the complexes, the BSSE and ZPE corrected stabilization energies (ΔE_{stab}) were calculated as mentioned before and are listed in table 5.1. From the values, it can be seen that BSSE and ZPE corrected ΔE_{stab} of 4T@CNT is higher than that of 4T-CNT by about 5-15 kcal/mol, depending on the functionals used. Based on this, it can be concluded that the endohedral complex is more stable than the exohedral analogues irrespective of the functionals used. To determine how different components of interaction energy (dispersion, electrostatic and induction) contribute to the stability of complexes, their percentage contributions to the interaction energies were calculated and are listed in table 5.2. It can be inferred from the table that both endo- and exohedral complexes are stabilized largely (> 60%) by dispersion forces. The electrostatic force between the components of each complex is attractive in nature and contributes substantially to the overall stability. The contribution of induction energy is almost negligible compared to other two types of forces and is nearly the same for both complexes. It is also observed that the contribution of dispersion forces for exohedral complex is slightly more than that for endohedral complex. Contrary to this, the contribution of electrostatic forces is less for exohedral counterparts.

5.3.2 Electronic properties

To get insight on the electronic properties of the above complexes, the values of ionization energy, electron affinity and energy gap between highest occupied and lowest unoccupied molecular orbital ($\Delta E_{\text{HOMO-LUMO}}$) were calculated and are listed in table 5.3. It can be seen clearly from the table that 4T has a higher IE and a lower EA than those of CNT. It can also be observed

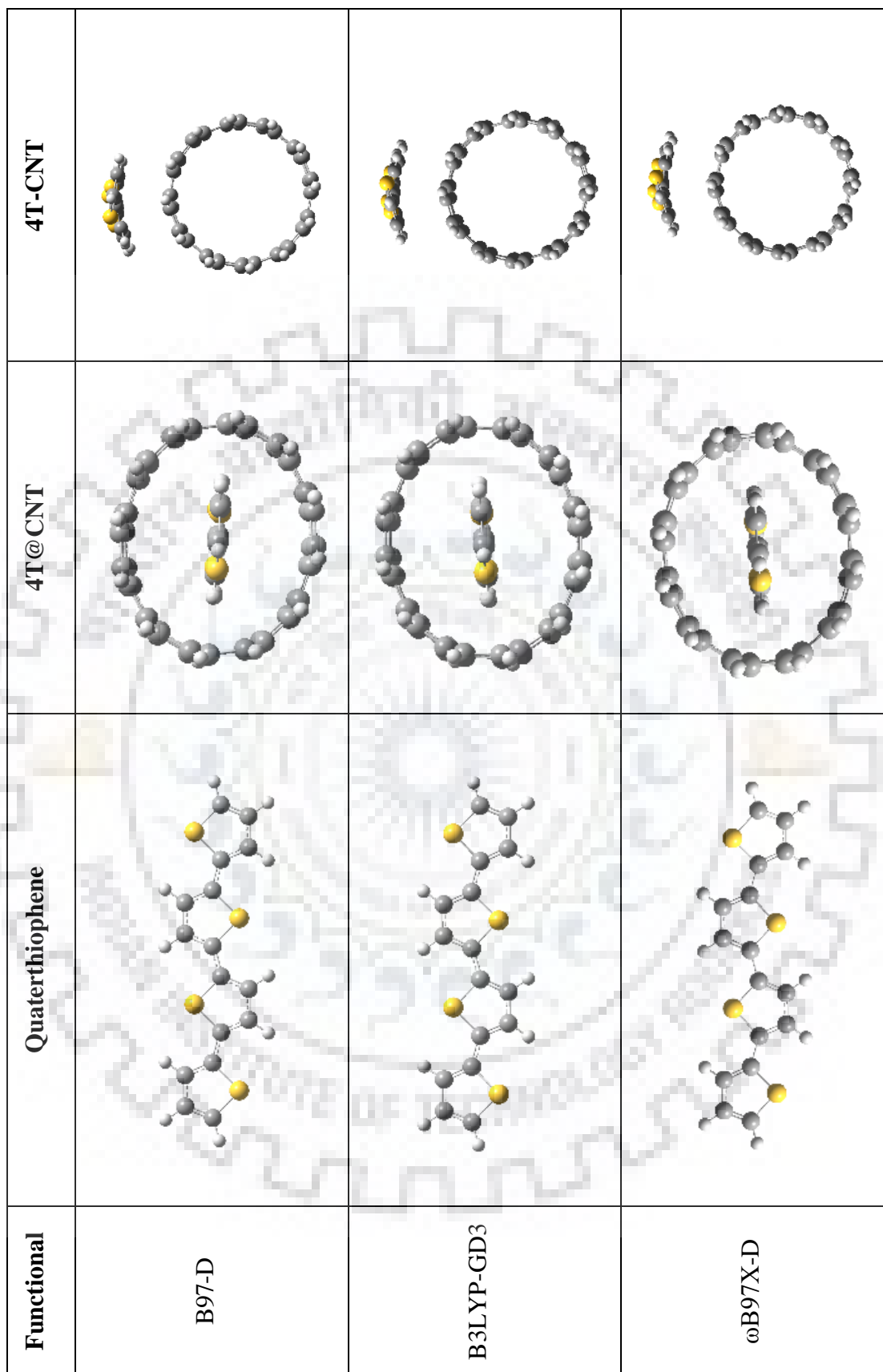


Figure 5.1 Optimized geometries of (a) 4T (b) 4T@CNT and (c) 4T-CNT obtained for different functionals using 6-31G(d,p) basis set.

Table 5.1 Stabilization energies (ΔE_{stab}) of endo- and exohedral complexes formed between CNT and 4T obtained for different functionals using 6-31G(d,p) basis set. All the energy values are in kcal/mol.

Complex	Functional	ΔE_{stab} without BSSE and ZPE corrections	ΔE_{stab} with BSSE and ZPE corrections
4T@CNT	B97-D	-58.92	-34.62
	B3LYP-GD3	-54.41	-30.09
	ω B97X-D	-50.79	-27.17
4T-CNT	B97-D	-29.40	-20.11
	B3LYP-GD3	-29.13	-20.32
	ω B97X-D	-30.11	-22.71

Table 5.2 Percentage contribution of various components of interaction energy for the complexes of CNT with 4T calculated using zeroth-order symmetry adapted perturbation theory (SAPT0) and 6-31G basis set.

Complex	Functional	Dispersion (%)	Electrostatic (%)	Induction (%)
4T@CNT	B97-D	61	34	5
	B3LYP-GD3	61	34	5
	ω B97X-D	60	34	6
4T-CNT	B97-D	63	31	6
	B3LYP-GD3	67	28	5
	ω B97X-D	66	28	6

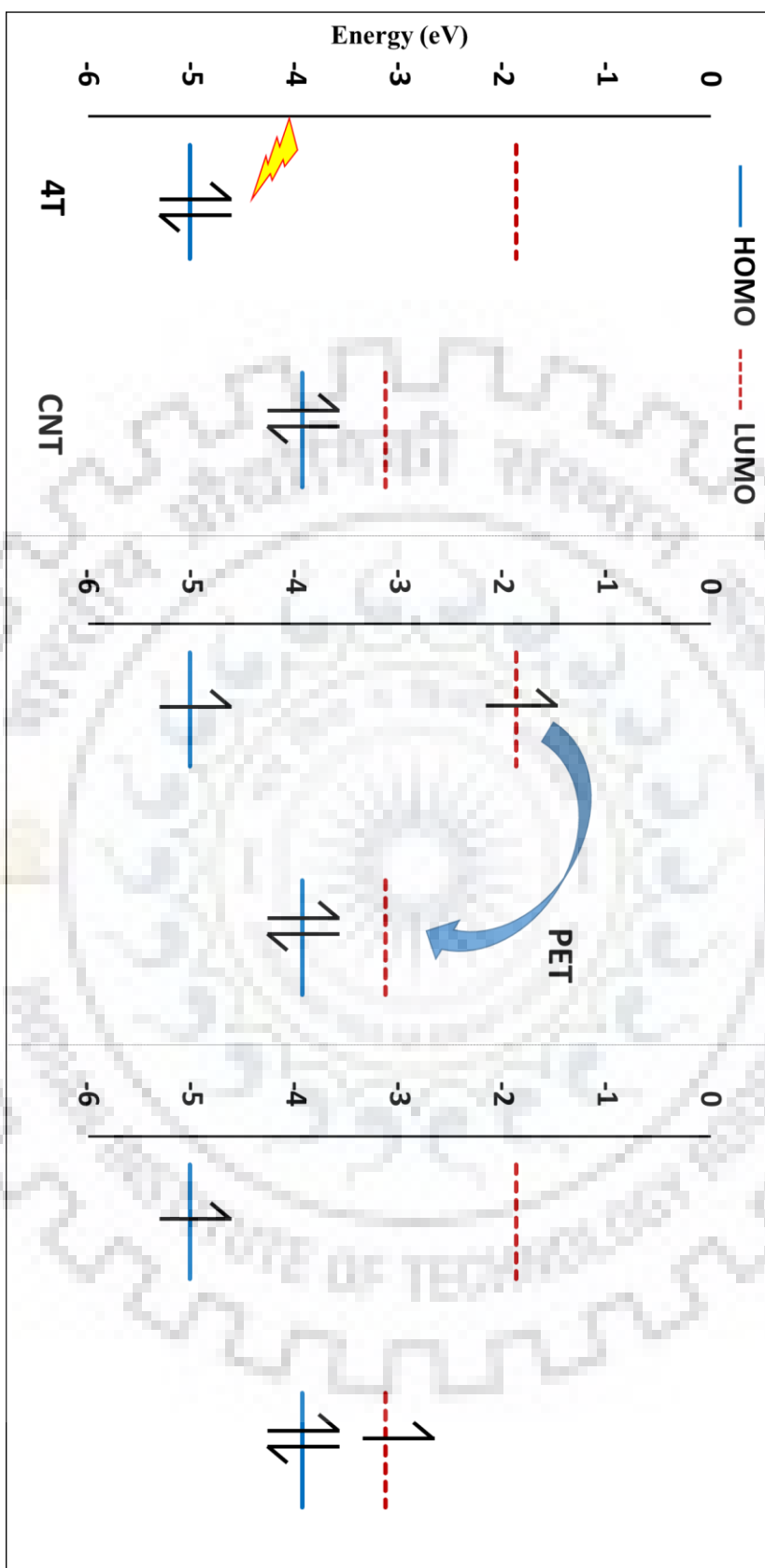


Figure 5.2 Schematic representation of the stepwise photoinduced electron transfer (PET) between 4T and CNT.

Table 5.3 Calculated values of ionization energy (IE), electron affinity (EA), energy gap between HOMO and LUMO ($\Delta E_{\text{HOMO-LUMO}}$) for 4T, CNT and their complexes obtained for different functionals using 6-31G(d,p) basis set. All the energy values are in eV.

Complex	Functional	VIE	AIE	VEA	AEA	$\Delta E_{\text{HOMO-LUMO}}$
4T	B97-D	6.01	5.89	-0.72	-0.82	1.87
	B3LYP-GD3	6.33	6.13	-0.59	-0.77	3.15 (3.13 ^a)
	ω B97X-D	6.86	6.49	-0.21	-0.56	6.93
(6,6)CNT	B97-D	4.93	4.90	-2.15	-2.17	0.80
	B3LYP-GD3	5.06	5.03	-2.06	-2.09	1.47
	ω B97X-D	5.50	5.43	-1.83	-1.90	3.97
4T@CNT	B97-D	— ^b	— ^b	-2.13	-2.15	0.64
	B3LYP-GD3	5.03	5.01	-2.04	-2.07	1.50
	ω B97X-D	5.48	5.43	-1.81	-1.87	3.98
4T-CNT	B97-D	4.86	4.83	-2.13	-2.15	0.80
	B3LYP-GD3	5.01	4.97	-2.04	-2.07	1.45
	ω B97X-D	5.45	5.37	-1.81	-1.88	3.96

^aFrom Reference [385], ^bConvergence criteria not met.

from the table that for 4T, the value of $\Delta E_{\text{HOMO-LUMO}}$ (3.15 eV) obtained using B3LYP-GD3 is more close to the reported value of 3.13 eV at B3LYP/6-31G(d) level.[385] Earlier studies have reported that B3LYP-GD3 is the ideal functional for evaluating the energy gap.[320, 322, 386] The findings of the present study suggest that B97-D underestimates and ω B97X-D overestimates the orbital energy gap in agreement with earlier studies.[387-389] From the values listed in table 5.3, it can be discerned that the above properties of CNT do not differ significantly from those of its complexes.

Based on the analysis of frontier molecular orbitals of 4T and CNT, the possible mechanism of photoinduced electron transfer between them was deduced and is shown in figure 5.2. As can be seen from the figure, the photoexcitation of electron takes place from HOMO of 4T to its LUMO. Further, the photoexcited electron gets transferred from LUMO of 4T to that of CNT. Thus, it can be concluded that the photoinduced electron transfer (PET) can take place from 4T to CNT and not vice-versa.

5.3.3 Charge transport properties

The carrier mobility is of great importance to understand the charge transport properties of an organic semiconductor. The essential parameter to calculate mobility (μ) is charge transfer rate constant (k), which in turn depends on the reorganization energy (λ) and the transfer integral (t) as well as center-to-center distance (d_{c-c}) between interacting molecules. Table 5.4 lists the values of the above mentioned parameters for PBI-CNT complexes obtained using the functional B97-D, B3LYP-GD3 and ω B97X-D. The tabulated values of reorganization energy for both types of complexes indicate that the hole reorganization energy (λ_+) is larger than the electron reorganization energy (λ_-), irrespective of the functional used. This is probably due to the higher structural relaxation of the complexes for the transport of holes than that of electrons. The transfer integral of electrons (t_-) is found to be greater than that of holes (t_+) for endohedral complex, irrespective of the level of calculations used. This also holds true for the transfer integrals of exohedral complex computed using ω B97X-D. For other functionals, the exohedral complex shows the same value of hole and electron transfer integrals. To achieve a high mobility, a low reorganization energy and a high transfer integral are needed. For both types of complexes, electron mobility is found to be higher than hole mobility thereby showing n-type charge transfer characteristics. These can be attributed to two factors: (i) $\lambda_- < \lambda_+$ and (ii) $t_- > t_+$. Compared to the exohedral complex, its endohedral analogue has higher ratio of electron mobility to hole mobility. It can be seen from the table that exohedral complex exhibits electron mobility of $2.65 \text{ cm}^2\text{V}^{-1}\text{s}^{-1}$ at B97-D level. Compared to this, a relatively higher electron mobility of $3.79 \text{ cm}^2\text{V}^{-1}$

Table 5.4 Calculated values of transfer integral (t), internal reorganization energy (λ), rate constant (k) and carrier mobility (μ) for the complexes at different distances between centre of 4T and that of nearby surface of CNT (d_{c-c}) obtained for different functionals using 6-31G(d,p) basis set.

Complex	Functional	Distance (Å)	λ_+ (eV)	t_+ (eV)	k_+ (s ⁻¹)	μ_+ [cm ² V ⁻¹ s ⁻¹]	λ_- (eV)	t_- (eV)	k_- (s ⁻¹)	μ_- [cm ² V ⁻¹ s ⁻¹]
4T@CNT	B97-D	3.60	— ^a	0.08	— ^a	— ^a	0.04	0.09	0.15×10^{15}	3.79
	B3LYP-GD3	3.65	0.07	0.07	0.02×10^{15}	0.52	0.06	0.10	0.07×10^{15}	1.82
	ω B97X-D	3.63	0.15	0.11	0.15×10^{13}	0.04	0.13	0.12	0.59×10^{13}	0.16
4T-CNT	B97-D	3.52	0.05	0.09	0.07×10^{15}	1.67	0.04	0.09	0.11×10^{15}	2.65
	B3LYP-GD3	3.53	0.08	0.11	0.03×10^{15}	0.74	0.07	0.11	0.05×10^{15}	1.21
	ω B97X-D	3.76	0.16	0.11	0.11×10^{13}	0.03	0.14	0.13	0.31×10^{13}	0.09

^aConvergence is not achieved.

s^{-1} is obtained for endohedral analogue at same level of theory. In contrast to the charge transfer characteristics of the complexes formed by CNT with indigo or PBI, the complexes of CNT with 4T exhibit n-type behaviour suggesting the complexes as promising for their applications in n-type transistors.

5.3.4 Optical absorption properties

The performance of different density functionals was assessed in the prediction of optical properties of 4T and its complexes with CNT. The simulated absorption spectra of 4T using different functional are depicted in figure 5.3a. For B97-D and B3LYP-GD3, a significant absorption takes place in the near ultraviolet-visible region of electromagnetic spectrum whereas the absorption occurs only in the near-infrared region for ω B97X-D. The maximum intensity for 4T is greater than one, irrespective of the functional used. Table 5.5 lists the values of maximum absorption wavelength (λ_{\max}), oscillator strength (f) and light-harvesting efficiency (LHE) for 4T. The λ_{\max} of 423 nm obtained at B3LYP-GD3 level is in good agreement with the reported value of 436 nm at B3LYP/6-31G(d,p) level.[390] Furthermore, the respective oscillator strengths of 1.19 and 1.20 obtained using B3LYP-GD3 and ω B97X-D are in excellent agreement with the value of 1.21 reported earlier at B3LYP/6-31G(d,p) level.[390] For all these functionals, very high light-harvesting efficiency (~94%) is attained. The excitation energy corresponding to HOMO \rightarrow LUMO transition of 4T obtained at B97-D, B3LYP-GD3 and ω B97X-D levels is 2.53, 2.93 and 3.61 eV, respectively. The excitation energy (2.74 eV) reported at CASPT2 level is more close to that calculated at B97-D and B3LYP-GD3 levels.[391] Thus, B97-D and B3LYP-GD3 results can be considered more reliable for determining the excitation energies.

Figures 5.3b and 5.3c display the absorption spectra of endo- and exohedral complexes, respectively. It can be seen from the figures that the complexes cover a wide spectral range (from visible to near-infrared region) for B97-D. For other functionals, the absorptions occur only in the visible region of the spectrum. Several peaks of relatively low intensity are also seen in the absorption spectra of the complexes, except for ω B97X-D. Table 5.6 lists the values of maximum absorption wavelength (λ_{\max}), light-harvesting efficiency (LHE) and molecular orbitals involved in the electronic transitions for the complexes. As evident from the table, the maximum absorption for the endohedral complex occurs at higher wavelength than that for its exohedral analogue. This suggests that the endohedral complex is more suitable for solar cell applications. The computed LHE for the complexes is greater than 95% at ω B97X-D level, which is also slightly larger than the LHE of 4T. The analysis of the molecular orbitals involved in the transition corresponding to λ_{\max} indicates the absence of any photoinduced charge transfer.

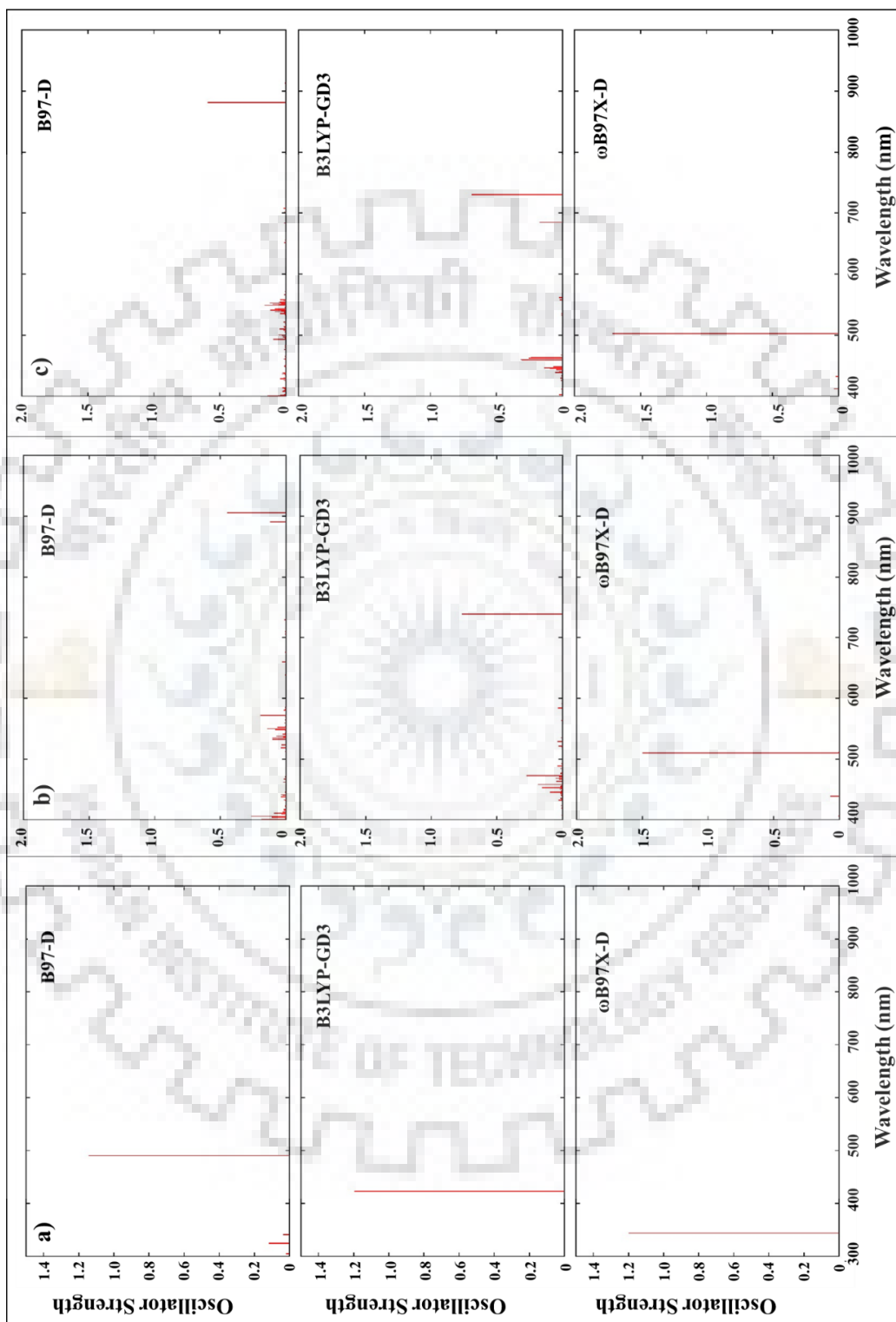


Figure 5.3 Simulated absorption spectra of (a) 4T (b) 4T@CNT and (c) 4T-CNT obtained for different functionals using 6-31G(d,p) basis set.


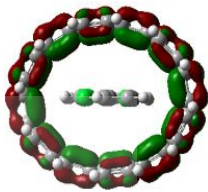
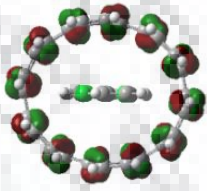
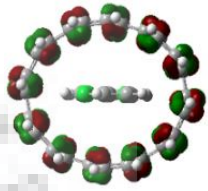
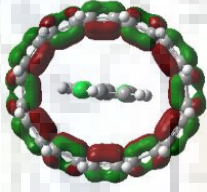

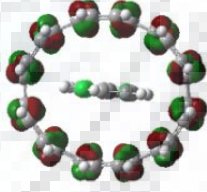
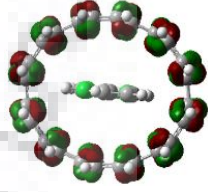
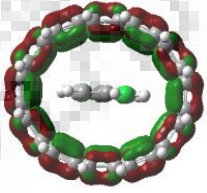
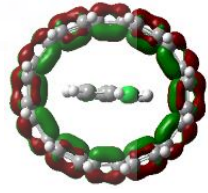
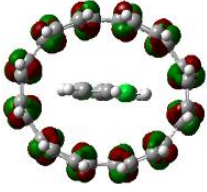
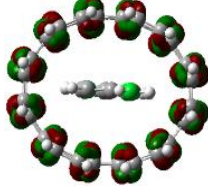
To further explore the charge transfer properties of the complexes, the molecular orbital analysis was performed for other absorption peaks of lower intensities and the results obtained at B3LYP-GD3 level are summarized in tables 5.7 and 5.8. As in the earlier cases, only those transitions for which oscillator strength greater than or equal to 0.05 and orbital contribution more than 15% were considered. For the endohedral complex, it is apparent from table 5.7 that wavelengths at 445, 453 and 458 nm are ascribed to charge transfer transitions. These transitions are contributed from HOMO-1 to outer unoccupied orbitals (LUMO+14 and LUMO+15). The values presented in table 5.8 indicates that the exohedral complex exhibits several charge transfer transitions between 448-462 nm as well as at relatively long wavelength (685 nm). These transitions are mostly contributed by those from the inner occupied molecular orbitals to LUMO or LUMO+4. An analysis of the molecular orbitals revealed the shift of electron density from 4T to CNT implying that 4T acts as an electron donor and CNT behaves as an electron acceptor in both endo- and exohedral complexes.

Table 5.5 Calculated values of maximum absorption wavelength (λ_{\max}), oscillator strength (f) and light-harvesting efficiency (LHE) of 4T obtained for different functionals using 6-31G(d,p) basis set.

Functional	λ_{\max} (nm)	f	LHE (%)
B97-D	490	1.14	93
B3LYP-GD3	423 (436) ^a	1.19	94
ω B97X-D	344	1.20	94

^aFrom Reference [390]

Table 5.6 The maximum absorption wavelength (λ_{\max}), light-harvesting efficiency (LHE) and the molecular orbitals involved in the electronic transitions of the complexes 4T@CNT and 4T-CNT obtained for different functionals using 6-31G(d,p) basis set.

System	Functional	λ_{\max} (nm)	LHE (%)	Molecular orbitals involved in the transitions	
	B97-D	906	65		
				HOMO-2	LUMO
					
				HOMO-1	LUMO+1
4T@CNT	B3LYP-GD3	738	83		
				HOMO-2	LUMO
					
				HOMO	LUMO+1
	ω B97X-D	510	97		
				HOMO-1	LUMO
					
				HOMO	LUMO+1

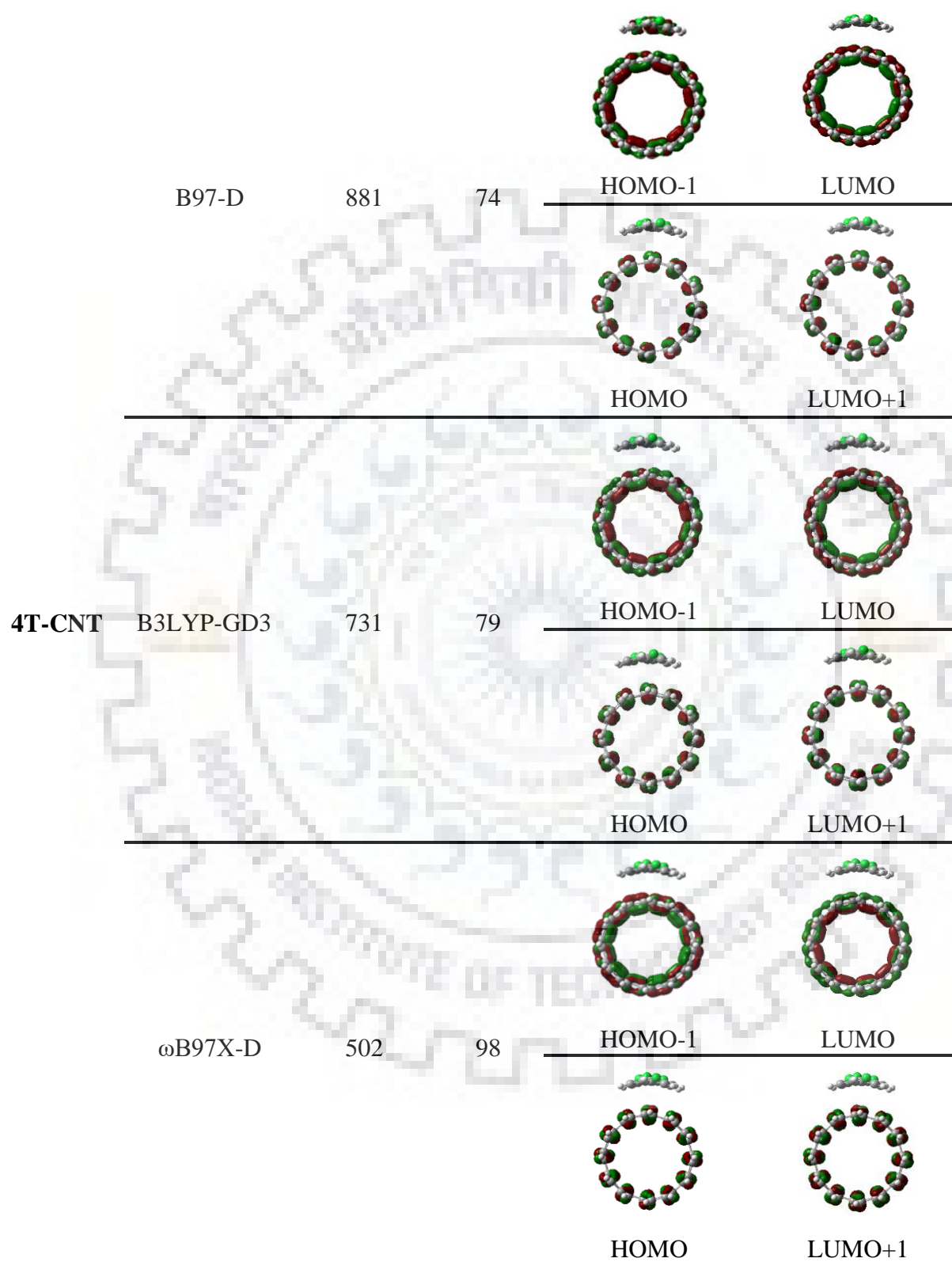
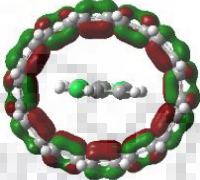
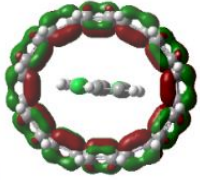
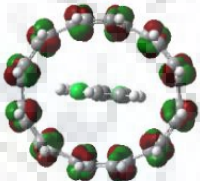
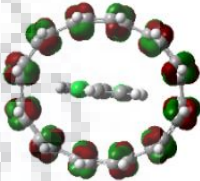

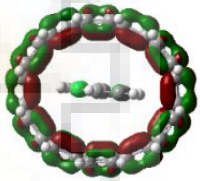
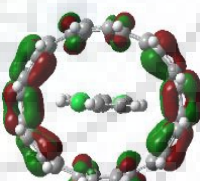
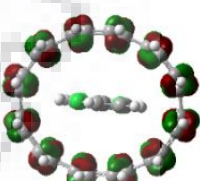
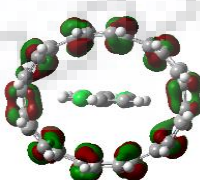
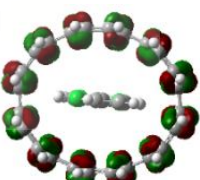


Table 5.7 The absorption wavelength (λ), oscillator strength (f), percentage orbital contribution and molecular orbitals involved in the transition of the complex 4T@CNT obtained for different functionals using 6-31G(d,p) basis set.

λ (nm)	f	Orbital contribution (%)	Molecular orbitals involved in the transitions	
738	0.76	48	 HOMO-2	 LUMO
		47	 HOMO	 LUMO+1
473	0.27	22	 HOMO-7	 LUMO
		20	 HOMO-5	 LUMO+1
468	0.05	67	 HOMO-8	 LUMO+1

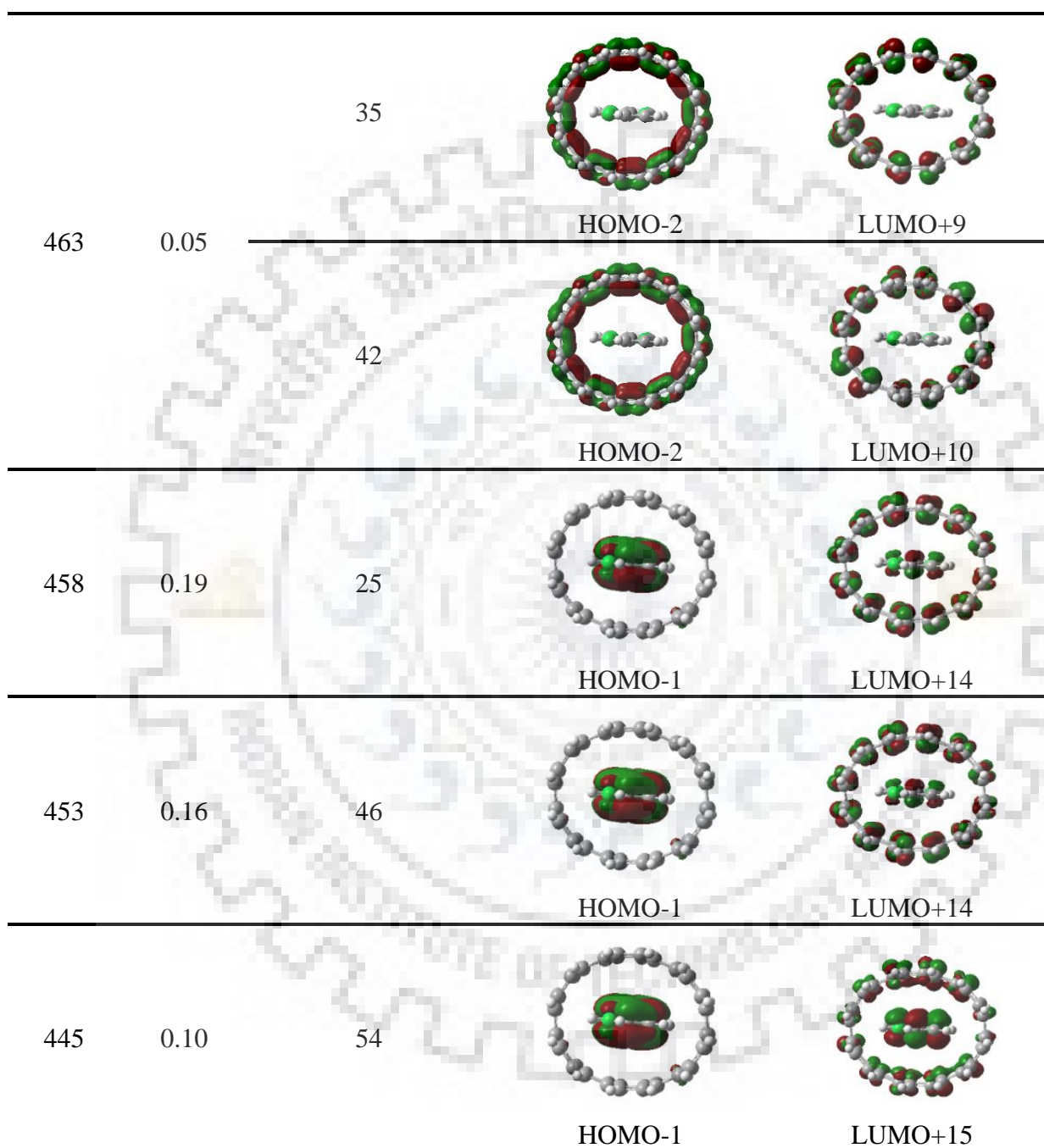

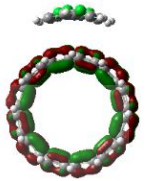
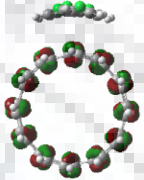
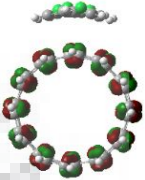



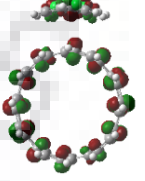
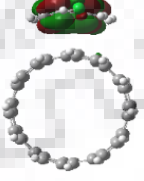
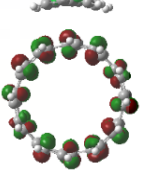
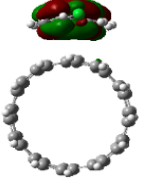
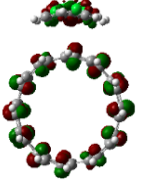
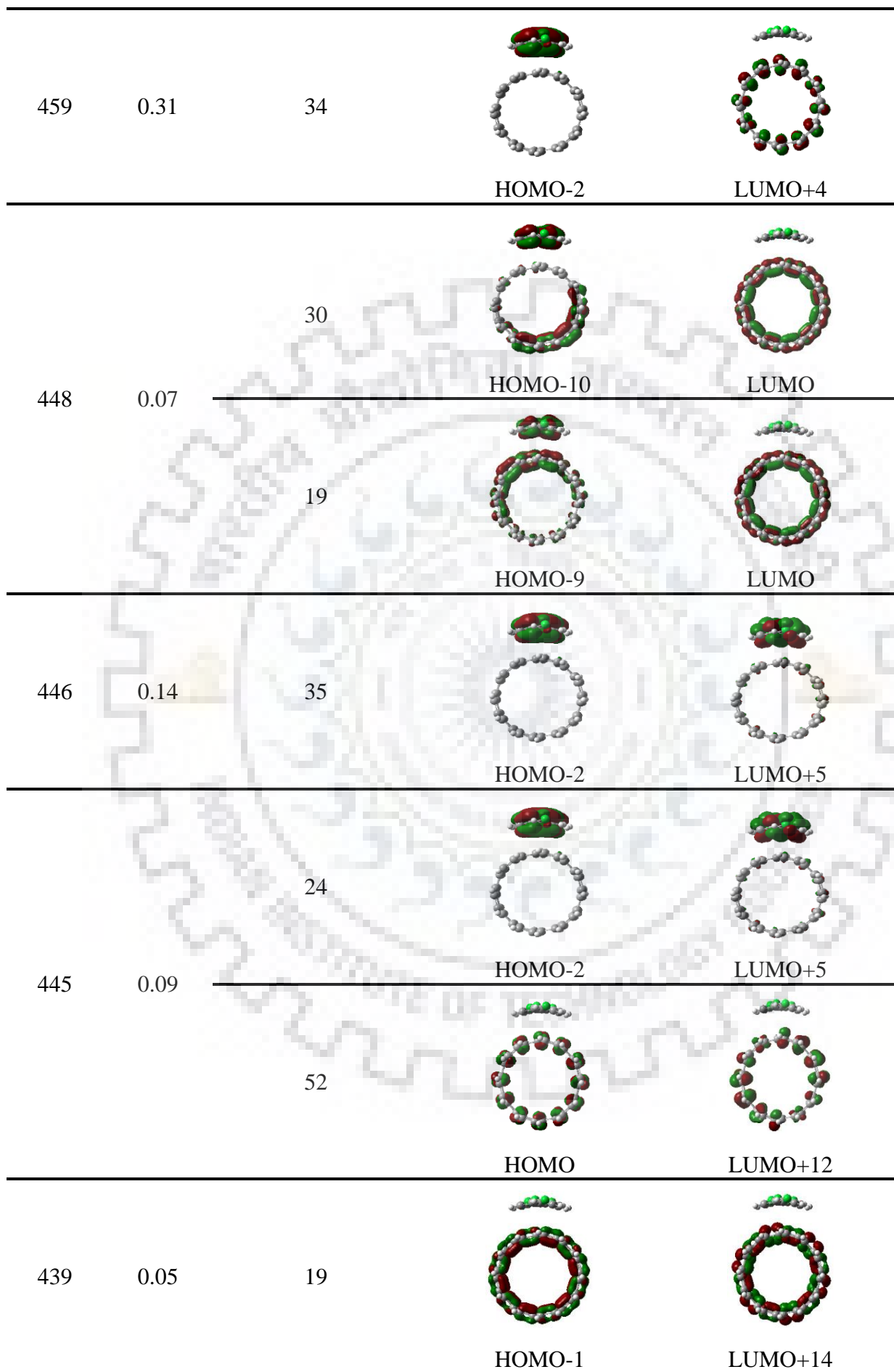


Table 5.8 The absorption wavelength (λ), oscillator strength (f), percentage orbital contribution and molecular orbitals involved in the transition of the complex 4T-CNT obtained for different functionals using 6-31G(d,p) basis set.

λ (nm)	f	Orbital contribution (%)	Molecular orbitals involved in the transitions	
731	0.68	44	 HOMO-1	 LUMO
		42	 HOMO	 LUMO+1
685	0.17	87	 HOMO-2	 LUMO
464	0.24	61	 HOMO-2	 LUMO+3
462	0.26	50	 HOMO-2	 LUMO+4
460	0.32	26	 HOMO-2	 LUMO+3



5.4 Conclusion

The optoelectronic and charge transport properties of endo- as well as exohedral complexes formed between CNT and 4T were investigated using various dispersion-corrected density functional methods in this chapter. The optimized geometries of the complexes were almost remained the same for different functionals. The calculated values of BSSE and ZPE corrected stabilization energies using B97-D functional for endo- and exohedral complexes are -35 and -20 kcal/mol, respectively, indicating that they are energetically stable. Moreover, it was observed that the endohedral complex was stabilized by about 5-15 kcal/mol relative to the exohedral complex, depending on the functional used. The stabilization of these complexes was due to dispersion, electrostatic and induction interactions. The dispersion interaction was more prominent in 4T-CNT, while the electrostatic interaction was predominant in 4T@CNT. It was found that the electronic properties such as ionization energy, electron affinity and energy gap between HOMO-LUMO of CNT do not change significantly on complexation with 4T. However, the optical and charge transport properties of 4T@CNT and 4T-CNT differed largely from those of their constituents. Although both endo- and exohedral complexes of CNT with 4T exhibited several charge transfer transitions in the excited states, they more likely occurred in the former case. The charge transfer transitions were accompanied by the transfer of electron density from donor 4T to acceptor CNT at wavelengths lying in the visible region of the electromagnetic spectrum. The complexes also showed very high light harvesting efficiency (> 95%) which suggest them suitable for solar cell applications.

In contrast to p-type nature of complexes of CNT with indigo and PBI, the complexes CNT with 4T showed higher value of electron mobility than hole mobility indicating that they can be used as n-type semiconductors. Thus, the complexes considered in this work are expected to have potential applications as n-type transistors in the realm of optoelectronics.



CHAPTER 6

Structure, Stability and Properties of the Complexes of Carbon Nanotube with Cycloparaphenylene and its Derivatives

6.1 Introduction

In chapters 3-5 of the present thesis, the encapsulation of different guest molecules such as indigo, perylene bisimide and quaterthiophene inside CNT were studied. The present chapter discusses the encapsulation of CNT within some macrocyclic systems. A recently synthesized macrocyclic system known as [10]cycloparaphenylene ([10]CPP) has been used for this purpose.[25] CPP is a ring-shaped molecule, which is composed of π -conjugated phenylene units connected at para-positions of each other. Within a decade after the synthesis of first CPP, another group of researchers successfully synthesized a series of CPPs with varying diameter ($[n]$ CPPs, where $n = 8-13$).[392] Their study revealed that the optoelectronic properties of $[n]$ CPPs change with the number of phenyl units. The optoelectronic properties of CPP are expected to be affected by the substitution of hydrogens with different functional groups or by doping of carbon atoms. Synthesis of various derivatives of CPP have been performed in the recent past to tune its properties. In 2014, Tran-Van and co-workers synthesized the derivatives of [8]CPP via [2+2+2] cycloaddition reaction and found that the optical properties of these derivatives differ largely from their unsubstituted analogue.[393] Very recently, Rio *et al.* synthesized halogen-substituted derivatives of CPP and demonstrated that the substitution of hydrogens of CPP by halogens leads to increase in the energy gap between highest occupied and lowest unoccupied molecular orbitals ($\Delta E_{\text{HOMO-LUMO}}$) of the resulting compounds.[394] Bachrach and Stück performed density functional theoretical studies on the doping of nitrogen atoms in the phenylene units of $[n]$ CPP ($n = 3-16$).[395] Various types of N- $[n]$ CPP derivatives considered in their study include pyridine, pyrazine, pyridazine and pyrimidine units in the ring structure of CPP. The dihedral angle between two successive nitrogen bearing units was found to be different for different N- $[n]$ CPP derivatives. A combined experimental and theoretical study on the optoelectronic properties of a series of aza[8]CPP by Darzi and colleagues showed a gradual decrease in $\Delta E_{\text{HOMO-LUMO}}$ and an increase in absorption wavelength with an increase in the number of nitrogen atoms.[396]

It has been reported that cycloparaphenylenes can host various fullerenes.[246, 397-401] In 2011, the endohedral complexes of $[n]$ CPP ($n = 8-12$) encapsulating C_{60} as guest species have been synthesized for the first time by Iwamoto and co-workers.[397] Their study showed that [10]CPP can be a suitable host for C_{60} as its diameter is large enough to accommodate the latter

species. Earlier studies have demonstrated that the cavity size of [11]CPP is suitable for the encapsulation of C_{70} and C_{82} . [398-401] Density functional theoretical studies using M06-2X functional and 6-31G(d) basis set for the inclusion complexes of [10]CPP and [11]CPP with C_{70} in lying and standing orientations, respectively, indicated a significant change in the structure of [11]CPP. [398] However, such a structural change was not observed for [11]CPP. A similar study on the stability of the complexes formed between C_{70} and [n]CPP ($n = 10-12$) for various orientations of C_{70} has also been reported by Yuan and co-workers. [246] In the most stable structure of each of the above complexes, C_{70} oriented in lying, standing and half-lying configurations with respect to the C_n -axis of [10]CPP, [11]CPP and [12]CPP, respectively. Using M06-2X functional and various basis sets, a potential energy surface analysis has been performed by Yuan *et al.* by moving C_{60} inside [8]CPP, [9]CPP and [10]CPP. Their results showed double-, triple- and single-well potentials for the respective complexes. [401]

In this chapter, the structural, stability and optoelectronic properties of a new class of host-guest complexes between CPP and CNT are investigated. The stability and optoelectronic properties of free CPP, CNT of length $\sim 11.7 \text{ \AA}$ and their complex are discussed. The optoelectronic properties are investigated for CPP, its various derivatives and their complexes with CNT. The schematic diagram of these systems is illustrated in figure 6.1. For the complexes, effect of the number of dopants and donor/acceptor substituents on the above-mentioned properties is also explored. To get insight on the translational motion of CPP over CNT, the change in potential energy due to the movement of CPP over a relatively long CNT of length $\sim 21.6 \text{ \AA}$ is studied. The energy barrier for the rotation of CPP around CNT is also examined.

6.2 Computational Methods

The geometry optimization and the vibrational frequency calculations were performed for all systems using Grimme's empirical dispersion corrected density functional B3LYP-GD3 and 6-31G(d,p) basis set. [201, 232] The above functional has been validated in earlier studies on several non-covalent complexes similar to the systems considered in the present study. [402, 403] The positive frequencies obtained for all the vibrational modes of the systems ensure the minima on the potential energy surface. The stabilization energy (ΔE_{stab}) of each complex was calculated and also, corrected for basis set superposition error (BSSE) as discussed in previous chapters. The zero-point energy (ZPE) corrections were further incorporated to BSSE corrected values of ΔE_{stab} . The contribution of different components of energy (electrostatic, exchange, induction and dispersion) was also determined using the symmetry adapted perturbation theory (SAPT) as

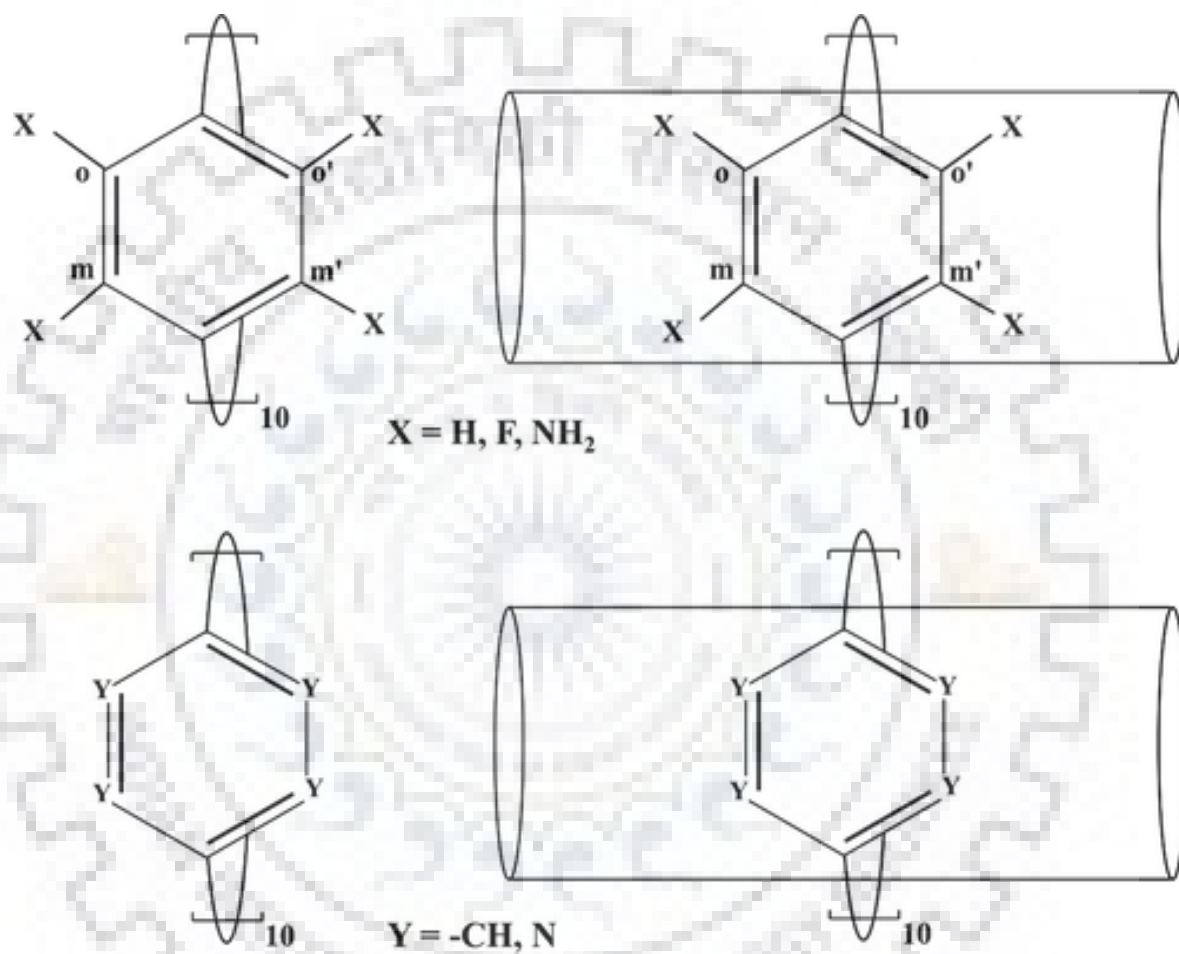


Figure 6.1 Schematic diagram of [10]CPP, its derivatives and their complexes with CNT.

reported in the studies of various non-covalent complexes [299-301]. Similar to the previous chapters, the calculations were performed using the zeroth-order SAPT approach in conjunction with 6-31G basis set as implemented in PSI4 suite of programs.[342] For various systems, the vertical ionization energy (IE) and vertical electron affinity (EA) were calculated. Both the cationic and anionic systems are in their doublet state. It is assured that these states has no spin contamination. To comprehend about the charge-transfer interactions between components, the frontier molecular orbital analysis was performed. The time-dependent density functional theoretical (TD-DFT) calculations were carried out to obtain the absorption wavelength (λ) and oscillator strength (f).[233] The light-harvesting efficiencies (LHE) were also determined as mentioned in previous chapters. All the above calculations were done using Gaussian 09 software package.[287] The optimized geometries and molecular orbital (MO) diagrams were generated using Gauss View 5.0 program.[288]

6.3 Results and discussion

6.3.1 Mechanically interlocked complex of CPP with CNT

The optimized geometries of [10]cycloparaphenylene (CPP), (6,6)-carbon nanotube (CNT) and their corresponding complex are shown in figure 6.2. As indicated in the figure, CPP has the diameters 13.3 and 13.9 Å along two perpendicular directions and CNT has a diameter of 8.1 Å. These values clearly indicate that CPP chosen is large enough to encapsulate CNT. CNT of length 11.7 Å was used as a guest to form inclusion complex with CPP. The resulting complex is labelled as CNT@CPP for further discussion. The interlayer distance of ~ 3.0 Å obtained for the complex is close to the π - π interacting complexes reported earlier [103, 297, 320, 404] In preceding chapters 3-5, CNT acted as a host for guest molecules indigo, PBI and 4T. Contrary to this, CNT behaves as a guest molecule for the host CPP in the present chapter. Owing to the encapsulation of CNT inside CPP, a slight increase in the diameter of the latter is observed in the complex. The stabilization energies (ΔE_{stab}) of the complex considered in the present chapter are listed in Table 6.1. The BSSE and ZPE corrected values of ΔE_{stab} for CNT@CPP is -8.93 kcal/mol. It can be seen from the table that the value of BSSE for the complex is large due to the relatively less distance between CPP and CNT (~ 3 Å) compared to 3.4 Å between two benzene rings in the dimeric structure. Also, more number of such rings in CNT-CPP leads to the reported BSSE. The stabilization of the complex can be attributed to the attractive π - π interactions between the π -electron clouds of CPP and CNT and to the C-H... π interactions between the C-H bonds of CPP and π -electrons of CNT. Table 6.2 summarizes the percentage contributions of

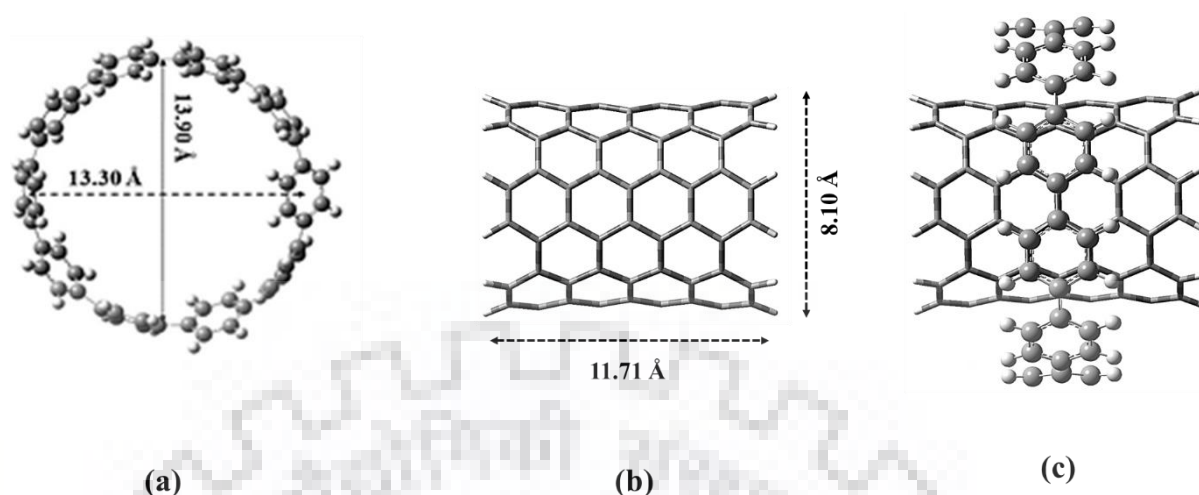


Figure 6.2 Optimized geometries of (a) [10]CPP, (b) CNT, and (c) the complex CNT@[10]CPP.

various energy components for the complex CNT@CPP. It is evident from the table that the complex is stabilized by dispersion forces followed by electrostatic and induction forces.

The ionization energy (IE) and electron affinity (EA) can be used as important parameters to describe the electron-donor/electron-acceptor nature of the compounds. For any compound, a low value of IE and a high value of EA are indicative of electron-donating and electron-accepting abilities, respectively. The calculated values of IE and EA for free molecules as well as their complex are given in table 6.3. In pristine state, CPP has an IE of 6.04 eV which is close to that of 6.24 eV reported earlier.[405] For CNT, the value of IE is 4.57 eV and that of EA is -2.38 eV. It can be also seen from the table that the IE of CNT is lower than the IE of CPP. On the other hand, the EA of CNT is more negative than that of CPP. Based on this, it can be envisaged that CNT acts as a better electron donor as well as an acceptor than CPP. This rules out the possibility of formation of donor-acceptor complex between CPP and CNT. Considering the IE of free CNT, a decrease of ~ 0.05 eV is observed for its complex. Similarly, EA of the complex is less negative than that of free CNT by ~ 0.1 eV. Therefore, only a slight change in the electronic properties of complex is observed compared to those of CNT. The frontier molecular orbitals of the above complex are shown in figure 6.3. The electron density in frontier orbitals of these complex resides only on CNT, ruling out the possibility of photoinduced charge transfer between the component species. Table 6.3 lists the values of the energies of HOMO and LUMO along with the energy gap between them. The $\Delta E_{\text{HOMO-LUMO}}$ of 3.49 eV for CPP is in agreement with the value of 3.53 eV reported earlier.[392] For CNT, the obtained value of $\Delta E_{\text{HOMO-LUMO}}$ is 0.53 eV. From the table, it can be seen that $\Delta E_{\text{HOMO-LUMO}}$ of the complex is slightly more than that of free CNT. This trend is opposite to that observed in the complexes indigo-CNT and PBI-CNT studied in

chapters 3 and 4. The energy gap between HOMO and LUMO of less than 1 eV for the above complex suggests it to be ideal for low energy gap semiconductor.

To investigate how the absorption properties of individual molecules vary on forming the complex, the time-dependent density functional theoretical calculations were performed. The values of maximum absorption wavelength (λ_{\max}) and the corresponding light-harvesting efficiency (LHE) for CPP and CNT are listed in table 6.4. For [10]CPP, the λ_{\max} lies at 350 nm which is close to the earlier reported value of 348 nm.[406] The λ_{\max} obtained is also very close to the experimental value of 338-339 nm reported for [n]CPPs ($n = 9, 12, 14, 15, 16$).[405] The maximum absorption wavelength (λ_{\max}) exhibited by CNT is ~ 320 nm and that of its complex with CPP is ~ 395 nm. It can be seen from the table that the LHE of the complex is relatively less than that of its individual components. The molecular orbitals involved in the transition corresponding to maximum absorption are depicted in figure 6.4. It can be observed from the figure that the electron density of the associated molecular orbitals for both complexes resides only on one of the components ruling out the possibility of charge transfer between the components. The absorption spectra of the above systems are depicted in figure 6.5. As can be seen from the figure, the optical absorption of CPP falls in the near-ultraviolet region of the electromagnetic spectrum. Compared to this, that of CNT and the complex CNT@[10]CPP spreads in the near-ultraviolet as well as visible region.

6.3.2 Amino and fluorine-substituted derivatives of CPP

To understand the effect of donor-acceptor substitution on the optoelectronic properties of CPP, a variety of amino- and fluorine-substituted CPP were designed. These derivatives of CPP were modelled by substituting hydrogen atoms of phenylene units with electron-donating amino and electron-withdrawing fluorine groups. Five different types of fluorine-substituted CPP were modelled as depicted in figure 6.6. For example, the fluorine-substituted compound (10F-[10]CPP) represents substitution of one fluorine atom in each phenyl units of [10]CPP. The di-substituted derivatives have two fluorine atoms per phenylene ring of CPP. Three different types of isomers of di-substituted derivatives are designated by (ortho, ortho)-, (ortho, meta)- and (ortho, meta')-20F-[10]CPP. Similarly, the tetra-substituted fluorine derivative is represented as 40F-[10]CPP. The same strategy is used for amino-substituted CPP as shown in figure 6.7. Close examination of the dihedral angles between adjacent phenylene units of the amino-substituted compounds revealed an increase in its value with the number of substituents. The compound 10NH₂-[10]CPP possesses a dihedral angle of $\sim 41^\circ$ between adjacent phenylene units. For the

Table 6.1 The values of stabilization energy (ΔE_{stab}) for the complexes of CPP, its substituted and doped derivatives with CNT. All the energy values are in kcal/mol.

Compound	Stabilization energy (ΔE_{stab})		
	Without BSSE and ZPE corrections	With BSSE correction	With BSSE and ZPE corrections
CNT@[10]CPP	-38.98	-10.07	-8.93
CNT@10NH ₂ -[10]CPP	-24.10	6.06	9.16
CNT@(ortho, ortho')20NH ₂ -[10]CPP	-19.33	18.30	28.44
CNT@(ortho, meta)20NH ₂ -[10]CPP	-11.85	19.87	26.27
CNT@(ortho, meta')20NH ₂ -[10]CPP	--- ^a	--- ^a	--- ^a
CNT@40NH ₂ -[10]CPP	334.88	377.80	377.15
CNT@10F-[10]CPP	-48.12	-14.62	-12.59
CNT@(ortho, ortho')20F-[10]CPP	-65.54	-29.03	-27.40
CNT@(ortho, meta)20F-[10]CPP	-54.20	-14.98	-13.30
CNT@(ortho, meta')20F-[10]CPP	-62.88	-26.77	-25.10
CNT@40F-[10]CPP	-197.00	-143.53	-142.88
CNT@10N-[10]CPP	-20.16	9.78	12.17
CNT@(ortho, ortho')20N-[10]CPP	11.54	42.59	44.55
CNT@(ortho, meta)20N-[10]CPP	17.12	48.86	49.99
CNT@(ortho, meta')20N-[10]CPP	9.41	40.17	41.67
CNT@40N-[10]CPP	26.75	60.17	61.91

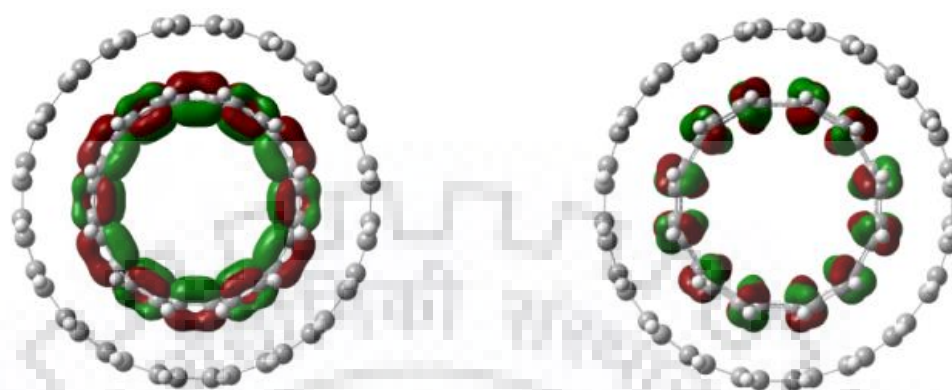
^aConvergence criteria was not achieved.

Table 6.2 Percentage contribution of various components of energy for the interactions of CPP, its fluorine-substituted derivatives with CNT.

Compound	Electrostatic	Dispersion	Induction
CNT@[10]CPP	38	57	5
CNT@10F-[10]CPP	37	58	5
CNT@(ortho, ortho')20F-[10]CPP	37	58	5
CNT@40F-[10]CPP	41	52	7

isomers (ortho, ortho')- and (ortho, meta)-20NH₂-[10]CPP, the dihedral angle is ~50° although it is in the range 17-33° for the isomer (ortho, meta')-20NH₂-[10]CPP. The less distortion for the structure of the latter isomer is probably due to the least steric hindrance between two amino groups that are relatively far apart from each other. The dihedral angle is maximum for the tetra-substituted amino derivative and is in the range 61-72°. The dihedral angle between the adjacent phenyl units for the mono- and di-fluorinated CPP is ~32°. Compared to this, the dihedral angle (~50°) for the tetra-fluorinated CPP is relatively large and is in agreement with the value of 47° reported by Rio and co-workers.[394]

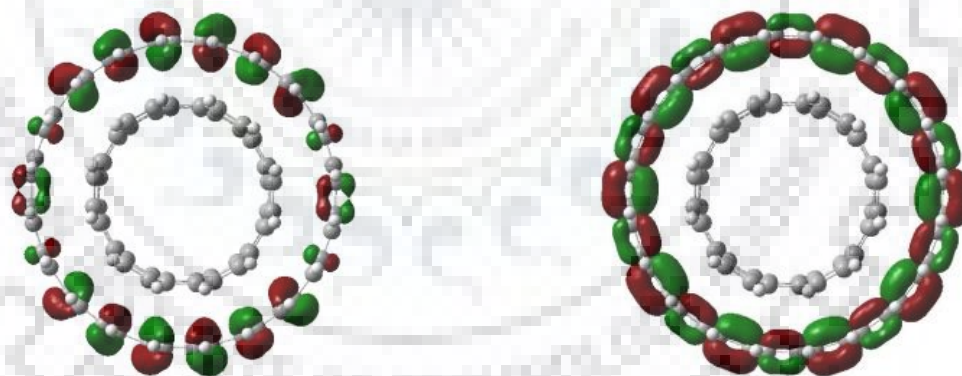
The electronic properties such as ionization energy (IE) and electron affinity (EA) were computed for above systems and are listed in table 6.3. From the table, it can be observed that IE of various NH₂-[10]CPP compounds lies within the range of 4.5-5.5 eV. Owing to the amino group, they show lower IE compared to that of the unsubstituted CPP. In general, the IE of amino-substituted derivatives is decreased with an increase in the number of substituents. On the other hand, EA of the above compounds becomes more positive with the number of substituents. Unlike the electron-donating amino-substituted CPPs, the electron-withdrawing fluorine-substituted CPPs show a higher IE and a more negative EA compared to unsubstituted CPP. Among various fluorinated derivatives, 40F-[10]CPP has maximum EA (-2.75 eV) reflecting its strong electron acceptor behaviour. From the above discussion, it can be concluded that the electronic properties of CPP can be tuned by varying the nature, number and position of the substituents. Table 6.3 also lists the energies of HOMO and LUMO (E_{HOMO} and E_{LUMO}) along with the energy gap between them ($\Delta E_{\text{HOMO-LUMO}}$). From the table, it is evident that the fluorine-substituted CPPs generally show a decrease in $\Delta E_{\text{HOMO-LUMO}}$ with an increase in the number of



HOMO

LUMO

Figure 6.3 Frontier molecular orbital of the complex CNT@[10]CPP.



HOMO-6

LUMO+2

Figure 6.4 The molecular orbital involved in the transition corresponding to the maximum absorption wavelength (λ_{max}) of the complex CNT@[10]CPP.

Table 6.3 Computed values of ionization energy (IE), electron affinity (EA), energy of HOMO (E_{HOMO}), energy of LUMO (E_{LUMO}) and energy gap between HOMO-LUMO ($\Delta E_{\text{HOMO-LUMO}}$) of [10]CPP, its substituted and doped derivatives, CNT and the corresponding complexes of CPP with CNT. All the energy values are in eV.

Compound	IE	EA	E_{HOMO}	E_{LUMO}	$\Delta E_{\text{HOMO-LUMO}}$
[10]CPP	6.04	-0.84	-5.18	-1.69	3.49
10NH ₂ -[10]CPP	5.21	-0.16	-4.41	-0.97	3.44
(ortho, ortho')20NH ₂ -[10]CPP	5.40	0.21	-4.60	-0.59	4.01
(ortho, meta)20NH ₂ -[10]CPP	5.46	0.05	-4.67	-0.74	3.93
(ortho, meta')20NH ₂ -[10]CPP	4.65	0.09	-3.87	-0.72	3.15
40NH ₂ -[10]CPP	4.93	0.48	-4.06	-0.29	3.77
10F-[10]CPP	6.43	-1.31	-5.58	-2.16	3.42
(ortho, ortho')20F-[10]CPP	6.75	-1.68	-5.90	-2.52	3.38
(ortho, meta)20F-[10]CPP	6.85	-1.68	-6.00	-2.53	3.47
(ortho, meta')20F-[10]CPP	6.74	-1.63	-5.88	-2.47	3.41
40F-[10]CPP	7.33	-2.75	-6.51	-3.57	2.94
10N-[10]CPP	6.40	-1.58	-5.52	-2.44	3.08
(ortho, ortho')20N-[10]CPP	7.20	-2.29	-6.30	-3.17	3.13
(ortho, meta)20N-[10]CPP	7.33	-2.19	-6.42	-3.07	3.35
(ortho, meta')20N-[10]CPP	6.95	-2.38	-6.06	-3.27	2.79
40N-[10]CPP	8.29	-3.99	-7.35	-4.93	2.42
CNT	4.57	-2.38	-3.74	-3.21	0.53
CNT@[10]CPP	4.51	-2.29	-3.70	-3.10	0.60
CNT@10F-[10]CPP	4.56	-2.35	-3.75	-3.15	0.60
CNT@(ortho, ortho')20F-[10]CPP	4.63	-2.45	-3.83	-3.24	0.59
CNT@(ortho, meta)20F-[10]CPP	4.58	-2.39	-3.77	-3.19	0.58
CNT@(ortho, meta')20F-[10]CPP	4.64	-2.46	-3.84	-3.25	0.59
CNT@40F-[10]CPP	4.94	-2.41	-4.13	-3.14	0.99

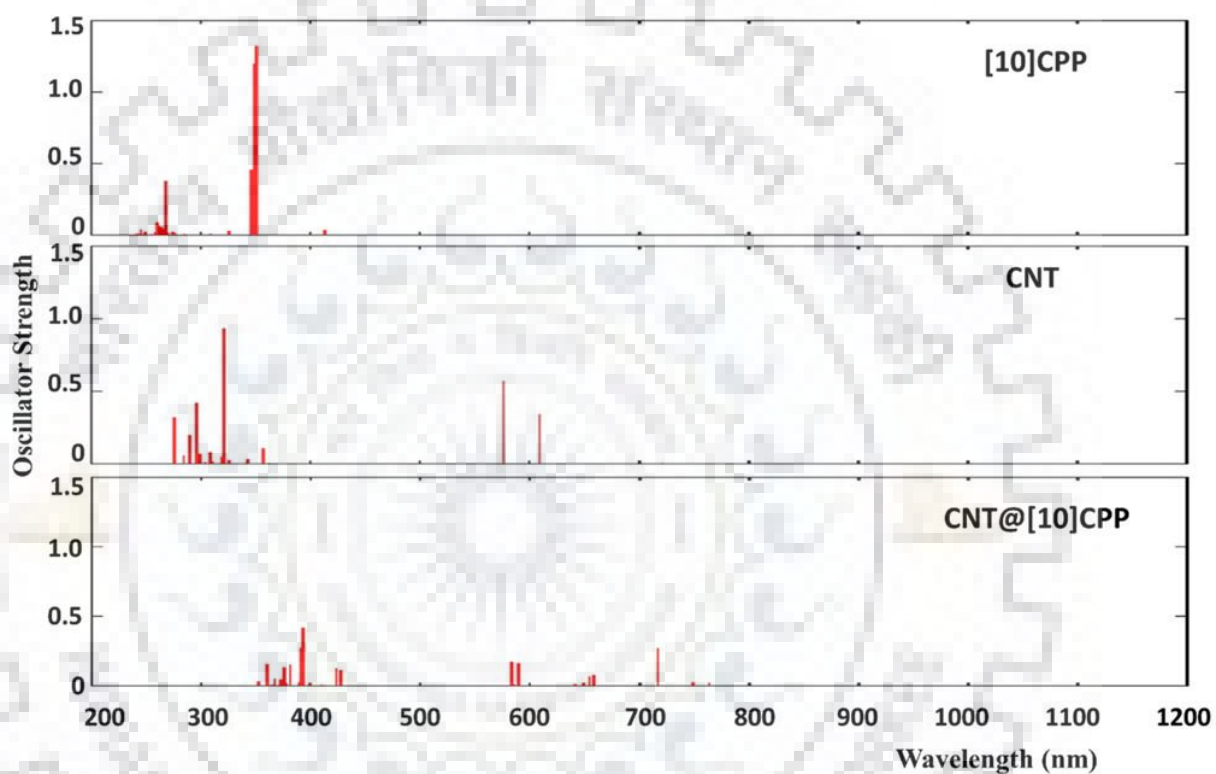


Figure 6.5 Absorption spectra of [10]CPP, CNT and the complex CNT@[10]CPP.

Table 6.4 The values of maximum absorption wavelength (λ_{\max}), light-harvesting efficiency (LHE) for [10]CPP, its substituted-/doped-derivatives, CNT and their corresponding complexes.

System	λ_{\max} (nm)	LHE (%)
[10]CPP	350	95
10N-[10]CPP	377	98
(ortho, ortho')20N-[10]CPP	368	99
(ortho, meta)20N-[10]CPP	406	42
(ortho, meta')20N-[10]CPP	401	99
40N-[10]CPP	528	7
10F-[10]CPP	357	95
(ortho, ortho')20F-[10]CPP	360	97
(ortho, meta)20F-[10]CPP	353	96
(ortho, meta')20F-[10]CPP	361	94
40F-[10]CPP	397	98
10NH ₂ -[10]CPP	375	91
(ortho, ortho')20NH ₂ -[10]CPP	337	75
(ortho, meta)20NH ₂ -[10]CPP	339	86
(ortho, meta')20NH ₂ -[10]CPP	442	89
40NH ₂ -[10]CPP	363	11
CNT	321	88
CNT@[10]CPP	393	61
CNT@10F-[10]CPP	403	49
CNT@ (ortho, ortho')20F-[10]CPP	397	57
CNT@ (ortho, meta)20F-[10]CPP	596	42
CNT@ (ortho, meta')20F-[10]CPP	401	55
CNT@40F-[10]CPP	551	52

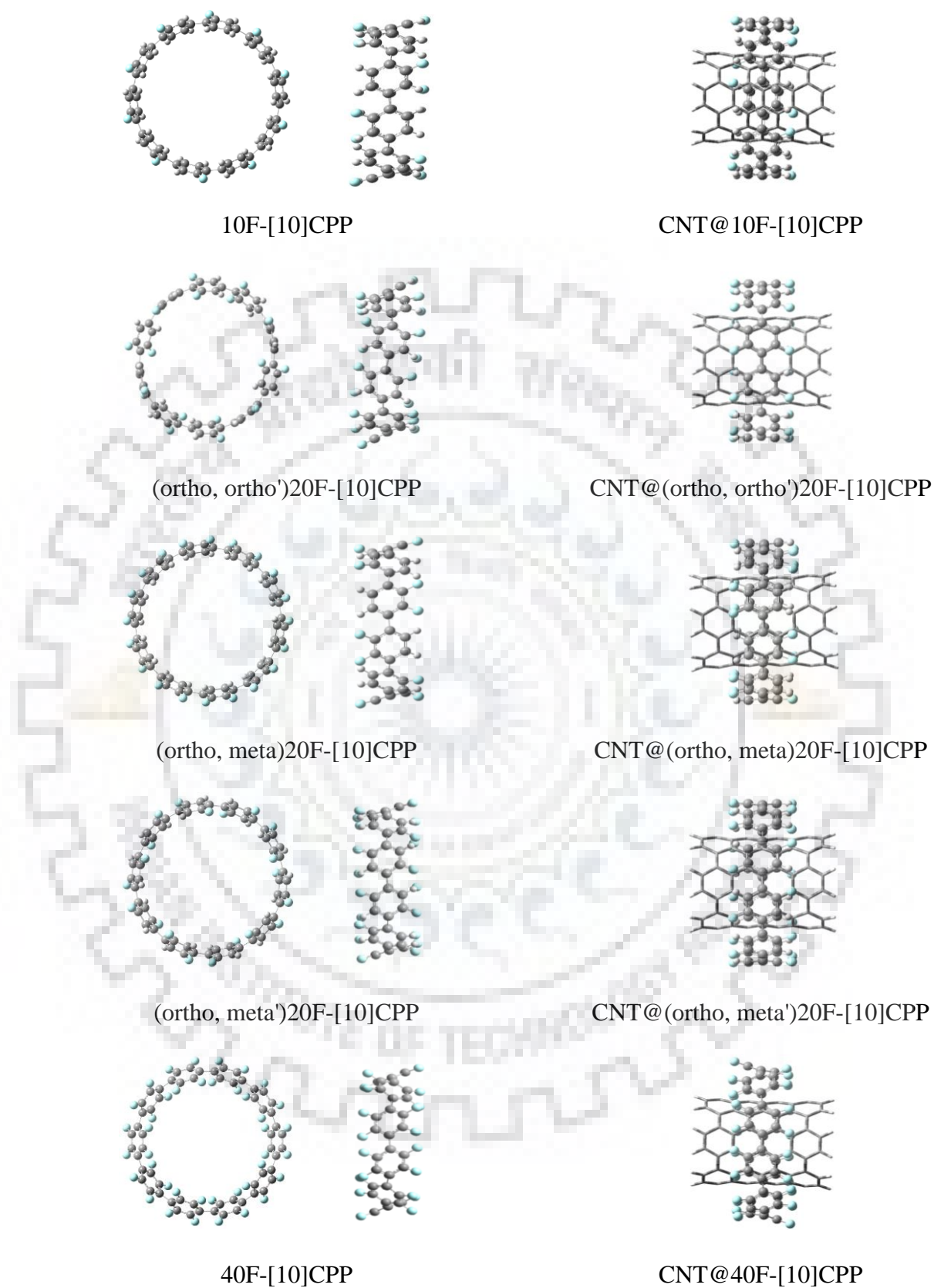


Figure 6.6 Optimized geometries of fluorine-substituted CPPs (side view and front view) and their complexes with CNT.

substituents. Compared to $\Delta E_{\text{HOMO-LUMO}}$ of 3.42 eV for 10F-[10]CPP, a marked decrease by 0.48 eV in $\Delta E_{\text{HOMO-LUMO}}$ is observed for 40F-[10]CPP. It should be emphasized that the least value of $\Delta E_{\text{HOMO-LUMO}}$ for tetra-fluorinated CPP derivative arises due to a significant decrease in the energy of LUMO without considerable change in the energy of HOMO compared to the respective energies of mono-substituted analogue. However, the amino-substituted CPPs do not show any trend in the values of $\Delta E_{\text{HOMO-LUMO}}$ with respect to the number or position of substituents. The calculated values of $\Delta E_{\text{HOMO-LUMO}}$ for the donor-/acceptor-substituted CPPs lie in the range 2.90-4.10 eV which make the above compounds attractive to be used as wide energy gap semiconductors.

The maximum absorption wavelengths (λ_{max}) for the amino/fluorine-substituted compounds of CPP are given in table 6.4. All these compounds absorb strongly in the near-ultraviolet region of the spectrum. In general, λ_{max} is decreased for the amino-substituted CPP and is increased for the fluorine substituted CPP with the number of substituents attached. The λ_{max} of fluorine-substituted CPP is red shifted by ~5-50 nm compared to the λ_{max} of free CPP, although such a regular shift is not observed for amino-substituted CPP.

Table 6.4 summarizes the LHE of CPP and its derivatives. From the table, it is clear that [10]CPP has a reasonably high LHE of ~95%. Compared to this, LHE of amino-substituted CPP is decreased and a large drop is noted for the tetra-substituted one. In contrast, the fluorine-substituted CPPs have LHE of more than 94% suggesting them as promising candidates for optoelectronic applications. Among the various fluorinated CPP, maximum LHE is obtained for 40F-[10]CPP. Thus, it can be inferred that substitution by donor/acceptor groups leads to considerable change in the optoelectronic properties of CPP.

6.3.3 Complexes of amino and fluorine-substituted CPP derivatives with CNT

The optimized geometries of the endohedral complexes of fluorine-substituted cycloparaphenylene with carbon nanotube are shown in figure 6.6 and those of amino-substituted cycloparaphenylene with carbon nanotube are shown in figure 6.7. For the amino-substituted complexes, the dihedral angle between two neighbouring phenyl units of CPP varies widely (4° - 23°). On the other hand, the dihedral angle between adjacent phenylene units of CPP is negligible for the mono- and di-substituted fluorinated complexes. In the case of tetra fluoro-substituted complex, the dihedral angle between adjacent phenylene units is increased to 25° - 30° . It should be also noted that the π - π stacking distance between CPP and CNT is ~2.90 Å for mono- and di-substituted complexes and ~2.71 Å for tetra-substituted complex. These π - π stacking distances are less than that for the unsubstituted analogue.

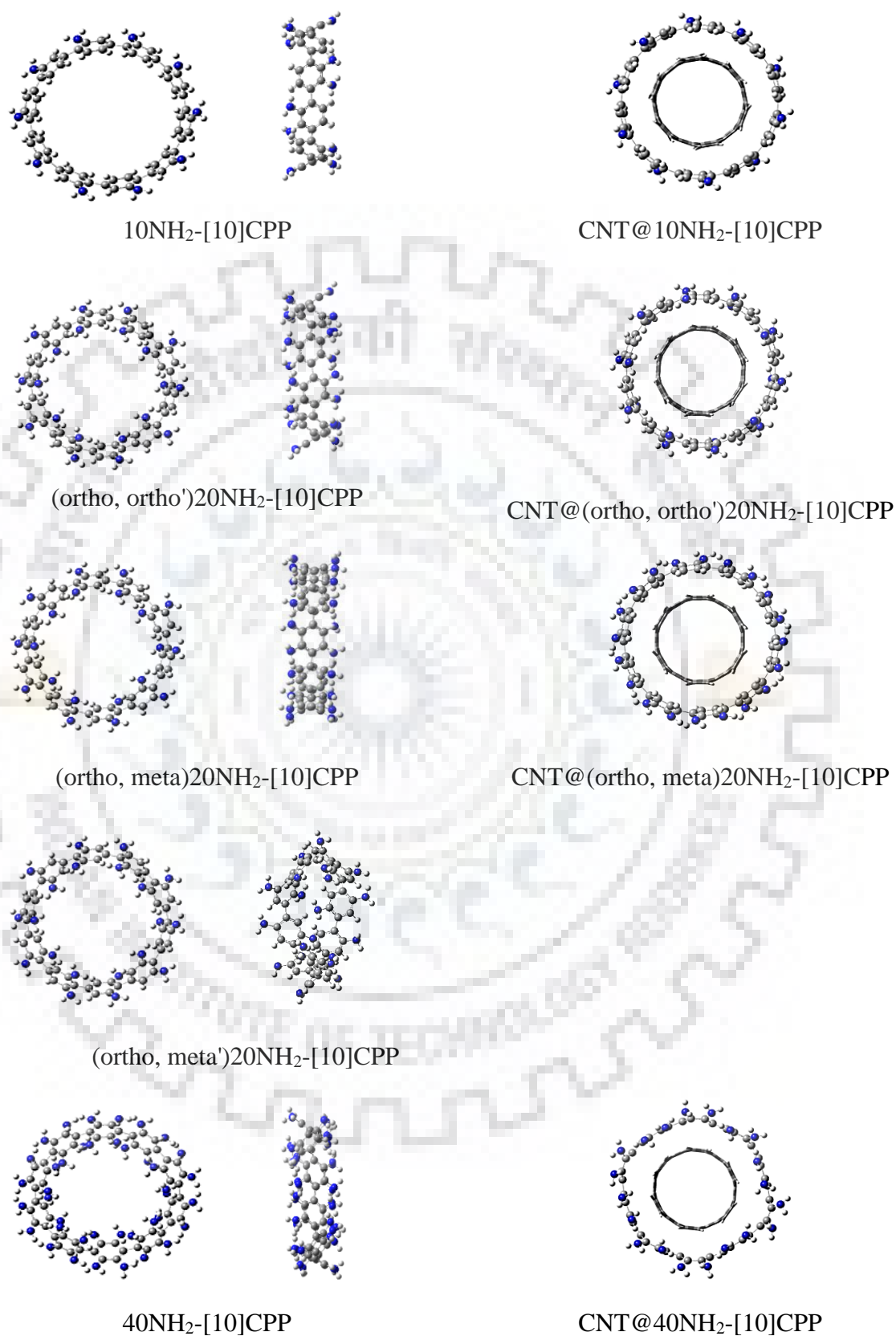
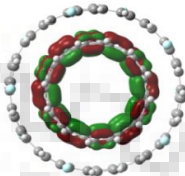
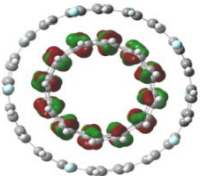

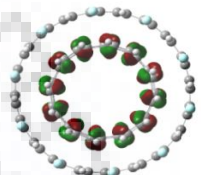
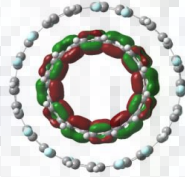
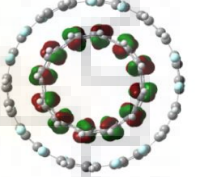
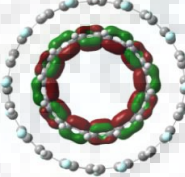
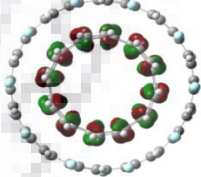
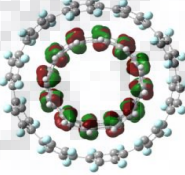
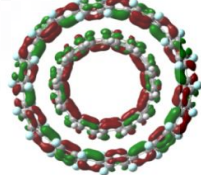


Figure 6.7 Optimized geometries of the amino-substituted derivatives of CPP (side view and front view) and their corresponding complexes with CNT.

To know the stability of the above complexes, their stabilization energy (ΔE_{stab}) was calculated. The BSSE and ZPE corrected values of ΔE_{stab} are given in table 6.1. It is evident from the values that the amino-substituted complexes are unstable, whereas the fluorine-substituted complexes are stable. From the table, it is also clear that ΔE_{stab} increases with the number of fluorine atoms on CPP for various fluorine-substituted complexes and are higher than that for the unsubstituted CPP-CNT complex. The large stabilization energy on adding fluorine atoms is expected from the multipole interactions. Considering the stability of fluorine substituted complexes, further discussion is limited only for such complexes. In order to understand how the substitution of fluorine affects the relative contribution of various components of interaction energy, the energy decomposition analysis was carried out for the fluorinated complexes. Table 6.2 lists the percentage contributions of dispersion, electrostatic and induction energies for the most stable fluorine-substituted complexes. It can be concluded from the values that the stabilization is mainly attained by dispersion interaction. As we move from mono-substituted to tetra-substituted complexes, the contribution of electrostatic energy is increased as expected. Owing to the enhancement of polarizability with additional fluorine atoms, the contribution of induction energy is maximum for tetra-substituted complex.

The calculated values of IE and EA for the fluorine-substituted complexes are provided in table 6.3. The values of IE lie in the range of 4.5-5.0 eV. With an increase in the number of substituents on CPP, IE of the complexes increases. On the other hand, EA of the complexes varies from -2.35 to -2.46 eV. However, no apparent trend is observed for EA with the number of substituents. All the fluorine substituted complexes show higher values of IE and EA compared to those of the unsubstituted complex. The frontier molecular orbital diagrams of the fluorine-substituted complexes are presented in table 6.5. As evident from the figure, the electron density of frontier orbitals resides only on CNT for the mono- and di-substituted complexes ruling out the possibility of charge transfer between the respective components. However, for tetra-substituted complex, the electron density of HOMO is delocalized over CNT whereas that of LUMO is delocalized over both components. Thus, in tetra fluorinated complex, photoinduced charge transfer takes place from donor CNT to acceptor 40F-[10]CPP. The energy gap between HOMO and LUMO ($\Delta E_{\text{HOMO-LUMO}}$) of various complexes is listed in table 6.1. From the table, it can be seen that the values of $\Delta E_{\text{HOMO-LUMO}}$ (~0.58-0.99 eV) of fluorinated complexes are close to that of bare CNT and are significantly less than that of the respective fluorinated CPP. The mono- and di-substituted complexes have nearly the same values of $\Delta E_{\text{HOMO-LUMO}}$ (~0.60 eV) and is increased by 0.40 eV for tetra-substituted complex.

Table 6.5 Frontier molecular orbitals of the fluorine-substituted derivatives with CNT.

Complex	HOMO	LUMO
CNT@10F-[10]CPP		
CNT@(ortho, ortho')20F-[10]CPP		
CNT@(ortho, meta)20F-[10]CPP		
CNT@(ortho, meta')20F-[10]CPP		
CNT@40F-[10]CPP		

The absorption maxima (λ_{\max}) and light-harvesting efficiency (LHE) of the fluorine-substituted complexes are listed in table 6.4. The λ_{\max} of the complexes lies in the range of 400-600 nm. It can be seen that the complexes have LHE of ~40-60 % which is significantly less with respect to the fluorine-substituted CPP analogues. As can be seen from figure 6.8, the fluorine-substituted CPPs absorb in the near-ultraviolet region and their complexes absorb in the range spanning from near-ultraviolet to near-infrared regions. The absorption of the complexes in the wide spectral range, despite their relatively low values of LHE, suggests them suitable for their possible applications in solar cells. The molecular orbitals involved in the electronic transitions corresponding to the absorption maximum of the complexes are given in table 6.6. For the mono-substituted complex, the transition from HOMO-2 to LUMO+4 can be assigned as a charge transfer transition as reflected from the isodensity surface plots of these molecular orbitals. The electron density of the former is located mainly on 10F-[10]CPP and that of the latter is localized on CNT. For the complexes of various isomers of di-substituted CPP, the electronic transitions take place between the molecular orbitals of CNT indicating the absence of charge transfer between the components. For tetra-substituted complex, charge transfer transition takes place from HOMO-5 delocalized on CNT to LUMO+2 delocalized on 40F-[10]CPP.

Considering the fact that B3LYP functional underestimates the absorption energy, a range-separated hybrid functional (ω B97X-D) was used to determine the absorption spectrum of [10]CPP, 40F-[10]CPP and the complex CNT@40F-[10]CPP. The absorption spectra of these species are given in figure 6.9. For [10]CPP, it is clear that from figure 6.5 that λ_{\max} (350 nm) obtained using B3LYP-GD3 method is closer to the experimental value of 340 nm [407] compared to that obtained for ω B97X-D (286 nm). However, it is worth to mention that the oscillator strength obtained for ω B97X-D (see figure 6.9) is more than that for B3LYP-GD3 (see figure 6.5). The calculated oscillator strength of [10]CPP for the range separated hybrid functional is more closer to that reported in an earlier study.[408] For 40F-[10]CPP and its complex CNT@40F-[10]CPP, the respective values of absorption maxima are decreased by 74 nm and 42 nm for ω B97X-D functional (see figure 6.9) with respect to those obtained using B3LYP-GD3 functional (see figure 6.8).

6.3.4 N-doped derivatives of CPP

To study the variation of electronic and optical properties of CPP with doping of nitrogens, various nitrogen-doped derivatives of CPP were modelled as shown in figure 6.10. Three different series of derivatives namely, 10N-[10]CPP, 20N-[10]CPP and 40N-[10]CPP were modelled. The three isomers of 20N-[10]CPP differ from each other with respect to the position

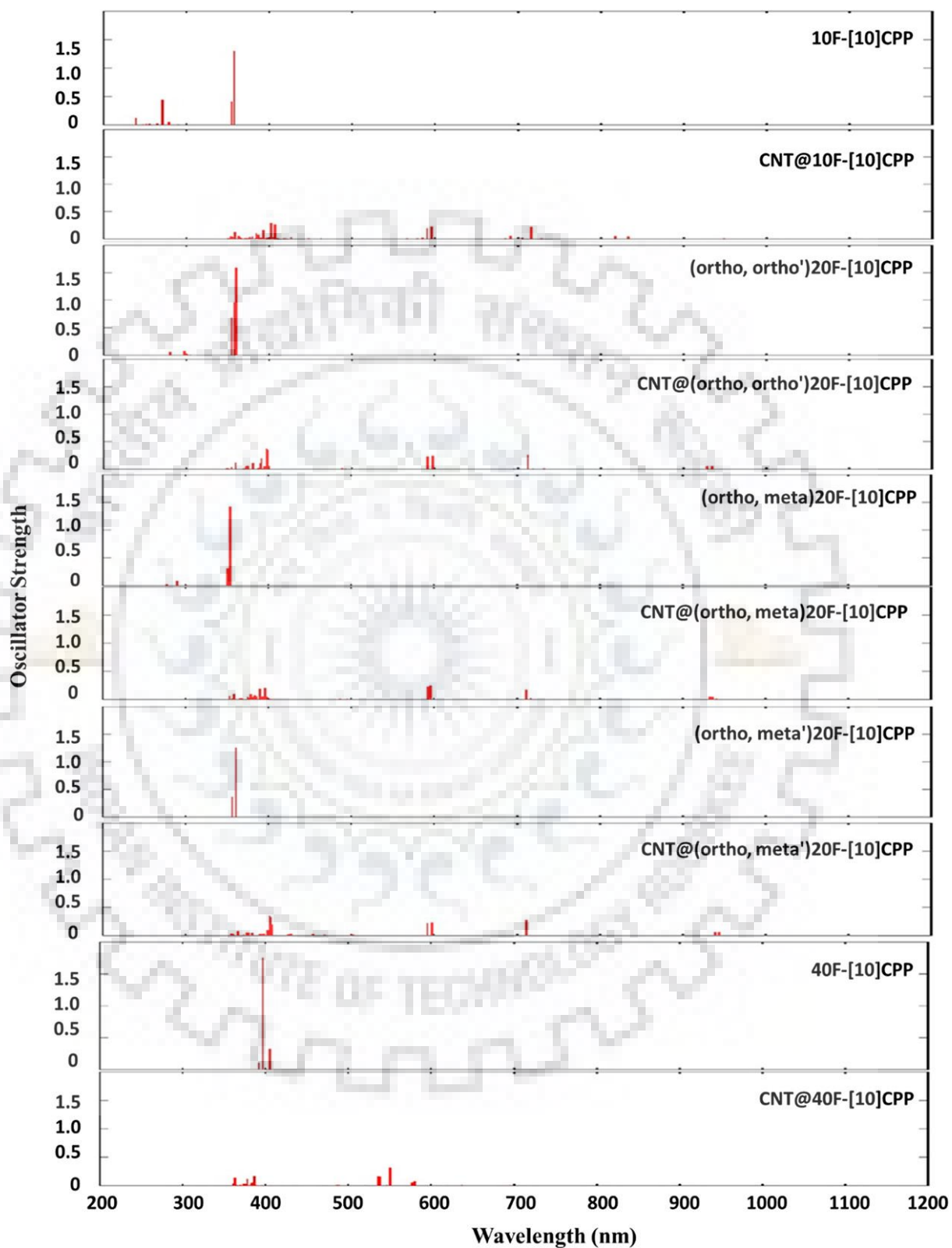


Figure 6.8 The absorption spectra of various fluorine-substituted derivatives of CPP and their complexes with CNT obtained at B3LYP-GD3/6-31G(d,p) level.

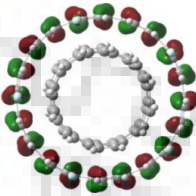
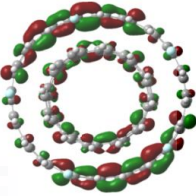
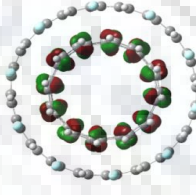
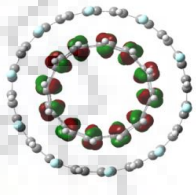
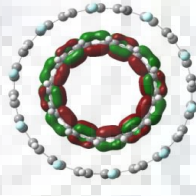
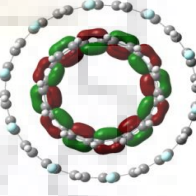
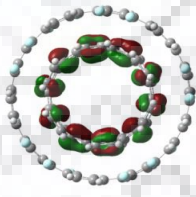
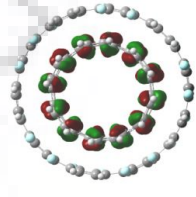
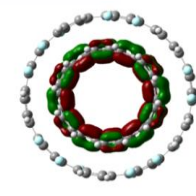
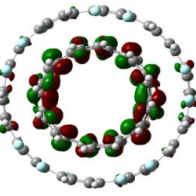
of nitrogen atoms and are denoted as (ortho, ortho')-, (ortho, meta)- and (ortho, meta')-20N-[10]CPP. The electronic properties such as IE and EA of the above compounds are presented in table 6.3. Due to their characteristic electron-accepting nature, all these compounds possess more negative EA than those of the unsubstituted CPP. The values of energy gap between HOMO and LUMO ($\Delta E_{\text{HOMO-LUMO}}$) for the nitrogen-doped CPPs are also listed in the same table. These compounds show $\Delta E_{\text{HOMO-LUMO}}$ of about 2.40-3.40 eV. Among various nitrogen-doped CPP compounds, 40N-[10]CPP exhibits the smallest value of $\Delta E_{\text{HOMO-LUMO}}$. The maximum absorption wavelengths (λ_{max}) of different nitrogen-doped derivatives are summarized in table 6.4. The compounds show λ_{max} in the range of 360-530 nm. Thus, it can be inferred that λ_{max} of nitrogen-doped CPP is shifted towards longer wavelength compared to that of unsubstituted CPP. The tetra-substituted derivative shows maximum shift in the absorption maximum, however, the oscillator strength corresponding to this transition is almost negligible. The red-shift of the absorption maximum for N-doped CPPs compared to that for pristine CPP is in agreement with a recent study by Graham and co-workers.[409]

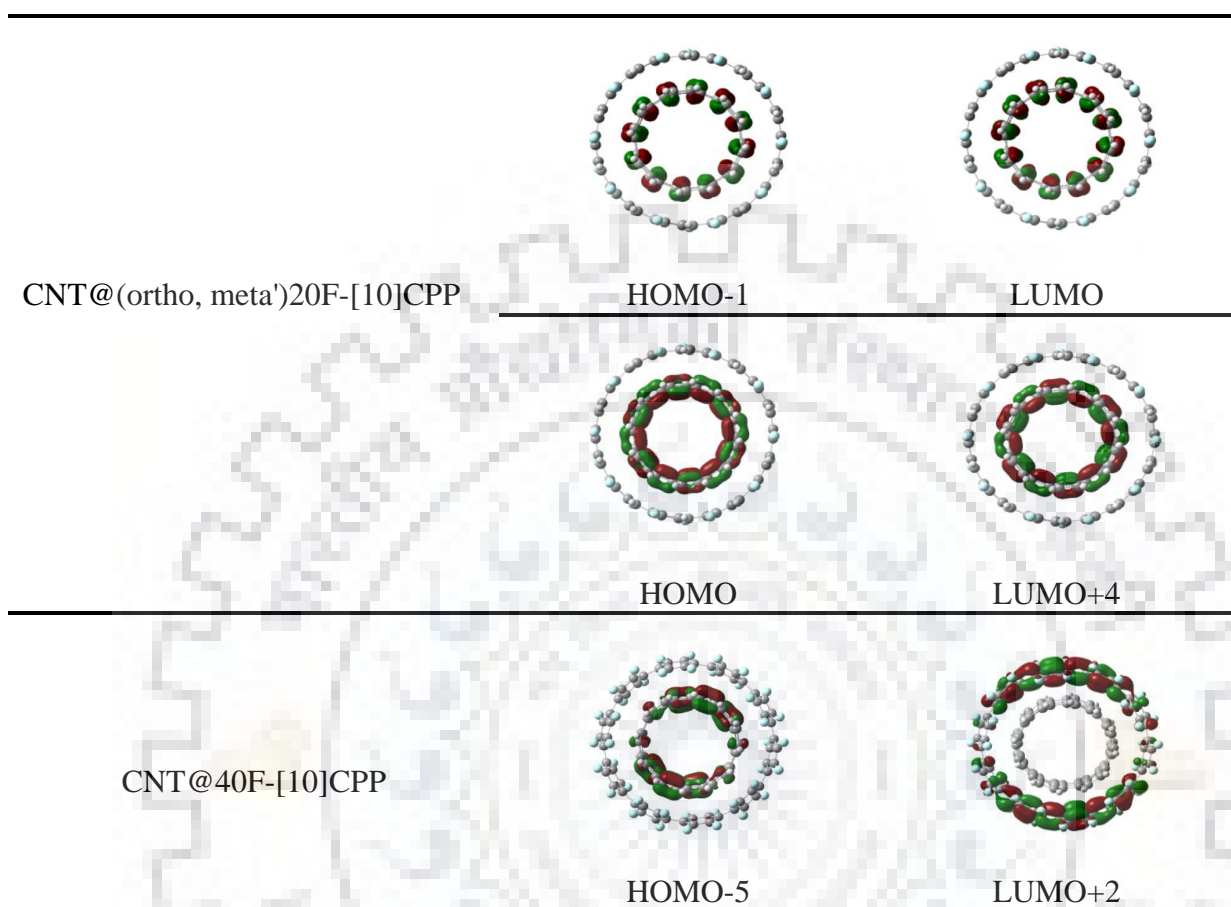
In order to explore the possibility of formation of the complexes between N-[10]CPP and CNT, various nitrogen-doped derivatives of CPP were used as hosts to form inclusion complexes of CNT. For this purpose, the CNT of length 11.7 Å was selected. The optimized geometries of the above complexes are also shown in figure 6.10. To examine their stability, BSSE and ZPE corrected stabilization energies (ΔE_{stab}) were calculated and are listed in table 6.1. The positive values of ΔE_{stab} indicate that the formation of such complexes are energetically unfavourable. Due to the instability, further examination of their electronic and optical properties was not performed.

6.3.5 Potential energy profiles for translational and rotational motions of CPP over CNT

To explore the complex CNT@CPP as a component in molecular machines,[109, 410, 411] the translational and rotational motions of CPP over the surface of CNT were investigated. For this purpose, the potential energy profile was generated for the movement of CPP over a relatively long CNT of length 21.6 Å. The optimized complex CNT@CPP in which the centres of both coincide was taken as the initial geometry. Later, the energy of CPP while moving along the tube axis was calculated without further optimization. Figure 6.11 depicts the change in potential energy as a function of translational movement of CPP over CNT for the ground as well as the excited states. It is clear from the figure that there is a slight barrier for the translational movement in its ground state (S_0). The translation energy profiles for the excited singlet and triplet states were obtained using the TD-DFT methods. For this purpose, the vertical excitation

Table 6.6 The molecular orbital involved in the electronic transition corresponding to the maximum absorption wavelength (λ_{\max}) of the complexes of fluorine-substituted derivatives with CNT.

Complex	Molecular orbitals	
CNT@10F-[10]CPP		
CNT@(ortho,ortho')20F-[10]CPP		
CNT@(ortho,ortho')20F-[10]CPP		
CNT@(ortho, meta)20F-[10]CPP		
CNT@(ortho, meta)20F-[10]CPP		



energy was calculated for each of the ground state configurations. Unlike in the ground state (S_0), there is no such barrier for the excited singlet (S_1) and triplet (T_1) states. This suggests that the movement of CPP can be controlled with external stimuli such as light thereby finding applications in molecular machines. Similarly, the potential energy profile for the rotational motion of CPP over CNT was also generated keeping geometric centres of both at the same point and is shown in figure 6.12. It can be noticed from the figure that the barrier of rotation is only 0.83 kcal/mol and is negligible. As in the case of [10]CPP, an investigation was also carried out for the translational and rotational movements of 40F-[10]CPP over CNT. The corresponding potential energy profiles are depicted in figures 6.13 and 6.14. As expected, the ground state energy barriers for translation and rotation movements are increased for the substituted system by about 42 and 12 kcal/mol, respectively. The above results suggest that CNT@CPP can be used in molecular architectures.[412]

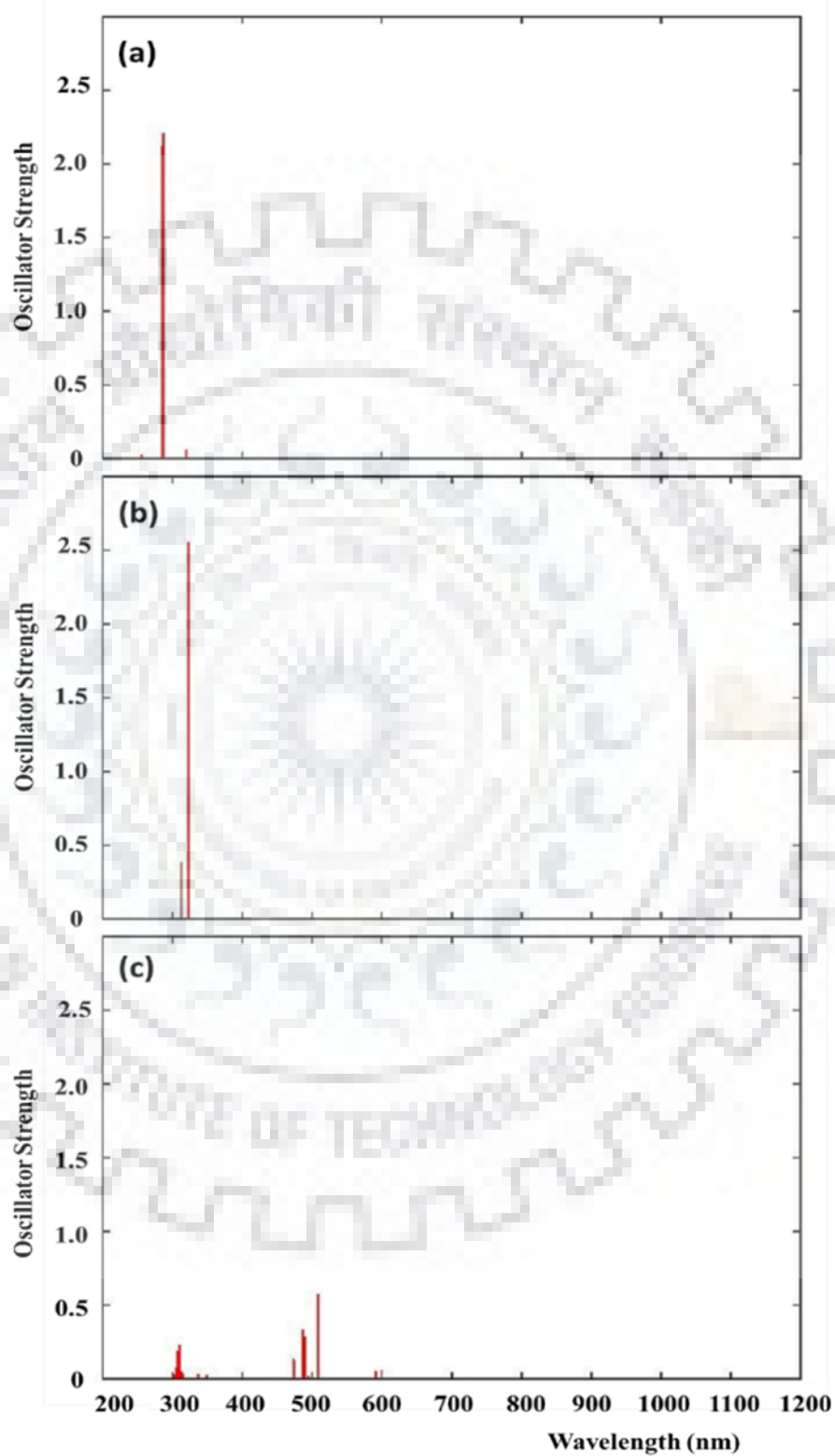


Figure 6.9 The absorption spectra of (a) [10]CPP, (b) 40F-[10]CPP and (c) CNT@40F-[10]CPP obtained at ω B97XD/6-31G(d,p) level.

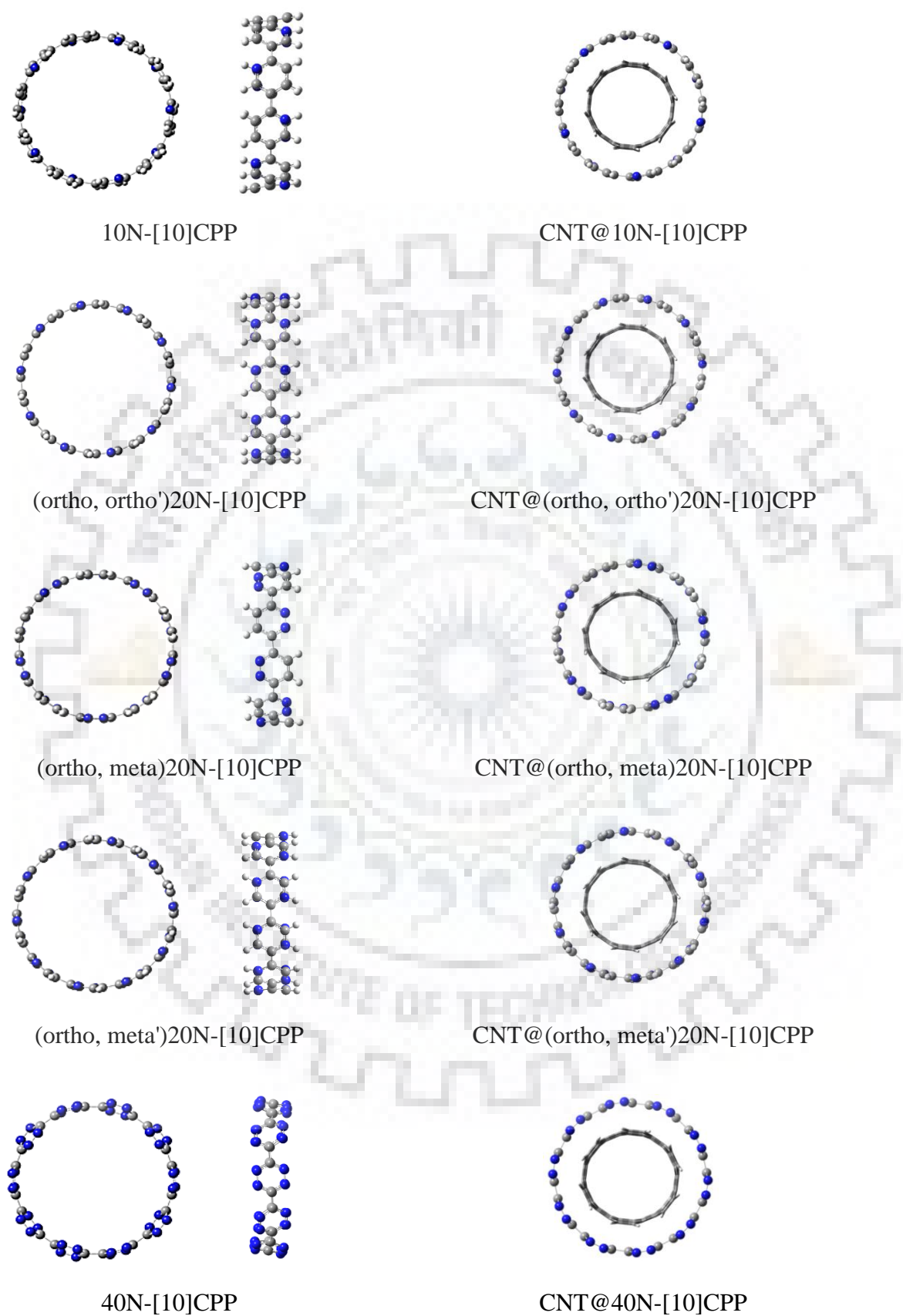


Figure 6.10 Optimized geometries of the nitrogen-doped derivatives of CPP (side view and front view) and their corresponding complexes.

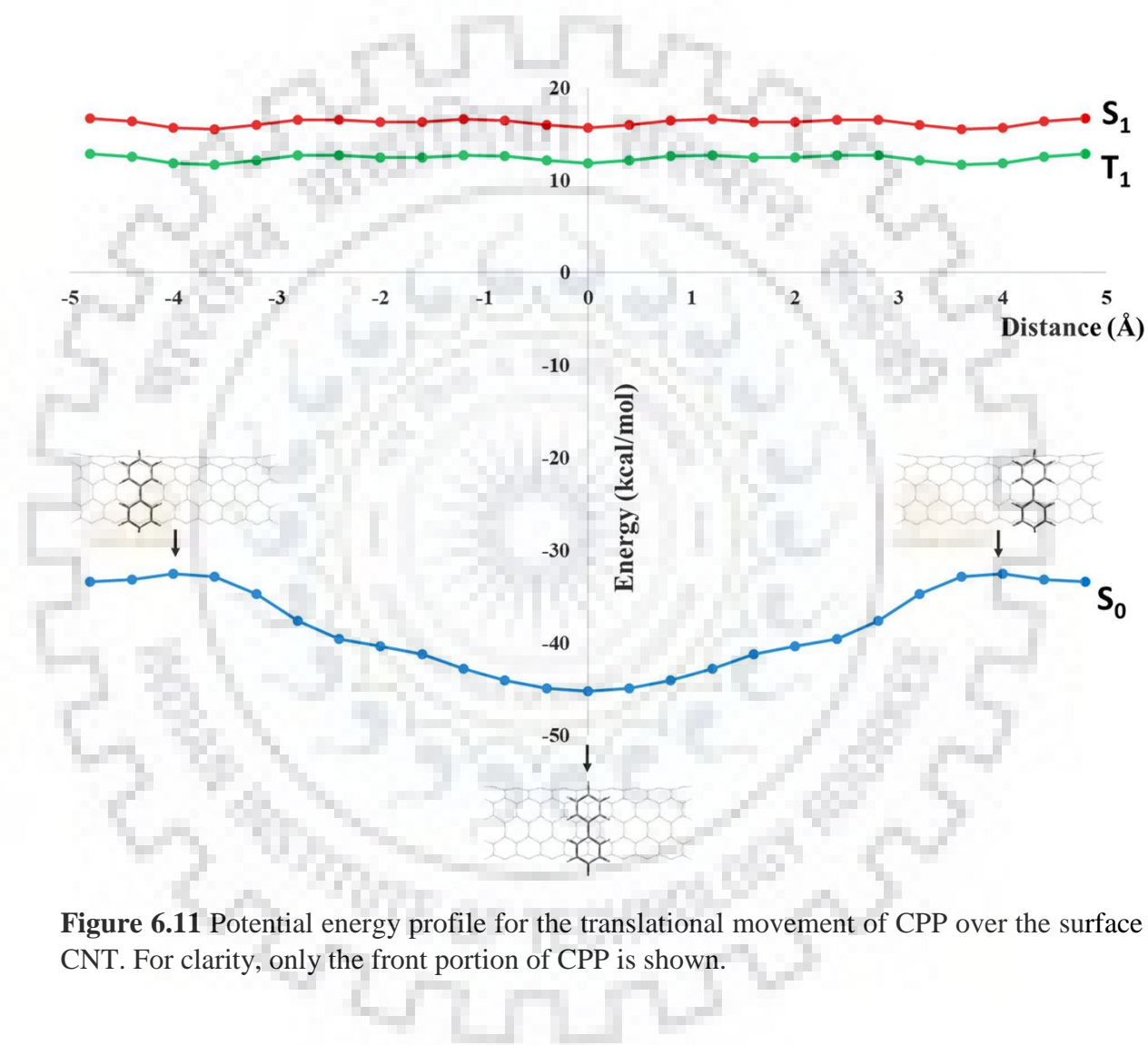


Figure 6.11 Potential energy profile for the translational movement of CPP over the surface of CNT. For clarity, only the front portion of CPP is shown.

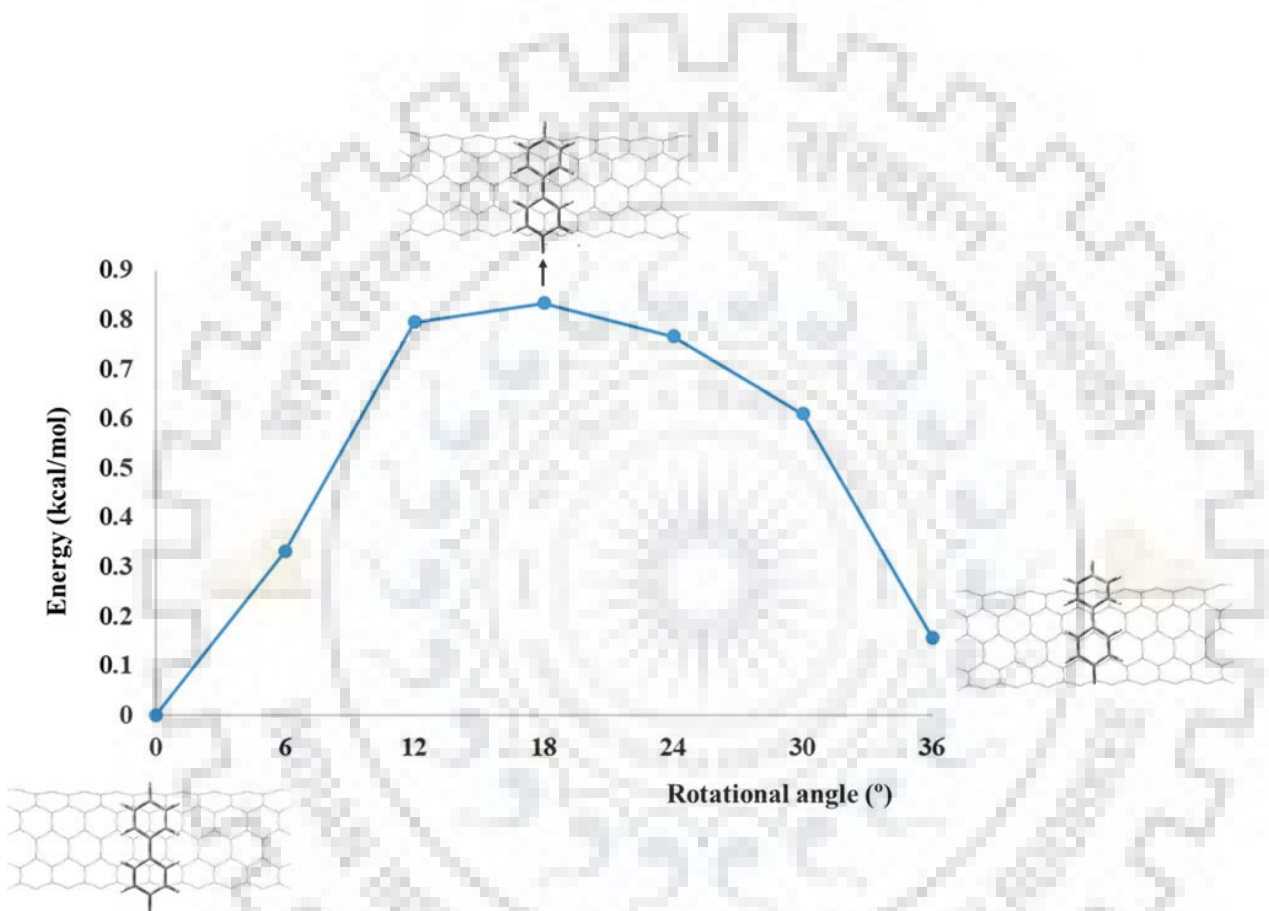


Figure 6.12 Potential energy profile for the rotation of CPP over the surface of CNT keeping their geometric centres coincide. For clarity, only the front portion of CPP is shown.

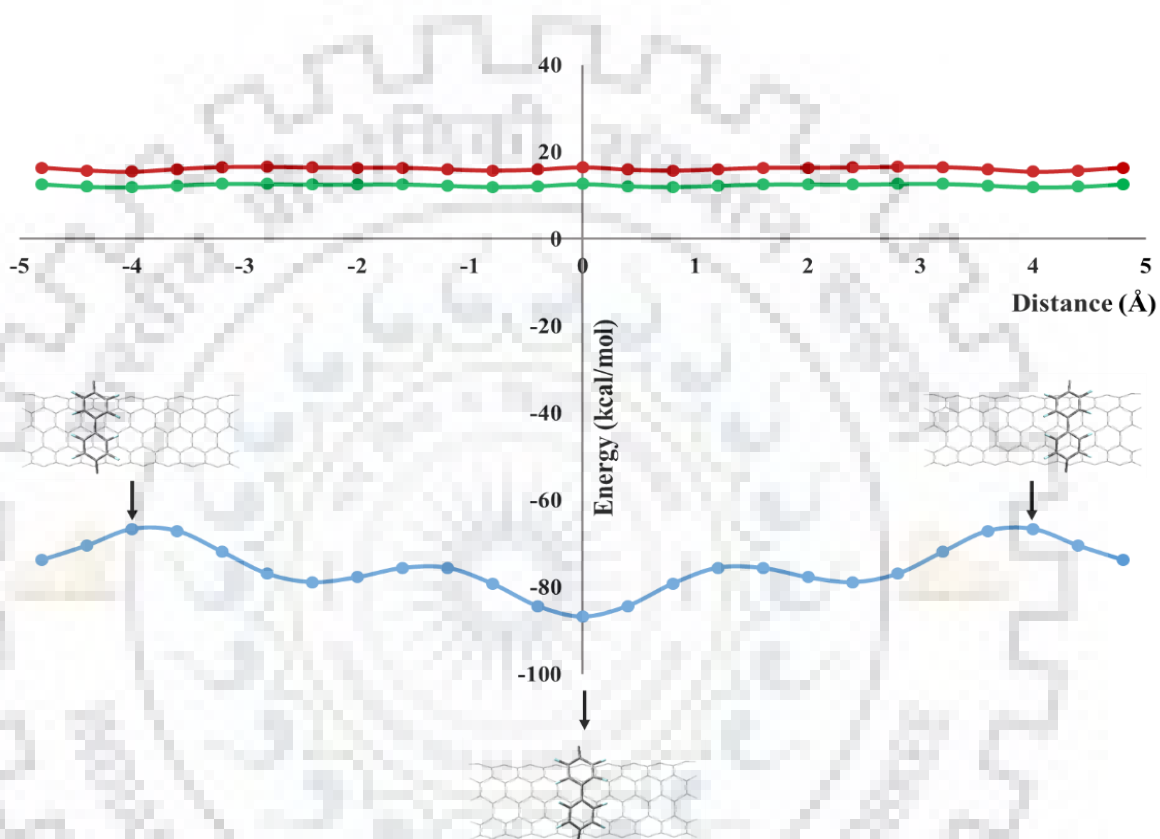


Figure 6.13 Potential energy profile for the translational movement of 40F-[10]CPP over the surface of CNT. For clarity, only the front portion of 40F-[10]CPP is shown.

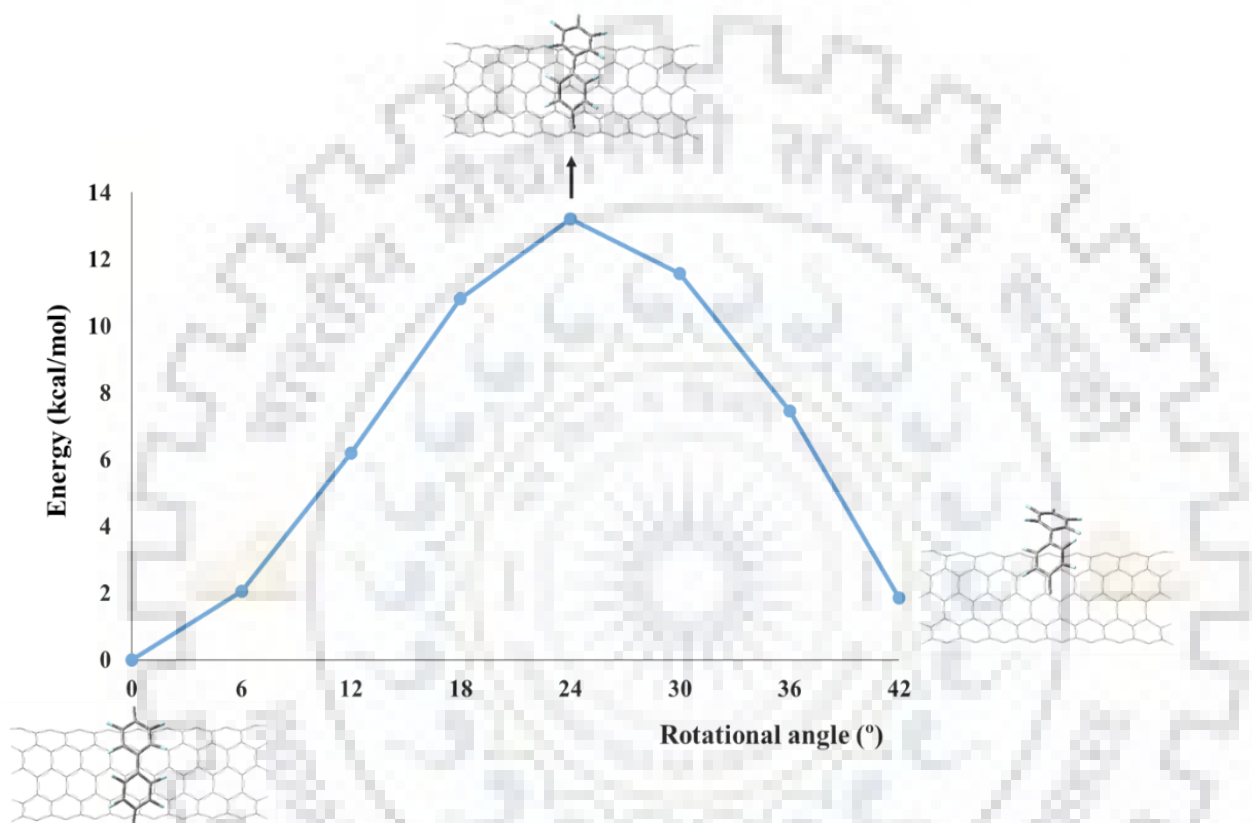


Figure 6.14 Potential energy profile for the rotation of 40F-[10]CPP over the surface of CNT keeping their geometric centres coincide. For clarity, only the front portion of 40F-[10]CPP is shown.

6.4 Conclusion

In summary, a systematic study on the structure and optoelectronic properties of CPP, its substituted as well as doped derivatives, CNT and the corresponding CPP-CNT complexes was carried out using the dispersion-corrected density functional theoretical methods. The negative value of stabilization energy for the unsubstituted complex indicated that it is energetically stable. Among the complexes of substituted- and doped-CPP with CNT, only the fluorinated ones were found to be stable. The energy decomposition analysis revealed that the complexes attain stability mainly due to the dispersion interaction between the individual components. Among various fluorinated complexes, the highly substituted one showed maximum contribution from the electrostatic energy term.

It was found that the substitution and doping of CPP alter the optoelectronic properties of bare CPP. Owing to the electron-donating ability of the amino substituted CPP, their IE values were found to be less than the IE value of bare CPP. Compared to EA of bare CPP, that of fluorine-substituted or nitrogen-doped CPP derivatives is relatively more negative due to their electron-withdrawing nature. In contrast to the wide energy gap between HOMO and LUMO of free CPP and its derivatives, a narrow energy gap (< 1 eV) was observed for the complexes. Such a small energy gap suggests them to be useful for their applications in organic semiconductors. Among various fluorine-substituted complexes, the tetrasubstituted complex has the maximum value of $\Delta E_{\text{HOMO-LUMO}}$. The study also showed that fluorinated complexes exhibit distinguishable properties. For example, photoinduced charge transfer behaviour was observed for the complex CNT@40F-[10]CPP in which the electron density is transferred from HOMO localized on CNT to LUMO delocalized over both the species. The fluorine-substituted complexes were absorbed in wide range of electromagnetic spectrum covering the near-ultraviolet and near-infrared regions compared to the absorption in near-ultraviolet and visible regions for their unsubstituted analogue. The photoinduced charge transfer phenomena in the fluorinated complexes was also reflected from the molecular orbitals involved in the transitions corresponding to the maximum absorption wavelengths. In the complex CNT@10F-[10]CPP, the charge transfer occurred from donor 10F-[10]CPP to acceptor CNT whereas in its tetra-fluorinated analogue, charge transfer occurred from donor CNT to acceptor 40F-[10]CPP. The wide range of absorption wavelength along with high light-harvesting efficiency suggests that these complexes are suitable for solar cell applications.

The potential energy profile for the translational motion of CPP/tetra-fluorinated CPP over the surface of CNT at ground and excited states were analysed. The barrier for the rotational motion of CPP or tetra-fluorinated CPP over CNT was also determined. Compared to the

translational and rotational energy barriers of unsubstituted complex, a remarkable increase in the barriers were obtained for the fluorinated complex. The translational and rotational movements of both unsubstituted and unsubstituted CPP over CNT suggests that these complexes can be used as components in molecular machines.



CHAPTER 7

Summary and Conclusions

In the present chapter, the works done in preceding four chapters are summarized. Different π - π interacting complexes of CNT with indigo, perylene bisimide, quaterthiophene and cycloparaphenylene were studied and their optoelectronic as well as charge transport properties are discussed. The main findings of the thesis are outlined as follows:

The structure as well as the properties of non-covalent complexes formed between CNT and indigo were investigated. Two types *viz.*, endohedral and exohedral complexes of indigo-CNT were considered. The negative values of stabilization energy obtained at B97-D/6-31G(d,p) level indicated that the complexes formed are stable. Among indigo@(n,n)CNT ($n = 6-8$), indigo@(7,7)CNT was found to be the most stable owing to the ideal diameter of (7,7)CNT for encapsulating indigo. The low values of $\Delta E_{\text{HOMO-LUMO}} (< 1 \text{ eV})$ for the complexes suggested that they can act as narrow energy gap semiconductors. The electron density distribution in the frontier molecular orbitals of the exohedral complexes showed a photoinduced charge transfer from donor CNT to acceptor indigo. However, no such charge transfer was observed for the endohedral complexes. Based on the Marcus theory, the carrier mobilities of the complexes were calculated. The results indicated that the complexes exhibit higher hole mobility than electron mobility thereby suggesting them as p-type semiconductors. The difference in hole and electron mobility of endohedral complexes was found to be relatively small compared to those of exohedral complexes. For endohedral complexes, the carrier mobilities varied inversely as the diameter of CNT is increased. The same behaviour was also observed for the exohedral complexes of indigo with relatively long CNT and those for which both ends are capped with fullerene segments. However, an opposite behaviour was seen for the exohedral complex in which indigo was oriented parallel rather than perpendicular to the tube-axis. The absorption properties obtained using TD-DFT method predicted that the complexes of CNT with indigo absorb strongly in the visible and the near-infrared regions. Along with this, several charge transfer transitions were found in the visible region thereby finding applications of the above complexes in solar cells. The role of hybrid B3LYP-GD3 and range-separated hybrid ω B97X-D functionals on the properties, especially optical absorption properties of the most stable complex indigo@(7,7)CNT was also examined. The results showed that both absorption wavelength and oscillator strength depend on the type of functional used.

Using various dispersion-corrected density functionals, the structure and properties of the complexes of CNT with perylene bisimide (PBI) were studied. The calculated stabilization energy indicated that the complex PBI-CNT is stable. The energy decomposition analysis showed that the

contribution of various components of energy towards the stabilization of the complex followed the order: dispersion > electrostatic > induction. PBI-CNT complex constituted a donor-acceptor system with CNT acting as an electron donor and PBI as an electron acceptor. Unlike the complex indigo-CNT, the complex PBI-CNT showed a significant decrease in $\Delta E_{\text{HOMO-LUMO}}$ compared to its free CNT analogue. The frontier molecular orbital analysis of the complex PBI-CNT revealed that electron density of HOMO is localized on CNT while that of LUMO is localized on PBI. In addition, the photoinduced electron transfer occurred from LUMO of CNT to that of PBI. Similar to indigo-CNT complexes, higher hole mobility than electron mobility was obtained for PBI-CNT making it suitable to be used as a p-type organic field-effect transistor. The studies on the absorption spectrum of the complex showed a wide range of absorption in the near ultraviolet-visible-near infrared regions of the electromagnetic spectrum suggesting it useful for optoelectronic applications. The above results were almost unchanged on increasing the length of CNT. The studies on the stability of endohedral complex of PBI with larger diameter (8,8)CNT revealed that it is more stable than its exohedral analogues.

The modelling and investigation of properties of endo- as well as the exohedral complexes of (6,6)CNT with 4T were also carried out using various dispersion-corrected density functionals. The stabilization energy of endohedral complex (4T@CNT) was found to be lower than its exohedral counterpart (4T-CNT). Similar to indigo-CNT complexes, the electronic properties such as ionization energy, electron affinity and energy gap between frontier molecular orbitals of CNT are not changed significantly due to the adsorption or the encapsulation of 4T. CNT acts as an acceptor in the complex 4T-CNT which is in contrast to the donor nature of CNT in the complexes indigo-CNT and PBI-CNT. Contrary to p-type charge transfer characteristics of the complexes of CNT with indigo or PBI, those with 4T exhibited n-type charge transfer characteristics due to higher electron mobility than hole mobility. Among the complexes of CNT with 4T, the endohedral one showed the highest electron mobility of $3.79 \text{ cm}^2\text{V}^{-1}\text{s}^{-1}$. The optical absorption studies of the complexes indicated several charge transfer transitions from electron donor 4T to electron acceptor CNT in the visible region of the electromagnetic spectrum which is in contrast to those observed for the complexes indigo-CNT and PBI-CNT. As it is known that pure CNT possesses p-type characteristic, its complexes with 4T have shown n-type characteristics. Thus, the above results unequivocally suggested that the charge-transfer characteristics of CNT can be altered on forming complexes with 4T.

The studies on CPP-CNT complexes which include various derivatives of CPP by doping nitrogens as well as by substituting donor amino or acceptor fluoro groups showed that only the unsubstituted or fluorine-substituted complexes are stable. The energy decomposition analysis suggested that the complexes are stabilized mainly by the dispersion interactions between constituent

units. The electrostatic interactions are more pronounced in the tetra-fluorinated complex compared to its unsubstituted analogue. The optical absorption properties indicated that the complexes of CPP with CNT absorb in the near-ultraviolet and visible regions whereas those of various fluorine-substituted CPP with CNT absorb in a wide range starting from near-ultraviolet to near-infrared region of the electromagnetic spectrum. Like the complexes indigo-CNT and PBI-CNT, a photoinduced charge transfer was also observed for the complex in which CNT acts as a donor and tetrafluorinated CPP acts as an acceptor. Similar to the complexes of CNT with indigo/PBI/4T, those with CPP and its fluorinated derivatives exhibited narrow energy gap between the highest occupied and the lowest unoccupied molecular orbitals suggesting their use in organic semiconductors. The high values of light-harvesting efficiency obtained for fluorine-substituted complexes indicate their use in photovoltaic devices. The studies also showed an energy barrier for the piston type movement of CNT in the complexes for the ground state, but not for the excited states. The barrier for rotation of bare and fluorinated CPP over CNT suggests the potential of these complexes as components in molecular wheels and shuttles.

In summary, the geometries of indigo, PBI and 4T are distorted largely on adsorbing over CNT than encapsulating inside CNT. CPP and its derivatives also undergo significant structural changes upon complexation with CNT. A small energy gap between HOMO and LUMO of the complexes suggests their semiconducting behaviour. They also exhibit very high values of both electron and hole mobility making them suitable for organic transistor devices. All the above complexes show several charge transfer transitions in the visible region of the electromagnetic spectrum and thus can be used in solar cell applications. Based on the above results, it can be concluded that π - π interacting complexes of CNT find potential applications in optoelectronic devices and more such complexes can be explored. Further, the above studies can be extended to know the effect of electric field on the charge transport properties of the complexes for their applications in organic field-effect transistors.



Appendix A

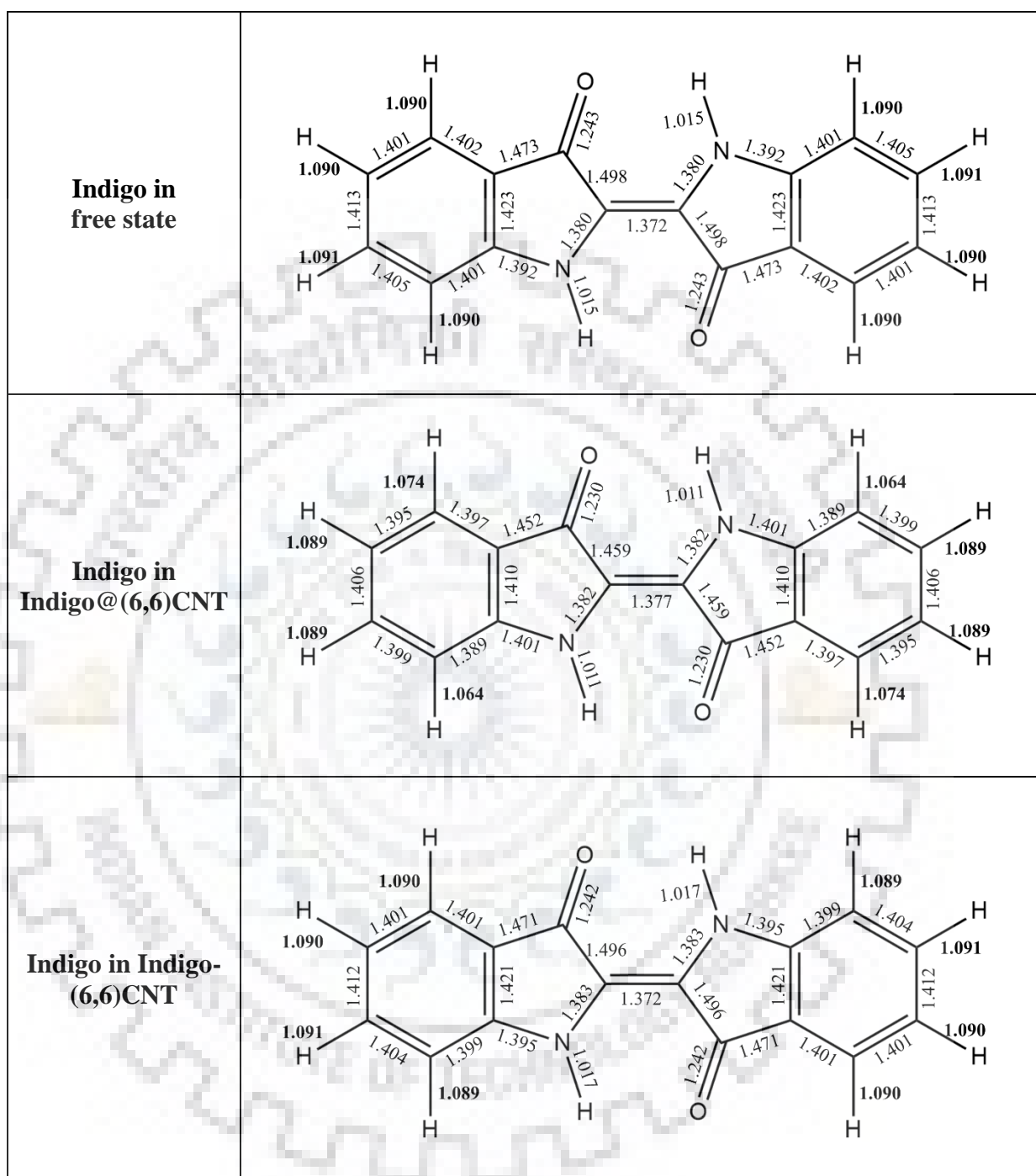


Figure A1. Schematic diagram of indigo in free state and indigo in its endo- and exohedral complexes with CNT. All the values shown in the above figures are in Å.

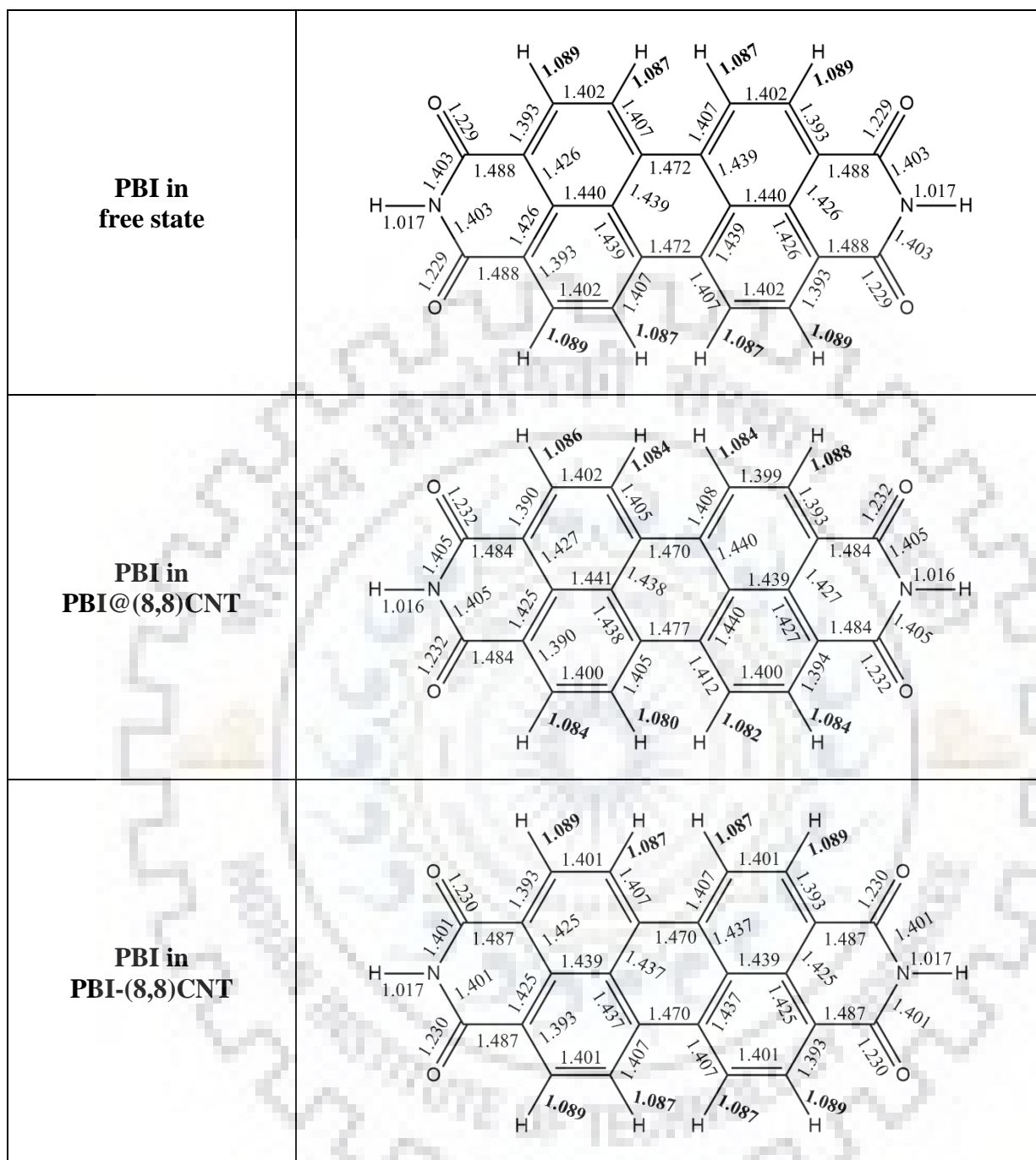


Figure A2. Schematic diagram of PBI in free state and PBI in its endo- and exohedral complexes with CNT. All the values shown in the above figures are in Å.

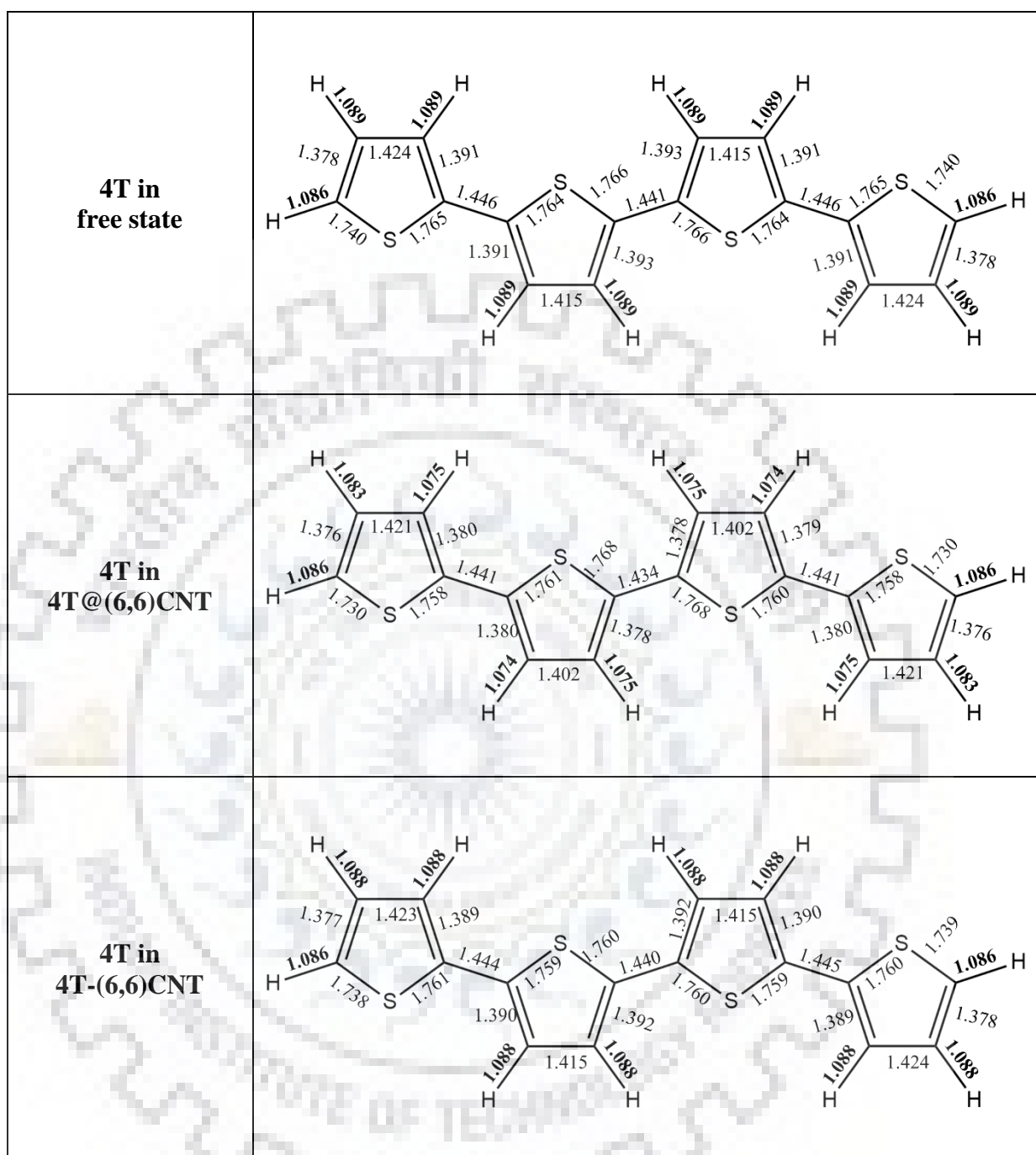


Figure A3. Schematic diagram of 4T in free state and 4T in its endo- and exohedral complexes with CNT. All the values shown in the above figures are in Å.



Bibliography

1. D. Jariwala, V. K. Sangwan, L. J. Lauhon, T. J. Marks, M. C. Hersam. Carbon nanomaterials for electronics, optoelectronics, photovoltaics, and sensing. *Chem. Soc. Rev.*, 42, 2824-60, 2013.
2. K. Higuchi, S. Kishimoto, Y. Nakajima, T. Tomura, M. Takesue, K. Hata, E. I. Kauppinen, Y. Ohno. High-Mobility, Flexible Carbon Nanotube Thin-Film Transistors Fabricated by Transfer and High-Speed Flexographic Printing Techniques. *Appl. Phys. Express*, 6, 085101, 2013.
3. S. Iijima. Helical microtubules of graphitic carbon. *Nature*, 354, 56-58, 1991.
4. P. L. McEuen, M. Bockrath, D. H. Cobden, J. G. Lu. One dimensional transport in carbon nanotubes. *Microelectron. Eng.*, 47, 417-420, 1999.
5. R. Saito, M. Fujita, G. Dresselhaus, M. S. Dresselhaus. Electronic structure of chiral graphene tubules. *Appl. Phys. Lett.*, 60, 2204-2206, 1992.
6. X. Tu, S. Manohar, A. Jagota, M. Zheng. DNA sequence motifs for structure-specific recognition and separation of carbon nanotubes. *Nature*, 460, 250, 2009.
7. X. Tu, A. R. Hight Walker, C. Y. Khripin, M. Zheng. Evolution of DNA Sequences Toward Recognition of Metallic Armchair Carbon Nanotubes. *J. Am. Chem. Soc.*, 133, 12998-13001, 2011.
8. B. Liu, F. Wu, H. Gui, M. Zheng, C. Zhou. Chirality-Controlled Synthesis and Applications of Single-Wall Carbon Nanotubes. *ACS Nano*, 11, 31-53, 2017.
9. Y. Wang, M. J. Kim, H. Shan, C. Kittrell, H. Fan, L. M. Ericson, W.-F. Hwang, S. Arepalli, R. H. Hauge, R. E. Smalley. Continued Growth of Single-Walled Carbon Nanotubes. *Nano Lett.*, 5, 997-1002, 2005.
10. R. E. Smalley, Y. Li, V. C. Moore, B. K. Price, R. Colorado, H. K. Schmidt, R. H. Hauge, A. R. Barron, J. M. Tour. Single Wall Carbon Nanotube Amplification: En Route to a Type-Specific Growth Mechanism. *J. Am. Chem. Soc.*, 128, 15824-15829, 2006.
11. Y. Yao, C. Feng, J. Zhang, Z. Liu. "Cloning" of Single-Walled Carbon Nanotubes via Open-End Growth Mechanism. *Nano Lett.*, 9, 1673-1677, 2009.
12. H. F. Wang, C. Yamada, J. Liu, B. L. Liu, X. M. Tu, M. Zheng, C. W. Zhou, Y. Homma. Re-growth of single-walled carbon nanotube by hot-wall and cold-wall chemical vapor deposition. *Carbon*, 95, 497-502, 2015.

13. S. M. Bachilo, L. Balzano, J. E. Herrera, F. Pompeo, D. E. Resasco, R. B. Weisman. Narrow (n,m)-Distribution of Single-Walled Carbon Nanotubes Grown Using a Solid Supported Catalyst. *J. Am. Chem. Soc.*, 125, 11186-11187, 2003.
14. G. Lolli, L. Zhang, L. Balzano, N. Sakulchaicharoen, Y. Tan, D. E. Resasco. Tailoring (n,m) Structure of Single-Walled Carbon Nanotubes by Modifying Reaction Conditions and the Nature of the Support of CoMo Catalysts. *J. Phys. Chem. B*, 110, 2108-2115, 2006.
15. Y. Yuan, H. E. Karahan, C. Yıldırım, L. Wei, Ö. Birer, S. Zhai, R. Lau, Y. Chen. "Smart poisoning" of Co/SiO₂ catalysts by sulfidation for chirality-selective synthesis of (9,8) single-walled carbon nanotubes. *Nanoscale*, 8, 17705-17713, 2016.
16. F. Yang, X. Wang, J. Si, X. Zhao, K. Qi, C. Jin, Z. Zhang, M. Li, D. Zhang, J. Yang, Z. Zhang, Z. Xu, L.-M. Peng, X. Bai, Y. Li. Water-Assisted Preparation of High-Purity Semiconducting (14,4) Carbon Nanotubes. *ACS Nano*, 11, 186-193, 2017.
17. F. Rao, T. Li, Y. Wang. Growth of "all-carbon" single-walled carbon nanotubes from diamonds and fullerenes. *Carbon*, 47, 3580-3584, 2009.
18. L. T. Scott, E. A. Jackson, Q. Zhang, B. D. Steinberg, M. Bancu, B. Li. A Short, Rigid, Structurally Pure Carbon Nanotube by Stepwise Chemical Synthesis. *J. Am. Chem. Soc.*, 134, 107-110, 2012.
19. A. Mueller, K. Y. Amsharov, M. Jansen. End-Cap Precursor Molecules for the Controlled Growth of Single-Walled Carbon Nanotubes. *Fuller. Nanotub. Car. N.*, 20, 401-404, 2012.
20. H. Omachi, Y. Segawa, K. Itami. Synthesis of Cycloparaphenylenes and Related Carbon Nanorings: A Step toward the Controlled Synthesis of Carbon Nanotubes. *Acc. Chem. Res.*, 45, 1378-1389, 2012.
21. H. Omachi, T. Nakayama, E. Takahashi, Y. Segawa, K. Itami. Initiation of carbon nanotube growth by well-defined carbon nanorings. *Nat. Chem.*, 5, 572, 2013.
22. X. Zhao, Y. Liu, S. Inoue, T. Suzuki, R. O. Jones, Y. Ando. Smallest Carbon Nanotube Is 3 Å in Diameter. *Phys. Rev. Lett.*, 92, 125502, 2004.
23. J. Ma, J. N. Wang, X. X. Wang. Large-diameter and water-dispersible single-walled carbon nanotubes: synthesis, characterization and applications. *J. Mater. Chem.*, 19, 3033-3041, 2009.
24. R. Zhang, Y. Zhang, F. Wei. Controlled Synthesis of Ultralong Carbon Nanotubes with Perfect Structures and Extraordinary Properties. *Acc. Chem. Res.*, 50, 179-189, 2017.

25. R. Jasti, J. Bhattacharjee, J. B. Neaton, C. R. Bertozzi. Synthesis, Characterization, and Theory of [9]-, [12]-, and [18]Cycloparaphenylene: Carbon NanoHoop Structures. *J. Am. Chem. Soc.*, 130, 17646-17647, 2008.
26. R. Jasti, C. R. Bertozzi. Progress and Challenges for the Bottom-Up Synthesis of Carbon Nanotubes with Discrete Chirality. *Chem. Phys. Lett.*, 494, 1-7, 2010.
27. S. Hitosugi, W. Nakanishi, T. Yamasaki, H. Isobe. Bottom-up synthesis of finite models of helical (n,m)-single-wall carbon nanotubes. *Nat. Commun.*, 2, 492, 2011.
28. S. Hitosugi, T. Yamasaki, H. Isobe. Bottom-up Synthesis and Thread-in-Bead Structures of Finite (n,0)-Zigzag Single-Wall Carbon Nanotubes. *J. Am. Chem. Soc.*, 134, 12442-12445, 2012.
29. W. Wang, Y.-X. Wang, H.-B. Yang. Bottom-up chemical synthesis of three-dimensional conjugated carbon nanostructures: from carbon nanocages to carbon nanotubes. *Org. Chem. Front.*, 1, 1005-1009, 2014.
30. Y. Wang, J. Zhang, J. Zang, E. Ge, H. Huang. Etching and cutting of multi-walled carbon nanotubes in molten nitrate. *Corros. Sci.*, 53, 3764-3770, 2011.
31. M. V. Shuba, A. G. Paddubskaya, P. P. Kuzhir, S. A. Maksimenko, V. K. Ksenevich, G. Niaura, D. Seliuta, I. Kasalynas, G. Valusis. Soft cutting of single-wall carbon nanotubes by low temperature ultrasonication in a mixture of sulfuric and nitric acids. *Nanotechnology*, 23, 495714, 2012.
32. F. Ren, S. A. Kanaan, F. Khalkhal, C. Z. Loebick, G. L. Haller, L. D. Pfefferle. Controlled cutting of single-walled carbon nanotubes and low temperature annealing. *Carbon*, 63, 61-70, 2013.
33. S. A. Miners, G. A. Rance, A. La Torre, S. M. Kenny, A. N. Khlobystov. Controlled oxidative cutting of carbon nanotubes catalysed by silver nanoparticles. *J. Mater. Chem. C*, 2, 8357-8363, 2014.
34. E. J. Weydemeyer, A. J. Sawdon, C.-A. Peng. Controlled cutting and hydroxyl functionalization of carbon nanotubes through autoclaving and sonication in hydrogen peroxide. *Chem. Commun.*, 51, 5939-5942, 2015.
35. M. Kierkowicz, E. Pach, A. Santidrián, S. Sandoval, G. Gonçalves, E. Tobías-Rossell, M. Kalbáč, B. Ballesteros, G. Tobias. Comparative study of shortening and cutting strategies of single-walled and multi-walled carbon nanotubes assessed by scanning electron microscopy. *Carbon*, 139, 922-932, 2018.
36. T. Kim, M. K. Kim, Y. Park, E. Kim, J. Kim, W. Ryu, H. M. Jeong, K. Kim. Cutting-Processed Single-Wall Carbon Nanotubes with Additional Edge Sites for Supercapacitor Electrodes. *Nanomaterials (Basel)*, 8, 464, 2018.

37. J. H. Warner, F. Schäffel, G. Zhong, M. H. Rummeli, B. Büchner, J. Robertson, G. A. D. Briggs. Investigating the Diameter-Dependent Stability of Single-Walled Carbon Nanotubes. *ACS Nano*, 3, 1557-1563, 2009.
38. A. V. Naumov, D. A. Tsyboulski, S. M. Bachilo, R. B. Weisman. Length-dependent optical properties of single-walled carbon nanotube samples. *Chem. Phys.*, 422, 255-263, 2013.
39. H. Kataura, Y. Kumazawa, Y. Maniwa, I. Umezu, S. Suzuki, Y. Ohtsuka, Y. Achiba. Optical properties of single-wall carbon nanotubes. *Synth. Met.*, 103, 2555-2558, 1999.
40. H. Kim, K. Chung, S. Lee, D. H. Kim, H. Lee. Near-infrared light-responsive nanomaterials for cancer theranostics. *Nanobiotechnol.*, 8, 23-45, 2016.
41. U. Kumar, S. Sikarwar, R. K. Sonker, B. C. Yadav. Carbon Nanotube: Synthesis and Application in Solar Cell. *J. Inorg. Organomet. Polym. Mater.*, 26, 1231-1242, 2016.
42. R. S. Park, G. Hills, J. Sohn, S. Mitra, M. M. Shulaker, H. S. P. Wong. Hysteresis-Free Carbon Nanotube Field-Effect Transistors. *ACS Nano*, 11, 4785-4791, 2017.
43. S. Wang, Q. Zeng, L. Yang, Z. Zhang, Z. Wang, T. Pei, L. Ding, X. Liang, M. Gao, Y. Li, L.-M. Peng. High-Performance Carbon Nanotube Light-Emitting Diodes with Asymmetric Contacts. *Nano Lett.*, 11, 23-29, 2011.
44. A. Rochefort, D. R. Salahub, P. Avouris. Effects of Finite Length on the Electronic Structure of Carbon Nanotubes. *J. Phys. Chem. B*, 103, 641-646, 1999.
45. Y. Matsuo, K. Tahara, E. Nakamura. Theoretical Studies on Structures and Aromaticity of Finite-Length Armchair Carbon Nanotubes. *Org. Lett.*, 5, 3181-3184, 2003.
46. F. Buonocore, F. Trani, D. Ninno, A. Di Matteo, G. Cantele, G. Iadonisi. Ab initio calculations of electron affinity and ionization potential of carbon nanotubes. *Nanotechnology*, 19, 025711, 2007.
47. L. V. Liu, W. Q. Tian, Y. K. Chen, Y. A. Zhang, Y. A. Wang. Theoretical studies on structures, ¹³C NMR chemical shifts, aromaticity, and chemical reactivity of finite-length open-ended armchair single-walled carbon nanotubes. *Nanoscale*, 2, 254-261, 2010.
48. M. T. Ahmadpour, S. J. Hashemifar, A. Rostamnejadi. Size effects on the structural, electronic, and optical properties of (5,0) finite-length carbon nanotube: An ab-initio electronic structure study. *J. Appl. Phys.*, 120, 014303, 2016.
49. G. Dumont, P. Boulanger, M. Côté, M. Ernzerhof. Peierls instability in carbon nanotubes: A first-principles study. *Phys. Rev. B*, 82, 035419, 2010.

50. T. W. Odom, J.-L. Huang, P. Kim, C. M. Lieber. Structure and Electronic Properties of Carbon Nanotubes. *J. Phys. Chem. B*, 104, 2794-2809, 2000.
51. D. Hedman, J. A. Larsson. Length dependent stability of single-walled carbon nanotubes and how it affects their growth. *Carbon*, 116, 443-447, 2017.
52. I. K. Petrushenko, N. A. Ivanov. Ionization potentials and structural properties of finite-length single-walled carbon nanotubes: DFT study. *Physica E Low Dimens. Syst. Nanostruct.*, 54, 262-266, 2013.
53. S. Okada. Electronic structure of finite-length carbon nanotubes: Crossover from fullerenes to nanotubes. *Nano*, 02, 51-57, 2007.
54. B. Gao, J. Jiang, Z. Wu, Y. Luo. Energy gaps, electronic structures, and x-ray spectroscopies of finite semiconductor single-walled carbon nanotubes. *J. Chem. Phys.*, 128, 084707, 2008.
55. K. R. S. Chandrakumar, K. Srinivasu, S. K. Ghosh. Nanoscale Curvature-Induced Hydrogen Adsorption in Alkali Metal Doped Carbon Nanomaterials. *J. Phys. Chem. C*, 112, 15670-15679, 2008.
56. A. Galano. On the influence of diameter and length on the properties of armchair single-walled carbon nanotubes: A theoretical chemistry approach. *Chem. Phys.*, 327, 159-170, 2006.
57. S. Chopra. Optical properties of sub 2 nm long (6,5) single-walled carbon nanotubes: first principles investigation. *Mol. Phys.*, 117, 71-78, 2019.
58. K. Milowska, M. Birowska, J. A. Majewski. Ab initio study of functionalized carbon nanotubes. *Acta Phys. Pol. A*, 116, 841-843, 2009.
59. T. Kar, B. Akdim, X. Duan, R. Pachter. A theoretical study of functionalized single-wall carbon nanotubes: ONIOM calculations. *Chem. Phys. Lett.*, 392, 176-180, 2004.
60. J. Zhao, H. Park, J. Han, J. P. Lu. Electronic Properties of Carbon Nanotubes with Covalent Sidewall Functionalization. *J. Phys. Chem. B*, 108, 4227-4230, 2004.
61. A. Setaro, M. Adeli, M. Glaeske, D. Przyrembel, T. Bisswanger, G. Gordeev, F. Maschietto, A. Faghani, B. Paulus, M. Weinelt, R. Arenal, R. Haag, S. Reich. Preserving π -conjugation in covalently functionalized carbon nanotubes for optoelectronic applications. *Nat. Commun.*, 8, 14281, 2017.
62. P. Singh, S. Campidelli, S. Giordani, D. Bonifazi, A. Bianco, M. Prato. Organic functionalisation and characterisation of single-walled carbon nanotubes. *Chem. Soc. Rev.*, 38, 2214-2230, 2009.

63. M. G. Williams, F. Gao, I. BenDhiab, A. Teplyakov. Carbon Nanotubes Covalently Attached to Functionalized Surfaces Directly through the Carbon Cage. *Langmuir*, 33, 1121-1131, 2017.
64. K. Balamurugan, P. Baskar, R. M. Kumar, S. Das, V. Subramanian. Effects of functionalization of carbon nanotubes on their dispersion in an ethylene glycol–water binary mixture – a molecular dynamics and ONIOM investigation. *Phys. Chem. Chem. Phys.*, 16, 24509-24518, 2014.
65. B. J. Nagare, D. Habale, S. Chacko, S. Ghosh. Hydrogen adsorption on Na–SWCNT systems. *J. Mater. Chem.*, 22, 22013-22021, 2012.
66. O. V. Kharissova, B. I. Kharisov, E. G. de Casas Ortiz. Dispersion of carbon nanotubes in water and non-aqueous solvents. *RSC Adv.*, 3, 24812-24852, 2013.
67. D. A. Britz, A. N. Khlobystov. Noncovalent interactions of molecules with single walled carbon nanotubes. *Chem. Soc. Rev.*, 35, 637-659, 2006.
68. Y.-L. Zhao, J. F. Stoddart. Noncovalent Functionalization of Single-Walled Carbon Nanotubes. *Acc. Chem. Res.*, 42, 1161-1171, 2009.
69. N. Saifuddin, A. Z. Raziah, A. R. Junizah. Carbon Nanotubes: A Review on Structure and Their Interaction with Proteins. *J. Chem.*, 2013, 18, 2013.
70. P. Bilalis, D. Katsigiannopoulos, A. Avgeropoulos, G. Sakellariou. Non-covalent functionalization of carbon nanotubes with polymers. *RSC Adv.*, 4, 2911-2934, 2014.
71. A. Di Crescenzo, V. Ettore, A. Fontana. Non-covalent and reversible functionalization of carbon nanotubes. *Beilstein J Nanotechnol.*, 5, 1675-1690, 2014.
72. D. Umadevi, S. Panigrahi, G. N. Sastry. Noncovalent Interaction of Carbon Nanostructures. *Acc. Chem. Res.*, 47, 2574-2581, 2014.
73. L. Meng, C. Fu, Q. Lu. Advanced technology for functionalization of carbon nanotubes. *Progress in Natural Science*, 19, 801-810, 2009.
74. J. Comer, R. Chen, H. Poblete, A. Vergara-Jaque, J. E. Riviere. Predicting Adsorption Affinities of Small Molecules on Carbon Nanotubes Using Molecular Dynamics Simulation. *ACS Nano*, 9, 11761-11774, 2015.
75. H. Murakami, T. Nomura, N. Nakashima. Noncovalent porphyrin-functionalized single-walled carbon nanotubes in solution and the formation of porphyrin–nanotube nanocomposites. *Chem. Phys. Lett.*, 378, 481-485, 2003.
76. J. K. Sprafke, S. D. Stranks, J. H. Warner, R. J. Nicholas, H. L. Anderson. Noncovalent Binding of Carbon Nanotubes by Porphyrin Oligomers. *Angew. Chem.*, 50, 2313-2316, 2011.

77. A. Najafi Chermahini, A. Teimouri, H. Farrokhpour. A DFT-D study on the interaction between lactic acid and single-wall carbon nanotubes. *RSC Adv.*, 5, 97724-97733, 2015.
78. M. K. Tripathy, N. K. Jena, A. K. Samanta, S. K. Ghosh, K. R. S. Chandrakumar. Effect of confinement on the structure and energetics of Zundel cation present inside the hydrophobic carbon nanotubes: an ab initio study. *Theor. Chem. Acc.*, 133, 1576, 2014.
79. T. Takenobu, T. Takano, M. Shiraishi, Y. Murakami, M. Ata, H. Kataura, Y. Achiba, Y. Iwasa. Stable and controlled amphoteric doping by encapsulation of organic molecules inside carbon nanotubes. *Nat. Mater.*, 2, 683, 2003.
80. H. Ulbricht, T. Hertel. Dynamics of C₆₀ Encapsulation into Single-Wall Carbon Nanotubes. *J. Phys. Chem. B*, 107, 14185-14190, 2003.
81. T. Shimada, Y. Ohno, K. Suenaga, T. Okazaki, S. Kishimoto, T. Mizutani, R. Taniguchi, H. Kato, B. Cao, T. Sugai, H. Shinohara. Tunable Field-Effect Transistor Device with Metallofullerene Nanopeapods. *Jpn. J. Appl. Phys.*, 44, 469-472, 2005.
82. W. Plank, H. Kuzmany, F. Simon, T. Saito, S. Ohshima, M. Yumura, S. Iijima, G. Rotas, G. Pagona, N. Tagmatarchis. Fullerene derivatives encapsulated in carbon nanotubes. *Phys. Status Solidi B*, 244, 4074-4077, 2007.
83. D. Baowan, N. Thamwattana, J. M. Hill. Encapsulation of C₆₀ fullerenes into single-walled carbon nanotubes: Fundamental mechanical principles and conventional applied mathematical modeling. *Phys. Rev. B*, 76, 155411, 2007.
84. J. H. Warner, A. A. R. Watt, L. Ge, K. Porfyrakis, T. Akachi, H. Okimoto, Y. Ito, A. Ardavan, B. Montanari, J. H. Jefferson, N. M. Harrison, H. Shinohara, G. A. D. Briggs. Dynamics of Paramagnetic Metallofullerenes in Carbon Nanotube Peapods. *Nano Lett.*, 8, 1005-1010, 2008.
85. Á. Botos, A. N. Khlobystov, B. Botka, R. Hackl, E. Székely, B. Simándi, K. Kamarás. Investigation of fullerene encapsulation in carbon nanotubes using a complex approach based on vibrational spectroscopy. *Phys. Status Solidi B*, 247, 2743-2745, 2010.
86. C.-c. Ling, Q.-z. Xue, D. Xia, M.-x. Shan, Z.-d. Han. Fullerene filling modulates carbon nanotube radial elasticity and resistance to high pressure. *RSC Adv.*, 4, 1107-1115, 2014.
87. L. Cui, Y. Feng, X. Zhang. Enhancement of heat conduction in carbon nanotubes filled with fullerene molecules. *Phys. Chem. Chem. Phys.*, 17, 27520-27526, 2015.
88. E. Munusamy, S. E. Wheeler. Endohedral and exohedral complexes of substituted benzenes with carbon nanotubes and graphene. *J. Chem. Phys.*, 139, 094703, 2013.
89. L. Stobinski, J. Mazurkiewicz, H. M. Lin, P. Tomasik. Complexes of carbon nanotubes with selected carotenoids. *J. Nanosci. Nanotechnol.*, 5, 2121-7, 2005.

90. A. Kumar, D. Singh, D. Kumar, D. Kumar. Quantum Mechanical Study of Nucleic Acid Interaction with Carbon Nanotubes in Interior and at Exterior Positions. *Adv. Sci. Lett.*, 24, 802-806, 2018.
91. H. Chang, J. D. Lee, S. M. Lee, Y. H. Lee. Adsorption of NH₃ and NO₂ molecules on carbon nanotubes. *Appl. Phys. Lett.*, 79, 3863-3865, 2001.
92. J. Dai, P. Giannozzi, J. Yuan. Adsorption of pairs of NO_x molecules on single-walled carbon nanotubes and formation of NO+NO₃ from NO₂. *Surf. Sci.*, 603, 3234-3238, 2009.
93. K. Srinivasu, M. Sundararajan. Can uranyl complexes encapsulate to carbon nanotubes? A periodic DFT study. *J. Chem. Sci.*, 129, 783-790, 2017.
94. A. Mejri, D. Vardanega, B. Tangour, T. Gharbi, F. Picaud. Encapsulation into Carbon Nanotubes and Release of Anticancer Cisplatin Drug Molecule. *J. Phys. Chem. B* 119, 604-611, 2015.
95. S. A. Sozykin, V. P. Beskachko. Structure of endohedral complexes of carbon nanotubes encapsulated with lithium and sodium. *Mol. Phys.*, 111, 930-938, 2013.
96. A. Roztoczyńska, J. Kozłowska, P. Lipkowski, W. Bartkowiak. Hydrogen bonding inside and outside carbon nanotubes: HF dimer as a case study. *Phys. Chem. Chem. Phys.*, 18, 2417-2427, 2016.
97. P. Kumar, C. N. Ramachandran, B. K. Mishra, N. Sathyamurthy. Interaction of rare gas dimers in the confines of a carbon nanotube. *Chem. Phys. Lett.*, 618, 42-45, 2015.
98. D. Chakraborty, P. K. Chattaraj. Confinement induced binding in noble gas atoms within a BN-doped carbon nanotube. *Chem. Phys. Lett.*, 621, 29-34, 2015.
99. R. M. Kumar, M. Elango, R. Parthasarathi, V. Subramanian. Density Functional Theory Studies on Ice Nanotubes. *J. Phys. Chem. A*, 115, 12841-12851, 2011.
100. L. M. Woods, Ş. C. Bădescu, T. L. Reinecke. Adsorption of simple benzene derivatives on carbon nanotubes. *Phys. Rev. B*, 75, 155415, 2007.
101. C.-J. M. Chin, M.-W. Shih, H.-J. Tsai. Adsorption of nonpolar benzene derivatives on single-walled carbon nanotubes. *Appl. Surf. Sci.*, 256, 6035-6039, 2010.
102. T. Kar, H. F. Bettinger, S. Scheiner, A. K. Roy. Noncovalent π - π Stacking and CH--- π Interactions of Aromatics on the Surface of Single-Wall Carbon Nanotubes: An MP2 Study. *J. Phys. Chem. C* 112, 20070-20075, 2008.
103. F. Tournus, S. Latil, M. I. Heggie, J. C. Charlier. π -stacking interaction between carbon nanotubes and organic molecules. *Phys. Rev. B*, 72, 075431, 2005.

104. D. Q. Yang, B. Hennequin, E. Sacher. XPS Demonstration of π - π Interaction between Benzyl Mercaptan and Multiwalled Carbon Nanotubes and Their Use in the Adhesion of Pt Nanoparticles. *Chem. Mater.*, 18, 5033-5038, 2006.
105. E. Cohen, H. Dodiuk, A. Ophir, S. Kenig, C. Barry, J. Mead. Evidences for π -interactions between pyridine modified copolymer and carbon nanotubes and its role as a compatibilizer in poly(methyl methacrylate) composites. *Compos. Sci. Technol.*, 79, 133-139, 2013.
106. E. M. Pérez, N. Martín. π - π interactions in carbon nanostructures. *Chem. Soc. Rev.*, 44, 6425-6433, 2015.
107. Y. Wang, Y. Bu. Noncovalent Interactions between Cytosine and SWCNT: Curvature Dependence of Complexes via π $\cdots\pi$ Stacking and Cooperative $\text{CH}\cdots\pi/\text{NH}\cdots\pi$. *J. Phys. Chem. B*, 111, 6520-6526, 2007.
108. G. Tian, H. Li, W. Ma, Y. Wang. Substituent effects in π -stacking of histidine on functionalized-SWNT and graphene. *Comput. Theor. Chem.*, 1062, 44-49, 2015.
109. J. Calbo, A. López-Moreno, A. de Juan, J. Comer, E. Ortí, E. M. Pérez. Understanding Noncovalent Interactions of Small Molecules with Carbon Nanotubes. *Chem. Eur. J.*, 23, 12909-12916, 2017.
110. S. Gorantla, S. Avdoshenko, F. Börrnert, A. Bachmatiuk, M. Dimitrakopoulou, F. Schäffel, R. Schönfelder, J. Thomas, T. Gemming, J. H. Warner, G. Cuniberti, J. Eckert, B. Büchner, M. H. Rummeli. Enhanced π - π interactions between a C_{60} fullerene and a buckle bend on a double-walled carbon nanotube. *Nano Res.*, 3, 92-97, 2010.
111. Z. Yang, Z. Wang, X. Tian, P. Xiu, R. Zhou. Amino acid analogues bind to carbon nanotube via π - π interactions: Comparison of molecular mechanical and quantum mechanical calculations. *J. Chem. Phys.*, 136, 025103, 2012.
112. T. Yumura, W. Yamamoto. Kinetic Control in the Alignment of Polar π -Conjugated Molecules inside Carbon Nanotubes. *J. Phys. Chem. C*, 122, 18151-18160, 2018.
113. S. L. Nogueira, S. K. Sahoo, T. Jarrosson, F. Serein-Spirau, J. P. Lère-Porte, E. A. Moujaes, A. Marletta, A. P. Santos, C. Fantini, C. A. Furtado, R. A. Silva. A new designed π conjugated molecule for stable single walled carbon nanotube dispersion in aqueous medium. *J. Colloid Interface Sci.*, 464, 117-125, 2016.
114. F. Moradi, M. Darvish Ganji, Y. Sarrafi. Remediation of phenol-contaminated water by pristine and functionalized SWCNTs: Ab initio van der Waals DFT investigation. *Diam. Relat. Mater.*, 82, 7-18, 2018.
115. X.-F. Zhang, X. Shao. π - π binding ability of different carbon nano-materials with aromatic phthalocyanine molecules: Comparison between graphene, graphene oxide and carbon nanotubes. *J. Photochem. Photobiol.*, 278, 69-74, 2014.

116. C. Rajesh, C. Majumder, H. Mizuseki, Y. Kawazoe. A theoretical study on the interaction of aromatic amino acids with graphene and single walled carbon nanotube. *J. Chem. Phys.*, 130, 124911, 2009.
117. D. Umadevi, G. N. Sastry. Quantum Mechanical Study of Physisorption of Nucleobases on Carbon Materials: Graphene versus Carbon Nanotubes. *J. Phys. Chem. Lett.*, 2, 1572-1576, 2011.
118. J. Chen, H. Liu, W. A. Weimer, M. D. Halls, D. H. Waldeck, G. C. Walker. Noncovalent Engineering of Carbon Nanotube Surfaces by Rigid, Functional Conjugated Polymers. *J. Am. Chem. Soc.*, 124, 9034-9035, 2002.
119. Y. J. Dappe. Encapsulation of organic molecules in carbon nanotubes: role of the van der Waals interactions. *J. Phys. D*, 47, 083001, 2014.
120. A. N. Enyashin, S. Gemming, G. Seifert. DNA-wrapped carbon nanotubes. *Nanotechnology*, 18, 245702, 2007.
121. T. Fujigaya, N. Nakashima. Non-covalent polymer wrapping of carbon nanotubes and the role of wrapped polymers as functional dispersants. *Sci. Technol. Adv. Mater.*, 16, 024802, 2015.
122. M. Numata, M. Asai, K. Kaneko, A.-H. Bae, T. Hasegawa, K. Sakurai, S. Shinkai. Inclusion of Cut and As-Grown Single-Walled Carbon Nanotubes in the Helical Superstructure of Schizophyllan and Curdlan (β -1,3-Glucans). *J. Am. Chem. Soc.*, 127, 5875-5884, 2005.
123. Y. Wang, H. Ai. Theoretical Insights into the Interaction Mechanism between Proteins and SWCNTs: Adsorptions of Tripeptides GXG on SWCNTs. *J. Phys. Chem. B*, 113, 9620-9627, 2009.
124. V. Z. Poenitzsch, D. C. Winters, H. Xie, G. R. Dieckmann, A. B. Dalton, I. H. Musselman. Effect of Electron-Donating and Electron-Withdrawing Groups on Peptide/Single-Walled Carbon Nanotube Interactions. *J. Am. Chem. Soc.*, 129, 14724-14732, 2007.
125. H. Hajova, Z. Kominkova, A. Santidrian, O. Frank, L. Kubac, F. Josefik, M. Kalbac. Preparation and Charge-Transfer Study in a Single-Walled Carbon Nanotube Functionalized with Poly(3,4-ethylenedioxythiophene). *J. Phys. Chem. C* 119, 21538-21546, 2015.
126. Y. Almadori, L. Alvarez, R. Arenal, R. Babaa, T. Michel, R. Le Parc, J.-L. Bantignies, B. Jouselme, S. Palacin, P. Hermet, J.-L. Sauvajol. Charge transfer in conjugated oligomers encapsulated into carbon nanotubes. *Phys. Status Solidi B*, 248, 2560-2563, 2011.

127. L. Alvarez, Y. Almadori, R. Arenal, R. Babaa, T. Michel, R. Le Parc, J. L. Bantignies, B. Jousselme, S. Palacin, P. Hermet, J. L. Sauvajol. Charge Transfer Evidence between Carbon Nanotubes and Encapsulated Conjugated Oligomers. *J. Phys. Chem. C*, 115, 11898-11905, 2011.
128. S. Fukuzumi. Nanocarbons as Electron Donors and Acceptors in Photoinduced Electron-Transfer Reactions. *ECS J. Solid State Sci. Technol.*, 6, M3055-M3061, 2017.
129. B. He, Q. Tang, J. Luo, Q. Li, X. Chen, H. Cai. Rapid charge-transfer in polypyrrole–single wall carbon nanotube complex counter electrodes: Improved photovoltaic performances of dye-sensitized solar cells. *J. Power Sources*, 256, 170-177, 2014.
130. J.-L. Xu, R.-X. Dai, Y. Xin, Y.-L. Sun, X. Li, Y.-X. Yu, L. Xiang, D. Xie, S.-D. Wang, T.-L. Ren. Efficient and Reversible Electron Doping of Semiconductor-Enriched Single-Walled Carbon Nanotubes by Using Decamethylcobaltocene. *Sci. Rep.*, 7, 6751, 2017.
131. M. Ohtani, S. Fukuzumi. Solubilization and photoinduced electron transfer of single-walled carbon nanotubes wrapped with coenzyme Q10. *Chem. Commun.*, 4997-4999, 2009.
132. J. E. Weaver, M. R. Dasari, A. Datar, S. Talapatra, P. Kohli. Investigating Photoinduced Charge Transfer in Carbon Nanotube–Perylene–Quantum Dot Hybrid Nanocomposites. *ACS Nano*, 4, 6883-6893, 2010.
133. V. Strauss, A. Roth, M. Sekita, Dirk M. Guldi. Efficient Energy-Conversion Materials for the Future: Understanding and Tailoring Charge-Transfer Processes in Carbon Nanostructures. *Chem*, 1, 531-556, 2016.
134. R. Voggu, C. S. Rout, A. D. Franklin, T. S. Fisher, C. N. R. Rao. Extraordinary Sensitivity of the Electronic Structure and Properties of Single-Walled Carbon Nanotubes to Molecular Charge-Transfer. *J. Phys. Chem. C*, 112, 13053-13056, 2008.
135. W. Wu, L. Liu, Y. Li, Z. X. Guo, L. Dai, D. Zhu. Charge Transfer Complex of TTF-Carbon Nanotubes. *Fullerenes, Nanotubes and Carbon Nanostruct.*, 11, 89-93, 2003.
136. E. L. Sceats, J. C. Green. Charge transfer composites of bis(cyclopentadienyl) and bis(benzene) transition metal complexes encapsulated in single-walled carbon nanotubes. *Phys. Rev. B*, 75, 245441, 2007.
137. S.-H. Jhi, S. G. Louie, M. L. Cohen. Electronic Properties of Oxidized Carbon Nanotubes. *Phys. Rev. Lett.*, 85, 1710-1713, 2000.
138. J. Zhao, J. P. Lu, J. Han, C.-K. Yang. Noncovalent functionalization of carbon nanotubes by aromatic organic molecules. *Appl. Phys. Lett.*, 82, 3746-3748, 2003.
139. F. Tournus, J. C. Charlier. Ab initio study of benzene adsorption on carbon nanotubes. *Phys. Rev. B*, 71, 165421, 2005.

140. J. Lu, S. Nagase, X. Zhang, D. Wang, M. Ni, Y. Maeda, T. Wakahara, T. Nakahodo, T. Tsuchiya, T. Akasaka, Z. Gao, D. Yu, H. Ye, W. N. Mei, Y. Zhou. Selective interaction of large or charge-transfer aromatic molecules with metallic single-wall carbon nanotubes: critical role of the molecular size and orientation. *J. Am. Chem. Soc.*, 128, 5114-5118, 2006.
141. A. K. Manna, S. K. Pati. Doping single-walled carbon nanotubes through molecular charge-transfer: a theoretical study. *Nanoscale*, 2, 1190-1195, 2010.
142. R. Kakkar, S. Sharma, B. Badhani. Density Functional Study of Functionalization of Carbon Nanotubes with Carbenes. *Can. Chem. Trans.*, 2, 434-449, 2014.
143. D. Umadevi, G. N. Sastry. Feasibility of carbon nanomaterials as gas sensors: a computational study. *Curr. Sci.*, 106, 1224-1234, 2014.
144. K. Balamurugan, V. Subramanian. Adsorption of Chlorobenzene onto (5,5) Armchair Single-Walled Carbon Nanotube and Graphene Sheet: Toxicity versus Adsorption Strength. *J. Phys. Chem. C*, 117, 21217-21227, 2013.
145. A. Bandyopadhyay, D. Ghosh, S. K. Pati. Trapping and sensing of hazardous insecticides by chemically modified single walled carbon nanotubes. *Phys. Chem. Chem. Phys.*, 19, 24059-24066, 2017.
146. A. S. Ivanov, T. Kar, A. I. Boldyrev. Nanoscale stabilization of zintl compounds: 1D ionic Li-P double helix confined inside a carbon nanotube. *Nanoscale*, 8, 3454-3460, 2016.
147. D. V. Rybkovskiy, A. Impellizzeri, E. D. Obraztsova, C. P. Ewels. Polyiodide structures in thin single-walled carbon nanotubes: A large-scale density-functional study. *Carbon*, 142, 123-130, 2019.
148. E. Kymakis, G. A. J. Amaratunga. Single-wall carbon nanotube/conjugated polymer photovoltaic devices. *Appl. Phys. Lett.*, 80, 112-114, 2002.
149. H. Ago, K. Petritsch, M. S. P. Shaffer, A. H. Windle, R. H. Friend. Composites of Carbon Nanotubes and Conjugated Polymers for Photovoltaic Devices. *Adv. Mater.*, 11, 1281-1285, 1999.
150. D. M. Guldi, G. M. A. Rahman, F. Zerbetto, M. Prato. Carbon Nanotubes in Electron Donor-Acceptor Nanocomposites. *Acc. Chem. Res.*, 38, 871-878, 2005.
151. C. Li, Y. Chen, S. A. Ntim, S. Mitra. Fullerene-multiwalled carbon nanotube complexes for bulk heterojunction photovoltaic cells. *Appl. Phys. Lett.*, 96, 143303, 2010.
152. A.-M. Dowgiallo, K. S. Mistry, J. C. Johnson, J. L. Blackburn. Ultrafast Spectroscopic Signature of Charge Transfer between Single-Walled Carbon Nanotubes and C₆₀. *ACS Nano*, 8, 8573-8581, 2014.

153. X. Li, M. Mariano, L. McMillon-Brown, J.-S. Huang, M. Y. Sfeir, M. A. Reed, Y. Jung, A. D. Taylor. Charge Transfer from Carbon Nanotubes to Silicon in Flexible Carbon Nanotube/Silicon Solar Cells. *Small*, 13, 1702387, 2017.
154. M. Mollahosseini, E. Karunaratne, G. N. Gibson, J. A. Gascón, F. Papadimitrakopoulos. Fullerene-Assisted Photoinduced Charge Transfer of Single-Walled Carbon Nanotubes through a Flavin Helix. *J. Am. Chem. Soc.*, 138, 5904-5915, 2016.
155. D. M. Guldi. Biomimetic Assemblies of Carbon Nanostructures for Photochemical Energy Conversion. *J. Phys. Chem. B*, 109, 11432-11441, 2005.
156. D. M. Guldi, G. M. A. Rahman, V. Sgobba, N. A. Kotov, D. Bonifazi, M. Prato. CNT–CdTe Versatile Donor–Acceptor Nanohybrids. *J. Am. Chem. Soc.*, 128, 2315-2323, 2006.
157. L.-M. Peng, Z. Zhang, S. Wang. Carbon nanotube electronics: recent advances. *Mater. Today*, 17, 433-442, 2014.
158. X. Cao, Y. Cao, C. Zhou. Imperceptible and Ultraflexible p-Type Transistors and Macroelectronics Based on Carbon Nanotubes. *ACS Nano*, 10, 199-206, 2016.
159. J. Park, J. Yoon, S. J. Kang, G.-T. Kim, J. S. Ha. High yield production of semiconducting p-type single-walled carbon nanotube thin-film transistors on a flexible polyimide substrate by tuning the density of ferritin catalysts. *Carbon*, 49, 2492-2498, 2011.
160. D.-m. Sun, M. Y. Timmermans, Y. Tian, A. G. Nasibulin, E. I. Kauppinen, S. Kishimoto, T. Mizutani, Y. Ohno. Flexible high-performance carbon nanotube integrated circuits. *Nat. Nanotechnol.*, 6, 156, 2011.
161. K. McGuire, N. Gothard, P. L. Gai, M. S. Dresselhaus, G. Sumanasekera, A. M. Rao. Synthesis and Raman characterization of boron-doped single-walled carbon nanotubes. *Carbon*, 43, 219-227, 2005.
162. C.-S. Park, C. J. Lee, E. K. Kim. Stable p-type properties of single walled carbon nanotubes by electrochemical doping. *Phys. Chem. Chem. Phys.*, 17, 16243-16245, 2015.
163. D. Kang, N. Park, J.-h. Ko, E. Bae, W. Park. Oxygen-induced p-type doping of a long individual single-walled carbon nanotube. *Nanotechnology*, 16, 1048-1052, 2005.
164. H. Oh, J.-J. Kim, W. Song, S. Moon, N. Kim, J. Kim, N. Park. Fabrication of n-type carbon nanotube field-effect transistors by Al doping. *Appl. Phys. Lett.*, 88, 103503, 2006.
165. R. Czerw, M. Terrones, J. C. Charlier, X. Blase, B. Foley, R. Kamalakaran, N. Grobert, H. Terrones, D. Tekleab, P. M. Ajayan, W. Blau, M. Rühle, D. L. Carroll. Identification of Electron Donor States in N-Doped Carbon Nanotubes. *Nano Lett.*, 1, 457-460, 2001.

166. R. Nouchi, H. Tomita, A. Ogura, H. Kataura, M. Shiraishi. Logic circuits using solution-processed single-walled carbon nanotube transistors. *Appl. Phys. Lett.*, 92, 253507, 2008.
167. T.-J. Ha, K. Chen, S. Chuang, K. M. Yu, D. Kiriya, A. Javey. Highly Uniform and Stable n-Type Carbon Nanotube Transistors by Using Positively Charged Silicon Nitride Thin Films. *Nano Lett.*, 15, 392-397, 2015.
168. M. Shim, A. Javey, N. W. Shi Kam, H. Dai. Polymer Functionalization for Air-Stable n-Type Carbon Nanotube Field-Effect Transistors. *J. Am. Chem. Soc.*, 123, 11512-11513, 2001.
169. J. Huang, Y.-Y. Jiang. Water-Processable Multiwalled Nanotube: Phenol-Induced Reversible Oxidation Process and Ambipolar Charge Transport Property. *Macromol. Mater. Eng.*, 303, 1700575, 2018.
170. K.-J. Baeg, H. J. Jeong, S. Y. Jeong, J. T. Han, G.-W. Lee. Enhanced ambipolar charge transport in staggered carbon nanotube field-effect transistors for printed complementary-like circuits. *Curr. Appl. Phys.*, 17, 541-547, 2017.
171. R. Martel, V. Derycke, C. Lavoie, J. Appenzeller, K. K. Chan, J. Tersoff, P. Avouris. Ambipolar Electrical Transport in Semiconducting Single-Wall Carbon Nanotubes. *Phys. Rev. Lett.*, 87, 256805, 2001.
172. D. Wei, Y. Zhang, Y. Yang, D. G. Hasko, D. Chu, K. B. K. Teo, G. A. J. Amaratunga, W. I. Milne. Transformation of Unipolar Single-Walled Carbon Nanotube Field Effect Transistors to Ambipolar Induced by Polystyrene Nanosphere Assembly. *ACS Nano*, 2, 2526-2530, 2008.
173. K. S. Vasu, D. Pramanik, S. Kundu, S. S. N. Jayaraman, M. Jain, P. K. Maiti, A. K. Sood. Opening of large band gaps in metallic carbon nanotubes by mannose-functionalized dendrimers: experiments and theory. *J. Mater. Chem. C*, 6, 6483-6488, 2018.
174. Z. Xu, W. Lu, W. Wang, C. Gu, K. Liu, X. Bai, E. Wang, H. Dai. Converting Metallic Single-Walled Carbon Nanotubes into Semiconductors by Boron/Nitrogen Co-Doping. *Adv. Mater.*, 20, 3615-3619, 2008.
175. A. Vijayaraghavan, K. Kanzaki, S. Suzuki, Y. Kobayashi, H. Inokawa, Y. Ono, S. Kar, P. M. Ajayan. Metal-Semiconductor Transition in Single-Walled Carbon Nanotubes Induced by Low-Energy Electron Irradiation. *Nano Lett.*, 5, 1575-1579, 2005.
176. G. Zheng, Q. Li, K. Jiang, X. Zhang, J. Chen, Z. Ren, S. Fan. Transition of Single-Walled Carbon Nanotubes from Metallic to Semiconducting in Field-Effect Transistors by Hydrogen Plasma Treatment. *Nano Lett.*, 7, 1622-1625, 2007.
177. Y. Umeno, T. Kitamura, A. Kushima. Metallic-semiconducting transition of single-walled carbon nanotubes under high axial strain. *Comput. Mater. Sci.*, 31, 33-41, 2004.

178. R. Voggu, S. Pal, S. K. Pati, C. N. R. Rao. Semiconductor to metal transition in SWNTs caused by interaction with gold and platinum nanoparticles. *J. Phys. Condens. Matter*, 20, 215211, 2008.
179. C. N. R. Rao, R. Voggu. Charge-transfer with graphene and nanotubes. *Mater. Today*, 13, 34-40, 2010.
180. R. Tsuchikawa, H.-Y. Ahn, S. Yao, K. D. Belfield, M. Ishigami. Photosensitization of carbon nanotubes using dye aggregates. *J. Phys. Condens. Matter*, 23, 202204, 2011.
181. B. R. Bunes, M. Xu, Y. Zhang, D. E. Gross, A. Saha, D. L. Jacobs, X. Yang, J. S. Moore, L. Zang. Photodoping and Enhanced Visible Light Absorption in Single-Walled Carbon Nanotubes Functionalized with a Wide Band Gap Oligomer. *Adv. Mater.*, 27, 162-167, 2015.
182. F. Cheng, P. Imin, C. Maunders, G. Botton, A. Adronov. Soluble, Discrete Supramolecular Complexes of Single-Walled Carbon Nanotubes with Fluorene-Based Conjugated Polymers. *Macromolecules*, 41, 2304-2308, 2008.
183. R. Yang, Z. Tang, J. Yan, H. Kang, Y. Kim, Z. Zhu, W. Tan. Noncovalent Assembly of Carbon Nanotubes and Single-Stranded DNA: An Effective Sensing Platform for Probing Biomolecular Interactions. *Anal. Chem.*, 80, 7408-7413, 2008.
184. E. Maligaspe, A. S. D. Sandanayaka, T. Hasobe, O. Ito, F. D'Souza. Sensitive Efficiency of Photoinduced Electron Transfer to Band Gaps of Semiconductive Single-Walled Carbon Nanotubes with Supramolecularly Attached Zinc Porphyrin Bearing Pyrene Glues. *J. Am. Chem. Soc.*, 132, 8158-8164, 2010.
185. W. R. Browne, B. L. Feringa. Making molecular machines work. *Nat. Nanotechnol.*, 1, 25-35, 2006.
186. J. F. Stoddart. The chemistry of the mechanical bond. *Chem. Soc. Rev.*, 38, 1802-1820, 2009.
187. A. Coskun, M. Banaszak, R. D. Astumian, J. F. Stoddart, B. A. Grzybowski. Great expectations: can artificial molecular machines deliver on their promise? *Chem. Soc. Rev.*, 41, 19-30, 2012.
188. F. Durola, V. Heitz, F. Reviriego, C. Roche, J.-P. Sauvage, A. Sour, Y. Trolez. Cyclic [4]Rotaxanes Containing Two Parallel Porphyrinic Plates: Toward Switchable Molecular Receptors and Compressors. *Acc. Chem. Res.*, 47, 633-645, 2014.
189. J. Akola, K. Rytönen, M. Manninen. Electronic Properties of Single-Walled Carbon Nanotubes inside Cyclic Supermolecules. *J. Phys. Chem. B*, 110, 5186-5190, 2006.
190. A. de Juan, E. M. Pérez. Getting tubed: mechanical bond in endohedral derivatives of carbon nanotubes? *Nanoscale*, 5, 7141-7148, 2013.

191. A. de Juan, Y. Pouillon, L. Ruiz-González, A. Torres-Pardo, S. Casado, N. Martín, Á. Rubio, E. M. Pérez. Mechanically Interlocked Single-Wall Carbon Nanotubes. *Angew. Chem. Int.*, 53, 5394-5400, 2014.
192. A. López-Moreno, E. M. Pérez. Pyrene-based mechanically interlocked SWNTs. *Chem. Commun.*, 51, 5421-5424, 2015.
193. A. López-Moreno, B. Nieto-Ortega, M. Moffa, A. de Juan, M. M. Bernal, J. P. Fernández-Blázquez, J. J. Vilatela, D. Pisignano, E. M. Pérez. Threading through Macrocycles Enhances the Performance of Carbon Nanotubes as Polymer Fillers. *ACS nano*, 10, 8012-8018, 2016.
194. L. de Juan-Fernández, P. W. Münich, A. Puthiyedath, B. Nieto-Ortega, S. Casado, L. Ruiz-González, E. M. Pérez, D. M. Guldi. Interfacing porphyrins and carbon nanotubes through mechanical links. *Chem. Sci.*, 9, 6779-6784, 2018.
195. Y. Luo, X. Yu. Light and electrically responsive materials based on aligned carbon nanotubes. *Eur. Polym. J.*, 82, 290-299, 2016.
196. H. Jintoku, Y. Matsuzawa, M. Yoshida. Switching the optical and electrical properties of carbon nanotube hybrid films using a photoresponsive dispersant as a dopant. *RSC Adv.*, 8, 11186-11190, 2018.
197. X. Zhang, Z. Yu, C. Wang, D. Zarrouk, J.-W. T. Seo, J. C. Cheng, A. D. Buchan, K. Takei, Y. Zhao, J. W. Ager, J. Zhang, M. Hettick, M. C. Hersam, A. P. Pisano, R. S. Fearing, A. Javey. Photoactuators and motors based on carbon nanotubes with selective chirality distributions. *Nat. Commun.*, 5, 2983, 2014.
198. Z. C. Tu, Z. C. Ou-Yang. A molecular motor constructed from a double-walled carbon nanotube driven by temperature variation. *J. Phys.: Condens. Matter* 16, 1287-1292, 2004.
199. Z. C. Tu, X. Hu. Molecular motor constructed from a double-walled carbon nanotube driven by axially varying voltage. *Phys. Rev. B*, 72, 033404, 2005.
200. S. Grimme. Semiempirical GGA-type density functional constructed with a long-range dispersion correction. *J. Comput. Chem.*, 27, 1787-1799, 2006.
201. S. Grimme, J. Antony, S. Ehrlich, H. Krieg. A consistent and accurate ab initio parametrization of density functional dispersion correction (DFT-D) for the 94 elements H-Pu. *J. Chem. Phys.*, 132, 154104, 2010.
202. J.-D. Chai, M. Head-Gordon. Long-range corrected hybrid density functionals with damped atom-atom dispersion corrections. *Phys. Chem. Chem. Phys.*, 10, 6615-6620, 2008.

203. W. Heisenberg. About quantum theoretical reinterpretation of kinematic and mechanical relations. *Z. Phys.*, 33, 879-893, 1925.
204. E. Schrödinger. An Undulatory Theory of the Mechanics of Atoms and Molecules. *Phys. Rev.*, 28, 1049-1070, 1926.
205. P. A. M. Dirac. On the theory of quantum mechanics. *Proc. R. Soc. Lond. A.*, 112, 661-677, 1926.
206. M. Born, R. Oppenheimer. On the quantum theory of molecules. *Ann. Phys. (Berl.)*, 389, 457-484, 1927.
207. M. A. X. Born. The interpretation of Quantum Mechanics. *Br. J. Philos. Sci.*, IV, 95-106, 1953.
208. H. A. Bethe, R. W. Jackiw, *Intermediate Quantum Mechanics*. Westview Press: Colorado, 1997.
209. A. Szabo, N. S. Ostlund, *Modern Quantum Chemistry : Introduction to Advanced Electronic Structure Theory*. Dover Publications: Mineola, N.Y., 2006.
210. P. W. Atkins, R. Friedman, *Molecular Quantum Mechanics*. Oxford University Press: Oxford; Toronto, 2011.
211. D. R. Hartree. The Wave Mechanics of an Atom with a Non-Coulomb Central Field. Part I. Theory and Methods. *Math. Proc. Camb. Philos. Soc.*, 24, 89-110, 1928.
212. V. Fock. Approximation method for solving the quantum mechanical multibody problem. *Z. Phys.*, 61, 126-148, 1930.
213. C. C. J. Roothaan. New Developments in Molecular Orbital Theory. *Rev. Mod. Phys.*, 23, 69-89, 1951.
214. G. G. Hall. The molecular orbital theory of chemical valency VIII. A method of calculating ionization potentials. *Proc. R. Soc. Lond. A.*, 205, 541-552, 1951.
215. E. Fermi. A statistical method for the determination of some properties of the atom *Rend. Accad. Naz.*, 6, 602-607, 1927.
216. J. C. Slater. A Simplification of the Hartree-Fock Method. *Phys. Rev.*, 81, 385-390, 1951.
217. P. A. M. Dirac. Note on Exchange Phenomena in the Thomas Atom. *Math. Proc. Camb. Philos. Soc.*, 26, 376-385, 2008.
218. P. Hohenberg, W. Kohn. Inhomogeneous Electron Gas. *Phys. Rev.*, 136, B864-B871, 1964.

219. W. Kohn, L. J. Sham. Self-Consistent Equations Including Exchange and Correlation Effects. *Phys. Rev.*, 140, A1133-A1138, 1965.
220. S. H. Vosko, L. Wilk, M. Nusair. Accurate spin-dependent electron liquid correlation energies for local spin density calculations: a critical analysis. *Can. J. Phys.*, 58, 1200-1211, 1980.
221. J. C. Slater, *Quantum Theory of Molecules and Solids. vol. 4.:The Self-Consistent Field for Molecules and Solids*. McGraw-Hill: New York, NY, 1974.
222. A. D. Becke. Density-functional thermochemistry. V. Systematic optimization of exchange-correlation functionals. *J. Chem. Phys.*, 107, 8554-8560, 1997.
223. A. D. Becke. Density-functional exchange-energy approximation with correct asymptotic behavior. *Phys. Rev. A*, 38, 3098-3100, 1988.
224. C. Lee, W. Yang, R. G. Parr. Development of the Colle-Salvetti correlation-energy formula into a functional of the electron density. *Phys. Rev. B*, 37, 785-789, 1988.
225. Y. Zhao, N. E. Schultz, D. G. Truhlar. Exchange-correlation functional with broad accuracy for metallic and nonmetallic compounds, kinetics, and noncovalent interactions. *J. Chem. Phys.*, 123, 161103, 2005.
226. J. Tao, J. P. Perdew, V. N. Staroverov, G. E. Scuseria. Climbing the Density Functional Ladder: Nonempirical Meta-Generalized Gradient Approximation Designed for Molecules and Solids. *Phys. Rev. Lett.*, 91, 146401, 2003.
227. A. D. Becke. Density-functional thermochemistry. III. The role of exact exchange. *J. Chem. Phys.*, 98, 5648-5652, 1993.
228. J.-D. Chai, M. Head-Gordon. Systematic optimization of long-range corrected hybrid density functionals. *J. Chem. Phys.*, 128, 084106, 2008.
229. T. Yanai, D. P. Tew, N. C. Handy. A new hybrid exchange-correlation functional using the Coulomb-attenuating method (CAM-B3LYP). *Chem. Phys. Lett.*, 393, 51-57, 2004.
230. S. Grimme. Semiempirical hybrid density functional with perturbative second-order correlation. *J. Chem. Phys.*, 124, 034108, 2006.
231. T. Schwabe, S. Grimme. Double-hybrid density functionals with long-range dispersion corrections: higher accuracy and extended applicability. *Phys. Chem. Chem. Phys.*, 9, 3397-3406, 2007.
232. L. Goerigk, S. Grimme. A thorough benchmark of density functional methods for general main group thermochemistry, kinetics, and noncovalent interactions. *Phys. Chem. Chem. Phys.*, 13, 6670-6688, 2011.

233. E. Runge, E. K. U. Gross. Density-Functional Theory for Time-Dependent Systems. *Phys. Rev. Lett.*, 52, 997-1000, 1984.
234. S. F. Boys, F. Bernardi. The calculation of small molecular interactions by the differences of separate total energies. Some procedures with reduced errors. *Mol. Phys.*, 19, 553-566, 1970.
235. A. B. Dalton, C. Stephan, J. N. Coleman, B. McCarthy, P. M. Ajayan, S. Lefrant, P. Bernier, W. J. Blau, H. J. Byrne. Selective Interaction of a Semiconjugated Organic Polymer with Single-Wall Nanotubes. *J. Phys. Chem. B*, 104, 10012-10016, 2000.
236. J. Chen, C. P. Collier. Noncovalent Functionalization of Single-Walled Carbon Nanotubes with Water-Soluble Porphyrins. *J. Phys. Chem. B*, 109, 7605-7609, 2005.
237. P. Salice, A. Gambarin, N. Daldosso, F. Mancin, E. Menna. Noncovalent Interaction between Single-Walled Carbon Nanotubes and Pyrene-Functionalized Gold Nanoparticles in Water-Soluble Nanohybrids. *J. Phys. Chem. C*, 118, 27028-27038, 2014.
238. P. Avouris. Molecular Electronics with Carbon Nanotubes. *Acc. Chem. Res.*, 35, 1026-1034, 2002.
239. C. Romero-Nieto, R. García, M. Á. Herranz, C. Ehli, M. Ruppert, A. Hirsch, D. M. Guldi, N. Martín. Tetrathiafulvalene-Based Nanotweezers—Noncovalent Binding of Carbon Nanotubes in Aqueous Media with Charge Transfer Implications. *J. Am. Chem. Soc.*, 134, 9183-9192, 2012.
240. P. J. Boul, D.-G. Cho, G. M. A. Rahman, M. Marquez, Z. Ou, K. M. Kadish, D. M. Guldi, J. L. Sessler. Sapphyrin–Nanotube Assemblies. *J. Am. Chem. Soc.*, 129, 5683-5687, 2007.
241. J. Lohrman, C. Zhang, W. Zhang, S. Ren. Semiconducting carbon nanotube and covalent organic polyhedron–C₆₀ nanohybrids for light harvesting. *Chem. Commun.*, 48, 8377-8379, 2012.
242. Z. Dai, L. Yan, S. M. Alam, J. Feng, P. R. D. Mariathomas, Y. Chen, C. M. Li, Q. Zhang, L.-J. Li, K. H. Lim, M. B. Chan-Park. Selective Small-Diameter Metallic Single-Walled Carbon Nanotube Removal by Mere Standing with Anthraquinone and Application to a Field-Effect Transistor. *J. Phys. Chem. C*, 114, 21035-21041, 2010.
243. R. J. Chen, S. Bangsaruntip, K. A. Drouvalakis, N. W. Kam, M. Shim, Y. Li, W. Kim, P. J. Utz, H. Dai. Noncovalent functionalization of carbon nanotubes for highly specific electronic biosensors. *Proc. Natl. Acad. Sci. U. S. A.*, 100, 4984-4989, 2003.
244. V. A. Karachevtsev, S. G. Stepanian, A. Y. Glamazda, M. V. Karachevtsev, V. V. Eremenko, O. S. Lytvyn, L. Adamowicz. Noncovalent Interaction of Single-Walled

- Carbon Nanotubes with 1-Pyrenebutanoic Acid Succinimide Ester and Glucoseoxidase. *J. Phys. Chem. C*, 115, 21072-21082, 2011.
245. P. Okrasinski, Z. Latajka, C. Hättig. Theoretical Study on Noncovalent Interactions in the Carbon Nanotube–Formic Acid Dimer System. *J. Phys. Chem. C*, 118, 4483-4488, 2014.
246. K. Yuan, Y.-J. Guo, X. Zhao. Nature of Noncovalent Interactions in the [n]Cycloparaphenylene \supset C70 (n = 10, 11, and 12) Host–Guest Complexes: A Theoretical Insight into the Shortest C70–Carbon Nanotube Peapod. *J. Phys. Chem. C*, 119, 5168-5179, 2015.
247. Y. Almadori, L. Alvarez, R. Le Parc, R. Aznar, F. Fossard, A. Loiseau, B. Jousselme, S. Campidelli, P. Hermet, A. Belhboub, A. Rahmani, T. Saito, J. L. Bantignies. Chromophore Ordering by Confinement into Carbon Nanotubes. *J. Phys. Chem. C*, 118, 19462-19468, 2014.
248. T. Yumura, H. Yamashita. Key factors in determining the arrangement of π -conjugated oligomers inside carbon nanotubes. *Phys. Chem. Chem. Phys.*, 17, 22668-22677, 2015.
249. M. Zaboli, H. Raissi. The influence of nicotine on pioglitazone encapsulation into carbon nanotube: the investigation of molecular dynamic and density functional theory. *J. Biomol. Struct. Dyn.*, 35, 520-534, 2017.
250. D. Kazachkin, Y. Nishimura, S. Irlle, K. Morokuma, R. D. Vidic, E. Borguet. Interaction of Acetone with Single Wall Carbon Nanotubes at Cryogenic Temperatures: A Combined Temperature Programmed Desorption and Theoretical Study. *Langmuir*, 24, 7848-7856, 2008.
251. H. Wang, B. Li, J. Yang. Electronic, Optical, and Mechanical Properties of Diamond Nanowires Encapsulated in Carbon Nanotubes: A First-Principles View. *J. Phys. Chem. C* 121, 3661-3672, 2017.
252. C. M. Chang, H. L. Tseng, A. de Leon, A. Posada-Amarillas, A. F. Jalbout. Theoretical Study of Amino Acids Encapsulation in Zigzag Single-Walled Carbon Nanotubes. *Comput. Theor. Nanosci.*, 10, 521-526, 2013.
253. Y. Wang, Z. Xu. Interaction mechanism of doxorubicin and SWCNT: protonation and diameter effects on drug loading and releasing. *RSC Adv.*, 6, 314-322, 2016.
254. S. Cuenot, C. Frétiigny, S. Demoustier-Champagne, B. Nysten. Surface tension effect on the mechanical properties of nanomaterials measured by atomic force microscopy. *Phys. Rev. B*, 69, 165410, 2004.
255. M. V. Veloso, A. G. Souza Filho, J. Mendes Filho, S. B. Fagan, R. Mota. Ab initio study of covalently functionalized carbon nanotubes. *Chem. Phys. Lett.*, 430, 71-74, 2006.

256. T. Kaneko, Y. Li, S. Nishigaki, R. Hatakeyama. Azafullerene Encapsulated Single-Walled Carbon Nanotubes with n-Type Electrical Transport Property. *J. Am. Chem. Soc.*, 130, 2714-2715, 2008.
257. B. B. Doudou, J. Chen, A. Vivet, C. Poilane, M. h. Ayachi. Size-dependent properties of amino-functionalized single walled carbon nanotubes. *Comput. Theor. Chem.*, 967, 231-234, 2011.
258. K. Milowska, M. Birowska, J. A. Majewski. Mechanical and electrical properties of carbon nanotubes and graphene layers functionalized with amines. *Diam. Relat. Mater.*, 23, 167-171, 2012.
259. G. García, I. Ciofini, M. Fernández-Gómez, C. Adamo. Confinement Effects on UV-Visible Absorption Spectra: β -Carotene Inside Carbon Nanotube as a Test Case. *J. Phys. Chem. Lett.*, 4, 1239-1243, 2013.
260. K. Z. Milowska, J. A. Majewski. Functionalization of carbon nanotubes with $-CH_n$, $-NH_n$ fragments, $-COOH$ and $-OH$ groups. *J. Chem. Phys.*, 138, 194704, 2013.
261. B. Nieto-Ortega, J. Villalva, M. Vera-Hidalgo, L. Ruiz-González, E. Burzurí, E. M. Pérez. Band-Gap Opening in Metallic Single-Walled Carbon Nanotubes by Encapsulation of an Organic Salt. *Angew. Chem. Int. Ed.*, 56, 12240-12244, 2017.
262. H. Kuzmany, A. Kukovecz, F. Simon, M. Holzweber, C. Kramberger, T. Pichler. Functionalization of carbon nanotubes. *Synth. Met.*, 141, 113-122, 2004.
263. H. A. Alturaif, Z. A. ALOthman, J. G. Shapter, S. M. Wabaidur. Use of Carbon Nanotubes (CNTs) with Polymers in Solar Cells. *Molecules*, 19, 17329-17344, 2014.
264. G. U. Sumanasekera, B. K. Pradhan, H. E. Romero, K. W. Adu, P. C. Eklund. Giant Thermopower Effects from Molecular Physisorption on Carbon Nanotubes. *Phys. Rev. Lett.*, 89, 166801, 2002.
265. S. Manzetti. Molecular and crystal assembly inside the carbon nanotube: encapsulation and manufacturing approaches. *Adv. Manuf.*, 1, 198-210, 2013.
266. A. Khorsand, S. Jamehbozorgi, R. Ghiasi, M. Rezvani. Structural, energetic and electrical properties of encapsulation of penicillamine drug into the CNTs based on vdW-DF perspective. *Physica E Low Dimens. Syst. Nanostruct.*, 72, 120-127, 2015.
267. L. Debbichi, Y. J. Dappe, M. Alouani. Effect of van der Waals interaction on energetics and transport properties of a single anthracene molecule adsorbed or confined inside a carbon nanotube. *Phys. Rev. B*, 85, 045437, 2012.
268. M. Shiraishi, S. Nakamura, T. Fukao, T. Takenobu, H. Kataura, Y. Iwasa. Control of injected carriers in tetracyano-p-quinodimethane encapsulated carbon nanotube transistors. *Appl. Phys. Lett.*, 87, 093107, 2005.

269. J. Lee, W. Lee, K. Sim, S.-h. Han, W. Yi. Field emission properties of single-walled carbon nanotube with amphoteric doping by encapsulation of TTF and TCNQ. *J. Vac. Sci. Technol., B: Microelectron. Nanometer Struct.–Process., Meas., Phenom.*, 26, 847-850, 2008.
270. K. Yanagi, K. Iakoubovskii, H. Matsui, H. Matsuzaki, H. Okamoto, Y. Miyata, Y. Maniwa, S. Kazaoui, N. Minami, H. Kataura. Photosensitive Function of Encapsulated Dye in Carbon Nanotubes. *J. Am. Chem. Soc.*, 129, 4992-4997, 2007.
271. A. I. Chernov, P. V. Fedotov, A. V. Talyzin, I. Suarez Lopez, I. V. Anoshkin, A. G. Nasibulin, E. I. Kauppinen, E. D. Obraztsova. Optical Properties of Graphene Nanoribbons Encapsulated in Single-Walled Carbon Nanotubes. *ACS Nano*, 7, 6346-6353, 2013.
272. S. Cambré, J. Campo, C. Beirnaert, C. Verlackt, P. Cool, W. Wenseleers. Asymmetric dyes align inside carbon nanotubes to yield a large nonlinear optical response. *Nat. Nanotechnol.*, 10, 248, 2015.
273. J. Campo, Y. Piao, S. Lam, C. M. Stafford, J. K. Streit, J. R. Simpson, A. R. Hight Walker, J. A. Fagan. Enhancing single-wall carbon nanotube properties through controlled endohedral filling. *Nanoscale Horiz.*, 1, 317-324, 2016.
274. R. G. A. Veiga, R. H. Miwa. Ab initio study of TCNQ-doped carbon nanotubes. *Phys. Rev. B*, 73, 245422, 2006.
275. F. Caruso, V. Atalla, X. Ren, A. Rubio, M. Scheffler, P. Rinke. First-principles description of charge transfer in donor-acceptor compounds from self-consistent many-body perturbation theory. *Phys. Rev. B*, 90, 085141, 2014.
276. J. Lu, S. Nagase, D. Yu, H. Ye, R. Han, Z. Gao, S. Zhang, L. Peng. Amphoteric and controllable doping of carbon nanotubes by encapsulation of organic and organometallic molecules. *Phys. Rev. Lett.*, 93, 116804, 2004.
277. E. D. Głowacki, G. Voss, L. Leonat, M. Irimia-Vladu, S. Bauer, N. S. Sariciftci. Indigo and Tyrian Purple – From Ancient Natural Dyes to Modern Organic Semiconductors. *Isr. J. Chem.*, 52, 540-551, 2012.
278. N. A. Poklonski, E. F. Kislyakov, N. N. Hieu, O. N. Bubel', S. A. Vyrko, A. M. Popov, Y. E. Lozovik. Uniaxially deformed (5,5) carbon nanotube: Structural transitions. *Chem. Phys. Lett.*, 464, 187-191, 2008.
279. T. Hasan, V. Scardaci, P. Tan, A. G. Rozhin, W. I. Milne, A. C. Ferrari. Stabilization and “Debundling” of Single-Wall Carbon Nanotube Dispersions in N-Methyl-2-pyrrolidone (NMP) by Polyvinylpyrrolidone (PVP). *J. Phys. Chem. C*, 111, 12594-12602, 2007.

280. C. Kördel, A. Setaro, P. Bluemmel, C. S. Popeney, S. Reich, R. Haag. Controlled reversible debundling of single-walled carbon nanotubes by photo-switchable dendritic surfactants. *Nanoscale*, 4, 3029-3031, 2012.
281. H. Yamashita, T. Yumura. The Role of Weak Bonding in Determining the Structure of Thiophene Oligomers inside Carbon Nanotubes. *J. Phys. Chem. C*, 116, 9681-9690, 2012.
282. S. Karthikeyan, V. Ramanathan, B. K. Mishra. Influence of the Substituents on the CH... π Interaction: Benzene–Methane Complex. *J. Phys. Chem. A*, 117, 6687-6694, 2013.
283. B. K. Mishra, R. Venkatnarayan. Substituents' influence on the C–H... π interaction in the T-shaped benzene dimer. *Theor. Chem. Acc.*, 137, 72, 2018.
284. B. J. Ransil. Studies in Molecular Structure. IV. Potential Curve for the Interaction of Two Helium Atoms in Single-Configuration LCAO MO SCF Approximation. *J. Chem. Phys.*, 34, 2109-2118, 1961.
285. M. Bixon, J. Jortner. Charge Transport in DNA Via Thermally Induced Hopping. *J. Am. Chem. Soc.*, 123, 12556-12567, 2001.
286. H. Liu, S. Kang, J. Y. Lee. Electronic Structures and Charge Transport of Stacked Annelated β -Trithiophenes. *J. Phys. Chem. B*, 115, 5113-5120, 2011.
287. M. J. Frisch, G. W. Trucks, H. B. Schlegel, G. E. Scuseria, M. A. Robb, J. R. Cheeseman, G. Scalmani, V. Barone, B. Mennucci, G. A. Petersson, H. Nakatsuji, M. Caricato, X. Li, H. P. Hratchian, A. F. Izmaylov, J. Bloino, G. Zheng, J. L. Sonnenberg, M. Hada, M. Ehara, K. Toyota, R. Fukuda, J. Hasegawa, M. Ishida, T. Nakajima, Y. Honda, O. Kitao, H. Nakai, T. Vreven, J. A. Montgomery, Jr., J. E. Peralta, F. Ogliaro, M. Bearpark, J. J. Heyd, E. Brothers, K. N. Kudin, V. N. Staroverov, T. Keith, R. Kobayashi, J. Normand, K. Raghavachari, A. Rendell, J. C. Burant, S. S. Iyengar, J. Tomasi, M. Cossi, N. Rega, J. M. Millam, M. Klene, J. E. Knox, J. B. Cross, V. Bakken, C. Adamo, J. Jaramillo, R. Gomperts, R. E. Stratmann, O. Yazyev, A. J. Austin, R. Cammi, C. Pomelli, J. W. Ochterski, R. L. Martin, K. Morokuma, V. G. Zakrzewski, G. A. Voth, P. Salvador, J. J. Dannenberg, S. Dapprich, A. D. Daniels, O. Farkas, J. B. Foresman, J. V. Ortiz, J. Cioslowski, D. J. Fox. *Gaussian 09, Revision D.01*, Gaussian, Inc., Wallingford CT, 2013.
288. D. Roy, K. Todd, M. John. Gauss View; Version 5; Semichem. *Semichem. Inc.: Shawnee Mission, KS, USA*, 2009.
289. P. Rademacher, K. Kowski. Photoelectron Spectrum and Electronic Structure of Indigo. *Chem. Ber.*, 125, 1773-1775, 1992.
290. A. Taherpour, A. Aghagolnezhad-Gerdroudbari, S. Rafiei. Theoretical and Quantitative Structural Relationship Studies of Reorganization Energies of [SWCNT(5,5)-Armchair-C_nH₂₀] (n=20-310) Nanostructures by Neural Network CFFBP Method. *Int. J. Electrochem. Sci.*, 7, 2468-2486, 2012.

291. Y. Li, D. Lu, K. Schulten, U. Ravaioli, S. V. Rotkin. Screening of Water Dipoles Inside Finite-Length Armchair Carbon Nanotubes. *J. Comput. Electron.*, 4, 161-165, 2005.
292. D. D. Tune, J. G. Shapter. The potential sunlight harvesting efficiency of carbon nanotube solar cells. *Energy Environ. Sci.*, 6, 2572-2577, 2013.
293. M. Kawahito, R. Yasukawa. Characteristics of Color Produced by Awa Natural Indigo and Synthetic Indigo. *Materials*, 2, 661-673, 2009.
294. A. V. Naumov, S. Ghosh, D. A. Tsyboulski, S. M. Bachilo, R. B. Weisman. Analyzing Absorption Backgrounds in Single-Walled Carbon Nanotube Spectra. *ACS Nano*, 5, 1639-1648, 2011.
295. J. Seixas de Melo, A. P. Moura, M. J. Melo. Photophysical and Spectroscopic Studies of Indigo Derivatives in Their Keto and Leuco Forms. *J. Phys. Chem. A*, 108, 6975-6981, 2004.
296. W. Wu, Y. Yang, Q. Yuan, D. Sun. The collapse of an elastic tube induced by encapsulated liquid droplets. *Soft Matter*, 9, 9774-9779, 2013.
297. A. Joshi, C. N. Ramachandran. Charge transport and optical properties of the complexes of indigo wrapped over carbon nanotubes. *Phys. Chem. Chem. Phys.*, 18, 14040-14045, 2016.
298. B. Jeziorski, R. Moszynski, K. Szalewicz. Perturbation Theory Approach to Intermolecular Potential Energy Surfaces of van der Waals Complexes. *Chem. Rev.*, 94, 1887-1930, 1994.
299. W. Wang, Y. Zhang, Y.-B. Wang. Noncovalent $\pi\cdots\pi$ interaction between graphene and aromatic molecule: Structure, energy, and nature. *J. Chem. Phys.*, 140, 094302, 2014.
300. S. M. Ryno, C. Risko, J.-L. Brédas. Noncovalent Interactions and Impact of Charge Penetration Effects in Linear Oligoacene Dimers and Single Crystals. *Chem. Mater.*, 28, 3990-4000, 2016.
301. M.-M. Li, Y.-B. Wang, Y. Zhang, W. Wang. The Nature of the Noncovalent Interactions between Benzene and C60 Fullerene. *J. Phys. Chem. A*, 120, 5766-5772, 2016.
302. W. Sun, Y. Bu, Y. Wang, Distinct Diameter Dependence of Redox Property for Armchair, Zigzag Single-walled, and Double-walled Carbon Nanotubes. In *Design and Applications of Nanomaterials for Sensors*, Seminario, J. M., Ed. Springer Netherlands: Dordrecht, 2014; pp 31-60.
303. C. Luo, A. K. K. Kyaw, L. A. Perez, S. Patel, M. Wang, B. Grimm, G. C. Bazan, E. J. Kramer, A. J. Heeger. General Strategy for Self-Assembly of Highly Oriented Nanocrystalline Semiconducting Polymers with High Mobility. *Nano Lett.*, 14, 2764-2771, 2014.

304. J. Liu, H. Zhang, H. Dong, L. Meng, L. Jiang, L. Jiang, Y. Wang, J. Yu, Y. Sun, W. Hu, A. J. Heeger. High mobility emissive organic semiconductor. *Nat. Commun.*, 6, 10032, 2015.
305. R. A. Marcus. On the Theory of Electron-Transfer Reactions. VI. Unified Treatment for Homogeneous and Electrode Reactions. *J. Chem. Phys.*, 43, 679-701, 1965.
306. K. F. Freed, J. Jortner. Multiphonon Processes in the Nonradiative Decay of Large Molecules. *J. Chem. Phys.*, 52, 6272-6291, 1970.
307. R. A. Marcus. Electron transfer reactions in chemistry. Theory and experiment. *Rev. Mod. Phys.*, 65, 599-610, 1993.
308. P. F. Barbara, T. J. Meyer, M. A. Ratner. Contemporary Issues in Electron Transfer Research. *J. Phys. Chem.*, 100, 13148-13168, 1996.
309. M. Irimia-Vladu, E. D. Głowacki, P. A. Troshin, G. Schwabegger, L. Leonat, D. K. Susarova, O. Krystal, M. Ullah, Y. Kanbur, M. A. Bodea, V. F. Razumov, H. Sitter, S. Bauer, N. S. Sariciftci. Indigo - A Natural Pigment for High Performance Ambipolar Organic Field Effect Transistors and Circuits. *Adv. Mater.*, 24, 375-380, 2012.
310. Y. Nonoguchi, K. Ohashi, R. Kanazawa, K. Ashiba, K. Hata, T. Nakagawa, C. Adachi, T. Tanase, T. Kawai. Systematic Conversion of Single Walled Carbon Nanotubes into n-type Thermoelectric Materials by Molecular Dopants. *Sci. Rep.*, 3, 3344, 2013.
311. J. E. Anthony, A. Facchetti, M. Heeney, S. R. Marder, X. Zhan. n-Type Organic Semiconductors in Organic Electronics. *Adv. Mater.*, 22, 3876-3892, 2010.
312. J.-M. Kim, S.-J. Yoo, C.-K. Moon, B. Sim, J.-H. Lee, H. Lim, J. W. Kim, J.-J. Kim. N-Type Molecular Doping in Organic Semiconductors: Formation and Dissociation Efficiencies of a Charge Transfer Complex. *J. Phys. Chem. C* 120, 9475-9481, 2016.
313. G. Qian, Z. Y. Wang. Near-Infrared Organic Compounds and Emerging Applications. *Chem. Asian J.*, 5, 1006-1029, 2010.
314. W. Ghann, H. Kang, T. Sheikh, S. Yadav, T. Chavez-Gil, F. Nesbitt, J. Uddin. Fabrication, Optimization and Characterization of Natural Dye Sensitized Solar Cell. *Sci. Rep.*, 7, 41470, 2017.
315. D. J. Bindl, A. J. Ferguson, M.-Y. Wu, N. Kopidakis, J. L. Blackburn, M. S. Arnold. Free Carrier Generation and Recombination in Polymer-Wrapped Semiconducting Carbon Nanotube Films and Heterojunctions. *J. Phys. Chem. Lett.*, 4, 3550-3559, 2013.
316. W. Orellana, S. O. Vásquez. Endohedral terthiophene in zigzag carbon nanotubes: Density functional calculations. *Phys. Rev. B*, 74, 125419, 2006.

317. G. Ning, N. Kishi, H. Okimoto, M. Shiraishi, T. Sugai, H. Shinohara. Structural Stability and Transformation of Aligned C60 and C70 Fullerenes in Double-Wall and Triple-Wall Carbon Nanotube-Peapods. *J. Phys. Chem. C*, 111, 14652-14657, 2007.
318. Z. Zhang, C. H. Turner. Structural and Electronic Properties of Carbon Nanotubes and Graphenes Functionalized with Cyclopentadienyl–Transition Metal Complexes: A DFT Study. *J. Phys. Chem. C*, 117, 8758-8766, 2013.
319. K. Miyaura, Y. Miyata, B. Thendie, K. Yanagi, R. Kitaura, Y. Yamamoto, S. Arai, H. Kataura, H. Shinohara. Extended-conjugation π -electron systems in carbon nanotubes. *Sci. Rep.*, 8, 8098, 2018.
320. A. Joshi, C. N. Ramachandran. Structural, optoelectronic and charge transport properties of the complexes of indigo encapsulated in carbon nanotubes. *Phys. Chem. Chem. Phys.*, 20, 15158-15167, 2018.
321. H. S. Kang, T. J. Sisto, S. Peurifoy, D. H. Arias, B. Zhang, C. Nuckolls, J. L. Blackburn. Long-Lived Charge Separation at Heterojunctions between Semiconducting Single-Walled Carbon Nanotubes and Perylene Diimide Electron Acceptors. *J. Phys. Chem. C*, 122, 14150-14161, 2018.
322. A. Joshi, C. N. Ramachandran. Optoelectronic Properties of Cycloparaphenylene–Carbon Nanotube Based Molecular Architectures. *J. Phys. Chem. C*, 122, 19904-19912, 2018.
323. C. Ehli, C. Oelsner, D. M. Guldi, A. Mateo-Alonso, M. Prato, C. Schmidt, C. Backes, F. Hauke, A. Hirsch. Manipulating single-wall carbon nanotubes by chemical doping and charge transfer with perylene dyes. *Nat. Chem.*, 1, 243, 2009.
324. C. Backes, C. D. Schmidt, K. Rosenlehner, F. Hauke, J. N. Coleman, A. Hirsch. Nanotube Surfactant Design: The Versatility of Water-Soluble Perylene Bisimides. *Adv. Mater.*, 22, 788-802, 2010.
325. C. Backes, C. D. Schmidt, F. Hauke, A. Hirsch. Perylene-Based Nanotweezers: Enrichment of Larger-Diameter Single-Walled Carbon Nanotubes. *Chem. Asian. J.*, 6, 438-444, 2011.
326. C. Backes, F. Hauke, A. Hirsch. The Potential of Perylene Bisimide Derivatives for the Solubilization of Carbon Nanotubes and Graphene. *Adv. Mater.*, 23, 2588-2601, 2011.
327. F. Ernst, T. Heek, A. Setaro, R. Haag, S. Reich. Energy Transfer in Nanotube-Perylene Complexes. *Adv. Funct. Mater.*, 22, 3921-3926, 2012.
328. R. F. Araújo, C. J. R. Silva, M. C. Paiva, M. M. Franco, M. F. Proença. Efficient dispersion of multi-walled carbon nanotubes in aqueous solution by non-covalent interaction with perylene bisimides. *RSC Adv.*, 3, 24535-24542, 2013.

329. Y. Tsarfati, V. Strauss, S. Kuhri, E. Krieg, H. Weissman, E. Shimoni, J. Baram, D. M. Guldi, B. Rytchinski. Dispersing Perylene Diimide/SWCNT Hybrids: Structural Insights at the Molecular Level and Fabricating Advanced Materials. *J. Am. Chem. Soc.*, 137, 7429-7440, 2015.
330. L. Hu, Y.-L. Zhao, K. Ryu, C. Zhou, J. F. Stoddart, G. Grüner. Light-Induced Charge Transfer in Pyrene/CdSe-SWNT Hybrids. *Adv. Mater.*, 20, 939-946, 2008.
331. C. Roquelet, B. Langlois, F. Violla, D. Garrot, J. S. Lauret, C. Voisin. Light harvesting with non covalent carbon nanotube/porphyrin compounds. *Chem. Phys.*, 413, 45-54, 2013.
332. D. R. Kauffman, A. Star. Electronically monitoring biological interactions with carbon nanotube field-effect transistors. *Chem. Soc. Rev.*, 37, 1197-1206, 2008.
333. T. Ketolainen, V. Havu, E. Ö. Jónsson, M. J. Puska. Electronic Transport Properties of Carbon-Nanotube Networks: The Effect of Nitrate Doping on Intratube and Intertube Conductances. *Phys. Rev. Applied* 9,034010, 2018.
334. R. B. Koizhaiganova, D. H. Hwang, C. J. Lee, S. Roth, U. Dettlaff-Weglikowska. N-type doping effect of single-walled carbon nanotubes with aromatic amines. *Phys. Status Solidi B*, 247, 2793-2796, 2010.
335. L. Brownlie, J. Shapter. Advances in carbon nanotube n-type doping: Methods, analysis and applications. *Carbon*, 126, 257-270, 2018.
336. A. Troeger, M. Ledendecker, J. T. Margraf, V. Sgobba, D. M. Guldi, B. F. Vieweg, E. Spiecker, S.-L. Suraru, F. Würthner. p-Doped Multiwall Carbon Nanotube/Perylene Diimide Derivative Photoelectrochemical Cells for Photocurrent Generation. *Adv. Energy Mater.*, 2, 536-540, 2012.
337. Y. Sun, W. Fu, Z. Li, Z. Wang. Tailorable Aqueous Dispersion of Single-Walled Carbon Nanotubes Using Tetrachloroperylene-Based Bolaamphiphiles via Noncovalent Modification. *Langmuir*, 30, 8615-8620, 2014.
338. S. Rajaram, R. Shivanna, S. K. Kandappa, K. S. Narayan. Nonplanar Perylene Diimides as Potential Alternatives to Fullerenes in Organic Solar Cells. *J. Phys. Chem. Lett.*, 3, 2405-2408, 2012.
339. C. B. Nielsen, S. Holliday, H.-Y. Chen, S. J. Cryer, I. McCulloch. Non-Fullerene Electron Acceptors for Use in Organic Solar Cells. *Acc. Chem. Res.*, 48, 2803-2812, 2015.
340. E. Erdoğan, B. Gündüz. Controlling of the optical properties of the solutions of the PTCDI-C8 organic semiconductor. *Electron. Mater. Lett.*, 12, 773-778, 2016.
341. M. C. R. Delgado, E.-G. Kim, D. A. d. S. Filho, J.-L. Bredas. Tuning the Charge-Transport Parameters of Perylene Diimide Single Crystals via End and/or Core

- Functionalization: A Density Functional Theory Investigation. *J. Am. Chem. Soc.*, 132, 3375-3387, 2010.
342. J. M. Turney, A. C. Simmonett, R. M. Parrish, E. G. Hohenstein, F. A. Evangelista, J. T. Fermann, B. J. Mintz, L. A. Burns, J. J. Wilke, M. L. Abrams, N. J. Russ, M. L. Leininger, C. L. Janssen, E. T. Seidl, W. D. Allen, H. F. Schaefer, R. A. King, E. F. Valeev, C. D. Sherrill, T. D. Crawford. Psi4: an open-source ab initio electronic structure program. *Wiley Interdisciplinary Reviews: Computational Molecular Science*, 2, 556-565, 2012.
343. V. Balzani, A. Juris, M. Venturi, S. Campagna, S. Serroni. Luminescent and Redox-Active Polynuclear Transition Metal Complexes. *Chem. Rev.*, 96, 759-834, 1996.
344. S. Goyal, A. Chattopadhyay, K. Kasavajhala, U. D. Priyakumar. Role of Urea–Aromatic Stacking Interactions in Stabilizing the Aromatic Residues of the Protein in Urea-Induced Denatured State. *J. Am. Chem. Soc.*, 139, 14931-14946, 2017.
345. T. Jaganade, A. Chattopadhyay, N. M. Pazhayam, U. D. Priyakumar. Energetic, Structural and Dynamic Properties of Nucleobase-Urea Interactions that Aid in Urea Assisted RNA Unfolding. *Sci. Rep.*, 9, 8805, 2019.
346. C. Brückner, C. Walter, B. Engels. Theoretical investigation of the interactions between the π -systems of molecular organic semiconductors and an analysis of the contributions of repulsion and electrostatics. *Int. J. Quantum Chem.*, 116, 1138-1152, 2016.
347. N. Alodia, T. Jaganade, U. D. Priyakumar. Quantum mechanical investigation of the nature of nucleobase-urea stacking interaction, a crucial driving force in RNA unfolding in aqueous urea. *J. Chem. Sci.*, 130, 158, 2018.
348. C. Zhang, T. Liu, W. Zeng, D. Xie, Z. Luo, Y. Sun, C. Yang. Thienobenzene-fused perylene bisimide as a non-fullerene acceptor for organic solar cells with a high open-circuit voltage and power conversion efficiency. *Mater. Chem. Front.*, 1, 749-756, 2017.
349. J. Calbo, A. Doncel-Giménez, J. Aragón, E. Ortí. Tuning the optical and electronic properties of perylene diimides through transversal core extension. *Theor. Chem. Acc.*, 137, 27, 2018.
350. M. Oltean, A. Calborean, G. Mile, M. Vidrighin, M. Iosin, L. Leopold, D. Maniu, N. Leopold, V. Chiş. Absorption spectra of PTCDI: A combined UV–Vis and TD-DFT study. *Spectrochim. Acta A*, 97, 703-710, 2012.
351. G. Gao, N. Liang, H. Geng, W. Jiang, H. Fu, J. Feng, J. Hou, X. Feng, Z. Wang. Spiro-Fused Perylene Diimide Arrays. *J. Am. Chem. Soc.*, 139, 15914-15920, 2017.
352. D. Casanova. Theoretical investigations of the perylene electronic structure: Monomer, dimers, and excimers. *Int. J. Quantum Chem.*, 115, 442-452, 2015.

353. C. Walter, V. Krämer, B. Engels. On the applicability of time-dependent density functional theory (TDDFT) and semiempirical methods to the computation of excited-state potential energy surfaces of perylene-based dye-aggregates. *Int. J. Quantum Chem.*, 117, e25337, 2017.
354. U. Salzner, A. Aydin. Improved Prediction of Properties of π -Conjugated Oligomers with Range-Separated Hybrid Density Functionals. *J. Chem. Theory Comput.*, 7, 2568-2583, 2011.
355. O. E. Kvyatkovskii, E. G. Donenko, I. B. Zakharova. Electronic Structure and Optical Properties of Charge-transfer Fullerene-porphyrin Complexes: ab initio Calculations. *Fuller. Nanotub. Car. N.*, 16, 530-533, 2008.
356. A. A. Kocherzhenko, X. A. Sosa Vazquez, J. M. Milanese, C. M. Isborn. Absorption Spectra for Disordered Aggregates of Chromophores Using the Exciton Model. *J. Chem. Theory Comput.*, 13, 3787-3801, 2017.
357. F. Baert, C. Cabanetos, A. Leliège, E. Kirchner, O. Segut, O. Alévêque, M. Allain, G. Seo, S. Jung, D. Tondelier, B. Geffroy, J. Roncali, P. Leriche, P. Blanchard. A bridged low band gap A–D–A quaterthiophene as efficient donor for organic solar cells. *J. Mater. Chem. C*, 3, 390-398, 2015.
358. B. M. Squeo, V. G. Gregoriou, Y. Han, A. Palma-Cando, S. Allard, E. Serpetzoglou, I. Konidakis, E. Stratakis, A. Avgeropoulos, T. D. Anthopoulos, M. Heeney, U. Scherf, C. L. Chochos. α,β -Unsubstituted meso-positioning thienyl BODIPY: a promising electron deficient building block for the development of near infrared (NIR) p-type donor–acceptor (D–A) conjugated polymers. *J. Mater. Chem. C*, 6, 4030-4040, 2018.
359. R. Sato, T. Kawamoto, T. Mori. Asymmetrical hole/electron transport in donor–acceptor mixed-stack cocrystals. *J. Mater. Chem. C*, 7, 567-577, 2019.
360. F. Garnier, R. Hajlaoui, A. El Kassmi, G. Horowitz, L. Laigre, W. Porzio, M. Armanini, F. Provasoli. Dihexylquaterthiophene, A Two-Dimensional Liquid Crystal-like Organic Semiconductor with High Transport Properties. *Chem. Mater.*, 10, 3334-3339, 1998.
361. F. Zhang, D. Wu, Y. Xu, X. Feng. Thiophene-based conjugated oligomers for organic solar cells. *J. Mater. Chem.*, 21, 17590-17600, 2011.
362. G. Barbarella, M. Melucci, G. Sotgiu. The Versatile Thiophene: An Overview of Recent Research on Thiophene-Based Materials. *Adv. Mater.*, 17, 1581-1593, 2005.
363. P. M. Beaujuge, J. M. J. Fréchet. Molecular Design and Ordering Effects in π -Functional Materials for Transistor and Solar Cell Applications. *J. Am. Chem. Soc.*, 133, 20009-20029, 2011.
364. H. Bedis, F. Kouki, H. Bouchriha. Effect of the oligothiophene chain length on the performance of organic photovoltaic cells. *Appl. Phys. A*, 110, 163-171, 2013.

365. T. Siegrist, C. Kloc, R. A. Laudise, H. E. Katz, R. C. Haddon. Crystal Growth, Structure, and Electronic Band Structure of α -4T Polymorphs. *Adv. Mater.*, 10, 379-382, 1998.
366. J. Gao, J. D. Roehling, Y. Li, H. Guo, A. J. Moulé, J. K. Grey. The effect of 2,3,5,6-tetrafluoro-7,7,8,8-tetracyanoquinodimethane charge transfer dopants on the conformation and aggregation of poly(3-hexylthiophene). *J. Mater. Chem. C*, 1, 5638-5646, 2013.
367. R. P. Ortiz, A. Facchetti, T. J. Marks, J. Casado, M. Z. Zgierski, M. Kozaki, V. Hernández, J. T. L. Navarrete. Ambipolar Organic Field-Effect Transistors from Cross-Conjugated Aromatic Quaterthiophenes; Comparisons with Quinoidal Parent Materials. *Adv. Funct. Mater.*, 19, 386-394, 2009.
368. R. S. Becker, J. Seixas de Melo, A. L. Maçanita, F. Elisei. Comprehensive Evaluation of the Absorption, Photophysical, Energy Transfer, Structural, and Theoretical Properties of α -Oligothiophenes with One to Seven Rings. *J. Phys. Chem.*, 100, 18683-18695, 1996.
369. S. Fomine, P. Guadarrama. Oligothiophene catenanes and knots: a theoretical study. *J. Phys. Chem. A*, 110, 10098-105, 2006.
370. J. Boixel, E. Blart, Y. Pellegrin, F. Odobel, N. Perin, C. Chiorboli, S. Fracasso, M. Ravaglia, F. Scandola. Hole-Transfer Dyads and Triads Based on Perylene Monoimide, Quaterthiophene, and Extended Tetrathiafulvalene. *Chem. Eur. J.*, 16, 9140-9153, 2010.
371. M. Aschi, A. Amadei, A. Pellegrino, N. Perin, R. Po'. Thermal and environmental effects on Oligothiophene low-energy singlet electronic excitations in dilute solution: a theoretical and experimental study. *Theor. Chem. Acc.*, 131, 1177, 2012.
372. P. Kamedulski, A. Kaczmarek-Kedziera, J. P. Lukaszewicz. Influence of intermolecular interactions on the properties of carbon nanotubes. *Bull. Mater. Sci.*, 41, 76, 2018.
373. A. Belhboub, P. Hermet, L. Alvarez, R. Le Parc, S. Rols, A. C. Lopes Selvati, B. Jousseme, Y. Sato, K. Suenaga, A. Rahmani, J. L. Bantignies. Enhancing the Infrared Response of Carbon Nanotubes From Oligo-Quaterthiophene Interactions. *J. Phys. Chem. C*, 120, 28802-28807, 2016.
374. J. Gao, P. Blondeau, P. Salice, E. Menna, B. Bártová, C. Hébert, J. Leschner, U. Kaiser, M. Milko, C. Ambrosch-Draxl, M. A. Loi. Electronic Interactions between "Pea" and "Pod": The Case of Oligothiophenes Encapsulated in Carbon Nanotubes. *Small*, 7, 1807-1815, 2011.
375. L. Picard, F. Lincker, Y. Kervella, M. Zagorska, R. DeBettignies, A. Peigney, E. Flahaut, G. Louarn, S. Lefrant, R. Demadrille, A. Pron. Composites of Double-Walled Carbon Nanotubes with bis-Quaterthiophene-Fluorenone Conjugated Oligomer: Spectroelectrochemical and Photovoltaic Properties. *J. Phys. Chem. C*, 113, 17347-17354, 2009.

376. T. Yumura, H. Yamashita. Modulating the Electronic Properties of Multimeric Thiophene Oligomers by Utilizing Carbon Nanotube Confinement. *J. Phys. Chem. C*, 118, 5510-5522, 2014.
377. K. Szalewicz, K. Patkowski, B. Jeziorski, Intermolecular Interactions via Perturbation Theory: From Diatoms to Biomolecules. In *Intermolecular Forces and Clusters II*, Wales, D. J., Ed. Springer Berlin Heidelberg: Berlin, Heidelberg, 2005; pp 43-117.
378. R. M. Parrish, L. A. Burns, D. G. A. Smith, A. C. Simmonett, A. E. DePrince, E. G. Hohenstein, U. Bozkaya, A. Y. Sokolov, R. Di Remigio, R. M. Richard, J. F. Gonthier, A. M. James, H. R. McAlexander, A. Kumar, M. Saitow, X. Wang, B. P. Pritchard, P. Verma, H. F. Schaefer, K. Patkowski, R. A. King, E. F. Valeev, F. A. Evangelista, J. M. Turney, T. D. Crawford, C. D. Sherrill. Psi4 1.1: An Open-Source Electronic Structure Program Emphasizing Automation, Advanced Libraries, and Interoperability. *J. Chem. Theory Comput.*, 13, 3185-3197, 2017.
379. D. Chakraborty, S. Pan, P. K. Chattaraj. Encapsulation of small gas molecules and rare gas atoms inside the octa acid cavitand. *Theor. Chem. Acc.*, 135, 119, 2016.
380. S. Pan, G. Jana, A. Gupta, G. Merino, P. K. Chattaraj. Endohedral gas adsorption by cucurbit[7]uril: a theoretical study. *Phys. Chem. Chem. Phys.*, 19, 24448-24452, 2017.
381. M. Elango, R. Parthasarathi, V. Subramanian, P. K. Chattaraj. Chemical reactivity patterns of [n]paracyclophanes. *J. Mol. Struct.*, 820, 1-6, 2007.
382. R. Li, P. Bäuerle, E. Umbach. Vibrational and geometric structure of quaterthiophene on Ag(111). *Surface Science*, 331-333, 100-104, 1995.
383. R. M. Kumar, M. Elango, R. Parthasarathi, D. Vijay, V. Subramanian. The role of C–H... π interaction in the stabilization of benzene and adamantane clusters#. *J. Chem. Sci.*, 124, 193-202, 2012.
384. A. L. Ringer, A. Senenko, C. D. Sherrill. Models of S/ π interactions in protein structures: comparison of the H₂S benzene complex with PDB data. *Protein Sci.*, 16, 2216-2223, 2007.
385. S. M. Bouzzine, S. Bouzakraoui, M. Bouachrine, M. Hamidi. Density functional theory (B3LYP/6-31G*) study of oligothiophenes in their aromatic and polaronic states. *J. Mol. Struc-Theochem.*, 726, 271-276, 2005.
386. B. Dede, D. Avci, D. Varkal, S. Bahçeli. Molecular, Spectroscopic, NBO and NLO Properties of 4-Methyl-5-thiazoleethanol: A Comparative Theoretical Study. *Acta Phys. Pol. A*, 134, 1083-1092, 2018.
387. S. A. Ayoub, J. B. Lagowski. Assessment of the performance of four dispersion-corrected DFT methods using optoelectronic properties and binding energies of organic monomer/fullerene pairs. *Comput. Theor. Chem.*, 1139, 15-26, 2018.

388. Z. Rostami, A. Hosseinian, A. Monfared. DFT results against experimental data for electronic properties of C60 and C70 fullerene derivatives. *J. Mol. Graph. Model.*, 81, 60-67, 2018.
389. A. I. Alrawashdeh, J. B. Lagowski. The role of the solvent and the size of the nanotube in the non-covalent dispersion of carbon nanotubes with short organic oligomers – a DFT study. *RSC Adv.*, 8, 30520-30529, 2018.
390. J. Aragó, P. M. Viruela, E. Ortí. From linear quaterthiophene to sulflower: A comparative theoretical study. *J. Mol. Struct-Theochem.*, 912, 27-31, 2009.
391. M. Rubio, M. Merchán, E. Ortí. A Theoretical Study on the Low-Lying Excited States of 2,2':5',2''-Terthiophene and 2,2':5',2'':5'',2'''-Quaterthiophene. *ChemPhysChem*, 6, 1357-1368, 2005.
392. T. Iwamoto, Y. Watanabe, Y. Sakamoto, T. Suzuki, S. Yamago. Selective and Random Syntheses of [n]Cycloparaphenylenes (n = 8–13) and Size Dependence of Their Electronic Properties. *J. Am. Chem. Soc.*, 133, 8354-8361, 2011.
393. A.-F. Tran-Van, E. Huxol, J. M. Basler, M. Neuburger, J.-J. Adjizian, C. P. Ewels, H. A. Wegner. Synthesis of Substituted [8]Cycloparaphenylenes by [2 + 2 + 2] Cycloaddition. *Org. Lett.*, 16, 1594-1597, 2014.
394. J. Rio, D. Erbahar, M. Rayson, P. Briddon, C. P. Ewels. Cyclotetrahalo-p-phenylenes: simulations of halogen substituted cycloparaphenylenes and their interaction with C60. *Phys. Chem. Chem. Phys.*, 18, 23257-23263, 2016.
395. S. M. Bachrach, D. Stück. DFT Study of Cycloparaphenylenes and Heteroatom-Substituted Nanohoops. *J. Org. Chem.*, 75, 6595-6604, 2010.
396. E. R. Darzi, E. S. Hirst, C. D. Weber, L. N. Zakharov, M. C. Lonergan, R. Jasti. Synthesis, Properties, and Design Principles of Donor–Acceptor Nanohoops. *ACS Cent. Sci.*, 1, 335-342, 2015.
397. T. Iwamoto, Y. Watanabe, T. Sadahiro, T. Haino, S. Yamago. Size-Selective Encapsulation of C60 by [10]Cycloparaphenylene: Formation of the Shortest Fullerene-Peapod. *Angew. Chem., Int. Ed.*, 50, 8342-8344, 2011.
398. T. Iwamoto, Y. Watanabe, H. Takaya, T. Haino, N. Yasuda, S. Yamago. Size- and Orientation-Selective Encapsulation of C70 by Cycloparaphenylenes. *Chem. – Eur. J.*, 19, 14061-14068, 2013.
399. T. Iwamoto, Z. Slanina, N. Mizorogi, J. Guo, T. Akasaka, S. Nagase, H. Takaya, N. Yasuda, T. Kato, S. Yamago. Partial Charge Transfer in the Shortest Possible Metallofullerene Peapod, La@C82@[11]Cycloparaphenylene. *Chem. – Eur. J.*, 20, 14403-14409, 2014.

400. Y. Nakanishi, H. Omachi, S. Matsuura, Y. Miyata, R. Kitaura, Y. Segawa, K. Itami, H. Shinohara. Size-Selective Complexation and Extraction of Endohedral Metallofullerenes with Cycloparaphenylene. *Angew. Chem., Int. Ed.*, 53, 3102-3106, 2014.
401. K. Yuan, C. H. Zhou, Y. C. Zhu, X. Zhao. Theoretical exploration of the nanoscale host-guest interactions between [n]cycloparaphenylenes (n = 10, 8 and 9) and fullerene C(6)(0): from single- to three-potential well. *Phys. Chem. Chem. Phys.*, 17, 18802-12, 2015.
402. N. Ramos-Berdullas, I. Pérez-Juste, C. Van Alsenoy, M. Mandado. Theoretical study of the adsorption of aromatic units on carbon allotropes including explicit (empirical) DFT dispersion corrections and implicitly dispersion-corrected functionals: the pyridine case. *Phys. Chem. Chem. Phys.*, 17, 575-587, 2015.
403. Đ. Nakarada, M. Etinski, M. Petković. Using Density Functional Theory To Study Neutral and Ionized Stacked Thymine Dimers. *J. Phys. Chem. A*, 120, 7704-7713, 2016.
404. X. Ye, Z.-H. Li, W. Wang, K. Fan, W. Xu, Z. Hua. The parallel π - π stacking: a model study with MP2 and DFT methods. *Chem. Phys. Lett.*, 397, 56-61, 2004.
405. J. C. Sancho-García, M. Moral, A. J. Pérez-Jiménez. Effect of Cyclic Topology on Charge-Transfer Properties of Organic Molecular Semiconductors: The Case of Cycloparaphenylene Molecules. *J. Phys. Chem. C*, 120, 9104-9111, 2016.
406. Y. Segawa, A. Fukazawa, S. Matsuura, H. Omachi, S. Yamaguchi, S. Irlé, K. Itami. Combined experimental and theoretical studies on the photophysical properties of cycloparaphenylenes. *Org. Biomol. Chem.*, 10, 5979-5984, 2012.
407. M. Fujitsuka, D. W. Cho, T. Iwamoto, S. Yamago, T. Majima. Size-dependent fluorescence properties of [n]cycloparaphenylenes (n = 8–13), hoop-shaped π -conjugated molecules. *Phys. Chem. Chem. Phys.*, 14, 14585-14588, 2012.
408. J. C. Sancho-García, C. Adamo, A. J. Pérez-Jiménez. Describing excited states of [n]cycloparaphenylenes by hybrid and double-hybrid density functionals: from isolated to weakly interacting molecules. *Theor. Chem. Acc.*, 135, 25, 2016.
409. C. Graham, M. Moral, L. Muccioli, Y. Olivier, Á. J. Pérez-Jiménez, J.-C. Sancho-García. N-doped cycloparaphenylenes: Tuning electronic properties for applications in thermally activated delayed fluorescence. *Int. J. Quantum Chem.*, 118, e25562, 2018.
410. J. M. Abendroth, O. S. Bushuyev, P. S. Weiss, C. J. Barrett. Controlling Motion at the Nanoscale: Rise of the Molecular Machines. *ACS Nano*, 9, 7746-7768, 2015.
411. E. M. Pérez. Putting Rings around Carbon Nanotubes. *Chem. - Eur. J.*, 23, 12681-12689, 2017.

412. M. Peplow. The tiniest Lego: a tale of nanoscale motors, rotors, switches and pumps. *Nature*, 525, 18-21, 2015.

